THE EFFECTS OF THREE-DIMENSIONAL MATRIX STIFFENING ON VASCULAR STRUCTURE AND INTEGRITY IN ANGIOGENESIS

A Dissertation

Presented to the Faculty of the Graduate School

of Cornell University

In Partial Fulfillment of the Requirements for the Degree of

Doctor of Philosophy

by

Brooke Nichol Mason

August 2014

THE EFFECTS OF THREE-DIMENSIONAL MATRIX STIFFENING ON VASCULAR STRUCTURE AND INTEGRITY IN ANGIOGENESIS

Brooke Nichol Mason, Ph. D.

Cornell University 2014

The extracellular environment is an essential mediator of blood vessel health and provides both chemical and mechanical stimuli to influence endothelial cell behavior. While historically there has been significant emphasis placed on the chemical regulators of angiogenesis, the role of the mechanical environment is less well known. Interestingly, the mechanical properties of tissues are altered in many disease states, leading to impaired vascular function.

Herein, we tune the mechanical properties of collagen-based scaffolds using non-enzymatic glycation to show that angiogenesis is differentially regulated by matrix stiffness. Importantly, our methods de-couple matrix stiffness from matrix density and fiber structure in collagen gels. Endothelial cell spreading increases with matrix stiffness, as do the number and length of angiogenic sprouts. Increased stiffness also promotes increased branching in sprouts that form from spheroids, and it disrupts endothelial barrier function.

In the first steps towards translating these findings in vivo, we used a murine tumor model of stiffening to show that vascular density and the localization of mural cells

are altered within murine mammary tumors where collagen cross-linking has been disrupted. Additionally, we studied breast tumors isolated from patients and found that a specific splice variant of fibronectin, a protein known to be required for neo-vessel formation which is typically associated with angiogenic blood vessels, is present within the vasculature of human breast tumors but not in patient-matched normal tissue. Together, these data show that the tumor vasculature is inherently different than that of normal tissue and suggest that matrix stiffness may play a role in these alterations.

To study the interplay and balance between chemical factors and matrix stiffness, we developed a versatile microfluidic platform to expose cells cultured on substrates of well-characterized, tunable stiffness to well-defined, stable chemical gradients. The utility of this platform was validated by imposing a chemical gradient onto vascular smooth muscle cells to show that podosomes preferentially form upstream in a gradient. We anticipate that this device, with modifications, can be adapted for the study of angiogenesis in response to simultaneous chemical cues and matrix stiffness.

Taken together, these data demonstrate that matrix stiffness regulates the formation and function of angiogenic vasculature. The data suggest that therapeutically targeting stiffness or endothelial cell response to stiffening may help maintain and restore vessel structure and function to minimize metastasis and aid in drug delivery.

BIOGRAPHICAL SKETCH

Brooke Nichol Mason was born in Saginaw, Michigan on December 27, 1985 to David and Peggy Smith and grew up with her younger sisters Renee and Melissa in Freeland, Michigan. She graduated as the Valedictorian of Freeland High School in 2004. Brooke attended Michigan Technological University and was actively involved in the Research Scholars Program. While an undergraduate, she worked in the laboratory of Michael R. Neuman at Michigan Tech and created thick film electrodes for fetal monitoring and in the laboratory of Thomas Stieglitz at the University of Freiburg in Germany and developed neural prosthetic encapsulation systems during a summer internship. Brooke also participated in the Michigan Tech International Business Ventures Enterprise as the Heart Monitor Team Leader where she worked to produce an infant heartbeat annunciator that she helped to introduce to physicians and midwives in Ghana. Brooke graduated summa cum laude with a Bachelors of Science in Biomedical Engineering in May 2008. She joined Cornell University's Ph.D. program in Biomedical Engineering in August 2008 and was awarded a National Science Foundation Graduate Assistant in Areas of National Need (GAANN) Fellowship. Brooke joined the laboratory of Cynthia A. Reinhart-King and her dissertation work focused on elucidating the role of three-dimensional extracellular matrix stiffness on endothelial cell function. She was named an Ashoka Campus Changemaker in 2009 and was awarded a National Science Foundation Graduate Research Fellowship in 2009, a National Science Foundation GK-12 Fellowship in 2012, and a Rebecca and James Morgan Graduate Fellowship in Biomedical Engineering in 2013. Brooke completed her Ph.D. in the summer of 2014. When not in the lab, Brooke enjoys spending time with her husband Blake, family, and friends. She also loves traveling, scuba diving, boating, cooking, and reading.

To my family and friends,

For your unconditional love and support.

ACKNOWLEDGMENTS

I would sincerely like to thank Dr. Cynthia Reinhart-King for the opportunity to complete my thesis work in her lab. Cindy, I am extremely grateful for your guidance and encouragement throughout my time at Cornell. From the beginning, your vision inspired me and you personally took the time to train and empower me to make the transition into biomaterials research. Your mentorship has helped me to learn to communicate science effectively and develop into an independent scientific researcher. I will be forever grateful for the time I spent in your lab at Cornell.

I would also like to recognize and thank my committee members Dr. Lawrence Bonassar and Dr. Richard Cerione for their support and supervision of this work.

I would like to acknowledge the collaborations I have had, especially Dr. Lawrence Bonassar, Dr. Jonathan Butcher, Dr. Rebecca Williams, Dr. Valerie Weaver, Dr. Sandra Shin, Dr. Nozomi Nishimura. Their input, discussions, and partnership greatly enriched my project work. Additionally, I would like to thank Dr. Joseph Califano, Dr. John Huynh, Dr. Casey Kraning-Rush, Dr. Francois Bordeleau, Dr. Christine Montague, Michael Mazzola, Sahana Somasegar, Shawn Carey, Julie Kohn, Alina Starchenko, Danielle LaValley, Yiming Kang, Na Young Kim, Dennis Zhou, and Allen Zhou for collaborations in original research and book chapters.

I gratefully thank the funding sources that have supported this work, including a National Science Foundation Graduate Assistant in Areas of National Need (GAANN) Fellowship, National Science Foundation Graduate Research Fellowship, National Science Foundation GK-12 Fellowship, and a Rebecca and James Morgan Graduate

Fellowship in Biomedical Engineering.

Thank you to Dr. Shivaun Archer, Dr. Chris Schaffer, and Nev Singhota for their guidance in regards to GK-12 education, teaching practices, and science outreach. I especially want to thank Ms. Laura Austen and her students at Elmira Southside High School for inviting me into their classroom and allowing me to become their "scientist in residence." Laura's collaboration and friendship have been especially meaningful to me.

I would especially like to thank and acknowledge my labmates who have become my family while at Cornell. Dr. Joseph Califano, Dr. John Huynh, and Dr. Casey Kraning-Rush, you all made the Reinhart-King (CRK) Lab an inviting home. To the rest of the CRK lab, Dr. Christine Montague, Dr. Libin Yuan, Dr. Saumendra Bajpai, Dr. Francois Bordeleau, Shawn Carey, Marsha Lampi, Julie Kohn, Alexandra McGregor, Aniqua Rahman, and Danielle LaValley, you were all a most welcome addition to our lab family and enlivened the group with your personalities, insights, and experiences. I was so fortunate to be part of the supportive and intellectually-stimulating environment of the CRK lab and not only share many scientific discussions but also meals, holidays, and vacation time with these wonderful people. Jason Kraning-Rush was also a pseudo-CRK lab member who was kind enough to always welcome me into his home for good company and a delicious meal.

I would also like to recognize Turi Alcoser. His profound vivacity and passion for science was contagious and will be remembered.

I must also acknowledge my friends Laura Hockaday and Heeyong Kang, Carissa and

Nathan Ball, Erica Pratt, Stephen and Kate Rosa, Lucas Dehn, Jennifer Richards, Jennifer Puetzer, Shawn and Teresa Carey (and P.J.), Katie and Alex Melville (and Evelyn), and many others. Their enduring companionship was a comfort throughout my time at Cornell.

I would like to thank all of the students I was fortunate to mentor during my time in the Reinhart-King Lab. I can only hope that Yuk Heng (Matthew) Tang, Brian Fleisher, Lulu Bai, Sahana Somasegar, Dennis Zhou, and Michael Mazzola learned as much from me as I did from them. It was truly my pleasure to work with all of them.

I would be remiss for not mentioning the people at Michigan Technological University who encouraged me to attend graduate school. I would sincerely like to thank Dr. Michael Neuman for being such a wonderful and caring advisor and for introducing me to research, allowing me to explore my interests under his reassuring guidance, and encouraging me to explore new opportunities. I would also like to thank Dr. Laura McCormick for being always willing to answer my incessant questions and for the helpful discussions we had about my research project and graduate school. I would also like to acknowledge Dr. Robert Gratz, Dr. Debra Charlesworth, Dr. Robert Warrington, and Anne Warrington for their mentoring and encouragement.

Thank you to Dr. Robert Grant for his mentorship and for allowing me to shadow him during the summer immersion program at Weill Cornell Medical College. His conversations and insights into how physicians use medical products have made me a better biomedical engineer and I will carry the experience and lessons learned with me throughout my career.

I would not be here today without the loving support of my family. My parents, sisters, grandparents, aunts, uncles, and cousins were influential role models who urged me to dream big dreams, prioritize my education, and strive to achieve my goals. When I was a child, my dad, David Smith, inspired me to learn about how machines function and my mom, Peggy Smith, shared her passion for human medicine with me - that is why I am a biomedical engineer today. Their belief in me and my abilities have empowered me to trust that I can realize my dreams.

I am extremely grateful to my husband Blake for urging me to follow my dreams and pursue my graduate education at Cornell and for then altering his own to join me in New York. Blake, your love and encouragement have been instrumental in helping me complete my dissertation. Even when you were working half a world away, your constant support emboldened me to persevere through the joys and trials of research. I am excited to begin the next chapter of our lives together.

TABLE OF CONTENTS

LIST OF FIGURES

Chapter 1: Introduction

Chapter 2: Tuning three-dimensional collagen matrix stiffness independently of collagen concentration modulates endothelial cell behavior

Chapter 3: Collagen cross-linking increases angiogenesis and disrupts barrier integrity

Chapter 4: Histological analysis of the tumor vasculature in humans and mice

Chapter 5: Development of a microfluidic device to study chemotactic and durotactic cues on cellular migration

Chapter 6: Exploring tissue perfusion and nutrient delivery in the classroom

Chapter 7: Conclusions and future directions

LIST OF ABBREVIATIONS

2D	Two dimensional
3D	Three dimensional
α-LOXab	Anti-lysyl oxidase inhibitory antibody
αSMA	Alpha smooth muscle actin
αSMA-	Alpha smooth muscle actin negative
αSMA+	Alpha smooth muscle actin positive
AGE	Advanced glycation endproducts
ANOVA	Analysis of variance
ATP	Adenosine triphosphate
BAEC	Bovine aortic endothelial cell
BAPN	Beta-aminopropionitrile
bFGF	Basic fibroblast growth factor
BME	Biomedical engineering
BSA	Bovine serum albumin
$CaCl_2$	Calcium chloride
CAM	Chorioallantoic membrane
CLIMB	Cornell Learning Initiative in Medicine and Bioengineering
CO_2	Carbon dioxide gas
Ctrl	Control
Ctsk	Cytoskeleton
DAB	3,3'-diaminobenzidine tetrahydrochloride
DAPI	4',6-diamidino-2-phenylindole
DAPT	N-[N-(3,5-difluorophenacetyl)-L-ananyl]-S-phenylglycine t-butyl ester

Dll4	Delta-like ligand 4
EC	Endothelial cell
ECM	Extracellular matrix
EDB-FN	Extra domain-B fibronectin
EGF	Epidermal growth factor
ELISA	Enzyme-linked immunosorbent assay
FITC	Fluorescein isothiocyanate
FN	Fibronectin
GFP	Green fluorescent protein
GK-12	Graduate STEM Fellows in K-12 Education
HEPES	4-(2-hydroxyethyl)-1-piperazineethanesulfonic acid
HRP	Horse radish peroxidase
HUVEC	Human umbilical vein endothelial cell
LOX	Lysyl oxidase
MCs	Mural cells
MMPs	Matrix metalloproteinases
MT-MMP	Matrix type matrix metalloproteinase
MW	Molecular weight
N-6	N-6-((acryloyl)amino) hexanoic acid, succinimidyl ester
NaCl	Sodium chloride
NaOH	Sodium hydroxide
Neu	FVB/N-Tg(MMTVneu)202Mul/J mice
NP-40	Tergitol-type NP-40
PA	Poly(acrylamide)
PBS	Phosphate-buffered saline
PDBu	Phorbol 12,13 dibutyrate

PDMS	Polydimethylsiloxane
PEG	Poly(ethylene glycol)
PyMT	FVB/N-Tg(MMTV-PyVT)634Mul/J mice
RAGE	Receptor for advanced glycation endproducts
RGD	Arginine-Glycine-Asparagine peptides
ROCK	Rho-associated coiled-coil containing protein kinase
SEM	Standard error of the mean
TCP	Tissue culture plastic
TPA	Phorbol-12-myristate-13-acetate
TRITC	tetramethylrhodamine isothicyanate
Triton	Octyl phenol ethoxylate
Tween	Polyoxyethylene 20 sorbitan monolaurate
VE-cadherin	Vascular endothelial cadherin
VEGF	Vascular endothelial growth factor
VSMCs	Vascular smooth muscle cells

LIST OF SYMBOLS

Symbol	Description	Units
A+B	Equilibrium stress	Pa = N/m^2
B	Instantaneous stress	Pa = N/m^2
^oC	Degree Celsius	Degree
d^2	Mean Square Displacement	μm^2
E	Young's Modulus	Pa = N/m^2
σ_{eq}	Equilibrium compressive modulus	Pa = N/m^2
P	Persistence	minutes
S	Migration Speed	μm/min
t	Time	sec or min
τ	Exponential time constant	sec

CHAPTER 1

INTRODUCTION

Portions of this chapter were published as a commentary titled "Controlling the mechanical properties of three-dimensional matrices via collagen cross-linking" in *Organogenesis*[1] or as a book chapter titled "Matrix Stiffness: A regulator of cellular behavior and tissue formation" in *Engineering Biomaterials for Regenerative Medicine: Novel Technologies for Clinical Applications*[2]

1.1 Abstract

The mechanical properties of the extracellular matrix play an important role in maintaining cellular function and overall tissue homeostasis. Recently, a number of hydrogel systems have been developed to investigate the role of matrix mechanics in mediating cell behavior within three-dimensional environments. However, many of the techniques used to modify the stiffness of the matrix also alter properties that are important to cellular function including matrix density, porosity, and binding site frequency, or rely on amorphous synthetic materials. In this dissertation, I will describe the fabrication, characterization and utilization of collagen gels that have been non-enzymatically glycated in their un-polymerized form to produce matrices of

[1] Mason BN, Reinhart-King CA. Controlling the mechanical properties of three-dimensional matrices via non-enzymatic collagen glycation. Organogenesis 2013; 9:70-5.

[2] Mason BN, Califano JP, Reinhart-King CA. Engineering Biomaterials for Regenerative Medicine: Novel Technologies for Clinical Applications. Bhatia SK, ed. 2012; 19-38.

varying stiffness. We show that the mechanical properties of the resulting collagen gels can be increased 3-fold without significantly altering the collagen fiber architecture. Applying these scaffolds to the question of angiogenesis, we find that endothelial cell spreading and outgrowth from multi-cellular spheroids changes as a function of the stiffness of the matrix. Our results demonstrate that non-enzymatic collagen glycation is a tractable technique that can be used to study the role of 3D stiffness in mediating cellular function. This introductory chapter will review some of the current methods that are being used to modulate matrix mechanics and discuss how the use of non-enzymatic collagen glycation can contribute to our knowledge of the factors regulating angiogenesis.

1.2 Introduction

The tissues and organs of the body are comprised of cells and extracellular matrices that are arranged to perform specific biological, chemical, and physical functions. Cells within tissues interact with the extracellular matrix and each other to receive and impart both chemical and mechanical cues that influence their behavior. Importantly, these interactions contribute to overall tissue homeostasis and cellular function and, if they are disturbed, can contribute to aberrant cell behavior and disease.

Altered tissue mechanical properties have been correlated with a number of disease states including cancer[1], diabetes[2], cardiovascular disease[3], wound healing[4], and asthma.[5] Each of these maladies is characterized by a unique set of conditions but, in all cases, the interaction of the cells with their extracellular environment is altered.

The composition, density, arrangement, and extent of cross-linking have all been shown to influence how cells interact with, move through, and remodel their surroundings.[6] Since it is difficult to control all of these parameters independently in an *in vivo* setting, a number of *in vitro* hydrogel systems have been designed to study their role in a controlled environment.

Studies using two-dimensional substrates have shown that changes in matrix stiffness are correlated with altered cellular morphology[7,8], traction force generation[9–11], cell-cell connectivity [3,12–14], differentiation [15], chemotactic response[16] and matrix deposition.[17] However, since most cells in the body reside within a three-dimensional environment, it is important to recapitulate their natural extracellular environment to assess cellular function.

Common methods to create three-dimensional matrices with tunable mechanical properties include altering the density and/or extent of cross-linking of natural or synthetic hydrogels, or creating mixed matrices comprised of multiple synthetic and/or natural hydrogels. Modifying the density of the matrix is a relatively simple way to alter the mechanical properties of a hydrogel system to allow for the investigation of three-dimensional cellular behavior. This technique has commonly been used with native biological proteins such as collagen[18,19] and fibrin[20] but is also used in other synthetic hydrogel systems such as poly(ethylene glycol).[21] Cross-linking approaches to control stiffness are most commonly used in synthetic hydrogel systems, but similar methods have been reported using natural matrices.[22,23]

While each of these techniques is capable of altering the stiffness of the matrix, they all have inherent advantages and disadvantages for studying the role of mechanical properties within a three-dimensional cell culture system. Specifically, changing the matrix density or cross-linking of a hydrogel can also influence porosity and hydraulic permeability[18,20], fibril arrangement and structure[19], and binding domain frequency[6] within the hydrogels. Consequently, it can be difficult to decouple the relative effects of the mechanical properties from the other physical and chemical factors that are concurrently affected.

This chapter will provide a brief overview of some of the current approaches to modulate matrix stiffness for three-dimensional studies of cellular behavior and review their general advantages and disadvantages.

1.3 Modulating 3D Hydrogel Mechanical Properties

Naturally-Derived Hydrogels

A number of native proteins and polymers have been utilized to make three-dimensional hydrogels for the investigation of cell response to matrix stiffening. Among the many extracellular matrix components that are present within the body, type I collagen, fibrin, and hyaluronic acid are among the most commonly used for creating three-dimensional matrices.[18,20,24] Importantly, these matrices allow cells to be seeded within a natural environment that is capable of being both degraded and remodeled as is done *in vivo* by cells.

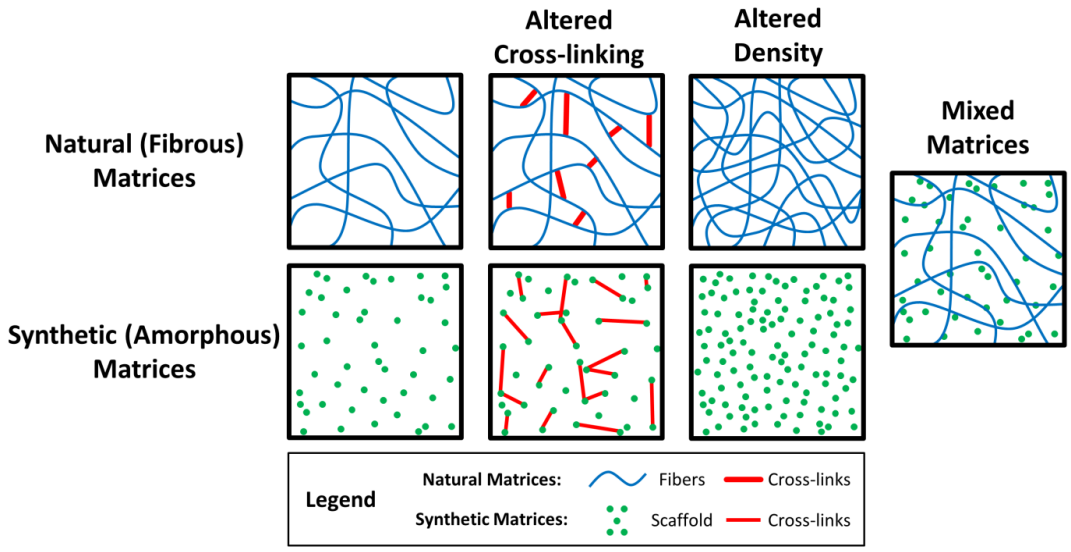

Figure 1.1. Methods commonly used to modulate matrix stiffness. The mechanical properties of both synthetic and natural matrices are commonly tuned by altering the number of cross-links and/or the density of the scaffold. Mixed matrices comprised of both synthetic and natural materials can be used to create hybrid in vitro environments that mimic the properties of in vivo tissues.

The most basic approaches utilizing natural matrices are those that increase the stiffness of the matrix by increasing the density (Figure 1.1). A number of studies have modified the density of collagen or fibrin hydrogels to study the influence of matrix mechanics on cellular behavior. By increasing the density of collagen matrices from 2 mg/ml to 20 mg/ml, the compressive modulus increases approximately 10-fold from approximately 175 Pa to 1800 Pa.[18,25] Similarly, by increasing the density of fibrin matrices from 2.5 mg/ml to 10 mg/ml, the compressive modulus increases from approximately 1.3 kPa to 9 kPa.[20]

The stiffness of some natural polymers can be modulated using differential cross-

linking to investigate cell behavior (Figure 1.1). For example, methacrylated hyaluronic acid is a matrix that is currently being used to dynamically modulate the stiffness of hydrogels via a two-step cross-linking process.[26] First, hydrogels are chemically cross-linked and then can be seeded with cells before a secondary photo cross-linking reaction is initiated. This is an especially interesting procedure because it allows the mechanics of the matrix to be temporally controlled from approximately 1.5 to 7.5 kPa while cellular behavior is simultaneously investigated. Unfortunately, since methacrylated hyaluronic acid is not naturally porous, methods had to be developed to create pores within the matrix. Poly(methyl methacrylate) microspheres are encapsulated during the initial polymerization reaction and subsequently dissolved before cells are seeded within the matrices to create large (~300 um) pores within the hydrogel. This potentially limits the ability of these matrices to truly recapitulate a three-dimensional, *in vivo*-like environment.

While hydrogels formed from naturally-derived materials provide an optimal environment for cell culture, it can be challenging to use natural matrices for studies of the effects of matrix stiffness. Specifically, since the matrix materials are biologically designed for cell adhesion, it is relatively difficult to decouple the role of binding site availability from matrix density. Additionally, the fibrous arrangement and structure of the matrices can be modified with changes to the density or cross-linking which further complicates the analysis of resultant cellular responses. Further, even when both the density and cross-linking of natural hydrogel matrices are modified, the resultant matrix stiffness is only tunable across a relatively narrow range (usually

100's to 1000's of Pa). Taken together, these complexities can make it difficult to pinpoint whether the cellular responses are due to changes in matrix stiffness or other factors.

Synthetic Hydrogels

To overcome some of the disadvantages inherent to hydrogels comprised of naturally-derived matrices, synthetic hydrogels have been created. The primary advantage of using synthetic hydrogels is that they can be formulated to investigate both mechanical and chemical properties on cellular function. Indeed, many synthetic hydrogel systems offer independent control of mechanical properties, adhesive binding sites, and chemical cues. One of the most popular synthetic materials used currently is poly(ethylene glycol) (PEG)[21,27–29] although other materials such as poly(caprolactone)[30] and poly(methyl methacrylate)[31] have also been used. Since these synthetic hydrogels were originally developed for other purposes and do not naturally contain cell binding domains, moieties such as Arg-Gly-Asp peptides (RGD) or laminin-like domains must be incorporated to facilitate cell adhesion. This allows for precise control and modulation of the frequency and availability of adhesive regions within the hydrogel.

Modulating the density and cross-linking of synthetic hydrogels are techniques that are commonly used to alter their mechanical properties (Figure 1.1). The density of PEG hydrogels has been used to investigate the role of three-dimensional cellular behaviors.[21] Additionally, a number of PEG hydrogel systems have been developed

that incorporate matrix metalloproteinase (MMP)-sensitive cross-links so that cells are capable of degrading their surrounding environment.[27,28] Systems have also been developed to selectively cross-link PEG gels using multiphoton microscopy resulting in hydrogels with micro-domains similar to those found in tissue structures.[32]

While synthetic hydrogels provide a highly tunable system for investigating cell behavior, they are generally amorphous and unlike the fibrous extracellular matrices within the body. Thus, while it is feasible to independently tune properties such as the stiffness, binding site availability, and degradability, synthetic hydrogels are sub-optimal because the cells are unable to actively remodel them and they do not recapitulate the fibrous nature of the *in vivo* environment.

Mixed Matrices

To overcome some of the disadvantages inherent to investigating matrix stiffness with hydrogels comprised of synthetic or natural materials alone, mixed matrices have been developed (Figure 1.1). For example, collagen has been combined with PEG [33], agarose [34], or fibrin[35] to create matrices with tunable mechanical properties. In each of these cases, the density, extent of cross-linking, or ratio of each component are altered to control the mechanical properties. As such, it is possible that the cellular behavior will be influenced by the matrix composition which is not completely decoupled from stiffness. While the data generated from cells embedded within these matrices may be complex, these systems lay an important foundation for the development of *in vitro* hydrogels that more closely mimic the properties of *in vivo*

tissues.

1.4 Non-enzymatic Collagen Glycation

We recently reported the use of non-enzymatic glycation of un-polymerized collagen to investigate the effects of matrix stiffening on endothelial cells.[25] Non-enzymatic glycation is a natural process whereby reducing sugars and proteins interact to produce extracellular matrix cross-linking within biological tissues.[36] These sugars create chemical alterations within the protein structures that ultimately result in protein-to-protein cross-links that mechanically alter the tissues. Specifically, the interaction of reducing sugars such as glucose or ribose with amino groups on proteins create Schiff bases which are able to rearrange into Amadori products.[37] The Amadori products can then form protein-to-protein cross-links that are commonly known as advanced glycation end products (AGE).[38] These AGE cross-links slowly accumulate on proteins *in vivo* during aging, and the rate and extent of accumulation is accelerated in individuals with diabetes.[38]

In vitro, non-enzymatic collagen glycation can be used to cross-link protein solutions prior to hydrogel polymerization (pre-glycation) or can cross-link polymerized protein matrices (post-glycation).[23] Post-glycation is the primary method whereby proteins *in vivo* are cross-linked. However, the high sugar concentrations necessary to achieve measurable changes in stiffness *in vitro* limit this technique to seeding cells on the surface of the matrices after the glycation reaction has been completed because cells cannot withstand the osmotic imbalance created by the glycating solutions.[39] During

pre-glycation, active sites are created within the collagen gels that will later become cross-links during collagen polymerization. Since the collagen solutions are treated with the glycating solutions prior to polymerization, cells can be embedded within the gels during the polymerization process and are not subjected to the osmotic imbalances created by the glycating solutions. Thus, by using the process of pre-glycation, the effects of 3D stiffness on cells embedded within collagen matrices can be investigated.

Many studies have investigated the effects of collagen glycation on endothelial cell behavior. In prior studies, investigators have seeded cells atop of post-glycated matrices or injected cells into matrices following glycation[39–42]. While these studies have provided valuable information, post-glycation is limited in its ability to investigate the effects of matrix stiffness on the behavior of cells embedded within the matrix. In our work, we utilized non-enzymatic pre-glycation (henceforth referred to as glycation) to investigate the effects of 3D matrix stiffness on collagen fiber structure and arrangement as well as on endothelial cell spreading and organization.[25] To glycate matrices, collagen solutions were incubated with 0 – 250 mM ribose for 5 days at 4^{O}C prior to polymerization. At the end of this incubation, the collagen solutions were mixed with sodium hydroxide to neutralize the pH, and complete medium or a suspension of endothelial cells was added to bring the final collagen density to 1.5 mg/ml. Collagen solutions were polymerized at 37^{O}C and 5% CO_2. Using these matrices, we investigated the mechanical properties, polymerization dynamics, collagen fiber distributions and structures, as well as individual and

collective endothelial cell responses.

In parsing out the effects of matrix stiffness on cell behavior, it is critical to also control for architecture and fiber arrangement within the collagen matrices. Our study was the first to examine the resultant fiber arrangements within pre-glycated polymerized matrices. Importantly, we found that there exists a range of ribose concentrations (0 – 100 mM) where the equilibrium compressive modulus of collagen can be increased approximately 3-fold from ~175 – 515 Pa while the arrangement and size of collagen fibrils is not significantly affected. Increasing the concentration of ribose to 150 mM or greater also results in increased matrix stiffness but the fibrous properties of the matrices change as well. Similarly, we found that the fibril formation rate was similar for collagen solutions that had been glycated with 0 – 100 mM ribose while the rates for solutions glycated with 150 – 250 mM ribose were significantly delayed and correlated with larger collagen fibers. Since it is known that the arrangement of fibrous features within matrices can influence cellular function, we focused on gels glycated with 0 – 100 mM ribose for our studies of endothelial cell behavior.

Disadvantages of collagen glycation

Although the non-enzymatic glycation of collagen mimics the stiffening of matrices naturally occurring *in vivo*, there are several drawbacks to using this method to investigate the effects of matrix stiffness on cell function. Specifically, collagen glycation alters the chemical composition of the matrix by creating AGE cross-links.

A variety of cell types, including endothelial cells, are known to have RAGE and the interactions between AGE and RAGE have been shown to influence cell behavior and cell-cell interactions.[43] Specifically, AGE/RAGE interactions have been implicated in altering endothelial cell response to shear stress[40], mechanical stretch[44], and barrier function.[45] A number of methods have been developed to inhibit the interaction of RAGE with AGE including blocking antibodies and pharmaceutical drugs.[46–48] However, like other cell-membrane receptors, RAGE can be replenished to the cell surface, making the long-term use of blocking antibodies less effective and very expensive. Additionally, the pharmaceutical drugs that have been used to inhibit the RAGE/AGE interaction are not specific to RAGE and also influence a wide variety of other cellular pathways and behaviors.[48–50] Thus, while glycation can recapitulate the mechanical stiffening that occurs naturally within the body, it can also engage RAGE. The respective contributions of these two factors to overall cell behavior can be difficult to decouple.

Advantages Collagen Glycation and Implications for Human Disease

Although it is challenging to completely decouple the role of matrix stiffness from AGE/RAGE signaling in our hydrogel system, collagen glycation does have many advantages over other current methods of matrix stiffening. Specifically, we demonstrated the ability to increase the stiffness of the collagen gels 3-fold independently of the overall collagen fiber arrangements. Our study was limited to 1.5 mg/ml gels but it is possible that increasing the density of the collagen gels will allow for a wider range of moduli to be achieved.

Since accumulation of AGE cross-links within tissues during aging is universal, using non-enzymatic glycation to investigate the role of matrix stiffening is relevant to understanding conditions *in vivo*. In fact, the presence of AGEs has been suggested to play a causative role in diseases such as diabetes[51], rheumatoid arthritis[52], atherosclerosis[53], Alzheimer's[54], and cataracts.[55] Our data has demonstrated that endothelial cells respond to the changes in matrix stiffness induced by non-enzymatic glycation. Importantly, our lab has also correlated aging with increased vascular stiffness and endothelial monolayer permeability which may contribute the increased prevalence in cardiovascular disease.[3] Thus, using non-enzymatic collagen glycation to investigate the impact of altering three-dimensional matrix stiffness on cellular behavior has the potential to inform how we manage and treat different disease conditions.

1.5 Angiogenesis and Disease

During angiogenesis, endothelial cells degrade the basement membrane and migrate from a pre-existing vessel into the surrounding extracellular matrix to form new blood vessels. Historically, there has been significant emphasis placed on the chemical regulators of angiogenesis such as vascular endothelial growth factor (VEGF)[56]. Indeed, it is well-known that VEGF plays an important role in endothelial cell migration, proliferation and angiogenesis. However, previous work from our lab has shown that the stiffness of the two-dimensional matrices regulates endothelial cell network formation and traction force generation, suggesting that matrix mechanical

properties also influence the formation of vascular structures[9,12]. In this dissertation, we will use non-enzymatic collagen glycation to study the role of three-dimensional matrix stiffness on angiogenesis.

In a number of disease conditions including cancer, diabetes, and aging, increased tissue stiffness is correlated with altered vascular formation and function[57,58]. In general, tumor tissues have altered mechanical properties as compared to native, healthy tissue[59–62]. In fact, breast cancer is often first detected by the patient or physician finding a palpable mass or lump that is stiffer than the surrounding tissue. Large tumors are associated with an increase in local ECM stiffness and angiogenesis, an in growth of newly sprouted blood vessels that facilitate increased tumor mass[58]. The increase in ECM stiffness is primarily due to increased collagen deposition and cross-linking within the tumor stroma[60], but a disruption in the tensional homeostasis of the cells may also contribute[1]. Additionally, the greater prevalence of reducing sugars such as glucose and ribose within the blood of diabetic patients leads to increased cross-link density of collagen and elastin, and consequently increased stiffness of the vasculature when compared with non-diabetics[2,63]. Importantly, in both cancer and diabetes, blood vessels are more malformed, tortuous, and leaky when compared to vessels within healthy tissues[64,65].

Herein, we utilize glycated collagen gels to study the role of three-dimensional stiffness on blood vessel formation. Since collagen is the primary component of the extracellular matrix and AGE cross-links are found within tumors and known to

mediate tissue stiffening in diabetes and aging[51,66,67], stiffening collagen gels with non-enzymatic glycation is a physiologically-relevant model for studying angiogenesis.

1.6 Conclusions

Researchers today have many options to consider when choosing a hydrogel system to investigate the role of matrix mechanics on cellular behavior. Naturally-derived matrices contain many of the essential elements required for cellular culture and can closely mimic the three-dimensional cellular environment. However, synthetic matrices tend to be more customizable so that the intricacies of individual parameters such as cellular adhesion and mechanosensing can be more closely studied. We have presented non-enzymatic collagen glycation as a highly tractable technique that utilizes a cross-linking mechanism that recapitulates *in vivo* tissue stiffening and is relevant to a number of disease states. Future work in the development of these materials should combine the advantages of these techniques to create matrices that allow for independent modulation of hydrogel parameters while mimicking the native extracellular environment. In my own work, as described in this dissertation, these materials were used to investigate the role of matrix stiffening on angiogenesis.

1.7 Organization of the Dissertation

The goal of this work is to investigate the role of three-dimensional matrix stiffness in regulating the structure and integrity of angiogenic blood vessels. We demonstrate that matrix stiffness influences the formation of angiogenic vasculature in vitro, ex ovo, and in histological sections from murine and human models.

In Chapter 2, we characterize the physical properties of collagen matrices that had been stiffened by non-enzymatic glycation cross-linking. We demonstrate that glycating collagen gels with 0-100 mM ribose only minimally changes collagen fiber distributions while increasing the compressive moduli of the gels three-fold. We embed endothelial cells within these glycated matrices and find that increased gel stiffness significantly alters angiogenic outgrowth from multi-cellular spheroids. This work is the first demonstration that increasing three-dimensional stiffness independently of matrix density increases angiogenic outgrowth.

In Chapter 3, we further investigate the role of extracellular matrix stiffness on angiogenic function. We find that increasing collagen density decreases angiogenic outgrowth from endothelial spheroids. We also determine that increasing matrix cross-linking increases angiogenic outgrowth both in vitro and in the ex ovo embryonic chick model. We further investigate the role of three-dimensional stiffness in mediating endothelial cell-cell junctions. We demonstrate that increasing matrix stiffness increases the widths of vascular endothelial cadherin "stalk" junctions. We also show that localization of vascular endothelial cadherin and the permeability of endothelial monolayers are significantly altered by matrix stiffness. This work is the first demonstration that three-dimensional matrix stiffness modulates vascular endothelial cadherin junction widths.

In Chapter 4, we use histology to investigate the role of tumor stiffness on the regulation of the vasculature in murine and human tumors. We determine that altered matrix stiffness correlates with differences in vascular density and mural cell localization in murine mammary tumors. Additionally, we find that the expression of a specific splice variant of fibronectin (EDB-FN) is expressed in the vasculature of human mammary tumors but not in patient-matched normal tissues.

In Chapter 5, we developed a microfluidic device to investigate the combined roles of matrix stiffness and chemical cues on endothelial cell migratory behavior. We also demonstrate that gradients of the phorbol ester PDBu stimulate podosomes in a directed manner in vascular smooth muscle cells.

Chapter 6 overviews my experience as an NSF STEM Fellow in GK-12 Education, where we developed laboratory activities and taught a science curriculum to high school students that focused on nutrient transport from the vasculature. In Chapter 7, conclusions and future directions are presented.

REFERENCES

1 Paszek MJ, Zahir N, Johnson KR, Lakins JN, Rozenberg GI, Gefen A, Reinhart-King CA, et al. Tensional homeostasis and the malignant phenotype. Cancer Cell 2005; 8:241–254.

2 DeLoach SS, Townsend RR. Vascular stiffness: its measurement and significance for epidemiologic and outcome studies. Clin J Am Soc Nephro 2008; 3:184–192.

3 Huynh J, Nishimura N, Rana K, Peloquin JM, Califano JP, Montague CR, King MR, et al. Age-related intimal stiffening enhances endothelial permeability and leukocyte transmigration. Sci Transl Med 2011; 3:112ra122.

4 Georges PC, Miller WJ, Meaney DF, Sawyer ES, Janmey PA. Matrices with compliance comparable to that of brain tissue select neuronal over glial growth in mixed cortical cultures. Biophys J 2006; 90:3012–3018.

5 Waters CM, Sporn PH, Liu M, Fredberg JJ. Cellular biomechanics in the lung. Am J Physiol Lung Cell Mol Physiol 2002; 283:L503–9.

6 Zaman MH, Trapani LM, Sieminski AL, Mackellar D, Gong H, Kamm RD, Wells A, et al. Migration of tumor cells in 3D matrices is governed by matrix stiffness along with cell-matrix adhesion and proteolysis. Proc Natl Acad Sci U S A 2006; 103:10889–10894.

7 Yeung T, Georges PC, Flanagan LA, Marg B, Ortiz M, Funaki M, Zahir N, et al. Effects of substrate stiffness on cell morphology, cytoskeletal structure, and adhesion. Cell Motil Cytoskeleton 2005; 60:24–34.

8 Pelham Jr. RJ, Wang Y. Cell locomotion and focal adhesions are regulated by substrate flexibility. Proc Natl Acad Sci U S A 1997; 94:13661–13665.

9 Califano JP, Reinhart-King CA. Substrate stiffness and cell area drive cellular traction stresses in single cells and cells in contact. Cell Mol Bioeng 2010; 3:68–75.

10 Reinhart-King CA, Dembo M, Hammer DA. Endothelial cell traction forces on RGD-derivatized polyacrylamide substrata. Langmuir 2003; 19:1573–1579.

11 Dembo M, Wang YL. Stresses at the cell-to-substrate interface during locomotion of fibroblasts. Biophys J 1999; 76:2307–2316.

12 Califano JP, Reinhart-King CA. A Balance of Substrate Mechanics and Matrix Chemistry Regulates Endothelial Cell Network Assembly. Cell Mol Bioeng 2008; 1:122–132.

13 Reinhart-King CA, Dembo M, Hammer DA. Cell-Cell Mechanical Communication through Compliant Substrates. Biophys J 2008; 95:6044–6051.

14 Krishnan R, Klumpers DD, Park CY, Rajendran K, Trepat X, Van Bezu J, Van Hinsbergh VWM, et al. Substrate stiffening promotes endothelial monolayer disruption through enhanced physical forces. Am J Physiol Cell Physiol 2011; 300:C146–C154.

15 Engler AJ, Sen S, Sweeney HL, Discher DE. Matrix elasticity directs stem cell lineage specification. Cell 2006; 126:677–689.

16 Jannat RA, Dembo M, Hammer DA. Neutrophil adhesion and chemotaxis depend on substrate mechanics. J Phys Condens Matter 2010; 22:194117.

17 Eisenberg JL, Safi A, Wei X, Espinosa HD, Budinger GS, Takawira D, Hopkinson SB, et al. Substrate stiffness regulates extracellular matrix deposition by alveolar epithelial cells. Res Rep Biol. 2011; 1–12.

18 Cross VL, Zheng Y, Won Choi N, Verbridge SS, Sutermaster BA, Bonassar LJ, Fischbach C, et al. Dense type I collagen matrices that support cellular remodeling and microfabrication for studies of tumor angiogenesis and vasculogenesis in vitro. Biomaterials 2010; 31:8596–8607.

19 Critser PJ, Kreger ST, Voytik-Harbin SL, Yoder MC. Collagen matrix physical properties modulate endothelial colony forming cell-derived vessels in vivo. Microvasc Res 2010; 80:23–30.

20 Ghajar CM, Blevins KS, Hughes CC, George SC, Putnam AJ. Mesenchymal Stem Cells Enhance Angiogenesis Early Matrix Metalloproteinase Upregulation. Tissue Eng 2006; 12:2875–88.

21 Ehrbar M, Sala A, Lienemann P, Ranga A, Mosiewicz K, Bittermann A, Rizzi SC, et al. Elucidating the role of matrix stiffness in 3D cell migration and remodeling. Biophys J 2011; 100:284–93.

22 Slaughter B V, Khurshid SS, Fisher OZ, Khademhosseini A, Peppas N a. Hydrogels in regenerative medicine. Adv Mater 2009; 21:3307–29.

23 Roy R, Boskey A, Bonassar LJ. Processing of type I collagen gels using nonenzymatic glycation. J Biomed Mater Res A 2010; 93A:843–851.

24 Seidlits SK, Drinnan CT, Petersen RR, Shear JB, Suggs LJ, Schmidt CE. Fibronectin-hyaluronic acid composite hydrogels for three-dimensional endothelial cell culture. Acta Biomater 2011; 7:2401–9.

25 Mason BN, Starchenko A, Williams RM, Bonassar LJ, Reinhart-King CA. Tuning three-dimensional collagen matrix stiffness independently of collagen concentration modulates endothelial cell behavior. Acta Biomater 2013; 9:4635–44.

26 Marklein RA, Soranno DE, Burdick JA. Magnitude and presentation of mechanical signals influence adult stem cell behavior in 3-dimensional macroporous hydrogels. Soft Matter 2012; 8:8113–20.

27 Kraehenbuehl TP, Zammaretti P, Van Der Vlies AJ, Schoenmakers RG, Lutolf MP, Jaconi ME, Hubbell JA. Three-dimensional extracellular matrix-directed cardioprogenitor differentiation: systematic modulation of a synthetic cell-responsive PEG-hydrogel. Biomaterials 2008; 29:2757–2766.

28 Kloxin AM, Kasko AM, Salinas CN, Anseth KS. Photodegradable hydrogels for dynamic tuning of physical and chemical properties. Science 2009; 324:59–63.

29 Zhang G, Drinnan CT, Geuss LR, Suggs LJ. Vascular differentiation of bone marrow stem cells is directed by a tunable three-dimensional matrix. Acta Biomater 2010; 6:3395–403.

30 Williamson MR, Woollard KJ, Griffiths HR. Gravity Spun Polycaprolactone Fibers for Applications in Vascular Tissue Engineering : Proliferation and Function of. Tissue Eng 2006; 12:45–51.

31 Quinn TM, Grodzinsky AJ. Longitudinal modulus and hydraulic permeability of poly(methacrylic acid) gels: effects of charge density and solvent content. Macromolecules 1993; 26:4332–4338.

32 Hoffmann JC, West JL. Three-dimensional photolithographic patterning of multiple bioactive ligands in poly(ethylene glycol) hydrogels. Soft Matter 2010; 6:5056.

33 Kong H, Liang Y, Jeong J, Devolder RJ, Cha C, Wang F, Tong YW. A cell-instructive hydrogel to regulate malignancy of 3D tumor spheroids with matrix rigidity. Biomaterials 2011; 32:9308–9315.

34 Ulrich T a, Jain A, Tanner K, MacKay JL, Kumar S. Probing cellular mechanobiology in three-dimensional culture with collagen-agarose matrices. Biomaterials 2010; 31:1875–1884.

35 Rao RR, Peterson AW, Ceccarelli J, Putnam AJ, Stegemann JP. Matrix composition regulates three-dimensional network formation by endothelial cells and mesenchymal stem cells in collagen/fibrin materials. Angiogenesis 2012; 15:253–264.

36 Maillard LC. Action des acides amines sur les sucres: formation des melanoides par voie methodique. Comptes Rendus de l'Academie des Sciences 1912; 154:66–68.

37 Hodge JE. The Amadori rearrangement. Adv Carbohydr Chem 1955; 10:169–205.

38 Ulrich P, Cerami A. Protein glycation, diabetes, and aging. Recent Prog Horm Res 2001; 56:1–21.

39 Roy R, Boskey AL, Bonassar LJ. Non-enzymatic glycation of chondrocyte-seeded collagen gels for cartilage tissue engineering. J Orthop Res 2008; 26:1434–1439.

40 Kemeny SF, Figueroa DS, Andrews AM, Barbee KA, Clyne AM. Glycated collagen alters endothelial cell actin alignment and nitric oxide release in response to fluid shear stress. J Biomech 2011; 44:1927–1935.

41 Basta G, Lazzerini G, Massaro M, Simoncini T, Tanganelli P, Fu C, Kislinger T, et al. Advanced glycation end products activate endothelium through signal-transduction receptor RAGE: a mechanism for amplification of inflammatory responses. Circulation 2002; 105:816–822.

42 Francis-Sedlak ME, Moya ML, Huang J-J, Lucas SA, Chandrasekharan N, Larson JC, Cheng M-H, et al. Collagen glycation alters neovascularization in vitro and in vivo. Microvasc Res 2010; 80:3–9.

43 Brett J, Schmidt AM, Yan SD, Zou YS, Weidman E, Pinsky D, Nowygrod R, et al. Survey of the distribution of a newly characterized receptor for advanced glycation end products in tissues. Am J Pathol 1993; 143:1699–1712.

44 Figueroa D, Kemeny S, Clyne A. Glycated Collagen Impairs Endothelial Cell Response to Cyclic Stretch. Cell Mol Bioeng 2011; 4:220–230.

45 Hirose A, Tanikawa T, Mori H, Okada Y, Tanaka Y. Advanced glycation end products increase endothelial permeability through the RAGE/Rho signaling pathway. FEBS Lett 2010; 584:61–6.

46 Ding Y, Kantarci A, Hasturk H, Trackman PC, Malabanan A, Van Dyke TE. Activation of RAGE induces elevated O2- generation by mononuclear phagocytes in diabetes. J Leukoc Biol 2007; 81:520–527.

47 Chen Y, Akirav EM, Chen W, Henegariu O, Moser B, Desai D, Shen JM, et al. RAGE ligation affects T cell activation and controls T cell differentiation. J Immunol 2008; 181:4272–8.

48 Basta G. Receptor for advanced glycation endproducts and atherosclerosis: From basic mechanisms to clinical implications. Atherosclerosis 2008; 196:9–21.

49 Liang C, Ren Y, Tan H, He Z, Jiang Q, Wu J, Zhen Y, et al. Rosiglitazone via upregulation of Akt/eNOS pathways attenuates dysfunction of endothelial progenitor cells, induced by advanced glycation end products. Br J Pharmacol 2009; 158:1865–73.

50 Matsui T, Takeuchi M, Yamagishi S. Nifedipine, a calcium channel blocker, inhibits inflammatory and fibrogenic gene expressions in advanced glycation end product (AGE)-exposed fibroblasts via mineralocorticoid receptor antagonistic activity. Biochem Biophys Res Commun 2010; 396:566–70.

51 Monnier VM, Kohn RR, Cerami A. Accelerated age-related browning of human collagen in diabetes mellitus. Proc Natl Acad Sci U S A 1984; 81:583–587.

52 Takahashi M, Kushida K, Ohishi T, Kawana K, Hoshino H, Uchiyama A, Inoue T. Quantitative analysis of crosslinks pyridinoline and pentosidine in articular cartilage of patients with bone and joint disorders. Arthritis Rheum 1994; 37:724–728.

53 Forbes JM, Teo L, Yee L, Thallas V, Lassila M, Candido R, Jandeleit-Dahm KA, et al. Advanced Glycation End Product Interventions Reduce Diabetes-Accelerated Atherosclerosis. Diabetes 2004; 53:1813–1823.

54 Vitek MP, Bhattacharya K, Glendening JM, Stopa E, Vlassara H, Bucala R, Manogue K, et al. Advanced glycation end products contribute to amyloidosis in Alzheimer disease. Proc Natl Acad Sci U S A 1994; 91:4766–4770.

55 Stitt AW. The maillard reaction in eye diseases. Ann N Y Acad Sci 2005; 1043:582–597.

56 Carmeliet P, Collen D. Molecular basis of angiogenesis. Role of VEGF and VE-cadherin. Ann N Y Acad Sci 2000; 902:244–249.

57 Levental KR, Yu H, Kass L, Lakins JN, Egeblad M, Erler JT, Fong SF, et al. Matrix crosslinking forces tumor progression by enhancing integrin signaling. Cell 2009; 139:891–906.

58 Trédan O, Galmarini CM, Patel K, Tannock IF, Tredan O. Drug resistance and the solid tumor microenvironment. J Natl Cancer Inst 2007; 99:1441–1454.

59 Nelson CM, Bissell MJ. Of extracellular matrix, scaffolds, and signaling: tissue architecture regulates development, homeostasis, and cancer. Annu Rev Cell Dev Biol 2006; 22:287–309.

60 Ng MR, Brugge JS. A stiff blow from the stroma: collagen crosslinking drives tumor progression. Cancer Cell 2009; 16:455–457.

61 Schedin P, Keely PJ. Mammary gland ECM remodeling, stiffness, and mechanosignaling in normal development and tumor progression. Cold Spring Harb Perspect Biol 2010; 3:a003228.

62 Yu H, Mouw JK, Weaver VM. Forcing form and function: biomechanical regulation of tumor evolution. Trends Cell Biol 2010; 21:47–56.

63 Brown XQ, Bartolak-Suki E, Williams C, Walker ML, Weaver VM, Wong JY. Effect of substrate stiffness and PDGF on the behavior of vascular smooth muscle cells: Implications for atherosclerosis. Journal of Cellular Physiology 2010; 225:115–122.

64 Carmeliet P, Jain RK. Angiogenesis in cancer and other diseases. Nature 2000; 407:249–257.

65 Martin A, Komada MR, Sane DC. Abnormal angiogenesis in diabetes mellitus. Med Res Rev 2003; 23:117–145.

66 Van Heijst JWJ, Niessen HWM, Hoekman K, Schalkwijk CG. Advanced glycation end products in human cancer tissues: detection of Nepsilon-(carboxymethyl)lysine and argpyrimidine. Ann N Y Acad Sci 2005; 1043:725–33.

67 Takino J-I, Yamagishi S-I, Takeuchi M. Cancer malignancy is enhanced by glyceraldehyde-derived advanced glycation end-products. J Oncol 2010; 2010:739852.

CHAPTER 2

TUNING THREE-DIMENSIONAL COLLAGEN MATRIX STIFFNESS INDEPENDENTLY OF COLLAGEN CONCENTRATION MODULATES ENDOTHELIAL CELL BEHAVIOR

Published in *Acta Biomaterialia* [1].

2.1 Abstract

Numerous studies have described the effects of matrix stiffening on cell behavior using two-dimensional synthetic surfaces; however less is known about the effects of matrix stiffening on cells embedded in three-dimensional *in vivo*-like matrices. A primary limitation in investigating the effects of matrix stiffness in three dimensions is the lack of materials that can be tuned to control stiffness independently of matrix density. Here, we use collagen-based scaffolds where the mechanical properties are tuned using non-enzymatic glycation of the collagen in solution, prior to polymerization. Collagen solutions glycated prior to polymerization result in collagen gels with a three-fold increase in compressive modulus without significant changes to the collagen architecture. Using these scaffolds, we show that endothelial cell spreading increases with matrix stiffness, as does the number and length of angiogenic sprouts and the overall spheroid outgrowth. Differences in sprout length are maintained even when the receptor for advanced glycation endproducts is inhibited.

[1] Mason BN, Starchenko A, Williams RM, Bonassar LJ, Reinhart-King CA. Tuning three-dimensional matrix stiffness independently of collagen concentration modulateds endothelial cell behavior. Acta Biomater 2013; 9:4732-44.

Our results demonstrate the ability to de-couple matrix stiffness from matrix density and structure in collagen gels, and that increased matrix stiffness results in increased sprouting and outgrowth.

2.2 Introduction

The importance of the mechanical properties of the extracellular matrix (ECM) in mediating cell health and behavior is now well accepted. Changes in matrix stiffness have been shown to promote cardiovascular disease[1,2] and cancer[3,4] by altering cellular morphology[5], differentiation[6], traction force generation[7], focal adhesion formation[8], and cell migration dynamics[9]. Additionally, the mechanical properties of the ECM have been found to be crucial regulators of the formation and arrangement of multi-cellular assemblies during tissue formation[10–13]. However, most studies investigating the role of matrix stiffening on cell behavior have primarily used 2D synthetic surfaces. As such, significantly less is known about the effects of matrix stiffening on cells embedded in three-dimensional (3D) *in vivo*-like matrices. This gap in knowledge is largely due to the lack of materials with tunable mechanical properties that are amenable to 3D cell culture.

Recent efforts to modulate 3D matrix stiffness have included modifying matrix density of natural proteins[14–17] and alginate[18], using synthetic polymers with tunable cross-linking densities such as poly(ethylene) glycol (PEG) to create hydrogel scaffolds[19,20], and creating mixed matrices of natural proteins and other hydrogels such as agarose[16,21,22]. Although these modifications are capable of generating 3D scaffolds

with tunable mechanical properties, they also change the fundamental structural properties of the culture system. For example, increasing the density of the matrix also causes changes in the porosity of the scaffold and the number of binding sites presented to the cells. Synthetic PEG-hydrogels offer the advantage of allowing for specific binding sequences to be incorporated at a specified density, independent of stiffness; however, PEG-hydrogels are amorphous and lack the native fiber structures found within most tissues. Alginate offers the ability to modulate stiffness in 3D, but it does not allow for cell migration because cells are unable to remodel it[18]. Therefore, while a number of approaches have been developed to modulate the stiffness of 3D culture, they each face limitations.

To develop and characterize 3D mechanically tunable scaffolds, we used non-enzymatic glycation to stiffen naturally-derived collagen[23,24]. Non-enzymatic glycation is a process whereby proteins are cross-linked by reducing sugars such as glucose or ribose through a sequence of chemical modifications known as the Maillard reaction[25,26]. During non-enzymatic glycation, reducing sugars interact with amino groups on proteins to form Schiff bases that can rearrange into Amadori products[27]. These Amadori products subsequently form advanced glycation endproducts (AGE) that accumulate on proteins and cause cross-link formation. A number of studies have utilized non-enzymatic glycation to create stiffer collagen scaffolds with increased mechanical integrity by incubating polymerized collagen gels with reducing sugar solutions[28,29]. However, since an excess of sugars create a hyperosmotic extracellular environment, this technique has been limited to stiffening scaffolds prior to seeding

cells onto the surface of the gels and does not allow cells to be embedded within the ECM scaffold prior to gel polymerization. Notably, others have used collagen gels glycated with glucose-6-phosphate post-polymerization to investigate endothelial cell response[30]. However, the limitations of this system include the inability to examine sparse cellular cultures and unclear effects to the collagen architecture as a result of cell injection. By glycating the collagen prior to polymerization, we are able to observe immediate spreading and migration effects or single cells or multi-cellular aggregates without disruption of the collagen architecture.

In addition to the role of AGEs in modulating the mechanical properties of the extracellular environment, some cells possess receptors for advanced glycation endproducts (RAGE) that can influence intracellular signaling[31,32]. Interestingly, the engagement of these receptors on cells is thought to be a factor in a number of disease states including diabetes, atherosclerosis, Alzheimer's, cataracts, and cancer[33–37] and RAGE signaling has been shown to affect endothelial cell responses[38].

Here, we glycate the collagen prior to polymerization, which allows for cell encapsulation at the time of gelation[23,24]. Using this technique, cells can be embedded within collagen gels and the collagen density can be kept constant while mechanical stiffness is varied. We characterized the fiber structure of glycated collagen gels and show that there exists a regime where stiffness can be increased three-fold with only minimal changes in fiber architecture and no change in collagen density.

To investigate the effects of changes in 3D matrix stiffness on cell behavior, we embedded individual bovine aortic endothelial cells (ECs) or cellular spheroids in collagen of varying stiffness. Our data indicate that both individual cell spreading and the growth of angiogenic sprouts increase with matrix stiffness. We also found that even when the AGE/RAGE interaction is inhibited, spheroid outgrowth increases with the stiffness of the matrix. Together, our study describes a tractable method for modulating 3D matrix stiffness independently of collagen structure, and using these materials, we demonstrate that matrix stiffness in 3D plays a critical role in modulating endothelial cell behavior.

2.3 Materials and Methods

Cell Culture

EC Culture

Bovine aortic endothelial cells (ECs) were purchased from VEC Technologies (Rensselaer, NY) and used until passage 12 as described previously[11]. Briefly, cells were fed every other day and grown to confluence at 37°C and 5% CO_2 in Medium 199 (Invitrogen, Carlsbad, CA) supplemented with 10% Fetal Clone III (HyClone, Logan, UT) and 1% each of MEM Amino Acids (Invitrogen), MEM Vitamins (Medtech, Manassas, VA), and penicillin-streptomycin (Invitrogen).

Spheroid Generation

ECs were suspended in complete Medium 199 supplemented with 0.25% Methocult (StemCell Technologies, Vancouver, BC, Canada) and seeded at 10,000 cells/well in

non-adherent 96-well round bottom plates (Costar, Corning Incorporated, Corning, NY). Plates were centrifuged to pellet the cells and placed on an orbital shaker at 37°C and 5% CO_2 for 2 hours to facilitate spheroid formation. EC spheroids were cultured for 2 days in the plates prior to embedding within collagen gels to allow for spheroid compaction.

Preparation of Collagen Gels

Isolation and Non-enzymatic Glycation of Collagen

Type I collagen was isolated from rat tail tendons (Pel-Freeze Biologicals, Rogers, AR) and extracted in 0.1% sterile acetic acid (JT Baker, Phillipsburg, NJ) at 4°C. The resulting solution was centrifuged to remove solids and the supernatant was lyophilized and then solubilized in 0.1% sterile acetic acid to form 10 mg/mL stock solutions. As described previously, collagen stock solutions were mixed with 0.5 M ribose to form glycated collagen solutions containing a final concentration of 0, 50, 100, 150, 200, or 250 mM ribose in 0.1% sterile acetic acid and incubated at 4°C for 5 days[23,24]. Glycated collagen solutions were neutralized with 1 M sodium hydroxide in 10X D-PBS buffer and mixed with HEPES (EMD Millipore, Billerica, MA) and sodium bicarbonate (JT Baker) in 10X D-PBS (Invitrogen) to form 1.5 mg/mL collagen gels with final concentrations of 1X D-PBS, 25 mM HEPES, and 44 mM sodium bicarbonate.

Fluorescent Labeling of Collagen

Collagen was labeled with tetramethylrhodamine isothicyanate (TRITC) (Invitrogen)

as described previously[39,40]. Briefly, lyophilized collagen was mixed with 0.1 M, pH 9 sodium bicarbonate (JT Baker) to achieve a final collagen concentration of 10 mg/ml. TRITC in DMSO was then added at a 1:30 dilution to the collagen and allowed to react in the dark for 24 hours at 4^{O}C. The labeled collagen solution was then dialyzed extensively against 0.1% sterile acetic acid using dialysis tubing with a 20,000 MW cutoff (Spectrum Laboratories, Inc., Rancho Dominguez, CA).

Cell and Spheroid Embedding

Isolated cells or spheroids were mixed with neutralized collagen solutions. Collagen gels were allowed to polymerize at 37°C and then overlaid with complete medium. Medium was changed at 1 hour and then every other day during experiments. When investigating the effects of the receptors for advanced glycation endproducts (RAGE) on spheroid outgrowth, a polyclonal anti-RAGE antibody (N-16, Santa Cruz Biotechnology, Inc., Santa Cruz, CA) was added to spheroids to inhibit the interaction of RAGE with AGE. The anti-RAGE antibody was at added at 10 ug/ml in complete medium to embedded spheroids after the spheroids had been incubated for a 1 hour with complete medium. Spheroids treated with the anti-RAGE antibody were monitored over the course of for 2 days for extension outgrowth[41–45]. In cases where isolated cells were not suspended within the gel, an equivalent volume of complete medium was added to the gel to maintain gel composition between experiments.

Collagen Polymerization Assay

The polymerization of collagen gels at 37°C was monitored by measuring the

absorbance of the collagen solutions every 3 minutes at 500 nm using a Synergy HT microplate reader (BioTek, Winooski, VT). Polymerization curves were fit with a variable slope sigmoidal dose-response curve and the slope of linear portion of the curve was reported as the fibril formation rate (GraphPad Prism, GraphPad Software, Inc, La Jolla, CA).

Mechanical Testing of Collagen Gels

The equilibrium compressive modulus of collagen gels was quantified as described previously[24]. Briefly, an Enduratec EL2100 frame (Bose, Eden Prairie, MN) with a 250-g load cell was used to measure the resultant forces of 75 micron displacements on 6 mm x 1.5 mm collagen gels in a confined compression chamber. A standard linear solid model of viscoelastic behavior was used to fit the stress relaxation data by using the equation, $\sigma_{eq} = A\,(1 - e^{-t/\tau}) + B$, where B is the instantaneous stress and $A + B$ is the equilibrium stress, t is time, and τ is the exponential time constant[24,39]. The equilibrium modulus was calculated as the slope of the linear region of the stress-strain curve. Similarly to other studies of collagen gel mechanical properties, we assumed that the collagen gels were isotropic and elastic[39,46].

Cellular Proliferation Assay

ECs were suspended at 250,000 cells/ml of collagen and cultured for up to 3 weeks. Collagen gels were collected at 0, 1, 2, 3 weeks and frozen at -20°C. The gels were digested for 14 hours at 60°C with papain and the DNA content of the gels was quantified with a Quant-iT PicoGreen dsDNA Kit (Invitrogen) using a Synergy HT

microplate reader (BioTek). Total DNA content per gel were normalized to DNA content at day 0 for each experiment and then experiments were averaged (N=3).

Imaging

Confocal Reflectance Collagen Imaging

The internal structure of collagen gels was visualized with confocal reflectance microscopy using a Zeiss LSM700 inverted laser scanning confocal microscope (Carl Zeiss, Oberkochen, Germany). Samples were illuminated with a 405 nm laser and optical slices 1 micron in depth were collected with a long working distance water-immersion C-Apochromat 40×/1.1 NA objective (Carl Zeiss)[47]. Image acquisition parameters were kept the same for all gels.

Image Autocorrelation Analysis

To compare the structural properties of the collagen gels, an autocorrelation analysis was performed on the confocal reflectance microscopy images[48,49]. Briefly, each image was translated with respect to itself in all directions (2D) and the average length of intensity correlation between the images was measured. The decay in the correlation between the images was used to determine the mean characteristic length of features (collagen fibers) within the image. The mean characteristic lengths were plotted for each image and coincide with the mean fibril length, the average fibril distribution and the extent of bundling within the collagen gel.

Single Cell and Spheroid Imaging and Analysis

Isolated cells were imaged on a Zeiss CSU-X1 (Carl Zeiss) spinning disc confocal and each z-stack was projected onto a single plane using the ImageJ maximum intensity feature (ImageJ 1.44p, NIH). The resulting 2D cellular images were used to quantify projected cell areas and perimeters (n = 138-148)[50–52]. Multi-cellular spheroids were imaged with brightfield on a Zeiss Axio Observer Z1m (Carl Zeiss) and with fluorescence on a Zeiss LSM700 point scanning confocal. Brightfield images of spheroids after 1 day in culture were compared to images of the spheroids at the time of embedding and analyzed for the number and length of extensions emanating from the spheroids (n = 18-23). Additionally, brightfield images were used to quantify the area of both control spheroids (n = 17-18) and spheroids treated with anti-RAGE antibody (n=16-23) over time. Control data sets of spheroid outgrowth were collected independently.

Staining

Cells within collagen gels were fixed with 3.7% (v/v) formaldehyde in PBS, permeabilized with 1% (v/v) Triton (JT Baker) in PBS, and stained for actin with Alexa Fluor 488 phalloidin (Invitrogen) in PBS/1% (w/v) bovine serum albumin (BSA, Sigma-Aldrich, St. Louis, MO) and for DNA with DAPI (Sigma-Aldrich) in purified deionized water.

Statistics

Data were analyzed using a one-way analysis of variance (ANOVA) and Tukey's

Honest Significant Difference test in JMP (SAS, v.8.0 and v.9.0) with statistical significance considered as $p<0.05$. All values are expressed as the mean ± SEM.

2.4 Results

Non-enzymatic Glycation Affects Collagen Gel Mechanical and Structural Properties

The mechanical properties of collagen gels were modulated by incubating un-polymerized collagen solutions with 0 – 250 mM ribose for 5 days prior to collagen neutralization and polymerization. The equilibrium compressive modulus was measured by applying a 5% stepwise strain to a confined collagen gel, measuring the resultant force, and fitting the data to a standard linear solid model of viscoelastic behavior. Collagen gels polymerized after non-enzymatic glycation have an increased equilibrium compressive modulus that varies approximately linearly with ribose concentration (Figure 2.1). Over the range of ribose concentrations tested, the

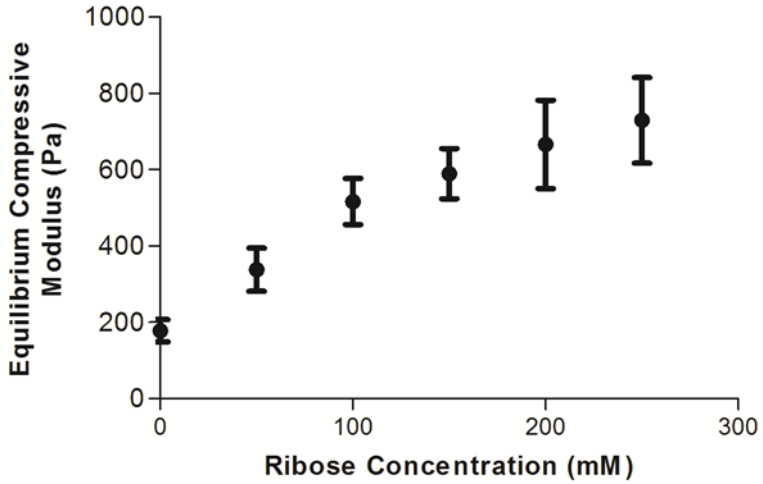

Figure 2.1. Collagen gel mechanical properties. The equilibrium compressive moduli of 1.5 mg/mL collagen gels were measured by confined compression testing. Data presented as mean ± SEM

compressive modulus of the collagen gels increased approximately four-fold (from ~175 Pa to ~730 Pa).

To investigate the effects of non-enzymatic glycation on collagen gel fiber architecture, the gels were imaged with confocal reflectance and fluorescence microscopy. Collagen solutions glycated with 0 – 100 mM ribose form gels that have qualitatively similar fiber distributions and arrangements; whereas collagen solutions treated with 150 – 250 mM ribose form gels with larger, more prominent collagen fibers when imaged either confocal reflectance (Figure 2.2a) or fluorescence microscopy (Figure 2.3). To further characterize the fiber architecture of the glycated collagen gels, an image autocorrelation analysis was performed. The autocorrelation mean radius is a measure of the size over which fibril structures persist in the image. The autocorrelation data indicated that collagen gels treated with 0 – 100 mM ribose have similar fibril sizes and arrangements, while higher ribose concentrations generate populations of larger fibrils in confocal reflectance images (Figure 2.2b).

Because differences in fiber structure have been shown previously to be correlated with differences in polymerization dynamics[53,54], the effects of non-enzymatic glycation on collagen gel polymerization dynamics were investigated with an absorbance assay. During polymerization, collagen fibril formation causes an increase in opacity that can be directly measured by absorbance. Collagen polymerization dynamics can generally be described by three stages and correspond to a sigmoidal curve that are observed with the absorbance assay: the nucleation phase is denoted by

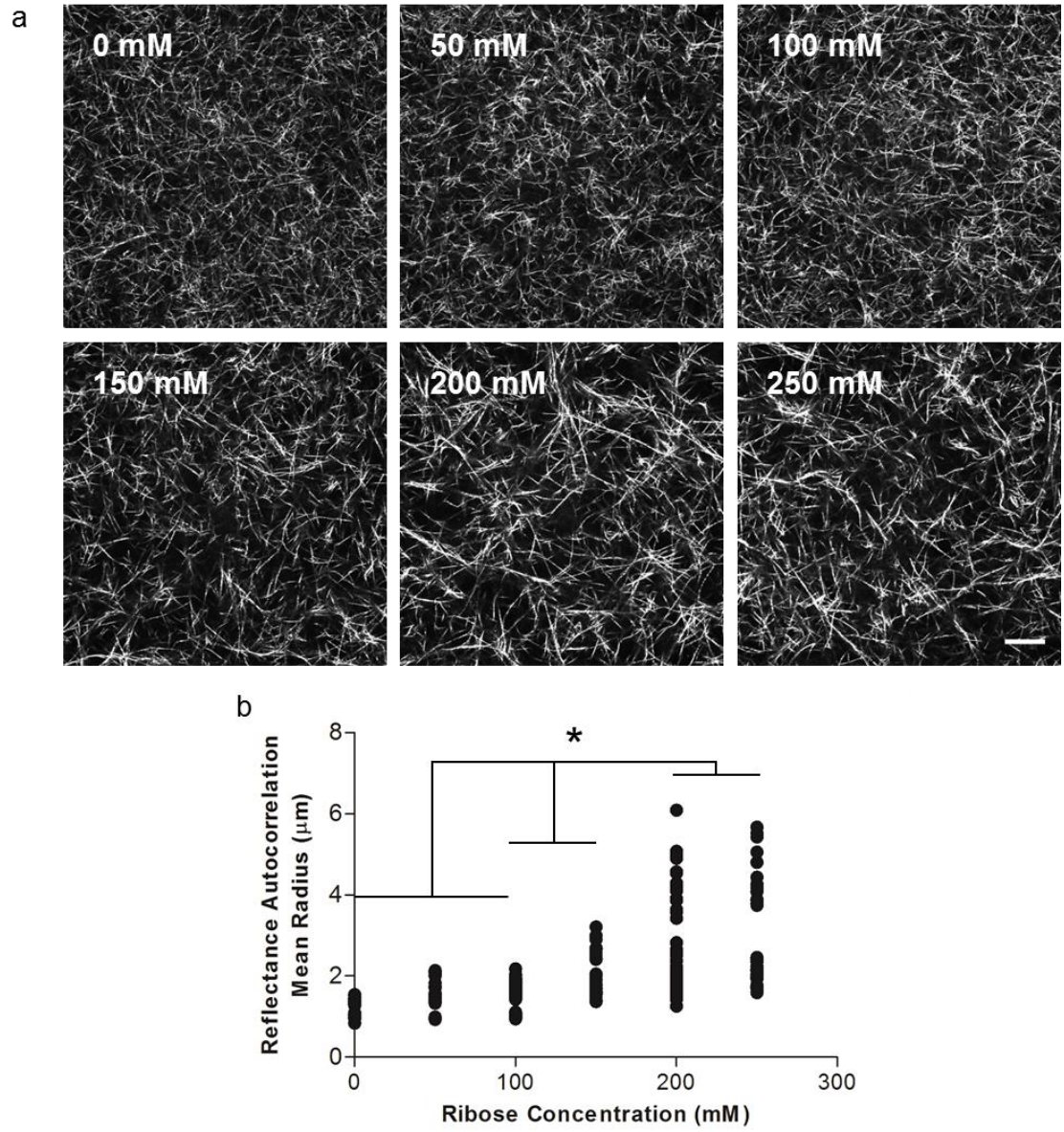

Figure 2.2 The effects of non-enzymatic glycation of collagen fibril arrangement. (a) Confocal reflectance microscopy was used to image the collagen gels formed from solutions that had been incubated with 0, 50, 100, 150, 200, or 250 mM ribose. (b) Collagen fiber organizations were compared using the image autocorrelation mean radius. Scale is 20 μm.

the toe region of the curve, the fibril formation phase is denoted by the linearly increasing portion of the curve, and the fibril stabilization phase is denoted by the plateau region of the curve. Non-enzymatic glycation increased the nucleation time of

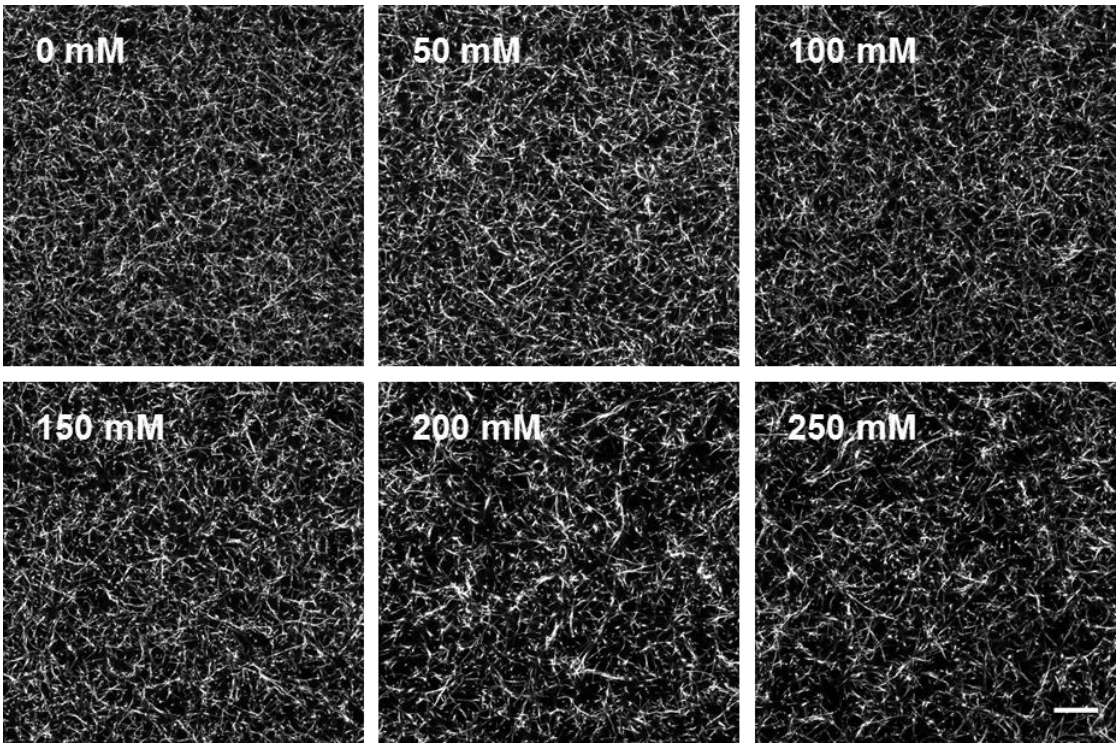

Figure 2.3. The effects of non-enzymatic glycation of fluorescently labeled collagen fibril arrangement. TRITC-labeled collagen was incubated with 0, 50, 100, 150, 200, or 250 mM ribose and imaged with fluorescence microscopy. Scale is 20 μm.

collagen fibril formation (Figure 2.4a). Notably, the rate of fibril formation showed a comparable trend to the autocorrelation data and was very similar for collagen incubated with 0 – 100 mM ribose and was significantly altered for collagen solutions that had been treated with 150 – 250 mM ribose (Figure 2.4b). These results indicate that the extent of glycation can alter the polymerization dynamics of collagen gels.

Endothelial Cell Viability and Proliferation in Glycated Collagen Gels

To evaluate the effect of collagen glycation on cell proliferation, ECs were embedded within collagen gels, and DNA content was quantified at 0, 7, 14, and 21 days. ECs

a

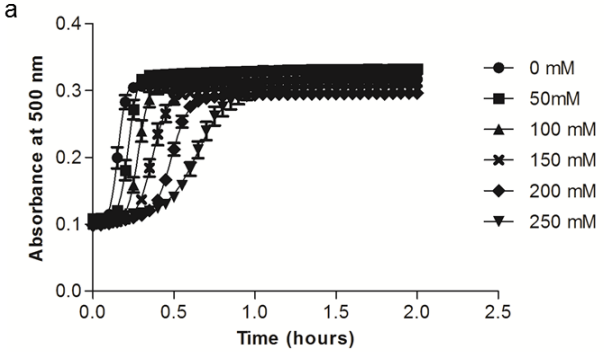

b

Ribose Concentration	95% Confidence Intervals of Fibril Formation Rate
0 mM	14.17 - 21.95
50 mM	12.77 - 18.07
100 mM	10.53 - 16.18
150 mM	7.338 - 10.49 ‡
200 mM	7.042 - 8.797 ‡
250 mM	3.631 - 4.835 ‡

‡ indicates $p < 0.05$ when compared to 0 mM condition

Figure 2.4. The effects of non-enzymatic glycation on the polymerization dynamics of collagen. (a) Collagen polymerization dynamics were measured as a function of ribose concentration based on absorbance readings at 500 nm during polymerization. (b) The fibril formation rates of glycated collagen polymerization were found by fitting a sigmoidal curve to the polymerization data in (a) and reporting the slope of the linear section of the curve. Data presented as mean ± SEM.

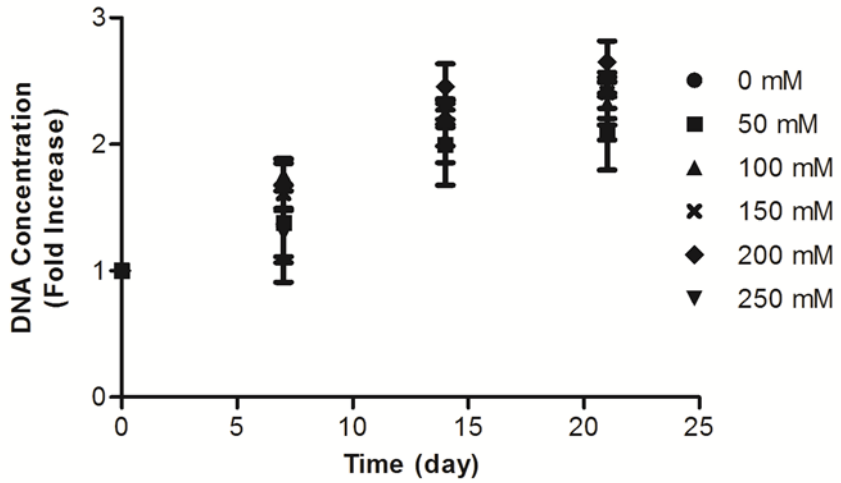

Figure 2.5. Endothelial cell proliferation within glycated collagen gels. ECs were embedded within collagen gels that had been glycated with 0, 50, 100, 150, 200, or 250 mM ribose. Cellular viability and proliferation was assessed by measuring the DNA content of gels at 0, 7, or 21 days. Data presented as mean ± SEM.

remained viable and proliferated at similar levels within glycated collagen gels and controls during the 3 week proliferation assay (Figure 2.5). These results indicate that

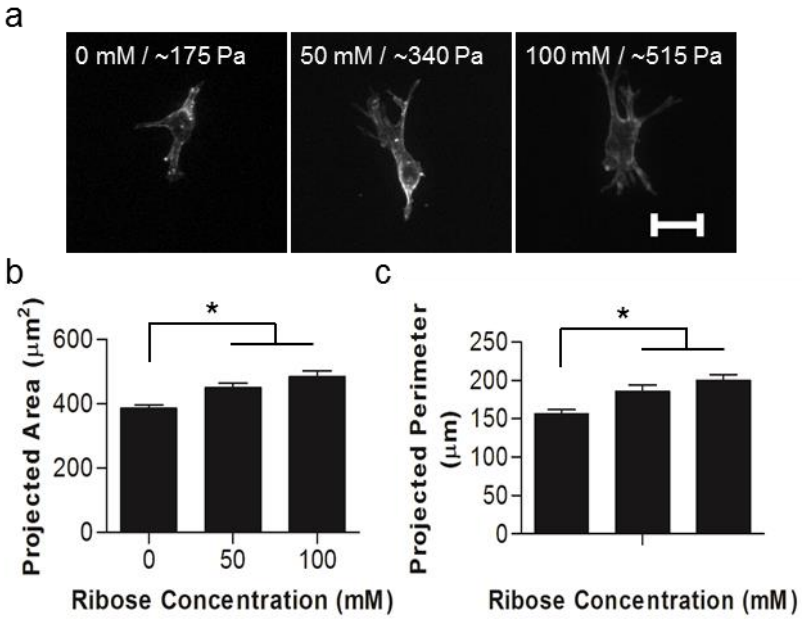

Figure 2.6. Single cell response to matrix stiffness. Isolated ECs were embedded within collagen gels formed from solutions that had been incubated with 0, 50, or 100 mM ribose. Cells were allowed to spread for 24 h and then were fixed and stained for actin. (a) ECs were imaged using confocal microscopy and the projected cell (b) area and (c) perimeter were determined. Data presented as mean ± SEM, * indicates $p < 0.05$, Scale is 20 μm.

collagen glycation prior to gel polymerization does not alter EC proliferative potential and that the cells remain viable within the gel.

Changes in 3D Matrix Stiffness Increase Cell Spreading

Studies using 2D planar substrates have reported that increased matrix stiffness results in increased cell spreading[55]. To assess whether modulating collagen stiffness independently of collagen organization caused cellular morphological changes in 3D matrices, ECs were embedded within collagen gels that had been glycated with 0 – 100 mM ribose and imaged with confocal microscopy. Ribose concentrations ranging from 0 – 100 mM were chosen because our data indicate that the structure of the

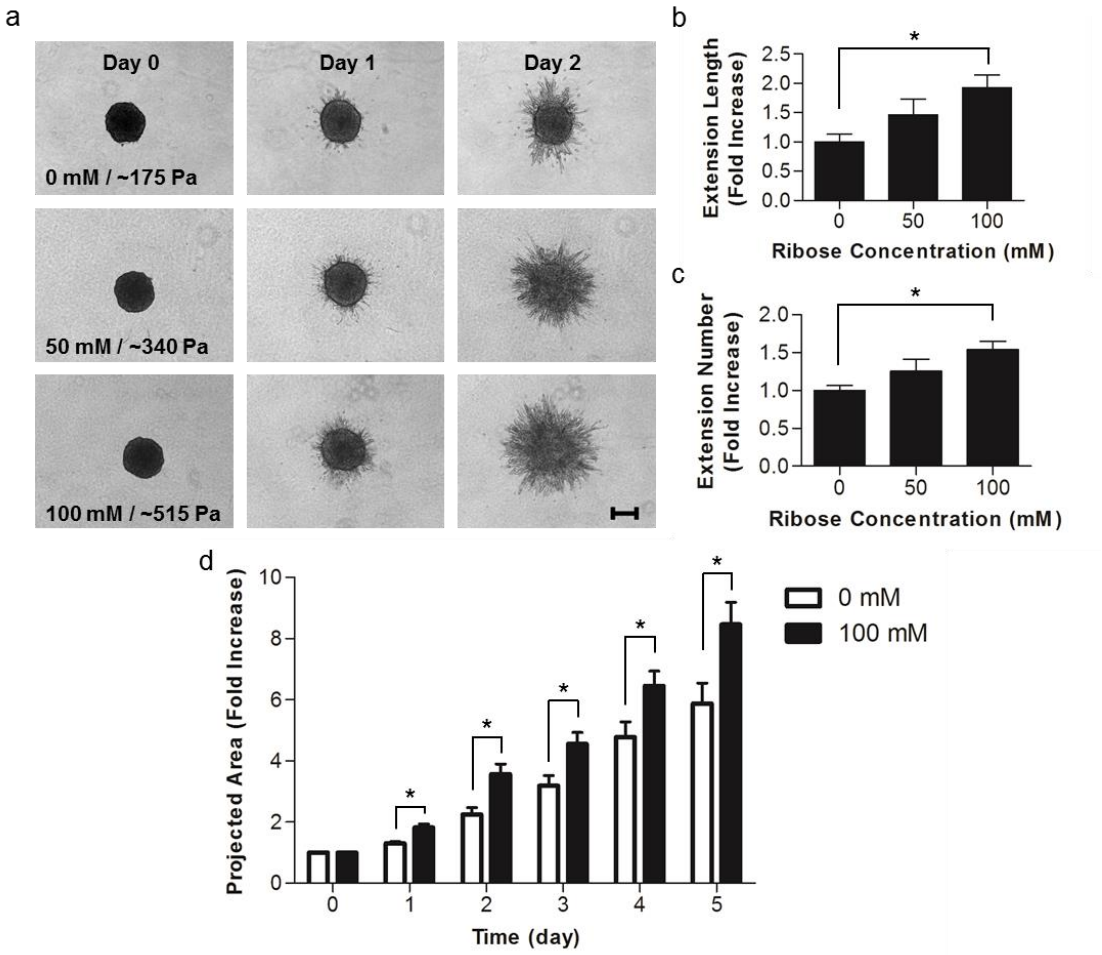

Figure 2.7. Angiogenic outgrowth response to matrix stiffness. Multicellular spheroids were embedded within collagen polymerized from solutions treated with 0, 50, or 100 mM ribose. (a) Spheroids were imaged using bright-field microscopy at 0, 1, and 2 days after embedding. (b) The total length of extensions and (c) the average number of extensions per spheroid were measured at day 1. (d) The projected spheroid area, including the extensions, was measured over the course of 5 days. Data presented as mean + SEM, * indicates $p < 0.05$, Scale is 200 μm.

collagen is only minimally altered (Figure 2.2 and Figure 2.3) while the compressive modulus increases from ~175 to ~515 Pa (Figure 2.1). ECs appeared well-spread with an elongated morphology and displayed defined actin fibrils in each stiffness condition studied (Figure 2.6a). Interestingly, EC projected area and perimeter were both significantly increased as a function of matrix stiffness (Figure 2.6b-c), indicating that

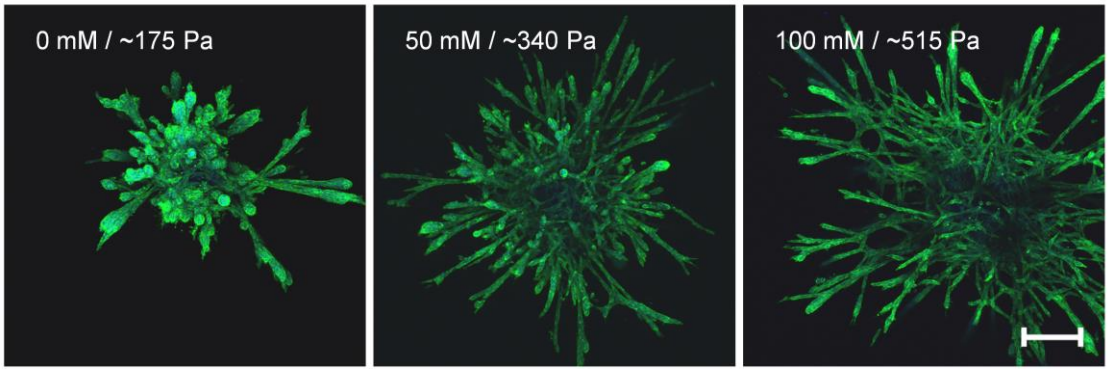

Figure 2.8. Long-term angiogenic outgrowth response to matrix stiffness. Multicellular spheroids were grown in collagen gels polymerized from solutions treated with 0, 50, or 100 mM ribose for 8 days. Spheroids were fixed and stained for actin and DAPI and imaged using confocal microscopy. Scale is 200μm.

stiffness is a mediator of cell spreading in 3D matrices.

Increased Matrix Stiffness Enhances Spheroid Outgrowth

Our lab has previously shown that endothelial cell network formation can be modulated by both matrix stiffness and ligand density in 2D[11]. To investigate whether endothelial sprouting is altered by collagen stiffness in 3D, EC spheroids were embedded within glycated collagen and the formation of sprouts from the spheroids was monitored over several days. Notably, increasing the stiffness of the collagen visibly altered the morphology of the outgrowths emanating from the spheroids (Figure 2.7a). While spheroids in all gels displayed a robust sprouting response, those cultured within the softer gels had fewer extensions that appeared to be less branched than the spheroids cultured within the stiffer, glycated gels. After only one day, spheroids within the stiffest collagen gels (100 mM ribose), had a two-fold increase in the total extension length per spheroid and a 1.5-fold increase in the average number of extensions per spheroids when compared to spheroids cultured within the soft

collagen gels (0 mM ribose) (Figure 2.7b-c). Additionally, spheroids in the stiffest collagen gels (100 mM ribose) had a significantly larger projected area during the entire 5 day analysis period than those in soft gels (0 mM ribose) (Figure 2.7d). These data indicate that 3D matrix stiffness altered endothelial sprouting dynamics. To determine if the differences in extension morphology persisted in long-term spheroid culture, EC spheroids were embedded and grown for 8 days. The resulting sprouts were stained for actin and DAPI and imaged using confocal microscopy (Figure 2.8). The morphology of spheroid outgrowth remained altered dependent upon collagen stiffness. To investigate the effects of AGE/RAGE signaling relative to stiffness on spheroid outgrowth, RAGE were inhibited with an anti-RAGE blocking antibody[41]. Notably, although the overall spheroid outgrowth was decreased with anti-RAGE treatment when compared to controls, the EC spheroid outgrowth remained significantly increased in the stiffer collagen gels at day 2 (Figure 2.9).

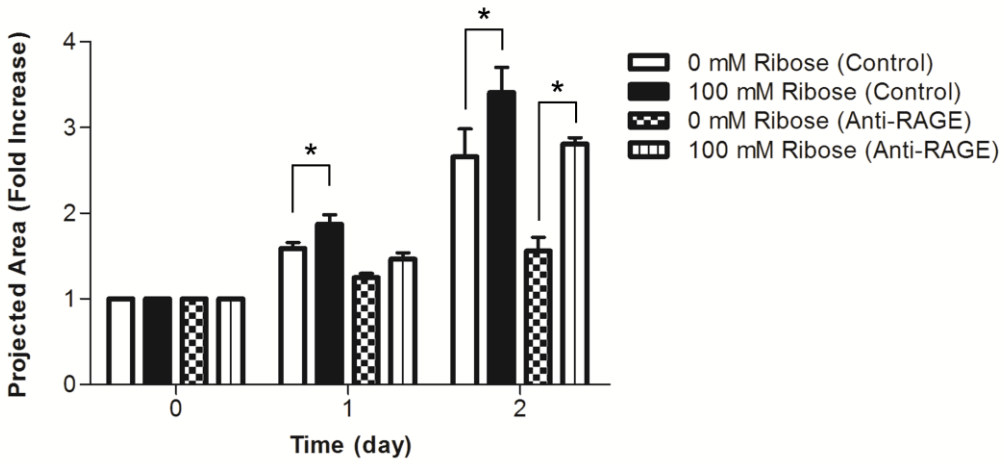

Figure 2.9. The effects of RAGE inhibition on spheroid outgrowth. Multicellular spheroids were embedded within collagen polymerized from solutions treated with 0 or 100 mM ribose and fed at 1 h with either complete media with or without 10 ug ml^{-1} anti-RAGE blocking antibody. (a) The projected spheroid areas were measured at days 0, 1 and 2 after embedding. Data presented as mean + SEM, * indicates $p < 0.05$.

2.5 Discussion

While numerous studies have investigated the role of matrix stiffness in mediating cell behavior on 2D substrates, much less is known about cell response to matrix stiffness in 3D matrices. Here, we describe and characterize a method to modulate the 3D stiffness of native, fibrillar collagen matrices while only minimally altering the inherent fiber structure, without the addition of synthetic materials. Using non-enzymatic glycation, collagen gel stiffness can be increased three-fold while only minimally changing the fiber architecture. Further, the method described permits isolated cells or multi-cellular spheroids to be embedded within the glycated collagen gels during polymerization so that the resulting cellular response to 3D stiffness can be studied. Our data indicate that increasing the collagen gel modulus from ~175 Pa to ~515 Pa caused changes in cell spreading and dramatic differences in the morphology of endothelial sprouts from spheroids. These results demonstrate the utility non-enzymatic glycation to alter 3D matrix mechanics with minimal changes in collagen fibril organization so that cell response to 3D changes in matrix stiffness can be studied.

Methods to glycate collagen have been explored previously in the literature. Several reports have described methods to glycate collagen gels once they have been polymerized[28,29] or to adsorb glycated collagen to glass or plastic[56]. However, neither of these methods allow for cells to be embedded within the collagen. Other studies have reported glycating collagen gels prior to polymerization[23,24,57], however it was

not clear what effect the process of glycation was having on the fiber architecture. Because fiber architecture is known to alter cell behavior[58], it is important to develop scaffolds where it is possible to control stiffness without altering fiber diameter or distribution. Here, we identify a range of ribose concentrations where stiffness can be increased with minimal changes to fiber architecture. Our data show that collagen glycated with 0 – 100 mM ribose exhibits a compressive modulus that varies over three fold (~175 Pa to ~515 Pa) (Figure 2.1) without significant changes to the fibril formation rates or fiber arrangements. At higher concentrations of ribose (150 – 250 mM), the compressive modulus of the gels increases, but a change in the fibril length scale (Figure 2.2 and Figure 2.3) and a decrease in the rate of gel polymerization (Figure 2.4) also occur. Therefore, while glycation can tune the moduli of collagen by four-fold, the changes in modulus that can be controlled while not producing statistically significant changes in fiber architecture fall within a narrower range. It is important to note that ligand availability and pore size can also affect cell behavior, although we did not directly test for these parameters.

Notably, the changes in fiber architecture due to glycation (Figure 2.2 and Figure 2.3) coincide with changes in the polymerization dynamics (Figure 2.4) of collagen treated with varying concentrations of ribose. Polymerization rate has been shown to be affected by a number of other parameters as well, including pH[59], temperature[60,61], and the presence of ions[62], where pore structure and fiber length and diameter are also altered. These results suggest that the polymerization rate of the collagen gels may be responsible for the changes in the fiber architecture we observe for collagen incubated

with high concentrations of ribose. Further modulation of the polymerization kinetics using temperature or pH may allow for the formation of highly glycated collagen gels that resemble the architecture of gels glycated with 0 – 100 mM ribose.

While stiffness has been shown to modulate numerous cellular behaviors, these reports are largely based on studies using 2D substrates. It is not clear how results based on the use of 2D substrates translate into behaviors in three dimensions. In previous work, we showed that changes in substrate stiffness resulted in changes in cell spreading[55]. Our data using 3D glycated gels indicate that, similar to our results obtained in 2D cultures, endothelial cells increase their spreading due to increased matrix stiffness. Unlike many studies using 2D substrates, we find no change in endothelial cell proliferation rates in 3D due to stiffness (Figure 2.5). These results may be attributed to the complex relationship of cell division with spreading and matrix deposition, degradation, and remodeling in 3D matrices[63,64]. However, just as cell response to matrix stiffness on 2D substrates has been found to be cell-type specific[5], it is likely that cell response in 3D matrices is also cell-type specific and should be further investigated.

In our study, we observed a significant increase in cellular spreading and extension formation with increasing matrix stiffness almost immediately (within 24 hours) after the individual cells and multi-cellular spheroids were embedded (Figure 2.6 and Figure 2.7) and these effects persisted throughout the entire course of our culture (8 days) (Figure 2.8). Interestingly, work by Francis-Sedlak et al. reported a transient

and opposite response to matrix stiffness when human umbilical vein endothelial cell aggregates were injected into gels glycated with glucose-6-phospate post-polymerization[30]. A number of differences in experimental design could attribute for these discrepancies including the density of the collagen matrices, cell type, or methods of glycation and cellular embedding. Additionally, collagen glycation has been shown to decrease adherent cell adhesion and mechanotransduction by modifying integrin binding sites[56,65–67]. Interestingly, we found that spheroids and isolated cells within the stiffer, glycated matrices have increased extension outgrowth and spreading when compared to those in non-glycated matrices (Figures 2.6 and 2.8). While we did not directly investigate cell adhesion in our study, our findings suggest that endothelial cells within glycated matrices integrate mechanical cues and increase their spreading, even if cell adhesion is disrupted when compared to the non-glycated matrices. Others have also shown that increasing the amount of non-enzymatic glycation cross-linking decreases the degradability of matrices[30,68,69]. It is notable that we saw the most spheroid outgrowth in the stiffest, least degradable and least adhesive collagen matrices (Figure 2.7). Future studies should elucidate whether our results are universal responses for all endothelial cell sources or specific to bovine aortic endothelial cells and further experiments should be performed to determine the relative effects of matrix density, glycation, and matrix degradation on cell outgrowth and function in collagen matrices.

In vivo, the cross-linking of matrix proteins via non-enzymatic glycation is a slow process that occurs naturally, resulting in AGE cross-links that cause tissue stiffening

with age. Cross-link accumulation is accelerated in diseases where blood sugar levels are not well-regulated such as diabetes[68–70]. Glycation has the most profound effect on components within the body that have a low turnover rate, including collagen[70]. Tissues including the vasculature[71], bone[72], cornea[73], and skin[73] and diseases such as Alzheimer's[74], rheumatoid arthritis[75], and end stage renal disease[76] have all been associated with the formation of glycation cross-links. In this study we have shown that collagen gel stiffness alters spheroid outgrowth when the AGE/RAGE interaction is inhibited (Figure 2.9). Notably, spheroid outgrowth decreased in RAGE inhibited spheroids when compared to control spheroids in matrices of the same stiffness, suggesting that the presence of the AGE/RAGE interaction may play a role in promoting extension formation and outgrowth. The concentrations and experimental time points we chose were similar to other studies using anti-RAGE antibodies for blocking[41–45]; however, it is not clear if the antibody completely blocks the interaction between AGE/RAGE at the concentrations used. To determine the relative roles of chemical vs. mechanical changes due to glycation, additional experiments are required and are an interesting area of future work given the effects of glycation on many major tissues in the body. Better models using collagen glycation may not only enable a greater understanding of how matrix stiffness affects cells in three dimensions but also how glycation can promote disease.

In both solid tumor growth and diabetes, tissues tend to stiffen[72,77] and, in both disease states, angiogenesis is perturbed and vessels tend to be malformed and present abnormally[78,79]. Our results suggest that the stiffening of the matrix may be one

mechanism which causes changes in the quantity and organization of blood vessels. In our study, differences in the number of extensions per spheroids were measurable as early as one day after embedding (Figure 2.7) indicating that the cells were integrating the stiffness cues into their behavior in the early stages of extension formation. Notably, the morphological differences in the extensions with stiffness were maintained throughout the entire length of culture, indicating that matrix stiffness likely plays a key role in angiogenesis.

2.6 Conclusions

The study describes a tractable technique for modifying collagen stiffness independently of gel density and fiber structure. By glycating the collagen while in solution, we were able to embed cells within collagen matrices to examine the effects of 3D stiffness on individual- and multi-cellular behaviors. These changes in stiffness significantly altered endothelial cell morphology and 3D sprouting from spheroids, indicating that the 3D mechanical environment is an essential mediator of cellular response. In the future, non-enzymatic glycation could be used to study the effects of extracellular matrix stiffness on a range of cell types that have previously been shown to be influenced by changes in matrix stiffness in 2D systems such as neurons[4], stem cells[6], and vascular smooth muscle cells[2].

REFERENCES

1 Huynh J, Nishimura N, Rana K, Peloquin JM, Califano JP, Montague CR, King MR, et al. Age-related intimal stiffening enhances endothelial permeability and leukocyte transmigration. Sci Transl Med 2011; 3:112ra122.

2 Isenberg BC, Dimilla PA, Walker M, Kim S, Wong JY. Vascular smooth muscle cell durotaxis depends on substrate stiffness gradient strength. Biophys J 2009; 97:1313–1322.

3 Paszek MJ, Zahir N, Johnson KR, Lakins JN, Rozenberg GI, Gefen A, Reinhart-King CA, et al. Tensional homeostasis and the malignant phenotype. Cancer Cell 2005; 8:241–254.

4 Ulrich TA, de Juan Pardo EM, Kumar S. The mechanical rigidity of the extracellular matrix regulates the structure, motility, and proliferation of glioma cells. Cancer Res 2009; 69:4167–4174.

5 Yeung T, Georges PC, Flanagan LA, Marg B, Ortiz M, Funaki M, Zahir N, et al. Effects of substrate stiffness on cell morphology, cytoskeletal structure, and adhesion. Cell Motil Cytoskeleton 2005; 60:24–34.

6 Engler AJ, Sen S, Sweeney HL, Discher DE. Matrix elasticity directs stem cell lineage specification. Cell 2006; 126:677–689.

7 Reinhart-King CA, Dembo M, Hammer DA. Endothelial cell traction forces on RGD-derivatized polyacrylamide substrata. Langmuir 2003; 19:1573–1579.

8 Beningo KA, Dembo M, Kaverina I, Small J V, Wang YL. Nascent focal adhesions are responsible for the generation of strong propulsive forces in migrating fibroblasts. J Cell Biol 2001; 153:881–888.

9 Pelham Jr. RJ, Wang Y. Cell locomotion and focal adhesions are regulated by substrate flexibility. Proc Natl Acad Sci U S A 1997; 94:13661–13665.

10 Guo WH, Frey MT, Burnham NA, Wang YL. Substrate rigidity regulates the formation and maintenance of tissues. Biophys J 2006; 90:2213–2220.

11 Califano JP, Reinhart-King CA. A Balance of Substrate Mechanics and Matrix Chemistry Regulates Endothelial Cell Network Assembly. Cell Mol Bioeng 2008; 1:122–132.

12 Reinhart-King CA, Dembo M, Hammer DA. Cell-Cell Mechanical Communication through Compliant Substrates. Biophys J 2008; 95:6044–6051.

13 Shebanova O, Hammer DA. Biochemical and Mechanical Extracellular Matrix Properties Dictate Mammary Epithelial Cell Assembly. Biotechnol J 2011; doi:10.1002/biot.201100188.

14 Kniazeva E, Putnam AJ. Endothelial cell traction and ECM density influence both capillary morphogenesis and maintenance in 3-D. Am J Physiol Cell Physiol 2009; 297:C179–87.

15 Shamloo A, Heilshorn SC. Matrix density mediates polarization and lumen formation of endothelial sprouts in VEGF gradients. Lab Chip 2010; 10:3061–3068.

16 Rao RR, Peterson AW, Ceccarelli J, Putnam AJ, Stegemann JP. Matrix composition regulates three-dimensional network formation by endothelial cells and mesenchymal stem cells in collagen/fibrin materials. Angiogenesis 2012; 15:253–264.

17 Sieminski AL, Hebbel RP, Gooch KJ. The relative magnitudes of endothelial force generation and matrix stiffness modulate capillary morphogenesis in vitro. Exp Cell Res 2004; 297:574–584.

18 Genes NG, Rowley JA, Mooney DJ, Bonassar LJ. Effect of substrate mechanics on chondrocyte adhesion to modified alginate surfaces. Arch Biochem Biophys 2004; 422:161–167.

19 Kraehenbuehl TP, Zammaretti P, Van Der Vlies AJ, Schoenmakers RG, Lutolf MP, Jaconi ME, Hubbell JA. Three-dimensional extracellular matrix-directed cardioprogenitor differentiation: systematic modulation of a synthetic cell-responsive PEG-hydrogel. Biomaterials 2008; 29:2757–2766.

20 Straley KS, Heilshorn SC. Independent tuning of multiple biomaterial properties using protein engineering. Soft Matter 2009; 5:114.

21 Ulrich T a, Jain A, Tanner K, MacKay JL, Kumar S. Probing cellular mechanobiology in three-dimensional culture with collagen-agarose matrices. Biomaterials 2010; 31:1875–1884.

22 Ulrich TA, Lee TG, Shon HK, Moon DW, Kumar S. Microscale mechanisms of agarose-induced disruption of collagen remodeling. Biomaterials 2011; 32:5633–5642.

23 Roy R, Boskey AL, Bonassar LJ. Non-enzymatic glycation of chondrocyte-seeded collagen gels for cartilage tissue engineering. J Orthop Res 2008; 26:1434–1439.

24 Roy R, Boskey A, Bonassar LJ. Processing of type I collagen gels using nonenzymatic glycation. J Biomed Mater Res A 2010; 93A:843–851.

25 Ulrich P, Cerami A. Protein glycation, diabetes, and aging. Recent Prog Horm Res 2001; 56:1–21.

26 Maillard LC. Action des acides amines sur les sucres: formation des melanoides par voie methodique. Comptes Rendus de l'Academie des Sciences 1912; 154:66–68.

27 Hodge JE. The Amadori rearrangement. Adv Carbohydr Chem 1955; 10:169–205.

28 Girton TS, Oegema TR, Tranquillo RT. Exploiting glycation to stiffen and strengthen tissue equivalents for tissue engineering. J Biomed Mater Res 1999; 46:87–92.

29 Francis-Sedlak ME, Uriel S, Larson JC, Greisler HP, Venerus DC, Brey EM. Characterization of type I collagen gels modified by glycation. Biomaterials 2009; 30:1851–1856.

30 Francis-Sedlak ME, Moya ML, Huang J-J, Lucas SA, Chandrasekharan N, Larson JC, Cheng M-H, et al. Collagen glycation alters neovascularization in vitro and in vivo. Microvasc Res 2010; 80:3–9.

31 Basta G, Lazzerini G, Massaro M, Simoncini T, Tanganelli P, Fu C, Kislinger T, et al. Advanced glycation end products activate endothelium through signal-transduction receptor RAGE: a mechanism for amplification of inflammatory responses. Circulation 2002; 105:816–822.

32 Brett J, Schmidt AM, Yan SD, Zou YS, Weidman E, Pinsky D, Nowygrod R, et al. Survey of the distribution of a newly characterized receptor for advanced glycation end products in tissues. Am J Pathol 1993; 143:1699–1712.

33 Thomas MC, Baynes JW, Thorpe SR, Cooper ME. The role of AGEs and AGE inhibitors in diabetic cardiovascular disease. Curr Drug Targets 2005; 6:453–474.

34 Reddy VP, Obrenovich ME, Atwood CS, Perry G, Smith MA. Involvement of Maillard reactions in Alzheimer disease. Neurotox Res 2002; 4:191–209.

35 Taguchi A, Blood DC, del Toro G, Canet A, Lee DC, Qu W, Tanji N, et al. Blockade of RAGE-amphoterin signalling suppresses tumour growth and metastases. Nature 2000; 405:354–360.

36 Stitt AW. The maillard reaction in eye diseases. Ann N Y Acad Sci 2005; 1043:582–597.

37 Reaven P, Merat S, Casanada F, Sutphin M, Palinski W. Effect of streptozotocin-induced hyperglycemia on lipid profiles, formation of advanced

glycation endproducts in lesions, and extent of atherosclerosis in LDL receptor-deficient mice. Arterioscler Thromb Vasc Biol 1997; 17:2250–2256.

38 Tezuka M, Koyama N, Morisaki N, Saito Y, Yoshida S, Araki N, Horiuchi S. Angiogenic effects of advanced glycation end products of the Maillard reaction on cultured human umbilical cord vein endothelial cells. Biochem Biophys Res Commun 1993; 193:674–680.

39 Cross VL, Zheng Y, Won Choi N, Verbridge SS, Sutermaster BA, Bonassar LJ, Fischbach C, et al. Dense type I collagen matrices that support cellular remodeling and microfabrication for studies of tumor angiogenesis and vasculogenesis in vitro. Biomaterials 2010; 31:8596–8607.

40 Hermanson GT. Bioconjugate techniques. New York: Academic Press 1996.

41 Ding Y, Kantarci A, Hasturk H, Trackman PC, Malabanan A, Van Dyke TE. Activation of RAGE induces elevated O2- generation by mononuclear phagocytes in diabetes. J Leukoc Biol 2007; 81:520–527.

42 Schmidt AM, Hori O, Chen JX, Li JF, Crandall J, Zhang J, Cao R, et al. Advanced glycation endproducts interacting with their endothelial receptor induce expression of vascular cell adhesion molecule-1 (VCAM-1) in cultured human endothelial cells and in mice. A potential mechanism for the accelerated vasculopathy of diabetes. J Clin Invest 1995; 96:1395–403.

43 Koka V, Wang W, Xiao RH, Shokei KM, Truong LD, Lan HY. Advanced glycation end products activate a chymase-dependent angiotensin II-generating pathway in diabetic complications. Circulation 2006; 113:1353–1360.

44 Mitola S, Belleri M, Urbinati C, Coltrini D, Sparatore B, Pedrazzi M, Melloni E, et al. Cutting edge: extracellular high mobility group box-1 protein is a proangiogenic cytokine. J Immunol 2006; 176:12–15.

45 Ren X, Shao H, Wei Q, Sun Z, Liu N. Advanced glycation end-products enhance calcification in vascular smooth muscle cells. J Int Med Res 2009; 37:847–54.

46 Quinn TM, Grodzinsky AJ. Longitudinal modulus and hydraulic permeability of poly(methacrylic acid) gels: effects of charge density and solvent content. Macromolecules 1993; 26:4332–4338.

47 Kraning-Rush CM, Carey SP, Califano JP, Smith BN, Reinhart-King CA. The role of the cytoskeleton in cellular force generation in 2D and 3D environments. Phys Biol 2011; 8:15009.

48 Carey SP, Kraning-Rush CM, Williams RM, Reinhart-King CA. Biophysical control of invasive tumor cell behavior by extracellular matrix

microarchitecture. Biomaterials 2012; 33:4157–4165.

49 Raub CB, Unruh J, Suresh V, Krasieva T, Lindmo T, Gratton E, Tromberg BJ, et al. Image Correlation Spectroscopy of Multiphoton Images Correlates with Collagen Mechanical Properties. Biophys J 2008; 94:2361–2373.

50 Lutolf MP, Raeber GP, Zisch AH, Tirelli N, Hubbell JA. Cell-Responsive Synthetic Hydrogels. Advanced Materials 2003; 15:888–892.

51 Raeber GP, Lutolf MP, Hubbell JA. Molecularly engineered PEG hydrogels: a novel model system for proteolytically mediated cell migration. Biophys J 2005; 89:1374–1388.

52 Kelm JM, Timmins NE, Brown CJ, Fussenegger M, Nielsen LK. Method for generation of homogeneous multicellular tumor spheroids applicable to a wide variety of cell types. Biotechnol Bioeng 2003; 83:173–180.

53 Brightman AO, Rajwa BP, Sturgis JE, McCallister ME, Robinson JP, Voytik-Harbin SL. Time-lapse confocal reflection microscopy of collagen fibrillogenesis and extracellular matrix assembly in vitro. Biopolymers 2000; 54:222–234.

54 Williams BR, Gelman RA, Poppke DC, Piez KA. Collagen fibril formation. Optimal in vitro conditions and preliminary kinetic results. J Biol Chem 1978; 253:6578–6585.

55 Califano JP, Reinhart-King CA. Substrate stiffness and cell area drive cellular traction stresses in single cells and cells in contact. Cell Mol Bioeng 2010; 3:68–75.

56 Kemeny SF, Figueroa DS, Andrews AM, Barbee KA, Clyne AM. Glycated collagen alters endothelial cell actin alignment and nitric oxide release in response to fluid shear stress. J Biomech 2011; 44:1927–1935.

57 Figueroa D, Kemeny S, Clyne A. Glycated Collagen Impairs Endothelial Cell Response to Cyclic Stretch. Cell Mol Bioeng 2011; 4:220–230.

58 Provenzano PP, Inman DR, Eliceiri KW, Trier SM, Keely PJ. Contact guidance mediated three-dimensional cell migration is regulated by Rho/ROCK-dependent matrix reorganization. Biophys J 2008; 95:5374–5384.

59 Gross J, Kirk D. The heat precipitation of collagen from neutral salt solutions: some rate-regulating factors. J Biol Chem 1958; 233:355–360.

60 Yang YL, Motte S, Kaufman LJ. Pore size variable type I collagen gels and their interaction with glioma cells. Biomaterials 2010; 31:5678–5688.

61 Raub CB, Suresh V, Krasieva T, Lyubovitsky J, Mih JD, Putnam AJ, Tromberg BJ, et al. Noninvasive assessment of collagen gel microstructure and mechanics using multiphoton microscopy. Biophys J 2007; 92:2212–2222.

62 Drouven BJ, Evans CH. Collagen fibrillogenesis in the presence of lanthanides. J Biol Chem 1986; 261:11792–11797.

63 Zhou X, Rowe RG, Hiraoka N, George JP, Wirtz D, Mosher DF, Virtanen I, et al. Fibronectin fibrillogenesis regulates three-dimensional neovessel formation. Genes Dev 2008; 22:1231–1243.

64 Lawrence BJ, Madihally S V. Cell colonization in degradable 3D porous matrices. Cell Adh Migr 2008; 2:9–16.

65 Boobink IWG, de Boer HC, Tekelenburg WLH, Banga J-D, de Groot PG. Effect of Extracellular Matrix Glycation on Endothelial Cell Adhesion and Spreading: Involvement of Vitronectin. Diabetes 1997; 46:87–93.

66 McCarthy AD, Uemura T, Etcheverry SB, Cortizo AM. Advanced glycation endproducts interefere with integrin-mediated osteoblastic attachment to a type-I collagen matrix. Int J Biochem Cell Biol 2004; 36:840–848.

67 Krantz S, Lober M, Thiele M, Teuscher E. Diminished adhesion of endothelial aortic cells on fibronectin and collagen layers after nonenzymatic glycation. Exp Clin Endocrinol 1988; 91:155–160.

68 Bunn HF, Gabbay KH, Gallop PM. The glycosylation of hemoglobin: relevance to diabetes mellitus. Science 1978; 200:21–27.

69 Monnier VM, Cerami A. Nonenzymatic browning in vivo: possible process for aging of long-lived proteins. Science 1981; 211:491–493.

70 Monnier VM, Kohn RR, Cerami A. Accelerated age-related browning of human collagen in diabetes mellitus. Proc Natl Acad Sci U S A 1984; 81:583–587.

71 Sims TJ, Rasmussen LM, Oxlund H, Bailey AJ. The role of glycation cross-links in diabetic vascular stiffening. Diabetologia 1996; 39:946–951.

72 Odetti P, Rossi S, Monacelli F, Poggi A, Cirnigliaro M, Federici M, Federici A. Advanced glycation end products and bone loss during aging. Ann N Y Acad Sci 2005; 1043:710–717.

73 Verzijl N, DeGroot J, Thorpe SR, Bank RA, Shaw JN, Lyons TJ, Bijlsma JW, et al. Effect of collagen turnover on the accumulation of advanced glycation end products. J Biol Chem 2000; 275:39027–39031.

74 Vitek MP, Bhattacharya K, Glendening JM, Stopa E, Vlassara H, Bucala R,

Manogue K, et al. Advanced glycation end products contribute to amyloidosis in Alzheimer disease. Proc Natl Acad Sci U S A 1994; 91:4766–4770.

75 Takahashi M, Kushida K, Ohishi T, Kawana K, Hoshino H, Uchiyama A, Inoue T. Quantitative analysis of crosslinks pyridinoline and pentosidine in articular cartilage of patients with bone and joint disorders. Arthritis Rheum 1994; 37:724–728.

76 Donnelly SM. Accumulation of glycated albumin in end-stage renal failure: evidence for the principle of "physiological microalbuminuria."Am J Kidney Dis 1996; 28:62–66.

77 Lopez JI, Kang I, You W-K, McDonald DM, Weaver VM. In situ force mapping of mammary gland transformation. Integr Biol (Camb) 2011; 3:910–921.

78 Ditzel J. Angioscopic Changes in the Smaller Blood Vessels in Diabetes Mellitus and their Relationship to Aging. Circulation 1956; 14:386–397.

79 Carmeliet P, Jain RK. Angiogenesis in cancer and other diseases. Nature 2000; 407:249–257.

CHAPTER 3

COLLAGEN CROSS-LINKING INCREASES ANGIOGENESIS AND DISRUPTS BARRIER INTEGRITY

Portions of this chapter are in preparation for submission.

3.1 Abstract

Tumor microvasculature tends to be malformed, more permeable and more tortuous than vessels in healthy tissue, effects that have been largely attributed to up-regulated VEGF expression. However, during solid tumor progression, tumor tissue tends to stiffen and tissue stiffness is known to alter cell behavior including the formation and stabilization of cell-cell contacts which are requisite for angiogenesis. Using cross-linked collagen gels, we investigated the effects of matrix stiffness on vessel growth and integrity during angiogenesis. Using in vitro and ex ovo models, our data indicate that angiogenic outrgrowth increases with matrix cross-linking but decreases with matrix density. Cross-linking also results in increased vessel branching, another hallmark of tumor vasculature. In addition to promoting increased outgrowth and branching, stiffness also disrupts endothelial barrier function. Importantly, we show that inhibiting matrix metalloproteinases with GM6001 significantly reduces angiogenic outgrowth in stiffer cross-linked gels and modifies sprout morphology. These results demonstrate that matrix stiffness, independently of exogenous growth factor cues and separately from matrix density, can alter vascular growth and integrity.

These data suggest that therapeutically targeting stiffness or endothelial cell response to stiffening in the tumor microenvironment may help maintain and restore vessel structure and function to minimize metastasis and aid in drug delivery.

3.2 Introduction

Tumor tissues generally have altered mechanical properties as compared to native, healthy tissue and solid tumors are associated with an increase in local extracellular matrix (ECM) stiffness and angiogenesis[1,2]. The in-growth of newly sprouted blood vessels is necessary for tumor growth and the tumor vasculature is typically malformed, leakier, and more tortuous than the vasculature of normal tissues[2,3]. Generally, the aberrant vasculature is viewed to be the result of up-regulated vascular endothelial growth factor (VEGF) expression resulting in chaotic vascular growth and failure to establish mature well-regulated networks. In fact, many studies have been focused on the role of increased VEGF expression in tumor angiogenesis[4–6]. Here, we propose a novel hypothesis, namely that ECM mechanical properties contribute to the aberrant vascular phenotype seen in tumors.

The increase in ECM stiffness of tumors is primarily due to both increased collagen deposition and increased cross-linking within the tumor stroma[7]. Increased ECM density and cross-linking are both known to be poor prognostic markers in a number of cancers[8–13]. Many studies have investigated the role of matrix density on angiogenesis and, in both collagen and fibrin matrices, have shown that angiogenesis decreases with increasing matrix concentration[14–18]. However, less is known about

how stiffening due to matrix cross-linking affects angiogenesis. In this study, we examine the effects of altering ECM stiffness through non-enzymatic glycation cross-linking to further understand the effects on the angiogenic response.

Non-enzymatic glycation is a process that occurs in vivo whereby proteins are cross-linked by reducing sugars such as glucose or ribose through a sequence of chemical modifications known as the Maillard reaction[19]. The process of non-enzymatic glycation forms cross-links termed advanced glycation endproducts (AGE). Importantly, AGEs have been found to be present in a number of different cancers and have been implicated in increased malignancy[20,21].

Here, we show that increasing the extent of collagen cross-linking leads to significantly more outgrowth and branching both in vitro and in an ex ovo embryonic chick model. We further show that the stiffness of the matrix plays an important role in endothelial cell-cell junctional integrity and endothelial monolayer permeability. Together, our study demonstrates matrix cross-linking plays a critical role in modulating the angiogenic potential and cell-cell associations of endothelial cells.

3.3 Materials and Methods

Cell Culture

EC culture

Human umbilical vein endothelial cells (HUVEC) were purchased from Invitrogen and used until passage 8. HUVECs were grown in M200 (Invitrogen) supplemented

with low-serum growth supplement (Invitrogen) and 5% fetal bovine serum (Invitrogen). Cells were fed every other day and grown to confluence in a 37^{O}C and 5% $C0_2$ incubator. Bovine aortic endothelial cells (BAEC) were purchased from VEC Technologies (Rensselaer, NY) and used until passage 12. BAECs were grown in M199 (Invitrogen, Carlsbad, CA) supplemented with 1% each of MEM amino acids (Invitrogen), MEM vitamins (Mediatech, Manassas VA), and penicillin-streptomycin (Invitrogen) and 10% fetal clone III (Hyclone, Logan, UT). For studies with GM6001 (EMD Millipore, Billerica, MA), GM6001 was diluted to 5 mM in dimethyl sulfoxide (DMSO; Sigma-Aldrich, St. Louis, MO) and then mixed with complete M199 to form a 5 μM solution.

Spheroid generation

Multicellular spheroids were prepared through forced aggregation as described previously[22]. Briefly, BAECs were suspended in complete M199 supplemented with 0.25% Methocult (Stem Cell Technologies, Vancouver, BC, Canada) and seeded into non-adherent 96-well round bottom plates (Corning Inc., Corning, NY) at 10,000 cells per well. Cells were pelleted by centrifugation and spheroids were formed by placing the plate on an orbital shaker for 2 hours and subsequently incubating the spheroids for 2 days prior to embedding within collagen gels.

Preparation of collagen gels

Isolation and non-enzymatic glycation of collagen

Type I collagen was isolated from rat tail tendons (Rockland Immunochemicals,

Gilbertsville, PA) as described previously[22]. Briefly, type I collagen was extracted in 0.1% acetic acid (JT Baker, Phillipsburg, NJ) at 4^{O}C, lyophilized, and solubilized in 0.1% sterile acetic acid to form 10 or 20 mg ml^{-1} stock solutions. Glycated collagen solutions were prepared by mixing collagen stock solutions with 0.5 M ribose to form solutions containing 0, 50, or 100 mM ribose in 0.1% sterile acetic acid on ice. Solutions were incubated for 5 days at 4^{O}C and then neutralized with 1N sodium hydroxide in 10x Dulbecco's Phosphate Buffered Saline (D-PBS; Invitrogen), mixed with HEPES (EMD Millipore) and sodium bicarbonate (JT Baker) in 10x D-PBS to form 1.5, 5, or 10 mg ml^{-1} collagen gels with final concentrations of 1x D-PBS, 25 mM HEPES and 44 mM sodium bicarbonate.

Cell and spheroid embedding

Spheroids or isolated cells were embedded within neutralized collagen solutions and allowed to polymerize at 37^{O}C and 5% CO_2 and then overlaid with complete medium. The medium was exchanged after 1 hour and then every other day during experiments. In cases were isolated cells were not suspended within the collagen gels, an equivalent volume of complete medium was added to the gel solutions prior to polymerization to maintain gel composition between experiments.

Vasculogenesis Assays

Vasculogenesis assays were seeded with HUVECs and fed every other day with CM200 supplemented with 40 ng ml^{-1} vascular endothelial growth factor (VEGF; R&D Systems, Minneapolis, MN), 40 ng ml^{-1} basic fibroblast growth factor (bFGF;

EMD Millipore), 50 ng ml^{-1} phorbol-12-myristate-13-acetate (TPA; EMD Millipore), and 50 μg ml^{-1} ascorbic acid (JT Baker)[17].

Mechanical testing of collagen gels

The equilibrium compressive moduli of collagen gels were quantified on an Enduratec EL2100 frame (Bose, Eden Prarie, MN) with at 250 g load cell measuring the resultant forces of 5% stepwise displacements on collagen gels in confined compression[22,23]. Briefly, a standard linear solid model of viscoelastic behavior was used to fit the relaxation data from 1.5, 5, or 10 mg ml^{-1} collagen gels and the equilibrium modulus was calculated as the slope of the stress-strain curve[17,23]. We assumed that the collagen gels were isotropic and elastic similarly to other studies of collagen gel mechanical properties[17,24].

Chicken embryo culture

Ex ovo chicken embryo culture was performed as previously described[25]. Briefly, fertilized white Leghorn chicken eggs were cultured for 72 hours at 37.5^{O}C and 60% humidity in a rocking incubator. The chicken embryos were then cracked into humidified hammocks and cultured *ex ovo* in a static incubator. At embryonic day 10, constructs consisting of two 5 mm x 5 mm squares of nylon mesh (Amazon Supply, Seattle, WA) sandwiched around 30 μl of 1.5 mg ml^{-1} collagen with that had been glycated with 0 or 100 mM ribose and containing 5 μg ml^{-1} VEGF (R&D Systems) were polymerized[26]. Constructs were placed onto the distal region of the chorioallantoic membrane (CAM) and returned to the incubator. At embryonic day 15,

the embryos were injected with 0.25% (w/v) fixable 70 kDa Texas Red-dextran (Invitrogen) in D-PBS into the vitelline veins and the dye was allowed to perfuse for 45 minutes. The collagen constructs were fixed for 1 hour in 3.7 vol% formaldehyde in PBS, removed from the CAM and washed with PBS. The vasculature within the collagen constructs was imaged using a Zeiss LSM700 (Carl Zeiss) confocal. Vascular density was scored by counting the number of mesh squares within a 6x6 region that had angiogenic vessels within the collagen[26] (n=40).

Release of VEGF from glycated collagen gels

Implants consisting of two 5 mm x 5 mm squares of nylon mesh and 30 μl of 1.5 mg ml^{-1} collagen that had been glycated with 0 or 100 mM ribose and containing 5 μg ml^{-1} VEGF (R&D Systems) were polymerized as described for chicken embryo culture. Individual constructs were placed in a 100 mm petri dish (VWR, Radnor, PA) containing 10 ml TBS with 0.05% Tween (JT Baker) and 0.1% BSA. Petri dishes were placed in an incubator at 37^{O}C and 5% CO_2 and 100 μl samples of the solution were obtained at 0, 1, 2, 4, 8, and 24 hours. Samples were frozen at -20^{O}C until quantification of VEGF release was performed using an ELISA according to the manufacturer's instructions (R&D Systems).

Polyacrylamide gel synthesis

Polyacrylamide (PA) hydrogels were synthesized as described previously[27–29]. Briefly, the ratio of acrylamide (40% w/v solution, Bio-Rad, Hercules, CA) and N,N'-methylene-bis-acrylamide (2% w/v solution, Bio-Rad) were varied to tune the

Young's moduli of the gels from 0.2 to 10 kPa. Substrates were functionalized with N-6-((acryloyl)amido)hexanoic acid, succinimidyl ester that was synthesized in our lab and covalently bound to 0.1 mg ml^{-1} type I rat tail collagen (Becton Dickinson, Franklin Lakes, NJ) or 0.1 mg ml^{-1} glycated collagen that had been prepared as described above[30,31].

Western Blot

Subconfluent BAECs on PA substrates ranging from 0.2-10 kPa or polystyrene were lysed with buffers to fractionate the Triton-soluble and Triton-insoluble proteins[32]. Triton-soluble fractions were extracted with 1% (w/v) NP-40 and 1 vol.% Triton in Tris-buffered saline (TBS; 10 mM Tris-HCl, 150 mM NaCl) with 2 mM CaCl2 (JT Baker) pH 7.5, and protease inhibitor cocktail (1:500, Sigma-Aldrich). The Triton-insoluble fractions were extracted with 0.5% (w/v) sodium dodecyl sulfate and 1% (w/v) NP-40 (JT Baker) in TBS. The supernatants were analyzed with a protein assay (Bio-Rad, Hercules, CA) and subjected to gel electrophoresis (15 μg per sample; 8% acrylamide gel) and Western blot. Antibodies to VE-cadherin (C-19, Santa Cruz Biotechnology, Santa Cruz, CA), and to β-actin (AC-15, Sigma-Aldrich) were detected by chemiluminescence on a Bio-Rad ChemiDoc imaging system. Densitometry of VE-cadherin was performed with Quantity One (v. 4.6.5; Bio-Rad) and expressed as a ratio to β-actin. Total cell VE-cadherin was calculated by adding the VE-cadherin/ β-Actin ratios for Triton-soluble and Triton-insoluble fractions and the VE-cadherin in each fraction was determined as a percent of the total VE-cadherin (N=3).

Permeability

BAECs on polyacrylamide substrates with Young's moduli from 0.2 to 10 kPa were used to measure endothelial cell permeability as described previously[33]. Briefly, 2-day post-confluent BAEC monolayers were immersed in a 10 μM solution of 40 kDa FITC-dextran (Sigma-Aldrich) for 5 minutes. Confocal z-slices were acquired using a Zeiss LSM700 microscope with a long working distance water-immersion C-Apochromat 40x/1.1 NA objective (Carl Zeiss). To calculate relative permeability, the intensity of the dextran accumulation within the gel was divided by the fluorescent intensity of the solution above the gel. These values were then normalized by the relative accumulation of dextran within gels without cells (n=21-56).

Immunocytochemistry

Cells and spheroids were fixed in 3.7 vol.% formaldehyde in 1x D-PBS, permeabilized with 1 vol.% Triton (JT Baker) in 1x D-PBS and blocked with 3% w/v bovine serum albumin (BSA, Sigma-Aldrich). Cells were stained for actin using Alexa Fluor 488 or Alexa Fluor 568 phalloidin (Invitrogen) and for nuclei with 4',6-diamidino-2-phenylindole (DAPI) (Sigma-Aldrich). BAECs were immunostained for VE-cadherin with a goat polyclonal VE-cadherin primary antibody (C-19, Santa Cruz Biotechnology) and Alexa Fluor 568 donkey anti-goat secondary antibody (Invitrogen).

Imaging

Confocal reflectance imaging

As described previously, the internal structure of collagen gels were visualized using confocal reflectance microscopy[22,34]. A Zeiss LSM 700 inverted laser scanning microscope (Carl Zeiss, Oberkochen, Germany) equipped with a 405 nm laser and a long working distance water-immersion C-Apochromat 40x/1.1 NA objective (Carl Zeiss) were used to acquire 1 μm optical slices of the collagen structure. Image acquisition parameters were the same for all gels.

Spheroid Outgrowth

BAEC multicellular spheroids were imaged with bright-field on a Zeiss Axio Observer Z1.m (Carl Zeiss) and with fluorescence on a Zeiss LSM700 point scanning confocal. Bright-field images of spheroids in culture were acquired daily for outgrowth studies. Spheroid outgrowth was compared across conditions by measuring the area of the spheroids with the resultant extensions over 5 days and normalizing to the area of the spheroid immediately after embedding within the collagen gel (n=7-14). For the GM6001 data, spheroid outgrowth was measured at day 3 and normalized to the area of the spheroid immediately after embedding in the collagen gel (n=19-28).

Spheroid Branching

Spheroids embedded in 1.5 mg ml^{-1} collagen for 5 days were stained for actin and nuclei. Images of the spheroids were acquired as z-stacks with 5 μm spacing using a EC Plan-Neofluar 10x/0.30 NA objective (Carl Zeiss). Maximum intensity

projections of the confocal z-stacks were analyzed for branching density by counting the number of branches per sprout length for five randomly chosen extensions per spheroid (n=35-55). Data were normalized to the 0 mM ribose condition.

Spheroid Sprout Width

Spheroids embedded in 1.5 mg ml^{-1} collagen for 3 days with and without GM6001 treatment were stained for actin and nuclei. Images of the spheroids were acquired as z-stacks with 5 μm spacing using a EC Plan-Neofluar 10x/0.30 NA objective (Carl Zeiss). Maximum intensity projections of the confocal z-stacks were analyzed for sprout width by drawing a line perpendicular to the sprout and fitting the intensity profile to with a two-Gaussian curve in MATLAB. The tip width was defined as the width of the two-Gaussian fit 20% above the background intensity (n=61-85).

VE-cadherin

BAEC spheroids embedded for 24 hours in 1.5 mg ml^{-1} collagen gels were stained for VE-cadherin and nuclei. Images of the sprouts emanating from the spheroids were acquired as z-stacks with 1 μm spacing using a long working distance water-immersion C-Apochromat 40x/1.1 NA objective (Carl Zeiss). The widths of endothelial cell junctions were analyzed as described previously using a custom-written MATLAB algorithm[33]. Briefly, z-stacks of were used to visually determine the focal plane for a given junction in ImageJ. A line was drawn perpendicular to the junction and the intensity profile was recorded and then fit with a two-Gaussian curve in MATLAB. The junctional width was defined as the width of the two-Gaussian fit

20% above the background intensity. Tip cell junctions were defined as the junction of the terminal cell with the rest of the sprout (n=80-105). Stalk cell junctions were defined as those between adjacent cells within the sprout (n=118-130).

Timelapse microscopy and single cell migration

Individual BAEC migration was monitored beginning 24 hours after embedding within collagen gels using a Zeiss Axio Observer Z1.m (Carl Zeiss) microscope equipped with motorized stage and an environmental chamber maintained at 37^{O}C and 5% CO_2. Images were acquired every 10 minutes for 15 hours. Cells were traced in ImageJ and centroid positions were used to calculate the mean-square displacement (d^2) to find cell migration speed (S) using the persistent random walk equation: $d^2 = 2S^2P\left[t - P\left(1 - e^{-(t/P)}\right)\right]$, where (t) is time interval, and (P) is the persistence time using a nonlinear least squares regression analysis as previously described[35–37] (n=46-68).

Vasculogenesis imaging and analysis

HUVECs were imaged using a Zeiss LSM700 (Carl Zeiss) after being embedded within 1.5 mg ml^{-1} gels for 7 days and stained for actin and nuclei. Images of cells were acquired as z-stacks with 5 μm spacing using an EC Plan-Neofluar 10x/0.30 NA objective (Carl Zeiss). Cellular structures were analyzed using a custom-written MATLAB algorithm for volume and tortuosity based on previously published methods[38,39]. Volume measurements were extracted as three-dimensional connected components from binary images processed with an adaptive thresholding method.

Tortuosity was defined as ratio of path length of lumen center divided by the Euclidean distance between the two distal tips of the lumen (n=51-70).

Statistics

Data were analyzed using a one-way analysis of variance (ANOVA) followed by a post-hoc Tukey's Honest Significant Difference test in JMP (SAS, v.10.0). To normalize the data distributions, spheroid branch density, VE-cadherin junction width, and permeability data were transformed by natural logarithm prior to running a Tukey's test. Statistical significance was considered as $p < 0.05$. All values are expressed as the mean ± standard error of the mean (SEM).

3.4 Results

Non-enzymatic collagen glycation and collagen density modulate the mechanical properties and fiber arrangements of collagen gels.

The individual and combined effects of non-enzymatic collagen glycation and collagen density on the mechanical and structural properties of collagen gels were studied. Non-enzymatic collagen glycation occurs when a non-reducing sugar such as ribose reacts with a free amino group on the collagen molecule to form a Schiff base (Figure 3.1A). The Schiff base can then undergo rearrangement to form an Amadori product and interact with a free amino group on an adjacent collagen fiber to create an advanced glycation endproduct (AGE) cross-link between the fibers. Accumulation of these AGE cross-links increases the stiffness of the collagen gels.

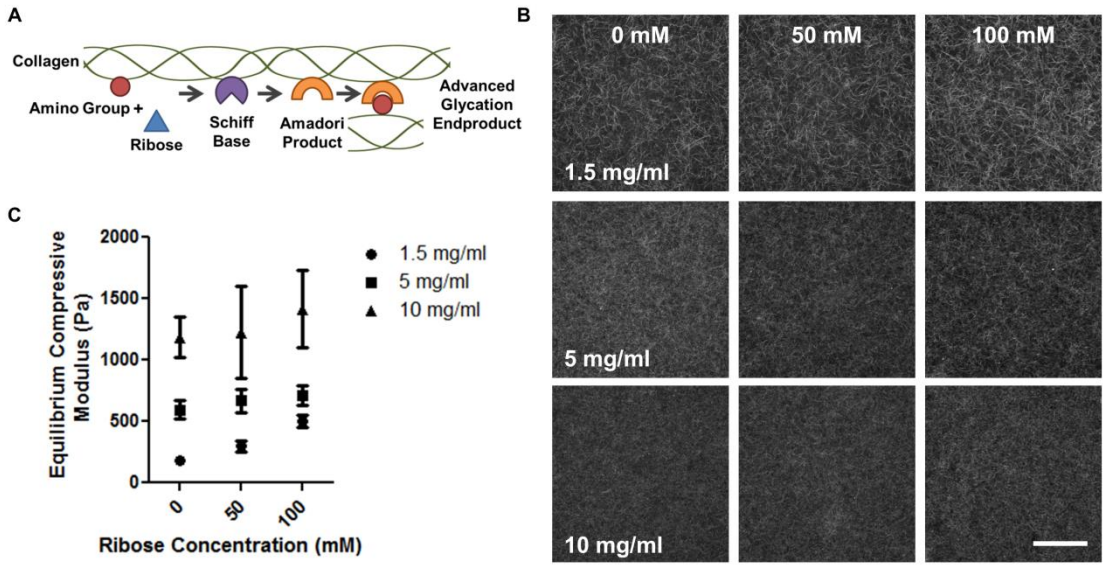

Figure 3.1. Matrix density and cross-linking alter collagen gel mechanical properties and fiber arrangements. (A) Schematic of the chemistry of collagen glycation. (B) Confocal reflectance microscopy images of 1.5, 5, and 10 mg ml-1 collagen gels glycated with 0, 50, or 100 mM ribose. (C) The equilibrium compressive moduli of the gels were measured by confined compression testing. Data presented as mean ± SEM, Scale is 50 μm.

We have previously shown that 1.5 mg ml^{-1} collagen gels glycated with 0-100 mM ribose have similar fiber arrangements while those glycated with 150-250 mM ribose have larger and more prominent collagen fibers[22]. Thus, we chose to use glycation concentrations of 0-100 mM ribose in this study. The process of non-enzymatic glycation was used to stiffen 1.5, 5, and 10 mg ml^{-1} collagen in vitro by incubating un-polymerized collagen solutions with 0, 50, or 100 mM ribose for 5 days at $4^{O}C$ prior to neutralization and polymerization. This incubation period allowed AGE precursors to form within the solubilized collagen so that cross-links could form upon polymerization of the gels[22,23].

To investigate the effects of collagen density and cross-linking on collagen gel fiber

architecture, gels were polymerized and the internal collagen fiber distributions were visualized with confocal reflectance microscopy. Increasing the density of the collagen visibly decreases the porosity and alters the size and distribution of fibers within the collagen gels (Figure 3.1B). However, collagen gels within a given density and glycated with 0-100 mM ribose form gels with qualitatively similar fiber architectures.

Confined compression testing was performed to investigate the mechanical properties of collagen gels by applying a 5% stepwise strain to a confined gel and measuring the resultant force. The equilibrium compressive modulus was calculated as the slope of the stress-strain curve by fitting the data to a standard linear solid model of viscoelastic behavior. Increasing the density of the collagen gels from 1.5 to 10 mg ml^{-1}, increases the equilibrium compressive modulus approximately 6-fold from ~180 Pa to ~ 1200 Pa (Figure 3.1C). Within a given density, increasing the extent of glycation from 0 to 100 mM also increases the modulus of the gels from ~180-500 Pa, ~600-715 Pa, and ~1200-1400 Pa, for 1.5, 5, and 10 mg ml^{-1} collagen gels, respectively.

Taken together, these results indicate that non-enzymatic glycation can modulate the mechanical properties of collagen gels within a defined range while only minimally altering the collagen fiber architecture. Altering the density of collagen modulates the stiffness of the gels to a greater extent, but also changes the collagen fiber distributions and arrangements within the gels. We used these two competing mechanisms of

stiffening collagen to investigate the relative roles of collagen stiffness and density on the outgrowth of angiogenic sprouts from multicellular spheroids into collagen gels.

Spheroid outgrowth is modulated by matrix density and collagen glycation

We have previously shown that increasing the stiffness of collagen matrices via non-enzymatic collagen glycation increases the angiogenic outgrowth of multicellular endothelial cell spheroids into 1.5 mg ml^{-1} collagen gels[22]. To investigate the individual and combined roles of stiffening gels via collagen glycation and density on endothelial cell (EC) outgrowth, EC spheroids were embedded within 1.5, 5, and 10 mg ml^{-1} gels glycated with 0, 50, or 100 mM ribose and imaged every 24 hours over 5 days. Increasing the density of the collagen matrix decreased the overall outgrowth of angiogenic sprouts from the spheroids (Figure 3.2A,B). However, at all densities, increasing the stiffness of the collagen via glycation increased the outgrowth response from the spheroids. EC spheroids invaded significantly further in collagen gels glycated with 100 mM ribose than with 0 mM ribose beginning at days 1 and 3 for 1.5 and 5 mg ml^{-1} collagen densities, respectively (Figure 3.2B). This trend is observed across all collagen densities, although it is not statistically significant at 10mg/ml. These data suggest that both the stiffness of the collagen matrix and the density can influence EC sprouting.

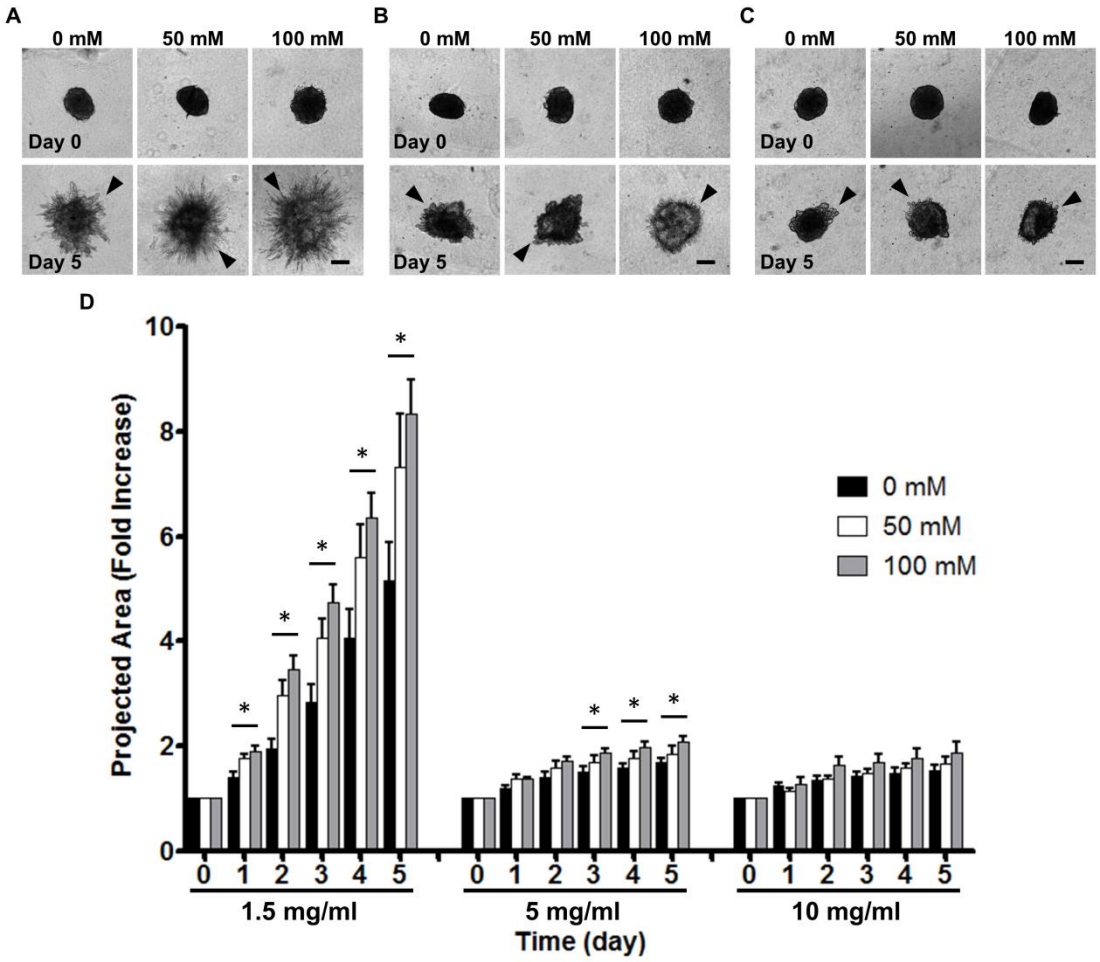

Figure 3.2. Collagen cross-linking and density alter the angiogenic sprouting response from multicellular spheroids. EC spheroids were embedded within (A) 1.5, (B) 5,or (C) 10 mg/ml collagen gels glycated with 0, 50, or 100 mM ribose and the angiogenic sprouting response (arrowheads) was monitored. (D) The projected spheroid area, including the extensions, was measured over the course of 5 days. Data presented as mean + SEM, * indicates $p<0.05$, Scale is 200 μm.

Spheroid branching is modulated by collagen glycation

To further analyze the effects of matrix stiffness on spheroid outgrowth, the density of branching along angiogenic sprouts in spheroids embedded for 5 days in 1.5 mg ml^{-1} collagen gels glycated with 0, 50, or 100 mM ribose was analyzed. Spheroids stained for actin and nuclei were imaged using confocal microscopy and the number of branches per sprout length was measured. Increasing the stiffness of the gels via non-

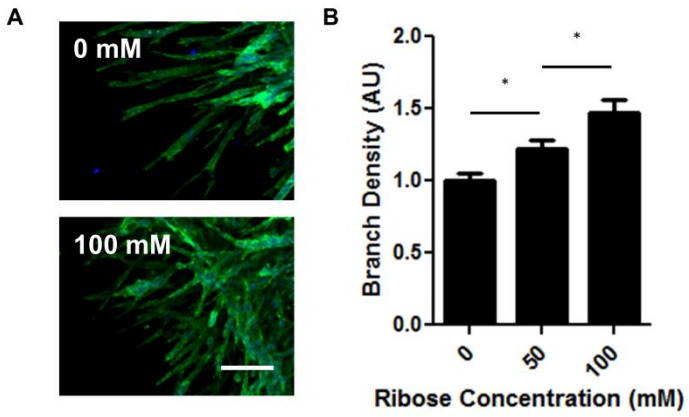

Figure 3.3. Matrix cross-linking alters angiogenic branching. EC multicellular spheroids were embedded within 1.5 mg/ml collagen gels glycated with 0, 50, or 100 mM ribose. (A) Spheroids were fixed, stained for actin (green) and nuclei (blue), and imaged using confocal microscopy after 5 days. (B) The number of branches per sprout length were counted and data were normalized to the 0 mM condition. Data presented as mean + SEM, * indicates $p<0.05$, Scale is 100 μm.

enzymatic glycation increased the density of branching in angiogenic outgrowths from spheroids (Figure 3.3A). Spheroids in stiffer gels (100 mM ribose) had an approximately 1.5-fold increase in branching when compared to those within softer (0 mM ribose) gels (Figure 3.3B). These data indicate that increasing matrix stiffness via non-enzymatic collagen glycation not only causes increased outgrowth from spheroids (Figure 3.2B) but also changes the morphology of the angiogenic sprouts that have formed.

Spheroid outgrowth requires matrix metalloproteinase activity

To understand the role of matrix metalloproteinase (MMP) activity on spheroid outgrowth, the broad spectrum MMP inhibitor, GM6001, was used. EC spheroids were embedded within 1.5 mg ml^{-1} collagen gels that had been glycated with 0 or 100 mM ribose and fed with either control media or media containing 5 μM GM6001. The

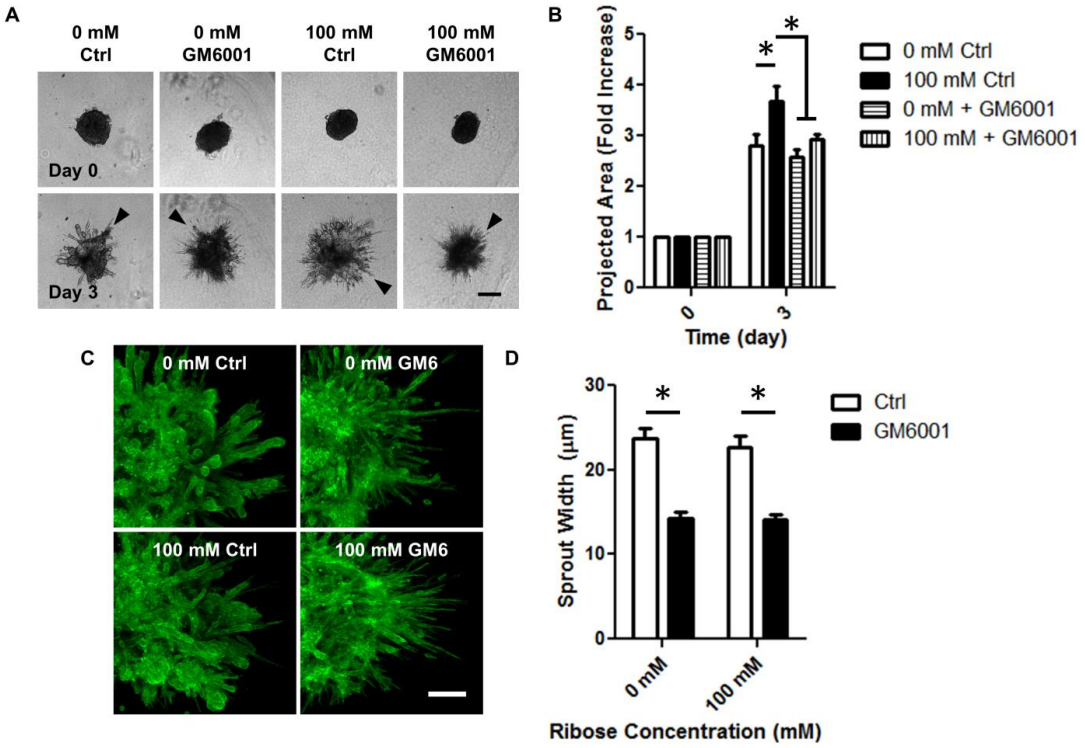

Figure 3.4. Spheroid outgrowth requires MMP activity. (A) EC multicellular spheroids were embedded within 1.5 mg ml^{-1} collagen gels glycated with 0 or 100 mM ribose and fed with complete medium with or without 5 μM GM6001. Scale is 200 μm. (B) Spheroid outgrowth was quantified after 3 days of culture and normalized to the Day 0 condition. (C) Spheroids were stained for actin (green) and nuclei (blue) and imaged with confocal microscopy. Scale is 100 μm. (D) The width of the angiogenic sprouts was measured by fitting the intensity profile of a line drawn perpendicular to the sprout with a two-Guassian curve. Data are presented as mean + SEM.

extent of spheroid outgrowth after 3 days of culture was quantified. Spheroids cultured with GM6001 in stiffer gels (100 mM ribose) had significantly less angiogenic outgrowth than spheroids in stiff controls (Figure 3.4A,B). Interestingly, spheroid outgrowth in stiffer gels (100 mM ribose) with GM6001 treatment was not significantly different than outgrowth within the softer gels (0 mM ribose) with or without GM6001 treatment. We observed that the morphologies of the angiogenic sprouts appeared to be altered with the GM6001 treatment. To investigate the role of

GM6001 on sprout morphology, spheroids were fixed and stained for actin and nuclear proteins and imaged using confocal microscopy (Figure 3.4C). Angiogenic sprout widths were measured by fitting the intensity profile to a two Gaussian curve. Sprouts in soft and stiff control gels (0 and 100 mM ribose) had similar morphologies while sprouts from spheroids cultured with GM6001 were much thinner than controls (Figure 3.4D). These data suggest that MMPs may be critical for the establishment of the wider, multicellular angiogenic sprouts seen in controls. Taken together, these data indicate that MMP activity is essential for the increased outgrowth that is seen in stiffer matrices.

Increased matrix stiffness increases angiogenesis in ex ovo chicken embryos

To investigate the role of matrix stiffness in mediating angiogenesis in a more physiologically-relevant model, we studied the formation of blood vessels in 1.5 mg ml^{-1} collagen gels glycated with 0 and 100 mM ribose using an *ex ovo* embryonic chicken model. Collagen implants were made by sandwiching 30 μl of collagen containing 5 μg ml^{-1} VEGF between two 5 mm x 5 mm pieces of nylon mesh and were placed onto the distal region of the chorioallantoic membrane (CAM) at embryonic day 10 (Figure 3.5A-C). To ensure that the elution of VEGF was not influenced by the stiffness of the gel, a VEGF ELISA was used to determine the release profile of VEGF. The ELISA analysis indicates that the release of VEGF from the collagen constructs was not affected by the stiffness of the gels (Figure 3.5D). On embryonic day 15, embryos were perfused with a 0.25% (w/v) solution of fixable 70 kDa Texas Red-dextran in D-PBS such that any open and patent angiogenic vessels in the

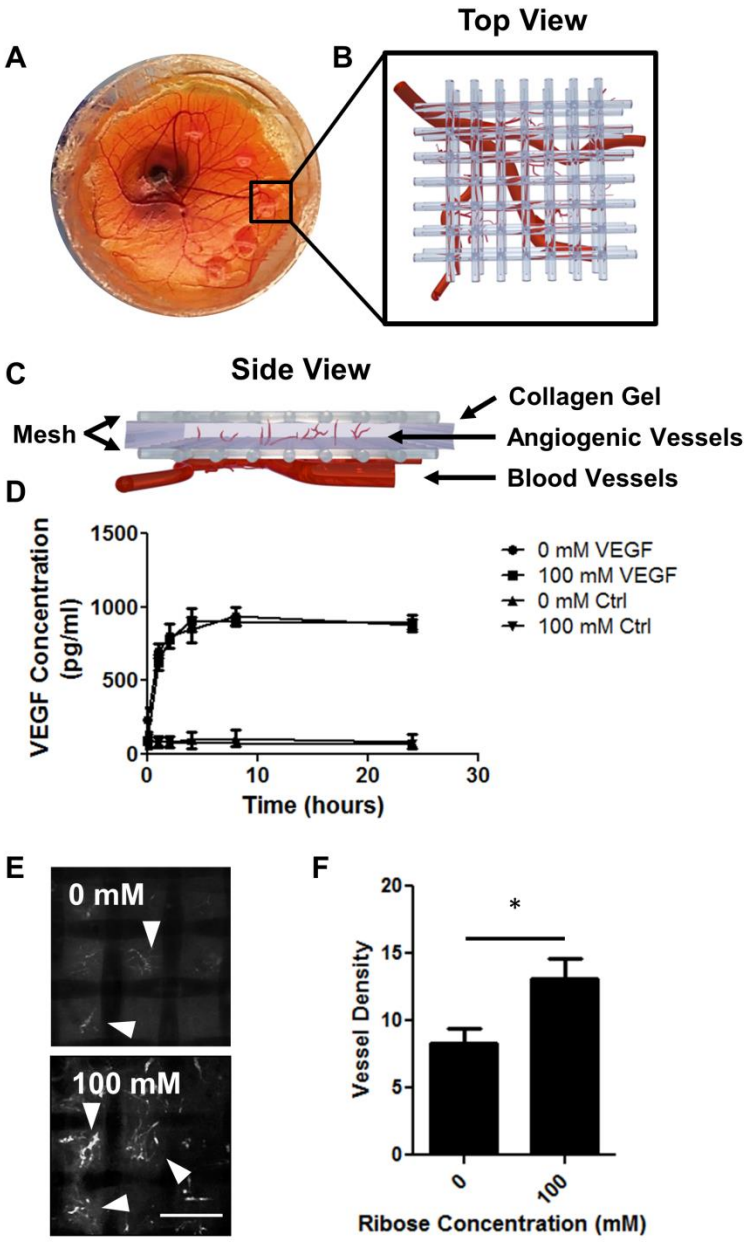

Figure 3.5. Matrix cross-linking alters angiogenic sprouting into collagen gels in the chick CAM model. (A) Collagen gels were placed on the chick CAM at day 10. Schematic views of the (B) top and (C) side of the collagen and nylon meshes depict angiogenic ingrowth into the collagen gels from the vasculature underlying the CAM. (D) VEGF release profiles over 24 hours from collagen glycated with 0 or 100 mM ribose were quantified by ELISA. (E) Angiogenic sprouting (arrowheads) into 1.5 mg/ml collagen gels glycated with 0 or 100 mM ribose were imaged with confocal microscopy and (F) the vessel density per gel was quantified. Data presented as mean + SEM, * indicates $p<0.05$, Scale is 200 μm.

collagen gels could be imaged via fluorescence. Collagen constructs were fixed with 3.7 vol.% formaldehyde in D-PBS and imaged using confocal microscopy. Vessels within the collagen gels appear as thin fluorescent sprouts (Figure 3.5E, arrowheads). Stiffer collagen gels (100 mM ribose) had significantly more angiogenic ingrowth than the more compliant (0 mM ribose) gels (Figure 3.5F). Importantly, these data indicate that angiogenesis in the CAM model is also modulated by the stiffness of the matrix.

Collagen stiffness influences single cell migration and persistence

To determine whether we could attribute the increased extent of angiogenic outgrowth with stiffness in vitro and ex ovo to the migration speed of ECs, we embedded ECs within 1.5 mg ml^{-1} collagen gels that had been glycated with 0, 50, or 100 mM ribose. The migration of the cells was monitored using timelapse microscopy, the cell centroid was tracked using ImageJ, and individual cell trajectories were plotted (Figure 3.6A). Centroid positions were used to quantify the mean-square displacement and cell speed and persistence were calculated by fitting the data to a persistent random walk model[35–37]. Surprisingly, as the stiffness of the gels increased, the speed of migration decreased (Figure 3.6B). However, the persistence time increased with increasing gel stiffness (Figure 3.6C). These data indicate that individual endothelial cells migrate slower within stiffer matrices and suggest that the increased extent of angiogenic outgrowth observed in stiffer collagen gels may be due to the increased persistence of cell migration.

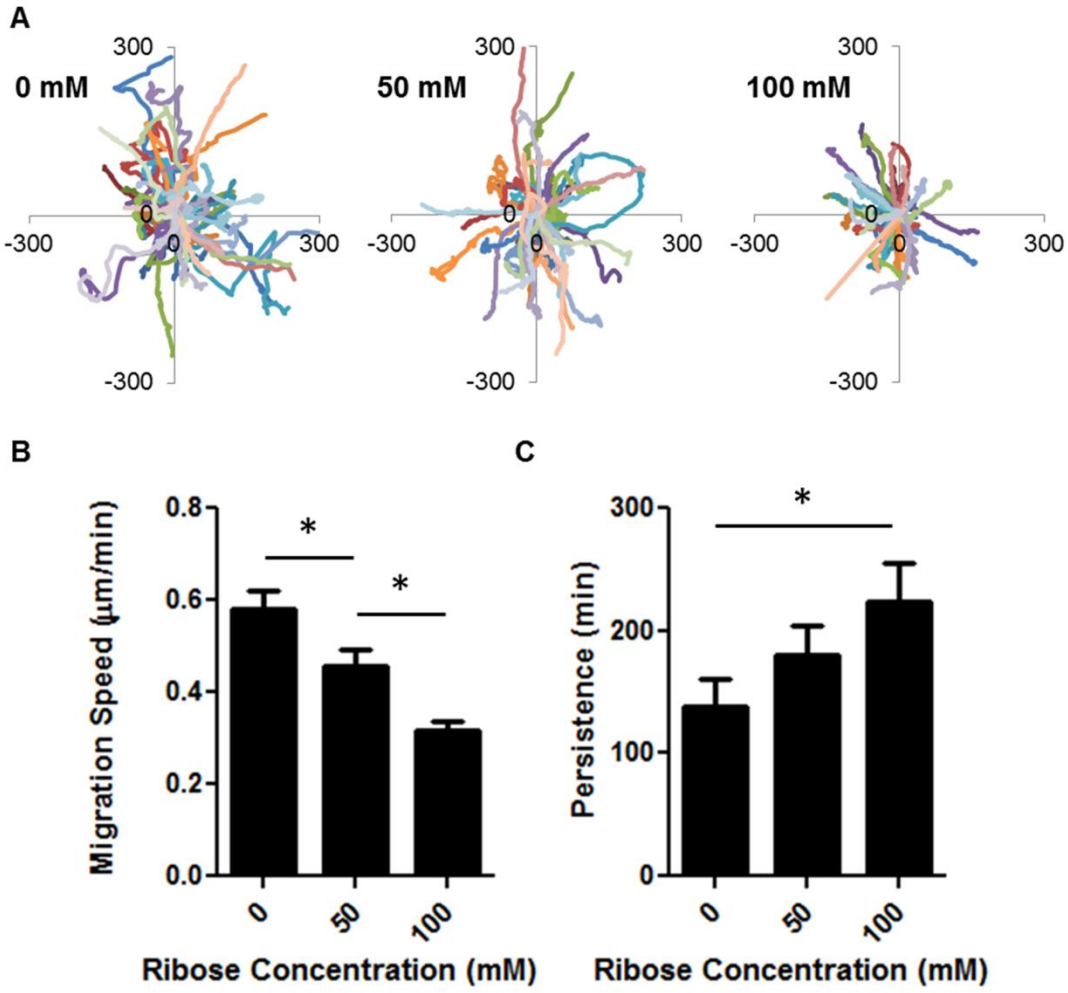

Figure 3.6. Endothelial cell migration is altered by matrix cross-linking. (A) Rose plots of individual EC migration within the 1.5 mg/ml collagen gels glycated with 0, 50, or 100 mM ribose. Scales of axes are μm. Migration (B) speed and (C) persistence were quantified. Data presented as mean + SEM.

Vasculogenesis formation is not altered with matrix stiffness

Since matrix stiffness results in differences in angiogenic outgrowth and branching, and single ECs have altered migration in response to matrix mechanical properties, we decided to study whether matrix stiffness influences the process of vasculogenesis. During vasculogenesis, single cells within a matrix migrate and proliferate to form

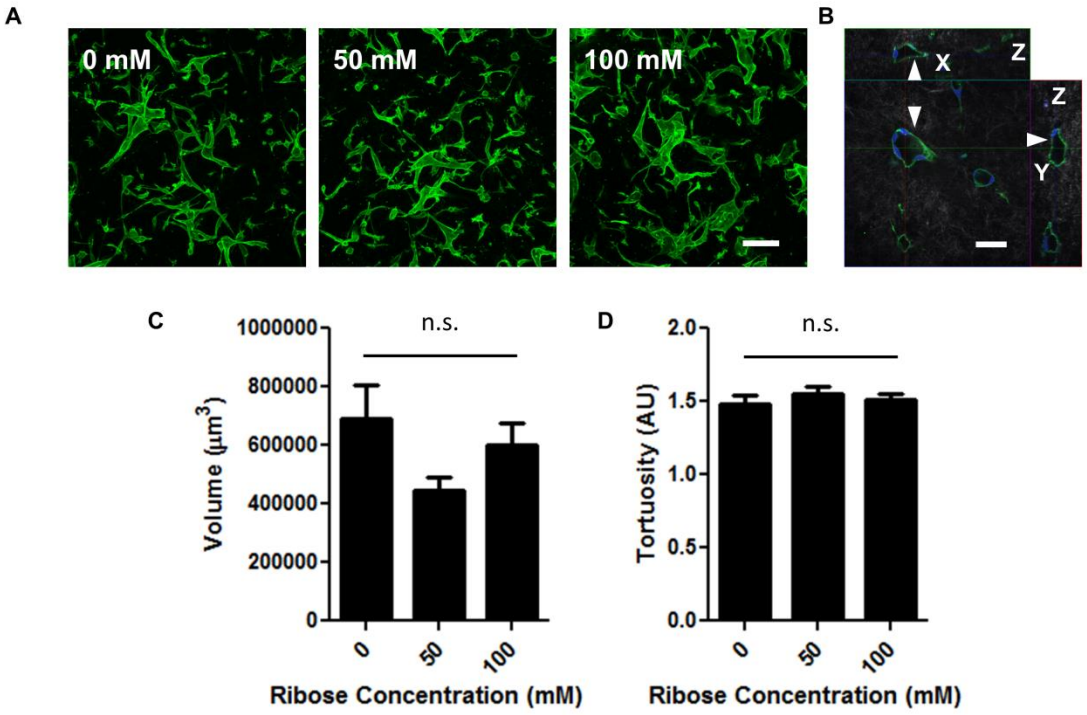

Figure 3.7. Vasculogenesis is not altered with matrix cross-linking in glycated collagen gels. (A) Maximum intensity projections of ECs stained for actin (green) within 1.5 mg/ml collagen gels glycated with 0, 50, or 100 mM ribose. Scale is 200 μm. (B) Orthogonal projection showing fully-enclosed lumens (arrowheads) formed by endothelial cells stained for actin (green) and DAPI (blue) with confocal reflectance of the collagen fibers. Scale is 50 μm. The (C) volume and (D) tortuosity of the vessel structures were measured using a customized Matlab code. Data presented as mean + SEM.

vascular structures. HUVECs were seeded within 1.5 mg ml^{-1} collagen gels that had been glycated with 0, 50, or 100 mM ribose and fed with CM200 supplemented with 40 ng ml^{-1} VEGF, 40 ng ml^{-1} bFGF, 50 ng ml^{-1} TPA and 50 μg ml^{-1} ascorbic acid[17]. After 7 days of culture, gels were fixed and stained for actin and nuclei and imaged using confocal microscopy. HUVECs formed qualitatively similar vasculogenic structures containing enclosed lumens in all conditions studied (Figure 3.7A,B). A custom MATLAB algorithm was used to quantify the volume and tortuosity of the HUVEC structures. Interestingly, there were not quantifiable differences in either the

volume or tortuosity of the resultant structures (Figure 3.7C,D). These results suggest that matrix stiffness does not significantly change the process of vasculogenesis.

Matrix stiffness influences VE-cadherin localization and endothelial monolayer permeability

Previous studies have shown that the barrier function within the tumor vasculature is impaired when compared to the vasculature in healthy tissue[3,40]. To understand the role of matrix stiffness on mediating endothelial junctional integrity, BAEC spheroids were embedded in 1.5 mg ml^{-1} collagen that had been glycated with 0, 50, or 100 mM ribose, fixed after 24 hours of outgrowth, and stained for vascular endothelial cadherin (VE-cadherin) and nuclei. Confocal images of the angiogenic outgrowth were acquired and VE-cadherin widths were measured by drawing a line perpendicular to the junction (Figure 3.8A). Interestingly, the VE-cadherin junctions of the tip cells were significantly wider than the junctions within the stalks (Figure 3.8B). Additionally, we found that the VE-cadherin junctions within the stiff (100 mM ribose) collagen were significantly wider than those within the softer (0 or 50 mM ribose) collagen gels.

To further study the role of matrix stiffness on mediating VE-cadherin junctional properties, BAECs were seeded onto soft (0.2 kPa) or stiff (10 kPa) polyacrylamide (PA) substrates. As we have shown previously, endothelial cell networks spontaneously assemble on soft PA substrates but not on stiff PA substrates (Figure 3.8C,D)[28]. Cells on soft substrates formed VE-cadherin junctions that were

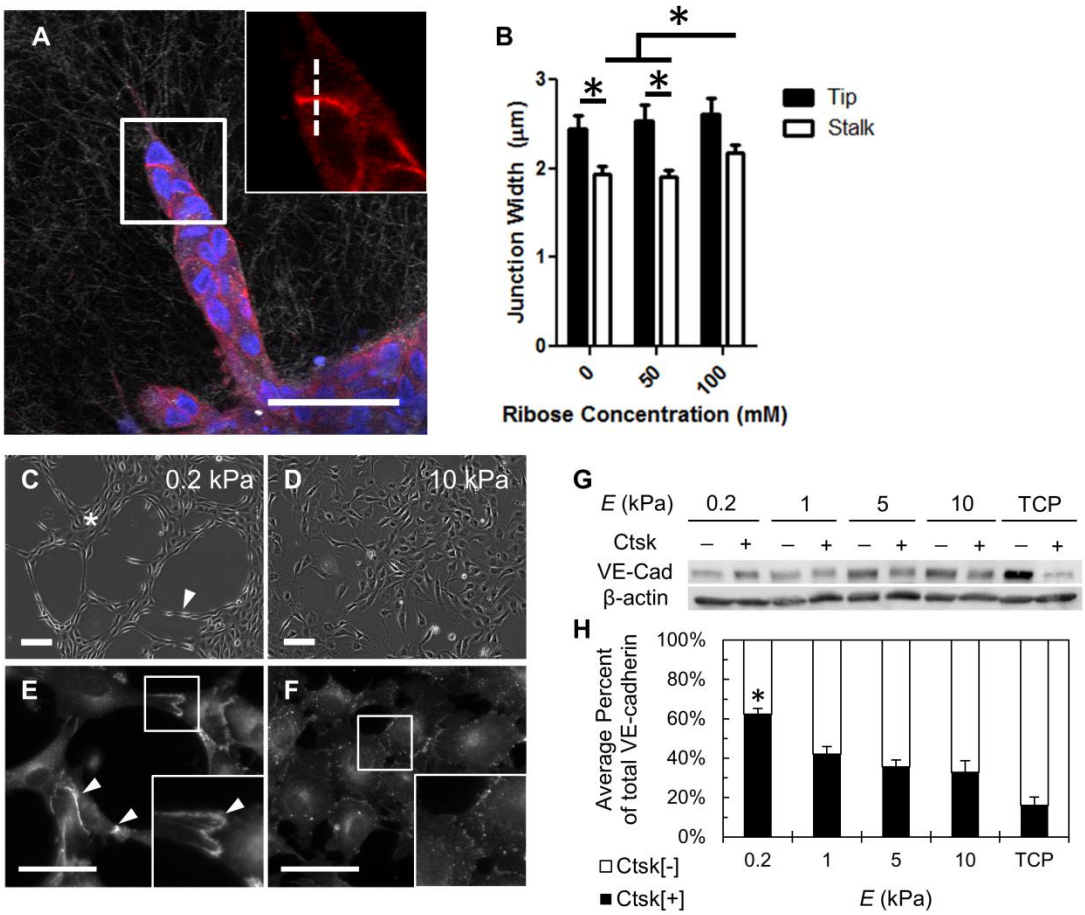

Figure 3.8. Matrix stiffness alters VE-cadherin expression and junction width. (A) EC spheroids were fixed 24 hours after embedding within 1.5 mg/ml collagen gels glycated with 0, 50, or 100 mM ribose and imaged with confocal microscopy to visualize VE-cadherin (red) and nuclei (blue) with confocal reflectance of the collagen fibers. The profile of VE-cadherin junctions were acquired by drawing a line perpendicular to the junction (dotted line) and (B) widths were quantified at the tip or within the stalk of the sprouts. Scale is 50 μm. ECs were seeded on (C) compliant (0.2 kPa) or (D) stiff (10 kPa) PA substrates. Scale is 100 μm. (E) On compliant substrates, VE-cadherin localization was continuous at cell-cell junctions (arrowheads). (F) On stiff substrates, VE-cadherin localization was punctate at cell-cell junctions. Scale is 50 μm. (G) Western blot and (H) quantification of VE-cadherin fractionated to localize association with the cytoskeleton (Ctsk +/-; E, Young's Modulus; TCP, tissue culture plastic). Insets are magnifications of boxed regions, Data presented as mean + SEM, * indicates $p<0.05$.

Figure 3.7C-F contributed by Dr. Joseph Califano

Figure 3.7G-H contributed by Dr. Christine Montague

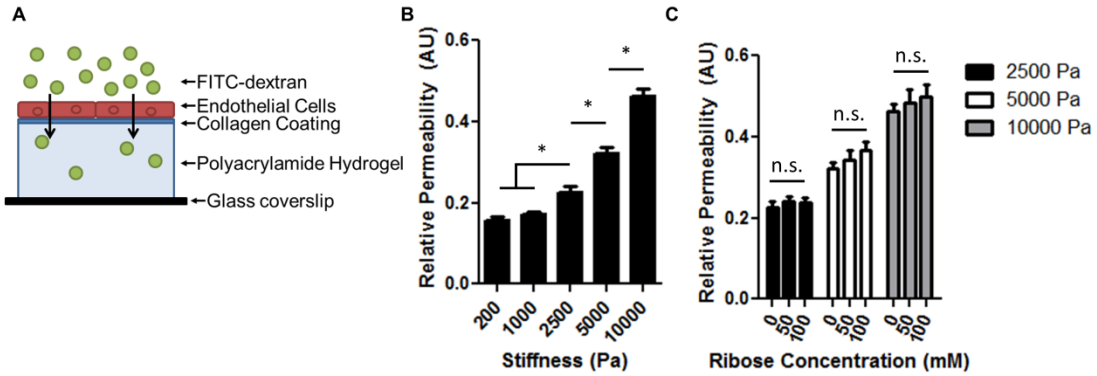

Figure 3.9. Endothelial cell permeability is modulated by collagen stiffness but not by collagen glycation. (A) Schematic of setup showing ECs grown to confluence on polyacrylamide hydrogels with elastic moduli ranging from 0.2-10 kPa and coated with 0.1 mg ml-1 of collagen glycated with 0, 50, or 100 mM ribose. The permeability of the ECs to 40kDa FITC-dextran was measured by monitoring the flux of fluorescence into the hydrogels in response to (B) stiffness and (C) collagen glycation. Data presented as mean + SEM, * indicates $p<0.05$.

continuous between cells while those on stiff substrates were punctate (Figure 3.8E,F; inset is a magnification of boxed region). To quantify the effect of matrix stiffness on VE-cadherin localization, BAECs plated on PA substrates ranging from 0.2 kPa to tissue culture plastic (TCP; polystyrene, E=3GPa[41]) were analyzed by Western blot. Triton was used to fractionate insoluble and soluble VE-cadherin fractions, where the cytoskeleton-associated (Ctsk) insoluble fraction corresponds to mature endothelial cell junctions[32]. The percentage of total VE-cadherin associated with the cytoskeleton was quantified and plotted (Figure 3.8H). A significantly greater proportion of total VE-cadherin was associated with the cytoskeleton (Ctsk[+]) in soft, 0.2 kPa gels and decreased with increasing substrate stiffness (black bars) while the soluble fraction (Ctsk[-]) increased proportionally with increasing substrate stiffness (white bars).

To further investigate how matrix stiffness and collagen glycation modulates VE-

cadherin integrity, the permeability of BAEC monolayers on PA gels ranging from 0.2 kPa to 10 kPa were measured as described previously[33]. BAEC monolayers were immersed in a 10 μM solution of 40 kDa FITC-dextran and the accumulation of dextran was measured relative to the fluorescent intensity above the gels (Figure 3.9A). We found that increasing the substrate stiffness significantly increases the permeability of endothelial cell monolayers (Figure 3.9B). Interestingly, we found no association between the extent of collagen glycation and endothelial permeability at a given stiffness (Figure 3.9C) suggesting that endothelial cells may be more responsive to the stiffness of their matrix than to the extent of collagen glycation. Together, these data indicate that the stiffness of the substrate modulates the integrity of VE-cadherin junctions, with compliant substrates encouraging the formation of tight and mature cell-cell interactions.

3.5 Discussion

While several studies have investigated the role of increasing three-dimensional matrix stiffness via matrix density on angiogenesis, much less is known about role of cross-linking on the formation of vascular structures. Here, we modulate matrix stiffness by increasing the amount of non-enzymatic glycation cross-linking. We show that increasing the extent of glycation increases the stiffness of the resultant collagen gels but only minimally changes the collagen fiber structure (Figure 3.1B,C). Additionally, we found that increasing the density of the matrices resulted in reduced angiogenic outgrowth from endothelial spheroids (Figure 3.2B) while increasing the cross-linking increased the extent of outgrowth and branching in endothelial spheroids

and in the ex ovo embryonic chick model (Figures 3.2B, 3.3B, and 3.5F). We also show that inhibiting MMP activity with GM6001 prevents the increased outgrowth from spheroids in cross-linked matrices and alters the resultant angiogenic sprout morphology (Figure 3.4). Interestingly, we demonstrate that endothelial cell-cell junctional properties are modulated by the stiffness of the matrix and that the localization of VE-cadherin and the permeability of endothelial monolayers are significantly altered by matrix stiffness (Figures 3.8A-H, 3.9B). Together, these results show that three-dimensional matrix stiffness plays an important role in regulating angiogenesis and vascular stability.

The Warburg effect, whereby cells produce energy through glycolysis instead of through oxidative phosphorylation, has been generally acknowledged to be a metabolic hallmark of cancer[42,43]. During glycolysis, glucose is converted into pyruvate to create adenosine triphosphate (ATP). Importantly, intermediates in the glycolytic pathway have been shown to be precursors of AGE cross-link formation[44,45]. Indeed, AGEs have been found in a number of different tumors types but the relationship between these cross-links and the integrity of the tumor vasculature has not been well-studied[20]. Our data suggest that increasing matrix stiffness through non-enzymatic glycation alters angiogenesis and endothelial cell-cell junctional integrity (Figures 3.2B, 3.8B). Future work should focus on understanding how processes such as the Warburg effect influence tumor vascular function in vivo.

In addition to the changes in ECM mechanics, the vasculature within tumors is known

to be more permeable than in normal tissues[3]. Our data demonstrate that increasing matrix stiffness increases endothelial cell-cell junction widths (Figure 3.8B) and modifies the localization of VE-cadherin from Ctsk[+] (mature, cell-cell junctions) to Ctsk[-] (soluble, cytoplasm) (Figure 3.8G,H). Further, we show that increasing the stiffness of the matrix also increases the permeability of endothelial monolayers (Figure 3.9B). Others have shown that increasing the amount of soluble VE-cadherin can induce endothelial membrane protrusions[46]. Recent work from the Gerhardt lab suggests that increased VE-cadherin dynamics lead to active endothelial cell movements within the sprout and branching morphogenesis[47]. Taken together, these observations provide a possible link between VE-cadherin localization and sprouting dynamics.

Methods to study the role of stiffness on angiogenesis in naturally-derived hydrogels have primarily focused on altering matrix density and have typically found that increased density decreases angiogenesis[15,17,18,48]. We also observed that increasing collagen density decreases angiogenic outgrowth from endothelial cells spheroids (Figure 3.2) but visibly altered the collagen fiber architecture (Figure 3.1B). However, glycation of 1.5, 5, or 10 mg ml^{-1} collagen with 0-100 mM ribose only minimally altered the resultant fiber arrangements in collagen gels (Figure 3.1B) while modulating the stiffness of the matrix (Figure 3.1C). Interestingly, when the stiffness of the matrix is increased through glycation, we observed increased angiogenic sprouting both in vitro ex ovo (Figures 3.2, 3.5F). Notably, work by Francis-Sedlak et al., showed a transient, decreased angiogenic sprouting in matrices that had been

stiffened by glycation with glucose-6-phospate[49]. However, prior work by Francis-Sedlak et al., showed that, collagen gels glycated with glucose-6-phosphate have a 2-fold increase in the volume fraction of insoluble materials when compared to collagen gels that were not glycated[50]. They attributed the increase in insoluble materials to increased fiber size or swelling of collagen fibers. In our previously published work, we quantified that autocorrelation mean radius to compare the fiber structural properties between glycated collagen gels and showed that 1.5 mg ml^{-1} gels that had been glycated with 0-100 mM ribose had only minimal differences in fiber structural properties; suggesting that large differences in fiber size or swelling do not exist in our system[22]. These differences in gel structural properties could account for the discrepancies in our experimental results. Additionally, recently published work investigating the effects of stiffening collagen matrices by using microbial transglutaminase or by varying the ratio of collagen monomers to oligomers supports our findings of increased angiogenic outgrowth in stiffer matrices[51,52].

Previously published work has shown that MMP activity is an important regulator of angiogenesis[15,53–55]. GM6001 is a broad-spectrum MMP inhibitor that is known to inhibit degradation of collagen by MMPs and, interestingly, has been shown to reduce the formation of angiogenic structures in response to matrix density of fibrin gels[15]. Here, we demonstrate that MMP activity is essential for the increased angiogenic response we observed within the stiffer, cross-linked, 1.5 mg ml^{-1} collagen gels (Figure 3.4). Surprisingly, we only observed a small decrease in angiogenic sprouting after 3 days of culture in the softer collagen gels with GM6001 treatment (Figure

3.4B). However, we did see a dramatic change in the sprout morphology from spheroids embedded within both the soft and stiff collagen gels and treated with GM6001 (Figure 3.4A,C,D). Prior studies have seen differences in the angiogenic sprouting response when using extended time periods (3-21 days)[15,54], different GM6001 concentrations (0.1-5 μM)[15,54,55], or increased collagen matrix density (2.5-3.75 mg ml^{-1})[54,55]. It is possible that culturing the spheroids for an increased time period or in higher density collagen gels with the GM6001 treatment would further demonstrate a decreased angiogenic response in gels that are less cross-linked. Taken together, these data show that MMPs are integral to the formation angiogenic sprouts from spheroids.

3.6 Conclusions

This chapter describes the effects of modulating matrix stiffness via AGE cross-linking on vessel architecture and integrity. Increasing collagen stiffness by increasing cross-linking at a given collagen density significantly increased the in vitro outgrowth from spheroids and ex ovo angiogenesis in the embryonic chick model while MMP inhibition prevented this response. Additionally, collagen stiffness modulated the extent of angiogenic branching, endothelial cell-cell junctional integrity, and permeability. These results indicate that three-dimensional matrix stiffness is an important regulator of angiogenesis and vascular integrity. While this study focuses on the biophysical mechanisms of angiogenesis, future work should further investigate the role of matrix stiffness on mediating the molecular mechanisms of angiogenic outgrowth.

REFERENCES

1 Levental KR, Yu H, Kass L, Lakins JN, Egeblad M, Erler JT, Fong SF, et al. Matrix crosslinking forces tumor progression by enhancing integrin signaling. Cell 2009; 139:891–906.

2 Trédan O, Galmarini CM, Patel K, Tannock IF, Tredan O. Drug resistance and the solid tumor microenvironment. J Natl Cancer Inst 2007; 99:1441–1454.

3 Hashizume H, Baluk P, Morikawa S, McLean JW, Thurston G, Roberge S, Jain RK, et al. Openings between defective endothelial cells explain tumor vessel leakiness. Am J Pathol 2000; 156:1363–80.

4 Carmeliet P. VEGF gene therapy: stimulating angiogenesis or angiomagenesis? Nat Med 2000; 6:1102–1103.

5 Jain RK. Normalization of tumor vasculature: an emerging concept in antiangiogenic therapy. Science 2005; 307:58–62.

6 Verheul HMW, Pinedo HM. The Role of Vascular Endothelial Growth Factor (VEGF) in Tumor Angiogenesis and Early Clinical Development of VEGFReceptor Kinase Inhibitors. Clin Breast Cancer 2000; 1:S80–S84.

7 Lu P, Weaver VM, Werb Z. The extracellular matrix: a dynamic niche in cancer progression. J Cell Biol 2012; 196:395–406.

8 Boyd NF, Lockwood G a, Byng JW, Tritchler DL, Yaffe MJ. Mammographic densities and breast cancer risk. Cancer Epidemiol Biomarkers Prev 1998; 7:1133–44.

9 McCormack VA, dos Santos Silva I. Breast density and parenchymal patterns as markers of breast cancer risk: a meta-analysis. Cancer Epidemiol Biomarkers Prev 2006; 15:1159–69.

10 Eriksson L, Czene K, Rosenberg LU, Törnberg S, Humphreys K, Hall P. Mammographic density and survival in interval breast cancers. Breast Cancer Res 2013; 15:R48.

11 Maskarinec G, Pagano IS, Little MA, Conroy SM, Park S-Y, Kolonel LN. Mammographic density as a predictor of breast cancer survival: the Multiethnic Cohort. Breast Cancer Res 2013; 15:R7.

12 Barker HE, Chang J, Cox TR, Lang G, Bird D, Nicolau M, Evans HR, et al. LOXL2-mediated matrix remodeling in metastasis and mammary gland involution. Cancer Res 2011; 71:1561–72.

13 Le Q-T, Harris J, Magliocco AM, Kong CS, Diaz R, Shin B, Cao H, et al. Validation of lysyl oxidase as a prognostic marker for metastasis and survival in head and neck squamous cell carcinoma: Radiation Therapy Oncology Group trial 90-03. J Clin Oncol 2009; 27:4281–6.

14 Kniazeva E, Putnam AJ. Endothelial cell traction and ECM density influence both capillary morphogenesis and maintenance in 3-D. Am J Physiol Cell Physiol 2009; 297:C179–87.

15 Ghajar CM, Blevins KS, Hughes CC, George SC, Putnam AJ. Mesenchymal Stem Cells Enhance Angiogenesis Early Matrix Metalloproteinase Upregulation. Tissue Eng 2006; 12:2875–88.

16 Shen CJ, Raghavan S, Xu Z, Baranski JD, Yu X, Wozniak M a, Miller JS, et al. Decreased cell adhesion promotes angiogenesis in a Pyk2-dependent manner. Exp Cell Res 2011; 317:1860–71.

17 Cross VL, Zheng Y, Won Choi N, Verbridge SS, Sutermaster BA, Bonassar LJ, Fischbach C, et al. Dense type I collagen matrices that support cellular remodeling and microfabrication for studies of tumor angiogenesis and vasculogenesis in vitro. Biomaterials 2010; 31:8596–8607.

18 Edgar LT, Underwood CJ, Guilkey JE, Hoying JB, Weiss J a. Extracellular matrix density regulates the rate of neovessel growth and branching in sprouting angiogenesis. PloS One 2014; 9:e85178.

19 Maillard LC. Action des acides amines sur les sucres: formation des melanoides par voie methodique. Comptes Rendus de l'Academie des Sciences 1912; 154:66–68.

20 Van Heijst JWJ, Niessen HWM, Hoekman K, Schalkwijk CG. Advanced glycation end products in human cancer tissues: detection of Nepsilon-(carboxymethyl)lysine and argpyrimidine. Ann N Y Acad Sci 2005; 1043:725–33.

21 Takino J-I, Yamagishi S-I, Takeuchi M. Cancer malignancy is enhanced by glyceraldehyde-derived advanced glycation end-products. J Oncol 2010; 2010:739852.

22 Mason BN, Starchenko A, Williams RM, Bonassar LJ, Reinhart-King CA. Tuning three-dimensional collagen matrix stiffness independently of collagen

concentration modulates endothelial cell behavior. Acta Biomater 2013; 9:4635–44.

23 Roy R, Boskey A, Bonassar LJ. Processing of type I collagen gels using nonenzymatic glycation. J Biomed Mater Res A 2010; 93A:843–851.

24 Quinn TM, Grodzinsky AJ. Longitudinal modulus and hydraulic permeability of poly(methacrylic acid) gels: effects of charge density and solvent content. Macromolecules 1993; 26:4332–4338.

25 Yalcin HC, Shekhar A, Rane AA, Butcher JT. An ex-ovo Chicken Embryo Culture System Suitable for Imaging and Microsurgery Applications. J Vis Exp 2010; 44:doi:10.3791/2154.

26 Nguyen M, Shing Y, Folkman J. Quantitation of Angiogenesis and Antiangiogenesis in the Chick Embryo Chorioallantoic Membrane. Microvasc Res 1994; 47:31–40.

27 Reinhart-King CA. Endothelial cell adhesion and migration. Methods Enzymol 2008; 443:45–64.

28 Califano JP, Reinhart-King CA. A Balance of Substrate Mechanics and Matrix Chemistry Regulates Endothelial Cell Network Assembly. Cell Mol Bioeng 2008; 1:122–132.

29 Kraning-Rush CM, Califano JP, Reinhart-King CA. Cellular Traction Stresses Increase with Increasing Metastatic Potential. PLoS One 2012; 7:e32572.

30 Pless DD, Lee YC, Roseman S, Schnaar RL. Specific cell adhesion to immobilized glycoproteins demonstrated using new reagents for protein and glycoprotein immobilization. J Biol Chem 1983; 258:2340–2349.

31 Califano JP, Reinhart-King CA. Substrate stiffness and cell area drive cellular traction stresses in single cells and cells in contact. Cell Mol Bioeng 2010; 3:68–75.

32 Lampugnani MG, Corada M, Caveda L, Breviario F, Ayalon O, Geiger B, Dejana E. The molecular organization of endothelial cell to cell junctions: differential association of plakoglobin, beta-catenin, and alpha-catenin with vascular endothelial cadherin (VE-cadherin). J Cell Biol 1995; 129:203–17.

33 Huynh J, Nishimura N, Rana K, Peloquin JM, Califano JP, Montague CR, King MR, et al. Age-related intimal stiffening enhances endothelial permeability and leukocyte transmigration. Sci Transl Med 2011; 3:112ra122.

34 Kraning-Rush CM, Carey SP, Califano JP, Smith BN, Reinhart-King CA. The role of the cytoskeleton in cellular force generation in 2D and 3D environments. Phys Biol 2011; 8:15009.

35 Stokes CL, Lauffenburger D a, Williams SK. Migration of individual microvessel endothelial cells: stochastic model and parameter measurement. J Cell Sci 1991; 99 (Pt 2):419–30.

36 Reinhart-King CA, Dembo M, Hammer DA. Cell-Cell Mechanical Communication through Compliant Substrates. Biophys J 2008; 95:6044–6051.

37 Kraning-Rush CM, Carey SP, Lampi MC, Reinhart-King C a. Microfabricated collagen tracks facilitate single cell metastatic invasion in 3D. Integr Biol (Camb) 2013; 5:606–16.

38 Hassouna MS, Farag a. a. Robust Centerline Extraction Framework Using Level Sets. 2005 IEEE Computer Society Conference on Computer Vision and Pattern Recognition (CVPR'05) 2005; 1:458–465.

39 Gonzalez RC, Woods RE. Digital Image Processing. Upper Saddle River, NJ: Prentice Hall 2011.

40 Dvorak HF, Nagy JA, Dvorak JT, Dvorak AM. Identification and characterization of the blood vessels of solid tumors that are leaky to circulating macromolecules. Am J Pathol 1988; 133:95–109.

41 Bonaccurso E, Cappella B, Graf K. Local mechanical properties of plasma treated polystyrene surfaces. J Phys Chem B 2006; 110:17918–24.

42 Hsu PP, Sabatini DM. Cancer cell metabolism: Warburg and beyond. Cell 2008; 134:703–7.

43 Hanahan D, Weinberg RA. Hallmarks of cancer: the next generation. Cell 2011; 144:646–74.

44 Phillips SA, Thornalley PJ. The formation of methylglyoxal from triose phosphates. Investigation using a specific assay for methylglyoxal. Eur J Biochem 1993; 212:101–105.

45 Hamada Y, Araki N, Koh N, Nakamura J, Horiuchi S, Hotta N. Rapid Formation of Advanced Glycation End Products by Intermediate Metabolites of Glycolytic Pathway and Polyol Pathway. Biochem Biophys Res Commun 1996; 228:339–345.

46 Kouklis P, Konstantoulaki M, Malik AB. VE-cadherin-induced Cdc42 signaling regulates formation of membrane protrusions in endothelial cells. J Biol Chem 2003; 278:16230–6.

47 Bentley K, Franco CA, Philippides A, Blanco R, Dierkes M, Gebala V, Stanchi F, et al. The role of differential VE-cadherin dynamics in cell rearrangement during angiogenesis. Nat Cell Biol 2014; 16:309–21.

48 Mason BN, Reinhart-King CA. Controlling the mechanical properties of three-dimensional matrices via non-enzymatic collagen glycation. Organogenesis 2013; 9:70–5.

49 Francis-Sedlak ME, Moya ML, Huang J-J, Lucas SA, Chandrasekharan N, Larson JC, Cheng M-H, et al. Collagen glycation alters neovascularization in vitro and in vivo. Microvasc Res 2010; 80:3–9.

50 Francis-Sedlak ME, Uriel S, Larson JC, Greisler HP, Venerus DC, Brey EM. Characterization of type I collagen gels modified by glycation. Biomaterials 2009; 30:1851–1856.

51 Lee P-F, Bai Y, Smith RL, Bayless KJ, Yeh a T. Angiogenic responses are enhanced in mechanically and microscopically characterized, microbial transglutaminase crosslinked collagen matrices with increased stiffness. Acta biomaterialia 2013; 9:7178–90.

52 Whittington CF, Yoder MC, Voytik-Harbin SL. Collagen-polymer guidance of vessel network formation and stabilization by endothelial colony forming cells in vitro. Macromol Biosci 2013; 13:1135–49.

53 Hotary K, Allen E, Punturieri A, Yana I, Weiss SJ. Regulation of cell invasion and morphogenesis in a three-dimensional type I collagen matrix by membrane-type matrix metalloproteinases 1, 2, and 3. J Cell Biol 2000; 149:1309–23.

54 Bayless KJ, Davis GE. Sphingosine-1-phosphate markedly induces matrix metalloproteinase and integrin-dependent human endothelial cell invasion and lumen formation in three-dimensional collagen and fibrin matrices. Biochem Biophys Res Commun 2003; 312:903–913.

55 Saunders WB, Bohnsack BL, Faske JB, Anthis NJ, Bayless KJ, Hirschi KK, Davis GE. Coregulation of vascular tube stabilization by endothelial cell TIMP-2 and pericyte TIMP-3. J Cell Biol 2006; 175:179–91.

CHAPTER 4

HISTOLOGICAL ANALYSIS OF THE TUMOR VASCULATURE IN HUMANS AND MICE

Portions of this chapter are in preparation for submission. Murine and human tumors were analyzed as part of collaborative projects with Dr. Valerie M. Weaver and Dr. Sandra Shin, respectively.

4.1 Abstract

The tumor vasculature is known to be more dense, disordered, and permeable than the vasculature in normal tissue. Additionally, cells within the tumor deposit and cross-link matrix proteins during the process of tumorigenesis, thereby creating a stiffer extracellular environment with altered protein expression. The objectives of the work presented in this chapter are two-fold. First, we sought to understand how the extracellular stiffness of murine mammary tumors influences vascular density and the association of mural cells with the vasculature. Secondly, based on previous data from our lab indicating that fibronectin expression is modulated by extracellular matrix stiffness[1], we investigated the expression an alternatively-spliced isoform of fibronectin in human mammary tissue and tumors. We show that vascular density and the localization of mural cells are altered within murine mammary tumors where collagen cross-linking has been disrupted. We further demonstrate that a specific splice variant of fibronectin (EDB-FN) typically associated with angiogenic blood

vessels is also found within the vasculature of human breast tumors but not in patient-matched normal tissue. Together, these data show that the tumor vasculature is inherently different than that of normal tissue and suggests that matrix stiffness may play a role in these alterations.

4.2 Introduction

During the process of the solid tumor formation, multiple changes occur to the physical and chemical environment of the extracellular matrix (ECM). Indeed, tumors are known to be stiffer than normal tissue and importantly, these mechanical changes have been correlated with altered cellular function and ECM deposition[2–4]. The ECM protein fibronectin (FN) has been suggested to be correlated with cancer severity[5,6]. However, it is unclear how tumor formation is related to the deposition and alternative splicing of new matrix proteins such as "extra domain B"-fibronectin (EDB-FN) by endothelial cells (EC). Additionally, blood vessels within solid tumors are known to be more dense, tortuous, and leaky when compared to those in normal, healthy tissues[7,8]. The presence of mural cells (MCs; pericytes and vascular smooth muscle cells) that stabilize and support the vasculature has been shown to be altered in solid tumors[9–11]. However, the role of matrix stiffness on MC-coverage of the tumor vasculature has not been studied. This chapter discusses the histological analysis of human and murine mammary tumors to investigate MC localization, vessel density, and fibronectin expression in the vasculature.

Staining of the vasculature in murine mammary tumors

The vascular density and MC localization of murine mammary tumors were studied as part of a collaborative project with Prof. Valerie M. Weaver at The University of California, San Francisco. Current work in the Weaver lab suggests that tumor stiffness influences the permeability of the vasculature in a number of murine models (unpublished). MCs are supporting cells that directly contact ECs and provide both physical and chemical cues to stabilize the vasculature. In the tumor vasculature, these cues are known to be dis-regulated and MC-coverage of vessels is altered[9,10,12]. In fact, decreases in MC-coverage have been implicated in increased vascular permeability and intravasation of tumor cells[10,11,13]. Here, we show that vascular density and MC-coverage were altered in mice that had been treated to inhibit lysyl oxidase activity or induce β_1 integrin clustering.

Fibronectin staining in human breast tumors

In order for angiogenesis to occur, the polymerization of the dimeric glycoprotein fibronectin by endothelial cells is required[14]. Notably, increased extracellular matrix stiffness, vascularity, and fibronectin expression are all correlated with increased breast cancer aggressiveness[3,15,16]. We have previously shown that matrix stiffening regulates the rate of angiogenesis as well as the resultant blood vessel architecture and integrity in vitro[17–19]. Previous work in the Reinhart-King lab has also shown that the synthesis and deposition of fibronectin is influenced by the stiffness of the ECM[20]. In recent work, we found that the expression of a specific splice variant of fibronectin (termed “extra domain B” fibronectin (EDB-FN)) that is normally only present during

embryonic development and with angiogenic blood vessels is regulated by ECM stiffness[21]. Here, we stained for the presence of EDB-FN in invasive ductal carcinomas and patient-matched normal mammary tissues. We found that EDB-FN is present in the vasculature of tumor tissue but is absent in normal mammary tissue. Since EDB-FN is generally undetectable within normal adult tissues, its presence in the in vivo breast tumor vasculature could lead to new clinical therapeutics.

4.3 Materials and Methods

CD31 and aSMA staining of Mouse Tumors

Mouse mammary tumor slides were provided by Dr. Valerie Weaver from The University of California, San Francisco. Immunohistochemistry slides were deparaffinized in xylene (VWR, Radnor, PA), rehydrated in graded ethanol (VWR), and washed in water. Heat activated antigen retrieval was performed in a pH 6, 0.01 M sodium citrate buffer (Sigma-Aldrich, St. Louis, MO) and slides were washed with 0.05% tween (JT Baker, Phillipsburg, NJ) in D-PBS (Invitrogen, Carlsbad, CA). Blocking was performed using a mouse-on-mouse kit (Vector Laboratories, Burlingame, CA) at the recommended concentrations. Endothelial cells and smooth muscle cells were stained with a rabbit polyclonal CD31 antibody (1:100; Santa Cruz Biotechnology, Dallas, TX) and a mouse monoclonal αSMA antibody (1:50; Dako, Carpinteria, CA), respectively, and for 1 hour at room temperature. The secondary antibodies were Alexa Fluor 568 donkey anti-rabbit (Invitrogen) and Alexa Fluor 488 goat anti-mouse (Invitrogen) and were incubated for 30 minutes at room temperature. All antibodies were applied using the diluent from the mouse-on-mouse kit. Nuclei

were counterstained with 4',6-diamidino-2-phenylindole (DAPI) (Sigma-Aldrich). Slides were mounted in Vectashield (Vector Laboratories) and imaged using a Zeiss LSM 700 with a water-immersion C-Apochromat 40x/1.1 NA objective (Carl Zeiss, Oberkochen, Germany).

Analysis of vessel density and αSMA+ vessels in mouse tumors

CD31 positive vessels with open lumens were scored as being αSMA positive (αSMA+) or αSMA negative (αSMA-). A vessel was identified as αSMA+ if any portion of the vessel was visibly in contact with αSMA staining. Vessel density was calculated by dividing the number of vessels scored for the αSMA+ by the sum of the area of DAPI staining in each image in ImageJ. Images were acquired using similar parameters.

EDB-FN staining of Human Tumors

Formalin-fixed, paraffin-embedded, invasive ductal carcinoma and patient-matched normal human breast tissue were provided by Dr. Sandra Shin from New York Presbyterian Hospital-Weill Cornell Medical College. For each tumor case, 4-μm-thick sections were deparaffinized in xylene, rehydrated in graded alcohols, and antigen retrieval was performed in a pH 6, 0.1 M citrate buffer. Envision+System-HRP (DAB) (Dako) was used for immunostaining according to the manufacturer's protocol. The sections were incubated overnight at $4^{O}C$ with a mouse anti-human EDB-FN antibody (1:200, BC1; Abcam, MA). Primary antibody was omitted for negative controls. Slides were counterstained with Harris hematoxylin (VWR) and

mounted with permount (Thermo Fisher Scientific, Waltham, MA). Slides were imaged on an A1 Axio Scope with an Axio Cam MRc5 color camera (Carl Zeiss).

4.4 Results

Modulating LOX activity changes MC-coverage and vessel density in murine tumors

To investigate the role of in vivo tumor stiffness on MC-coverage of the vasculature, sections of mammary tumors from FVB/N-Tg(MMTV-PyVT)634Mul/J mice (herein described as PyMT mice) that had been treated to inhibit lysyl oxidase (LOX), were used. Lysly oxidase (LOX), a collagen cross-linker, is frequently elevated in tumors and has been shown to cause matrix stiffening[22,23]. Previous studies have shown that lysyl oxidase activity is inhibited in mice that have been treated with beta-aminopropionitrile (BAPN) or an anti-LOX inhibitory antibody (α-LOXab)[2,24].

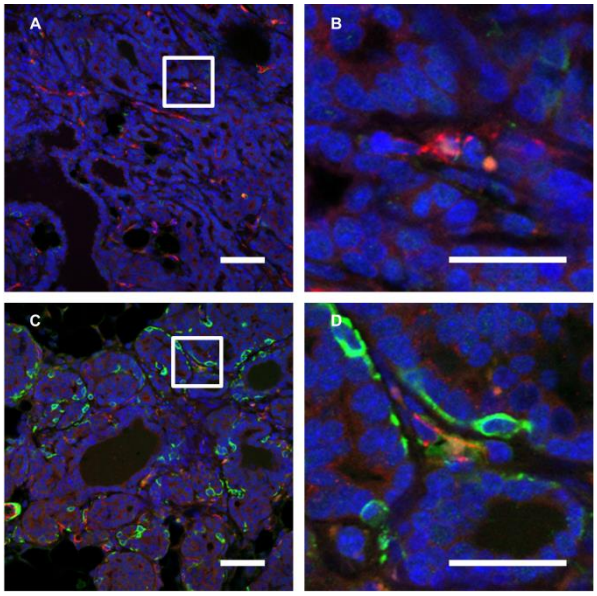

Figure 4.1. Immunohistochemical staining of murine breast tissue for αSMA (green), CD31 (red), and nuclei (blue). (A) PyMT tumor section with outlined region (B) showing an αSMA- vessel. (C) PyMT tumor treated with BAPN with (D) showing an αSMA+ vessel. Scale in A,C is 50 μm, Scale in B,D is 25 μm.

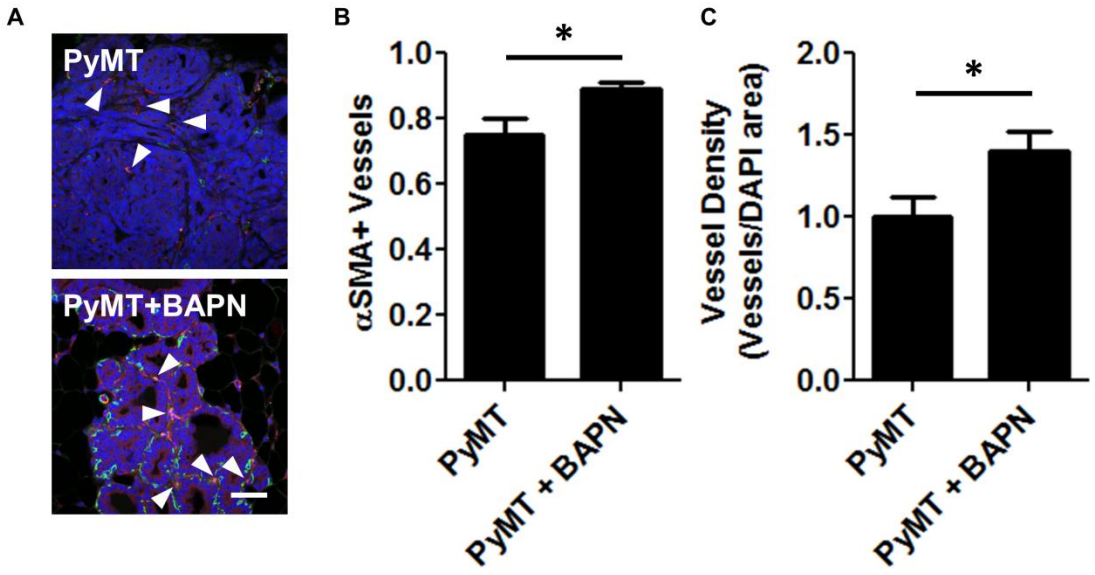

Figure 4.2. Vessel density and α-SMA expression are increased in BAPN-treated PyMT mice. (A) Immunohistochemical staining of murine breast tissue for α-SMA (green), CD31 (red), and nuclei (blue) with arrowheads denoting vessels. Quantification of the percentage of (B) α-SMA(+) vessels and (C) vessel density. Data presented as mean + SEM, * indicates $p<0.05$, Scale is 50 μm.

Tumor sections from PyMT mice treated with BAPN or α-LOXab were stained for CD31, αSMA, or nuclei and vessels were identified as being αSMA-negative (αSMA-) (Figure 4.1A,B) or αSMA-positive (αSMA+) (Figure 4.1C,D). Interestingly, BAPN-treated PyMT mice had a significantly greater proportion of αSMA+ vessels and an increased vessel density compared to PyMT control mice (Figure 4.2). Surprisingly, PyMT mice treated with α-LOXab had a decreased proportion of αSMA+ vessels (Figure 4.3B). While the number of vessels was slightly increased in vessels treated with the α-LOXab, the trend was not significant (Figure 4.3A,C). These data indicate that modulating the activity of LOX in the tumor was capable of altering the density of the vasculature and its association with MCs.

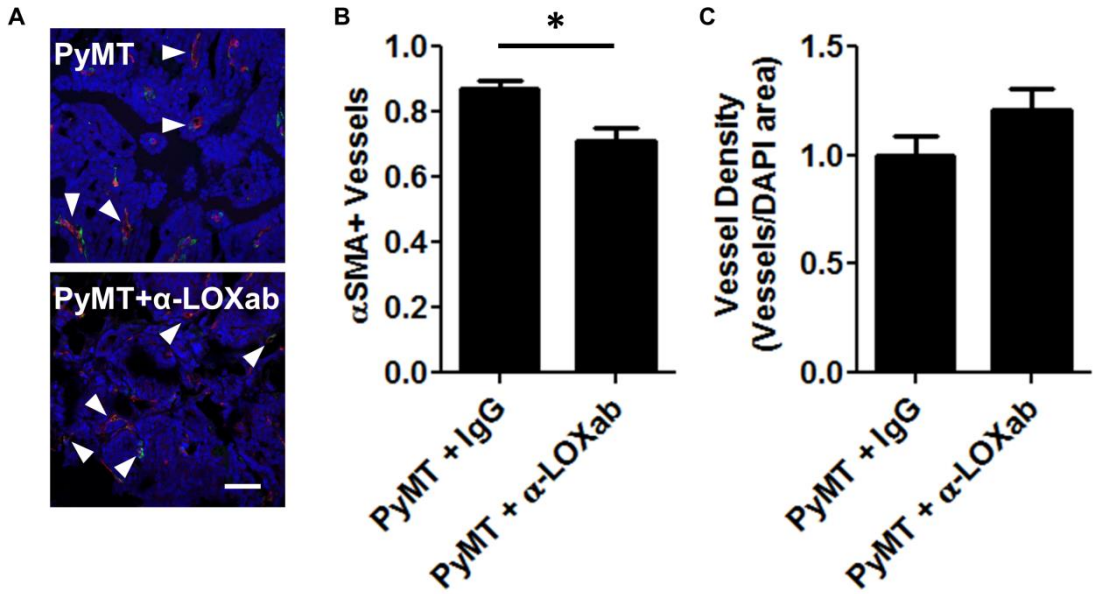

Figure 4.3. α-SMA expression is decreased in PyMT mice treated with α-LOX antibody. (A) Immunohistochemical staining of murine breast tissue for α-SMA (green), CD31 (red), and nuclei (blue) with arrowheads denoting vessels. Quantification of the percentage of (B) α-SMA(+) vessels and (C) vessel density. Data presented as mean + SEM, * indicates $p<0.05$, Scale is 50 μm.

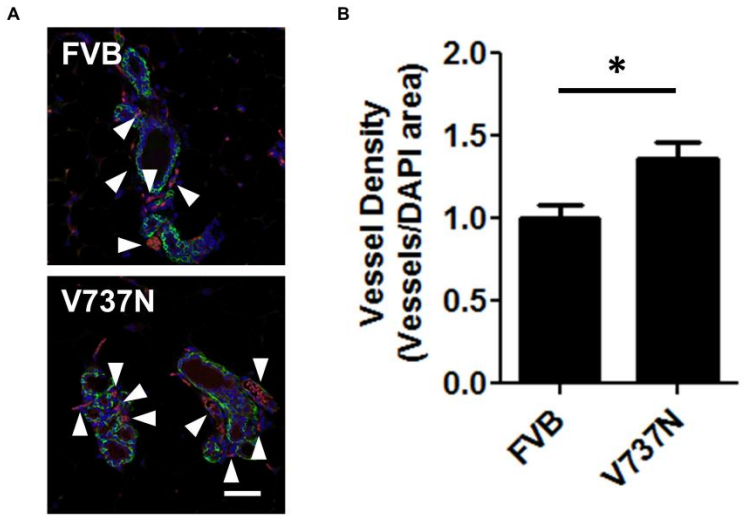

Figure 4.4. Vessel density is increased in V737N mice compared to FVB mice. (A) Immunohistochemical staining of murine breast tissue for α-SMA (green), CD31 (red), and nuclei (blue) with arrowheads denoting vessels. (B) Quantification of the vessel density. Data presented as mean + SEM, * indicates $p<0.05$, Scale is 50 μm.

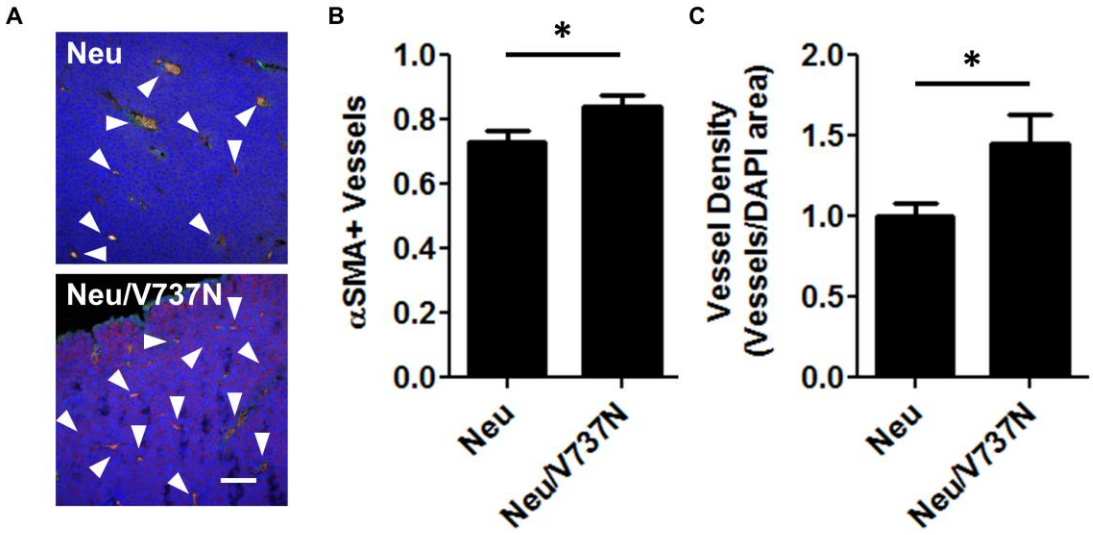

Figure 4.5. Vessel density and α-SMA expression are increased in Neu/V737N mice. (A) Immunohistochemical staining of murine breast tissue for α-SMA (green), CD31 (red), and nuclei (blue) with arrowheads denoting vessels. Quantification of the percentage of (B) α-SMA(+) vessels and (C) vessel density. Data presented as mean + SEM, * indicates $p<0.05$, Scale is 50 μm.

Increased integrin clustering increases MC-coverage and vessel density in murine tumors

To study the role of β_1 integrin clustering on MC localization within the microvasculature, FVB/N-Tg(MMTVneu)202Mul/J mice, also known as MMTV-Her-2/neu mice (herein described as Neu mice), with or without a mutation for V737N β_1 integrin clustering were used. Previous studies have shown that the V737N mutant induces focal adhesion formation and increased tumor size but the effects of the mutation on MC localization are unknown[3]. Normal tissue sections from FVB control or V737N mice or tumor sections from Neu or Neu/V737N mice were stained for CD31, αSMA, or nuclei and vascular density was quantified. Additionally, the proportion of αSMA+ vessels was quantified for Neu or Neu/V737N tumors. We found that V737N mice had significantly increased vascular density when compared to

FVB controls (Figure 4.4). Interestingly, increasing β_1 integrin clustering in Neu mice increased the extent of αSMA+ vessels and vascular density within the tumors compared to Neu tumors alone (Figure 4.5). These data show that V737N tumors exhibited increased vascular density compared to FVB controls and suggest that increasing β_1 integrin clustering alters the association of MCs with the vasculature.

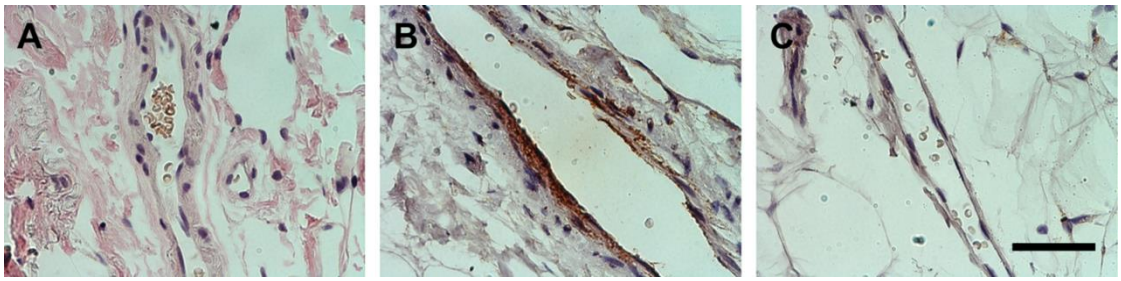

Figure 4.6. EDB-FN is expressed in human breast tumor vasculature. Immunohistochemical staining of human breast tissue for EDB-FN showing (A) negative control of the tumor vasculature, (B) strong EDB-FN staining in the tumor vasculature, and (C) no immunoreactivity for EDB-FN in the normal tissue vasculature. Images were acquired at same exposure settings, Scale is 50 μm.

EDB-FN is expressed in the human tumor vasculature

To determine if human breast tumors express EDB-FN, sections of invasive ductal carcinomas and patient-matched normal breast tissue were stained for EDB-FN. Our results show strong EDB-FN staining in the vessel wall within the tumor vasculature and no EDB-FN staining in normal breast tissue (Figure 4.6). These observations indicate that FN in the tumor vasculature has been alternatively spliced to contain the EDB-region and suggest that targeting EDB-FN may be one way to localize therapeutics to the tumor vasculature.

4.5 Discussion

While several studies have shown a decrease in MC coverage of the vasculature in tumors, much less is known about how the extracellular matrix mechanical properties of the tumor regulate MC localization of matrix deposition of FN splice variants. Here, we have used histological staining and analysis to study the localization of MCs and vascular density in mouse tumors and the localization of EDB-FN human tissue. We show that modulating LOX activity or β_1 integrin clustering altered the vascular density and localization of MCs. We also show that EDB-FN is localized to the tumor vasculature but was not seen in the vasculature of normal tissues.

LOX-mediated cross-linking is known to play a role in tumor matrix stiffening and has been implicated in the promotion of breast cancer metastasis[22,23,25]. The inhibition of LOX through treatment with BAPN or α-LOXab has been previously shown to decrease collagen cross-linking, focal adhesion, and tumor incidence[3,26]. However, our results unexpectedly indicated that the localization of MCs with the tumor vasculature was increased in PyMT tumors treated with BAPN and decreased in those treated with α-LOXab (Figures 4.2,4.3). We speculate that the differences in MC localization in the BAPN and the α-LOXab are due to tumor stage and progression. In fact, the tissue sections we analyzed for mice treated with α-LOXab were later stage than those from BAPN-treated mice (15 weeks vs. 10 weeks). Our collaborators have confirmed that while inhibiting stiffness with either BAPN or α-LOXab reduced vascular permeability in 9-12 week old animals, there ceases to be differential effects of matrix stiffness on vascular permeability in late stage, 15 week, tumors.

The V737N mutation replaces a hydrophobic valine with asparagine in the β_1 integrin to promote clustering through increased hydrogen bonding[27]. Interestingly, increased spreading, integrin clustering, and force generation are observed when the V737N mutation is expressed in mammary epithelial cells plated on soft substrates in vitro[27]. The β_1 integrin has been implicated as a key regulator in the regulation of EC tube formation, basement membrane matrix deposition, and EC-MC interactions[28]. Our data indicate that increasing β_1 integrin clustering with the V737N mutation in Neu tumors increases vascular density and the localization of MCs with the vasculature (Figure 4.5). These results suggest that enhancing integrin clustering may be one way to enhance MC-EC association.

EDB-FN is often referred to as oncofetal-fibronectin because of its expression in fetal development and cancer. Importantly, we have recently found that expression of EDB-FN is regulated by matrix stiffness[21]. Here, we found that EDB-FN was expressed in the vasculature of human invasive ductal carcinomas while it is absent in patient-matched normal tissue Figure 4.6). These results suggest that EDB-FN could be utilized as a specific marker to target tumor vasculature.

4.6 Conclusions

This chapter describes the histological staining of mammary tumors to study protein composition, MC localization, and vascular density. We found that murine mammary tumors modulate the extent of MC-coverage and density of the vasculature when LOX

activity is inhibited or β_1 integrin clustering is induced. Additionally we found that EDB-FN is expressed in human mammary tumors but not in patient-matched controls. Together, these data indicate that the process of tumorigenesis drastically changes the composition and density of the vasculature.

REFERENCES

1 Califano JP. Substrate stiffness regulates capillary network assembly. 2012.

2 Lopez JI, Kang I, You W-K, McDonald DM, Weaver VM. In situ force mapping of mammary gland transformation. Integr Biol (Camb) 2011; 3:910–921.

3 Levental KR, Yu H, Kass L, Lakins JN, Egeblad M, Erler JT, Fong SF, et al. Matrix crosslinking forces tumor progression by enhancing integrin signaling. Cell 2009; 139:891–906.

4 Baluk P, Morikawa S, Haskell A, Mancuso M, McDonald DM. Abnormalities of basement membrane on blood vessels and endothelial sprouts in tumors. Am J Pathol 2003; 163:1801–15.

5 Park J, Schwarzbauer JE. Mammary epithelial cell interactions with fibronectin stimulate epithelial-mesenchymal transition. Oncogene 2014; 33:1649–57.

6 Von Au A, Vasel M, Kraft S, Sens C, Hackl N, Marx A, Bermejo JL, et al. Circulating Fibronectin Controls Tumor Growth. Neoplasia 2013; 15:925–938.

7 Vakoc BJ, Lanning RM, Tyrrell J a, Padera TP, Bartlett L a, Stylianopoulos T, Munn LL, et al. Three-dimensional microscopy of the tumor microenvironment in vivo using optical frequency domain imaging. Nature medicine 2009; 15:1219–23.

8 McDonald DM, Choyke PL. Imaging of angiogenesis: from microscope to clinic. Nature medicine 2003; 9:713–25.

9 Morikawa S, Baluk P, Kaidoh T, Haskell A, Jain RK, McDonald DM. Abnormalities in pericytes on blood vessels and endothelial sprouts in tumors. Am J Pathol 2002; 160:985–1000.

10 Yonenaga Y, Mori A, Onodera H, Yasuda S, Oe H, Fujimoto A, Tachibana T, et al. Absence of smooth muscle actin-positive pericyte coverage of tumor vessels correlates with hematogenous metastasis and prognosis of colorectal cancer patients. Oncology 2005; 69:159–66.

11 Welén K, Jennbacken K, Tesan T, Damber J-E. Pericyte coverage decreases invasion of tumour cells into blood vessels in prostate cancer xenografts. Prostate Cancer Prostatic Dis 2009; 12:41–6.

12 Jain RK, Booth MF. What brings pericytes to tumor vessels ? J Clin Invest 2003; 1134–1136.

13 Hellström M, Gerhardt H, Kalén M, Li X, Eriksson U, Wolburg H, Betsholtz C. Lack of pericytes leads to endothelial hyperplasia and abnormal vascular morphogenesis. J Cell Biol 2001; 153:543–553.

14 Zhou X, Rowe RG, Hiraoka N, George JP, Wirtz D, Mosher DF, Virtanen I, et al. Fibronectin fibrillogenesis regulates three-dimensional neovessel formation. Genes Dev 2008; 22:1231–1243.

15 Bae YK, Kim A, Kim MK, Choi JE, Kang SH, Lee SJ. Fibronectin expression in carcinoma cells correlates with tumor aggressiveness and poor clinical outcome in patients with invasive breast cancer. Hum Pathol 2013; 44:2028–2037.

16 Visscher DW, Smilanetz S, Drozdowicz S, Wykes SM. Prognostic significance of image morphometric microvessel enumeration in breast carcinoma. Anal Quant Cytol Histol 1993; 15:88–92.

17 Mason BN, Starchenko A, Williams RM, Bonassar LJ, Reinhart-King C a. Tuning three-dimensional collagen matrix stiffness independently of collagen concentration modulates endothelial cell behavior. Acta Biomater 2013; 9:4635–44.

18 Huynh J, Nishimura N, Rana K, Peloquin JM, Califano JP, Montague CR, King MR, et al. Age-related intimal stiffening enhances endothelial permeability and leukocyte transmigration. Sci Transl Med 2011; 3:112ra122.

19 Mason BN, Mazzola MC, Somasegar S, Califano JP, Montague CR, Kang Y, LaValley D, et al. Collagen cross-linking increases angiogenesis and disrupts barrier integrity. In Preparation 2014;

20 Califano JP, Reinhart-King CA. A Balance of Substrate Mechanics and Matrix Chemistry Regulates Endothelial Cell Network Assembly. Cell Mol Bioeng 2008; 1:122–132.

21 Califano JP, Mason BN, Yuan L, Charest JM, Shin SJ, Reinhart-King CA. Substrate stiffness alters fibronectin matrix deposition via cell shape and traction force polarity. In Preparation 2014;

22 Erler JT, Bennewith KL, Nicolau M, Dornhofer N, Kong C, Le QT, Chi JT, et al. Lysyl oxidase is essential for hypoxia-induced metastasis. Nature 2006; 440:1222–1226.

23 Pfeiffer BJ, Franklin CL, Hsieh FH, Bank RA, Phillips CL. Alpha 2(I) collagen deficient oim mice have altered biomechanical integrity, collagen content, and collagen crosslinking of their thoracic aorta. Matrix Biol 2005; 24:451–458.

24 Pickup MW, Laklai H, Acerbi I, Owens P, Gorska AE, Chytil A, Aakre M, et al. Stromally derived lysyl oxidase promotes metastasis of transforming growth factor-β-deficient mouse mammary carcinomas. Cancer Res 2013; 73:5336–46.

25 El-Haibi CP, Bell GW, Zhang J, Collmann AY, Wood D, Scherber CM, Csizmadia E, et al. Critical role for lysyl oxidase in mesenchymal stem cell-driven breast cancer malignancy. Proc Natl Acad Sci U S A 2012; 109:17460–5.

26 Mouw JK, Yui Y, Damiano L, Bainer RO, Lakins JN, Acerbi I, Ou G, et al. Tissue mechanics modulate microRNA-dependent PTEN expression to regulate malignant progression. Nat Med 2014; 20:360–7.

27 Paszek MJ, Zahir N, Johnson KR, Lakins JN, Rozenberg GI, Gefen A, Reinhart-King CA, et al. Tensional homeostasis and the malignant phenotype. Cancer Cell 2005; 8:241–254.

28 Stratman AN, Malotte KM, Mahan RD, Davis MJ, Davis GE. Pericyte recruitment during vasculogenic tube assembly stimulates endothelial basement membrane matrix formation. Blood 2009; 114:5091–5101.

CHAPTER 5

DEVELOPMENT OF A MICROFLUIDIC DEVICE TO STUDY CHEMOTACTIC AND DUROTACTIC CUES ON CELLULAR MIGRATION

Portions of this chapter are in preparation for submission[1].

5.1 Abstract

Cell behavior is influenced by both the local mechanical and chemical microenvironment. To study the interplay and balance between chemical and mechanical cues, we developed a microfluidic device to expose cells cultured on substrates of well-characterized, tunable stiffness to well-defined, stable chemical gradients. The device utilizes source, culture, and sink channels to regulate the cellular chemical environment while simultaneously permitting control of the mechanical environment using polyacrylamide (PA) substrates of known stiffness. This device was used to study two distinct phenomena: the formation of podosomes in vascular smooth muscle cells (VSMCs), and the combined roles of chemotaxis and durotaxis in endothelial cells (ECs). Herein, we describe the device design and gradient generation characterization. While we found that the microfluidic device was not well-suited to experiments involving the chemotaxis of ECs to vascular endothelial growth factor, we did demonstrate that gradients of the phorbol ester PDBu stimulated podosomes in a directed manner in VSMCs. Together, these data demonstrate that the described microfluidic platform could be amenable to the study of chemotaxis,

durotaxis, or molecular activation in a number of cellular systems.

5.2 Introduction

Cells within the vasculature are continuously exposed to different chemical and mechanical stimuli. The effects of chemical factors such as vascular endothelial growth factor (VEGF) on endothelial cell (EC) behavior have been extensively studied and it is well established that ECs migrate up a gradient to higher concentrations of VEGF. The stiffness of the extracellular matrix (ECM) has also been shown to play an important role on EC and vascular smooth muscle cell (VSMC) function[2–4]. However, the combined effects of ECM stiffness and chemotactic factors have not been well-studied. Here, we develop a microfluidic device to test the additive and potentially synergistic effects of combining chemical gradients and mechanical cues. Because there is no suitable tool currently available to study chemical gradients and matrix mechanics simultaneously, we developed a microfluidic device that maintains a stable concentration gradient and simultaneously allows cells to be seeded on matrices of tunable compliance. We utilized this device to study the migratory response of ECs to matrix stiffness and VEGF and also investigated the formation of podosomes in VSMCs stimulated with gradients of the phorbol ester PDBu.

EC Migration

Angiogenesis is important to many biological processes including wound healing and cancer progression. During angiogenesis, ECs migrate from a pre-existing vessel into the surrounding tissue to form new vessels. A better understanding of EC migration

can lead to therapeutics to regulate angiogenesis and promote better wound healing or inhibit tumor vascularization.

VEGF is an important protein involved in EC migration, proliferation, and angiogenesis and it is well known that ECs tend to migrate towards increasing concentrations. In addition, it has become apparent that matrix mechanics play an important role in dictating cell behavior[5,6]. Indeed, there is an important balance between the extracellular matrix compliance and chemistry in EC function[3,7]. However, the extent to which matrix mechanics influence EC migration during chemotaxis has not been explored, as most chemotaxis studies have been done on polystyrene or glass.

To study the interplay and balance between chemical and mechanical cues, we have developed a microfluidic device to expose cells cultured on substrates of well-characterized, tunable stiffness to well-defined, stable chemical gradients. The device utilizes source, culture, and sink channels to regulate the cellular chemical environment while simultaneously permitting control of the mechanical environment using polymer substrates of known stiffness. We have used this device to investigate the combined roles of chemotaxis and durotaxis on EC migration.

Using this novel device, the migration of EC was measured in response to linear gradients of vascular endothelial growth factor (VEGF) on collagen-functionalized substrates. ECs adhere, migrate, and proliferate within the microfluidic culture

channel. Unfortunately, ECs did not undergo chemotaxis within the device for reasons we discuss. Although we found that this device is not amenable to EC migration with VEGF, it could be used to study the combined roles of chemotaxis and durotaxis in response to other chemotactic molecules.

Podosome Formation

Podosomes are dynamic actin-rich cellular structures capable of adhering to and degrading extracellular matrix (ECM)[8–10]. As such, podosomes are largely found in invasive cell types, including macrophages, osteoclasts, and dendritic cells[11,12]. More recently, vascular smooth muscle cells (VSMCs) have also been shown to form podosomes when induced by phorbol esters or growth factors[13,14]. Podosomes are thought to mediate VSMC migration and may contribute to intimal hyperplasia in response to vascular injury or atherosclerosis[8,14,15]. However, very little is known about the chemical and physical cues in the microenvironment that induce and mediate podosome formation. Here, we show that chemical gradients of phorbol esters can trigger directed podosome formation.

5.3 Materials and Methods

Cell culture

A7R5 rat aortic smooth muscle cells were maintained in DMEM (Invitrogen, Carlsbad, CA) supplemented with 10% fetal bovine serum (Invitrogen) and 1% of penicillin-streptomycin (Invitrogen) at 37°C in a 5% CO_2 incubator. Cells were transfected with 1 μg ml^{-1} actin-eGFP (a gift from David Holowka, Department of

Chemistry and Chemical Biology, Cornell University, Ithaca, NY) in 3 μg ml^{-1} Lipofectamine 2000 (Invitrogen). Media was replenished after 4 hours of lipofection.

Bovine aortic endothelial cells (Vec Technologies, Rensselaer, NY) were used until passage 12. Cells were fed every other day with M199 (Invitrogen) supplemented with 10% Fetal Clone III (HyClone, Logan, UT) and 1% each of MEM amino acids (Invitrogen), MEM vitamins (Mediatech, Manassas, VA), and penicillin-streptomycin at kept in a 37°C in a 5% CO_2 incubator.

Polyacrylamide gel synthesis

Polyacrylamide (PA) hydrogels were synthesized as described previously by varying the ratio of acrylamide (40% w/v solution, Bio-Rad, Hercules, CA) and N,N'-methylene-bis-acrylamide (2% w/v solution, Bio-Rad) to tune the Young's moduli of the gels[3,16,17]. The PA gels were made on a 3 x 1 in. glass slide so they could be incorporated into the microfluidic device manifold. PA substrates were functionalized with N-6-((acryloyl)amido)hexanoic acid, succinimidyl ester (N-6) that was synthesized in our lab and bound to 0.1 mg ml^{-1} type I rat tail collagen (Becton Dickinson, Franklin Lakes, NJ)[4,18].

Microfluidic device

Fabrication and assembly

Microfluidic channels were cast by pouring an agarose solution over a silicon master mold as described previously[19]. Briefly, an etched silicon wafer patterned with

positive reliefs was used to create a mold of the channel features. A polydimethlysiloxane (PDMS) (Dow Corning, Midland, MI) rectangular spacer was placed around the section of the silicon mold that was to be casted so the height of the resulting agarose mold could be precisely controlled. A heated, 3% (w/v) solution of agarose (Fisher Scientific, Pittsburg, PA) in PBS was poured into the center of the spacer. The agarose was allowed to gel over the positive reliefs of the channels while being compressed by a glass slide. Once the agarose gelled, the glass slide was removed and a punch was used to create holes over the port areas of the channels.

To construct the microfluidic device, the agarose mold containing the channels was inserted between a plexiglass manifold and a glass slide or polyacrylamide gel. A multichannel precision peristaltic pump (Mettler Toledo, Columbus, OH) was used to generate a stable flow of the chemotactic agent through the source chamber. The chemotactic agent was cleared from the device via media flowing in the sink channel at an identical rate, thereby creating a linear gradient of the chemical through the agarose gel and over the cells in the culture channel.

Validation of linear gradient

To validate the generation of a linear gradient, 0.1 mM of 10kDA FITC-dextran (Sigma-Aldrich) was flowed through the source channel, and the resultant fluorescent gradient was imaged. The pixel intensities of the images were measured in ImageJ and graphed as a function of distance away from the source channel (Figure 5.3).

Stimulation of EC migration with VEGF

To investigate the effect of substrate stiffness on EC response to a VEGF gradient, we utilized the microfluidic device to generate stable gradients of VEGF. A 5 kPa PA hydrogel was seeded with ECs, cells were allowed to spread overnight, and a microfluidic device was assembled with the cell-seeded PA slide. A multichannel precision peristaltic pump was used to generate a stable flow of 32ng ml^{-1} of VEGF in complete media through the source chamber of the microfluidic device. The VEGF was cleared from the device via complete media flowing in the sink channel at an identical rate, thereby creating a linear gradient of VEGF through the agarose gel. As a control, measurements were made using an identical chamber with complete media flowing through both the source and sink channels of the device. Cell migration was monitored with time-lapse microscopy beginning 1 hour after the beginning of VEGF or complete media flow for a period of 6 hours. Cell trajectories were tracked using ImageJ.

Stimulation of podosomes in A7R5 cells with PDBU

A glass slide was seeded with transfected VSMCs expressing actin-eGFP. Cells were allowed to spread overnight and a microfluidic device was assembled with the cell-seeded slide. All channels of the microfluidic device were primed with complete media. The peristaltic pump was used to generate a stable flow of 2 μM phorbol 12,13 dibutyrate (PDBu) (Sigma-Aldrich) through the source chamber and cleared from the device via media flowing in the sink channel at an identical rate.

Timelapse microscopy was used to monitor the formation of podosomes in real-time. To quantify the location of podosomes within individual cells, cells were segmented into two halves, and the number of podosomes was counted within each half. Cells with a majority of podosomes located closer to the PDBu source were labeled "proximal," those with podosomes located closer to the sink were labeled "distal," and those with equal number of podosomes throughout were labeled "equal."

5.4 Results and Discussion

Microfluidic device fabrication and characterization

To create a device that was capable of modulating both the mechanical and chemical

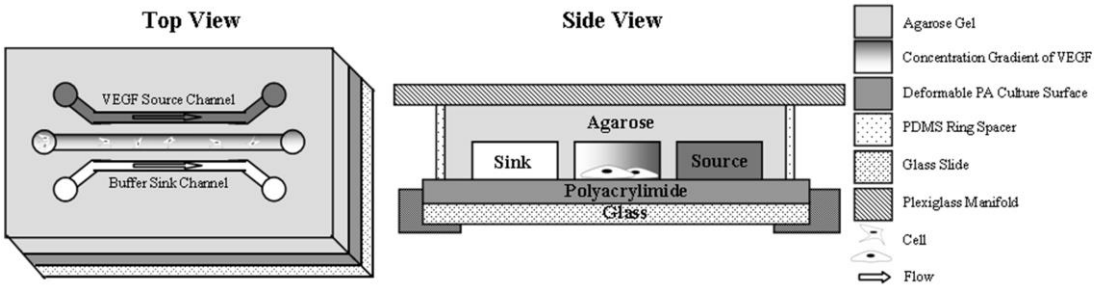

Figure 5.1. Schematic of microfluidic device assembly. Microfluidic channels were cast in agarose and assembled over polyacrylamide hydrogels within a manifold.

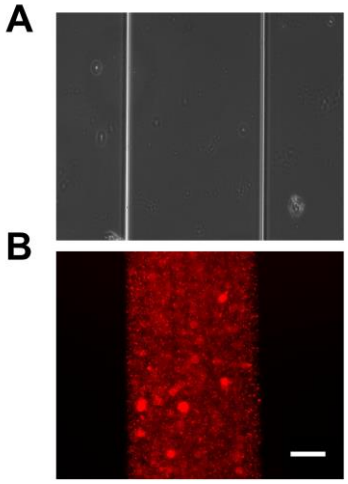

Figure 5.2. Microfluidic channels seal tightly with PA gels. (A) Phase contrast image of microfluidic channel and (B) fluorescence image of the same channel showing that 0.5 μm beads are completely contained within the channel. Scale is 50 μm.

environment of cells in culture, we modified an agarose-based, three-channel microfluidic device that has been previously used to study bacterial and mammalian cell chemotaxis[20,21]. A PA hydrogel substrate functionalized with N-6 and bound to 0.1 mg ml^{-1} collagen was incorporated into the device to control the stiffness of the substrate cells were seeded upon (Figure 5.1).

To determine whether the microfluidic device was operating as intended and created a stable, linear chemical gradient, a series of characterization tests were performed. To ensure that the agarose-molded channels sealed tightly to the PA substrate, a microfluidic device was assembled and 0.5 μm fluorescent beads were injected into the channels. Phase images were taken to localize the channels and fluorescence images were acquired to determine if there was any flow between the PA hydrogel and agarose (Figure 5.2). We found that the agarose sealed well to the PA substrate and beads were completely contained within the channels. Concentration gradients were quantified within the culture channel by using a 10kDa FITC-dextran fluorescent biomarker with a similar mobility as VEGF[22]. Phase images of the channels were acquired and matched to fluorescence images of the resultant gradient (Figure 5.3A,B). The intensity profiles of the fluorescence images were measured using ImageJ. We found that the device creates a nearly linear gradient from the source to the sink channel. The gradient was established within 30 minutes and was stable over the 16 hour experiment (Figure 5.3C). To ensure that the microfluidic device was suitable for long-term cell culture, microfluidic devices were assembled with PA gels seeded with ECs. ECs remained viable and proliferated within the channels

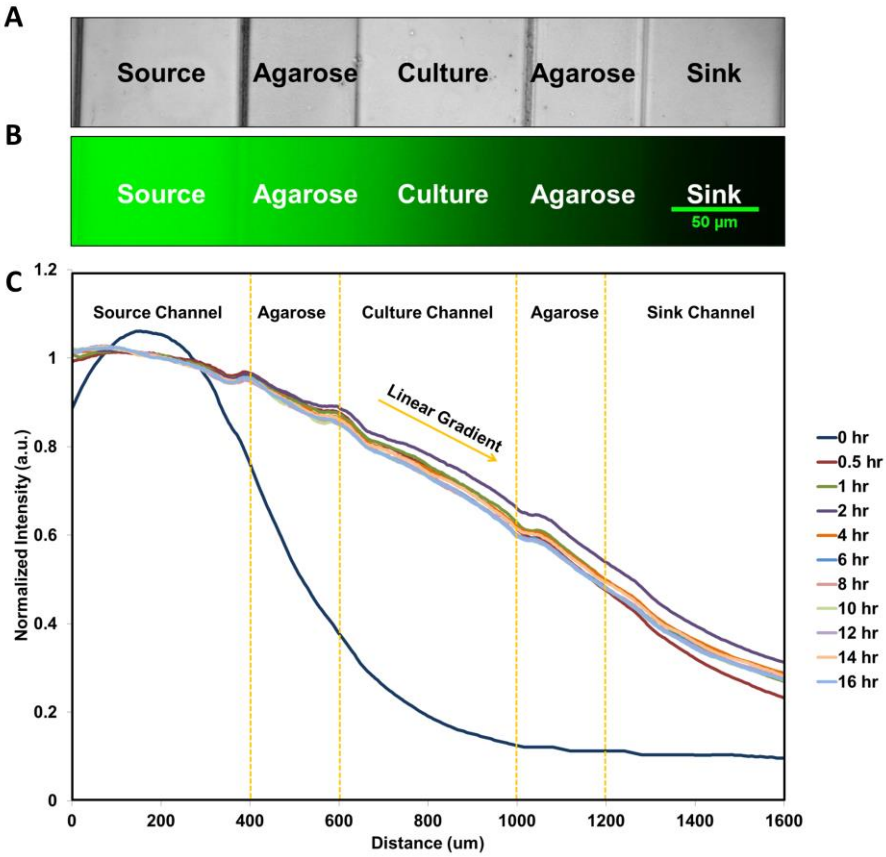

Figure 5.3. Example of gradient generation in the microfluidic device. Chemotactic agents in complete medium were flowed through the source channel and complete medium was flowed through the sink at an identical rate, creating a linear gradient of the chemotactic agent through the agarose. (A) Phase images showing the channels within the microfluidic device and (B) fluorescence images showing an established gradient. (C) Monitoring the fluorescence intensity through the source, culture, and sink channels over time indicated that gradients are established within 30 minutes and remained stable over the 16 hour study. Scale is 50 µm.

throughout the course of the 3-day experiment (data not shown). These data demonstrate that we were able to incorporate PA gels to control the stiffness of the substrate and that the resultant microfluidic device was amenable to cell culture and capable of generating and maintaining a linear chemical gradient.

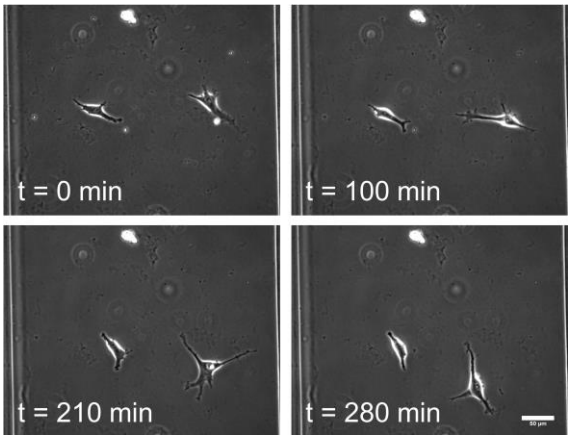

Figure 5.4. Timelapse images of ECs within the microfluidic device. Images show endothelial cells migrating within the channel over time. Scale is 50 μm.

EC chemotactic response to VEGF is limited in the microfluidic device

To investigate the combined chemotactic and durotactic response of ECs, ECs were seeded on a 5 kPa PA substrate, allowed to attach overnight, and assembled into a microfluidic device. A VEGF gradient was created by flowing 32 ng ml^{-1} VEGF into the source channel while complete medium was flowed into the sink channel. Cell migration in response to VEGF or control (no chemical) gradients were imaged using timelapse microscopy (Figure 5.4). Cells were traced using ImageJ and the trajectories were plotted (Figure 5.5). Surprisingly, the presence of VEGF did not elicit a chemotactic response from ECs. Similar results were obtained when chemotactic experiments were extensively repeated with glass and 0.5 kPa – 30 kPa substrates, with different concentrations of VEGF, or when human umbilical vein endothelial cells were used.

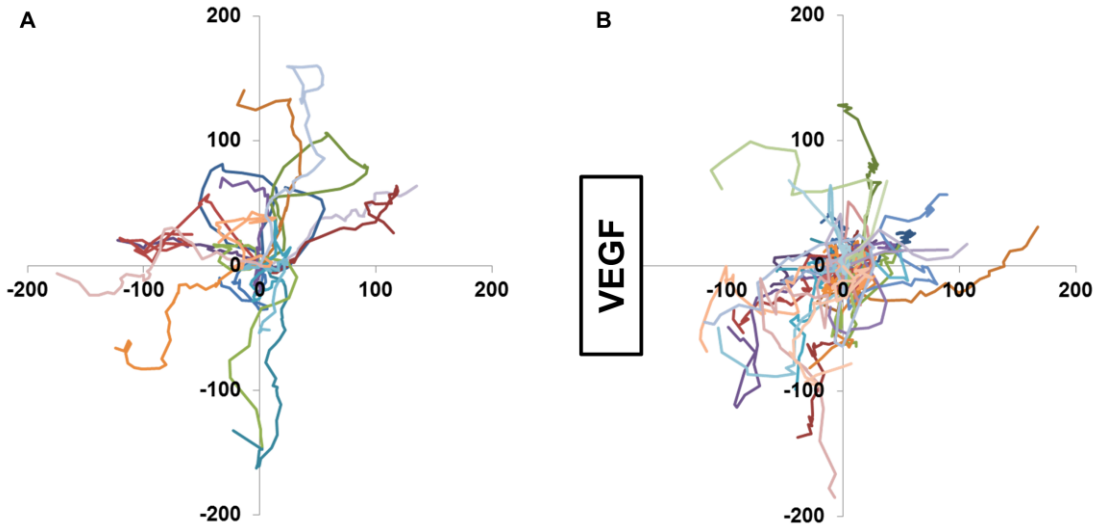

Figure 5.5. Cell trajectories of ECs within a microfluidic device demonstrate no preferential migration of ECs to VEGF. ECs were tracked for 6 hours in microfluidic devices with either (A) complete medium in both the source and sink channel (as a control) or (B) 32 ng/ml VEGF flowing through the source channel (location of VEGF channel marked).

VEGF has been repeatedly and consistently shown to have a chemotactic effect on ECs and adaptations of this device have been successfully used for a number of studies to generate chemical gradients across cells[20,21,23–26]. In combination with the lack of chemotaxis we have reported, these observations suggest that the formation and establishment of the VEGF chemotactic gradient was somehow prevented within our device. We hypothesize that VEGF was being sequestered within the agarose, thus precluding gradient formation. While we were able to demonstrate the establishment of a gradient using a 10 kDa FITC-dextran molecule with similar mobility to VEGF (Figure 5.3), experiments using a fluorescently-tagged VEGF were cost-prohibitive. However, investigating and validating gradient generation with fluorescently-tagged VEGF could help explain why these experiments were unsuccessful.

Importantly, even though we found that this device was not well-suited to the investigation of EC chemotaxis to VEGF, it could be used for other studies. For example, other studies have demonstrated the compatibility of agarose-based devices with epidermal growth factor (EGF) but these studies have not investigated the effects of mechanical stiffness on cellular function[26]. EGF is known to be a key factor in tumor growth and cancer cell invasion. During tumor metastasis, cancer cells migrate from the primary tumor and through a mechanically heterogeneous stromal environment to secondary metastatic sites. Since cancer cells are exposed to gradients of EGF and diverse mechanical environments during metastasis, it would be interesting to investigate the combined role of matrix mechanics and chemical gradients using the described microfluidic device.

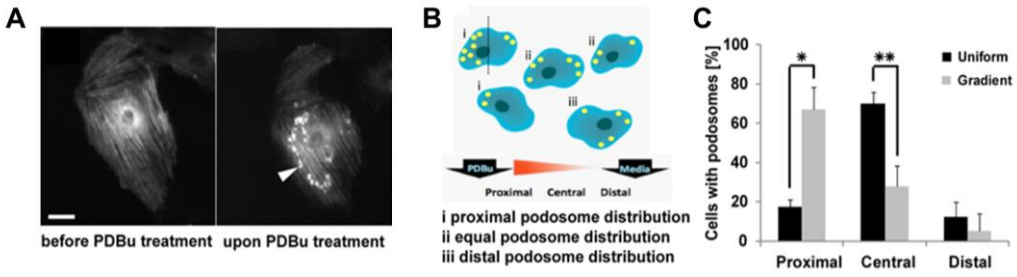

Figure 5.6. VSMCs form podosomes locally at the leading edge in response to a chemical gradient. (A) Representative images of VSMCs exhibiting podosomes after stimulation with a PDBu gradient. (B) Cartoon schematic of methods to quantify podosome location within the cell. Cells with a majority of podosomes located closer to the PDBu source were labeled "proximal," those with podosomes located closer to the sink were labeled "distal," and those with equal number of podosomes throughout were labeled "equal." (C) Quantification of the percentage of cells exhibiting podosomes proximal, central or distal to the PDBu source before and after PDBu gradient generation.

Podosomes are directionally formed towards increasing PDBu concentrations

To investigate the formation and localization of podosomes in VSMCs in respect to chemical cues, we used the microfluidic device to create linear chemical gradients of PDBu. Using this device, we stimulated actin-eGFP transfected VSMCs with a gradient of PDBu which resulted in robust podosome formation (Figure 5.6A). To characterize the location of podosome formation relative to the gradient, we quantified the percentage of cells that exhibited podosomes in response to the chemical gradient as a function of their position relative to the nucleus and the source channel of the gradient (Figure 5.6B). When stimulated uniformly by flowing PDBu through both the source and sink channels, the majority of cells formed podosomes with no preferential distribution (Figure 5.6C, dark bars). Interestingly, when stimulated with a linear gradient of PDBu, approximately 70% of cells formed podosomes proximal to the source channel. These data indicate that VSMC can respond to gradients by locally forming podosomes in the direction of the gradient.

Podosomes are thought to be important for cellular adhesion, matrix degradation, and migration[9,12,27]. While chemical cues are known to trigger the formation of podosomes, the formation of podosomes in response to chemical gradients has not been well studied. Our results show that VSMCs exposed to gradients of PDBu form podosomes that are localized proximally to increased concentrations (Figure 5.6). Interestingly, VSMC podosome formation has been suggested to contribute to the migration of VSMCs during atherosclerosis. These results suggest that chemical

gradients may have the ability to assist in mediating this response.

5.5 Conclusions

Cells within our body exist within a complex and dynamic environment filled with chemical and mechanical stimuli. This chapter describes the development and characterization of a microfluidic device to simultaneously investigate the effects of well-defined mechanical and chemical cues on cells. Chemical gradients within the device are established within 30 minutes of initiating flow of the chemotactic molecule and are maintained long-term allowing for observation of cell responses such as migration or cell activation. Interestingly, we found that PDBu gradients generated the directional formation of podosomes in VSMCs. Together, these results demonstrate that the described microfluidic device can be used to study cellular response to chemical and mechanical stimuli in different cell models.

REFERENCES

1 Kim NY, Huynh J, Mason BN, Carey SP, Kohn JC, Vouyouka A, Reinhart-King CA. Biophysical Inducation of Vascular Smooth Muscle Cell Podosomes. In Preparation.

2 Reinhart-King CA, Dembo M, Hammer DA. The dynamics and mechanics of endothelial cell spreading. Biophys J 2005; 89:676–689.

3 Califano JP, Reinhart-King CA. A Balance of Substrate Mechanics and Matrix Chemistry Regulates Endothelial Cell Network Assembly. Cell Mol Bioeng 2008; 1:122–132.

4 Califano JP, Reinhart-King CA. Substrate stiffness and cell area drive cellular traction stresses in single cells and cells in contact. Cell Mol Bioeng 2010; 3:68–75.

5 Discher DE, Janmey P, Wang Y-LL. Tissue cells feel and respond to the stiffness of their substrate. Science 2005; 310:1139–43.

6 Paszek MJ, Zahir N, Johnson KR, Lakins JN, Rozenberg GI, Gefen A, Reinhart-King CA, et al. Tensional homeostasis and the malignant phenotype. Cancer Cell 2005; 8:241–254.

7 Califano JP, Reinhart-king CA. Mechanical and Chemical Signaling in Angiogenesis. Berlin, Heidelberg: Springer Berlin Heidelberg 2013.

8 Burgstaller G, Gimona M. Podosome-mediated matrix resorption and cell motility in vascular smooth muscle cells. Am J Physiol Heart Circ Physiol 2005; 288:H3001–H3005.

9 Murphy DA, Courtneidge SA. The “ins” and “outs” of podosomes and invadopodia: characteristics, formation and function. Nat Rev Mol Cell Biol 2011; 12:413–426.

10 Linder S. The matrix corroded: podosomes and invadopodia in extracellular matrix degradation. Trends Cell Biol 2007; 17:107–117.

11 Linder S, Nelson D, Weiss M, Aepfelbacher M. Wiskott-Aldrich syndrome protein regulates podosomes in primary human macrophages. Proc Natl Acad Sci U S A 1999; 96:9648–9653.

12 Buccione R, Orth JD, McNiven MA. Foot and mouth: podosomes, invadopodia and circular dorsal ruffles. Nat Rev Mol Cell Biol 2004; 5:647–657.

13 Hai C-M, Hahne P, Harrington EO, Gimona M. Conventional protein kinase C mediates phorbol-dibutyrate-induced cytoskeletal remodeling in a7r5 smooth muscle cells. Exp Cell Res 2002; 280:64–74.

14 Quintavalle M, Elia L, Condorelli G, Courtneidge SA. MicroRNA control of podosome formation in vascular smooth muscle cells in vivo and in vitro. J Cell Biol 2010; 189:13–22.

15 Mak AS. P53 Regulation of Podosome Formation and Cellular Invasion in Vascular Smooth Muscle Cells. Cell Adh Migr 2011; 5:144–149.

16 Reinhart-King CA, Dembo M, Hammer DA. Cell-Cell Mechanical Communication through Compliant Substrates. Biophys J 2008; 95:6044–6051.

17 Kraning-Rush CM, Carey SP, Lampi MC, Reinhart-King C a. Microfabricated collagen tracks facilitate single cell metastatic invasion in 3D. Integr Biol (Camb) 2013; 5:606–16.

18 Pless DD, Lee YC, Roseman S, Schnaar RL. Specific cell adhesion to immobilized glycoproteins demonstrated using new reagents for protein and glycoprotein immobilization. J Biol Chem 1983; 258:2340–2349.

19 Cheng S-Y, Heilman S, Wasserman M, Archer S, Shuler ML, Wu M. No Title. Lab on a Chip 2007; 7:763–769.

20 Cheng S-Y, Heilman S, Wasserman M, Archer S, Shuler ML, Wu M. A hydrogel-based microfluidic device for the studies of directed cell migration. Lab Chip 2007; 7:763.

21 Diao J, Young L, Kim S, Fogarty E a., Heilman SM, Zhou P, Shuler ML, et al. A three-channel microfluidic device for generating static linear gradients and its application to the quantitative analysis of bacterial chemotaxis. Lab Chip 2006; 6:381.

22 Berk D a, Yuan F, Leunig M, Jain RK. Fluorescence photobleaching with spatial Fourier analysis: measurement of diffusion in light-scattering media. Biophys J 1993; 65:2428–36.

23 Haessler U, Kalinin Y, Swartz MA, Wu M. An agarose-based microfluidic platform with a gradient buffer for 3D chemotaxis studies. Biomed Microdevices 2009; 11:827–835.

24 Haessler U, Pisano M, Wu M, Swartz M a. Dendritic cell chemotaxis in 3D under defined chemokine gradients reveals differential response to ligands CCL21 and CCL19. Proc Natl Acad Sci U S A 2011; 108:5614–9.

25 Kalinin Y, Neumann S, Sourjik V, Wu M. Responses of Escherichia coli

bacteria to two opposing chemoattractant gradients depend on the chemoreceptor ratio. J Bacteriol 2010; 192:1796–800.

26 Kim BJ, Hannanta-anan P, Chau M, Kim YS, Swartz M a, Wu M. Cooperative roles of SDF-1α and EGF gradients on tumor cell migration revealed by a robust 3D microfluidic model. PLoS One 2013; 8:e68422.

27 Linder S, Kopp P. Podosomes at a glance. J Cell Sci 2005; 118:2079–82.

CHAPTER 6

EXPLORING TISSUE PERFUSION AND NUTRIENT DELIVERY IN THE CLASSROOM

6.1 Abstract

In June 2012, I was selected to be a fellow in Cornell's National Science Foundation Graduate STEM Fellows in K-12 Education (NSF GK-12) program. As part of this year-long fellowship, I had the privilege of working with Ms. Laura Austen, a high school biology teacher at Elmira Southside High School. During this time, I became the "scientist in residence" in Ms. Austen's classes and developed a number of lectures and inquiry-based laboratories to engage the students in experiential learning. This chapter will discuss my experiences with the program and detail the laboratories I developed to introduce the students blood vessel transport and tissue perfusion.

6.2 Introduction

Connections between the science curriculum that is taught in schools and real-world problems are not obvious to middle and high school students although such connections have been shown to be critical for student performance in STEM fields. The NSF funded Cornell Learning Initiative in Medicine and Bioengineering (CLIMB) GK-12 program pairs biomedical engineering (BME) graduate students (fellows) with local high school science teachers to provide opportunities for students to experience science and integrate knowledge across disciplines. The goals of the

NSF GK-12 program are to enhance the content of the science curriculum in a local classroom by interacting extensively with the teacher to introduce them to a research environment, developing new inquiry-based activities, and becoming a resident scientist in the classroom. GK-12 fellows, work with teachers both in the research lab on an original research project as well as in the classroom where new science experiments and activities are implemented based on the fellow's BME research. This program has allowed collaborations with high school teachers to develop and utilize simple, yet highly effective approaches to engage high school students in inquiry-based approaches to science to promote learning and retention. The GK12 fellow becomes a resident scientist, utilizing biomedical engineering as an integrative glue to connect the separate science disciplines (biology, chemistry, and physics) to relevant health issues.

I was paired with Laura Austen, a teacher from Elmira Southside High School who teaches the New York State Regents Living Environment course and an Advanced College Education General Biology course. During the summer of 2012, Laura familiarized herself with a number of techniques in the Reinhart-King lab including cell culture, hydrogel synthesis, microscopy, and immunofluorescence to complete a novel research project. During the academic year, I became a scientist in residence in Laura's classroom. Together, we developed a curriculum designed around the theme of blood vessel mechanics from my graduate research and incorporating the concept of diffusion to reinforce information learned in one of the New York State mandated laboratories for the Living Environments class. In addition, we created a number of

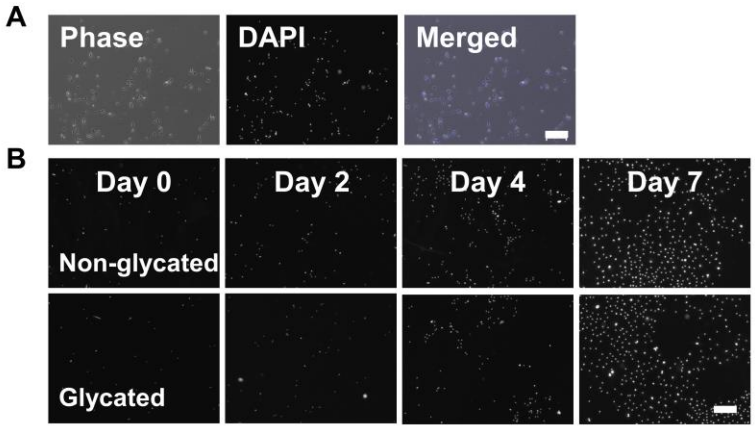

Figure 6.1. Proliferation on polyacrylamide hydrogels. (A) ECs on PA gels imaged imaged showing a phase image, DAPI staining, or merged image. (B) DAPI images of ECs on PA substrates coated with glycated or non-glycated collagen. Scale is 200 μm.

other modules and revised experimental protocols to promote inquiry-based learning, organized a "lunch with scientists" for junior and senior students, and held a field trip where the students toured the science facilities in the Biomedical Engineering Department, Veterinary School, and Nanofab Facilities at Cornell University. Working with Laura at Elmira Southside was an eye-opening experience that allowed me to learn how to translate and communicate complex scientific information into material that is relevant to high school students.

6.3 Results from Laura's summer research

Laura worked with me in the Reinhart-King lab during the summer of 2012 to experience how research is conducted in an academic setting. Her project was to determine the role of collagen glycation on endothelial cell proliferation. I taught Laura how to make polyacrylamide hydrogel substrates that were coated with collagen that had been glycated with 0 – 100 mM ribose. She also learned how to culture

endothelial cells, seed them on the polyacrylamide hydrogels, and then fix, stain, and image the cells after 0, 2, 4, or 7 days in culture (Figure 6.1). I wrote a custom algorithm in ImageJ to count the number of cells per field of view and Laura used this to process the image and analyzed the amount of endothelial cell proliferation on glycated or non-glycated substrates (Figure 6.2A). Laura determined that the endothelial cell proliferation was not a function of collagen glycation (Figure 6.2B). Laura created a poster that highlighted the work she completed over the summer and displayed it in her classroom as an example of how scientists communicate data to one another. Our experiences together in the research lab were instrumental in forming the basis for our curriculum materials.

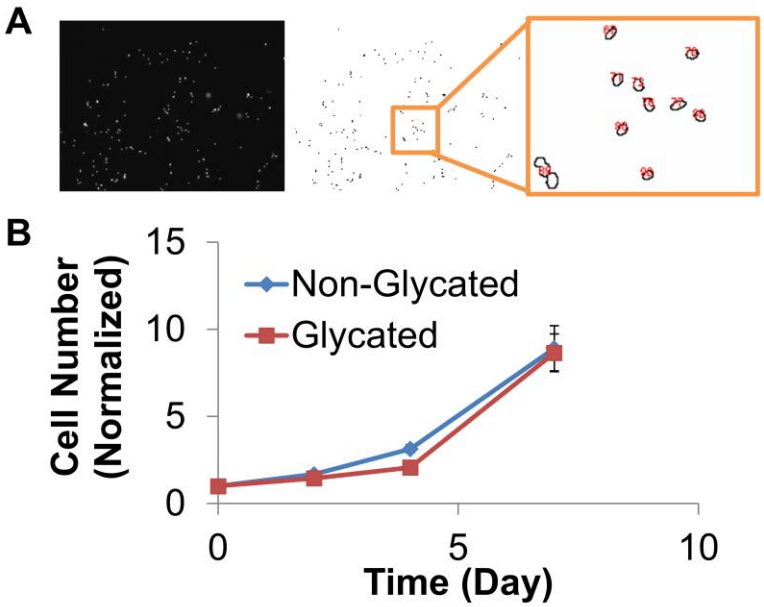

Figure 6.2. Proliferation on PA gels coated with glycated or non-glycated collagen. (A) Cells were stained with DAPI and counted using a custom ImageJ algorithm. (B) The average cell number per image was plotted against time. The number of cells increases on both glycated and non-glycated gels with time. Data were normalized to the Day 0 cell number. Scale is 200 μm.

6.4 Curriculum Development

The curriculum Laura and I developed includes two separate modules to investigate how the density of our tissues can influence nutrient transport and to relate how the foods and drinks we consume relate to our blood sugar levels. The transport module here utilizes gelatin-coated petri dishes that can be used to model the diffusion of molecules from the vasculature into the surrounding tissue. The blood sugar module utilizes dialysis tubing, glucose meters, and a variety of drinks (such as water, milk, soda, juice, or sport drinks) to help students understand how the foods we eat influence the blood sugar levels in our bodies. This inexpensive, inquiry-based experiment can be easily integrated into a high school biology classroom to reinforce the fundamentals of diffusion by connecting it to the core concepts of the circulatory and transport system within our bodies. Students who complete this module significantly increase their knowledge about the circulatory system and the factors that regulate tissue perfusion and become more proficient at using the scientific method to design experiments and collect data.

6.5 Materials and Methods

The transport of molecules and perfusion of tissues via the circulatory system

Introduction

This experimental module utilizes gelatin-coated petri dishes to simulate "tissues" of different densities. "Blood vessels" are created within the 'tissues' by using a biopsy punch to remove circular areas of the gelatin. Tissue perfusion is simulated by adding a small amount of red food coloring to the 'blood vessels' and measuring the extent of

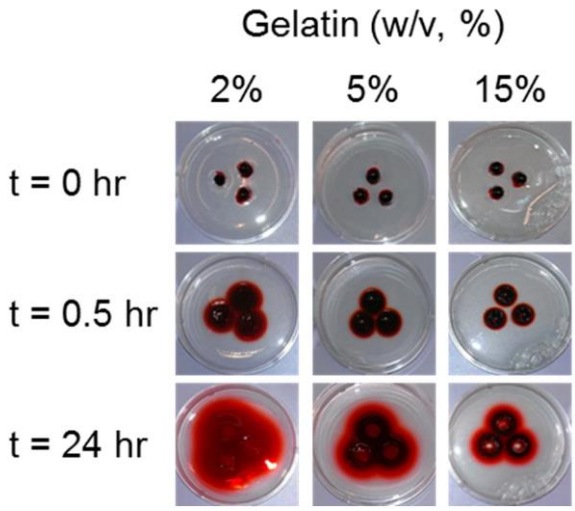

Figure 6.3. The transport of molecules and perfusion of tissues via the circulatory system. Gelatin density modulates the diffusion of food coloring from the "blood vessels."

diffusion over the course of 2 days.

Materials and Methods

The following materials are needed for each group: One each of a 35 mm petri dish coated with 2%, 5% and 15% gelatin solution (5 ml/dish), 6 mm biopsy punch or straw, red food coloring, liquid droppers or pipettes, paper towels.

Classroom Procedure

The entire exercise was performed in three New York State High School Regents Living Environments classes. Students were provided with background information about the circulatory system and basic tissue composition after which they were asked to complete a pre-test to gauge their knowledge of the topic before the experimental module was begun. At the beginning of the experiment, the students were allowed to choose the density of their tissue samples and asked to hypothesize about the optimal vascular distribution (number and arrangement of punches) and tissue density that

would be needed to achieve diffusion throughout the entire tissue construct. Figure 6.3 shows an example of diffusion within gelatin of different densities. Throughout the experiment, students collected both qualitative and quantitative data and were asked to use all the steps of the scientific method. At the completion of the experiment, students were given a post-test to assess the effectiveness of the module.

The relationship of the food we eat to blood sugar levels

Introduction

In this laboratory, students investigated how different drinks can influence blood sugar levels. Students will simulated the absorbance of nutrients into the blood stream from different liquids using dialysis tubing filled with fluid to model the blood vessel. They tested the amount of glucose that has entered the blood vessel using a glucose meter and compare between the conditions they chose.

Materials and Methods

The following materials are needed for each group: Dialysis tubing, drinks (water, milk, soda, juice, and sports drink), beakers, glucose meter, glucose meter test strips, red food coloring, pipettes or droppers, toothpicks.

Classroom Procedure

The entire exercise was performed in three New York State High School Regents Living Environments classes. Students were provided with background information about the circulatory and digestive systems and were asked to complete a pre-test to

gauge their knowledge of the topic before the experimental module was begun. At the beginning of the experiment, the students were allowed to choose which drink conditions they wanted to test and asked to hypothesize about how the drinks would influence the sugar levels of the vessels made out of dialysis tubing. Throughout the experiment, students collected both qualitative and quantitative data and were asked to use all the steps of the scientific method. At the completion of the experiment, students were given a post-test to assess the effectiveness of the module.

6.6 Results from the lab exercises

Overall, this experimental module was very effective at helping the students develop mental connections about diffusion, the circulatory system, and the digestive system. An anonymous survey indicated that the students were excited about the experiment and particularly enjoyed creating their own experimental protocol to do hypothesis testing. Data from the post-test indicates that the students incorporated their experiences from the laboratory into their knowledge base (Figure 6.4).

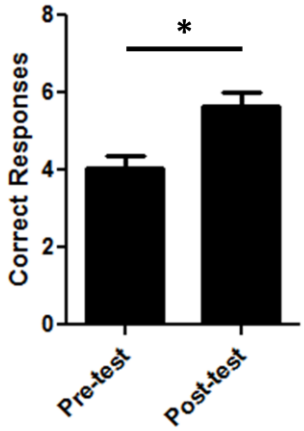

Figure 6.4. Pre-test and post-test results from the curriculum module. Students performed significantly better on the post-tests.

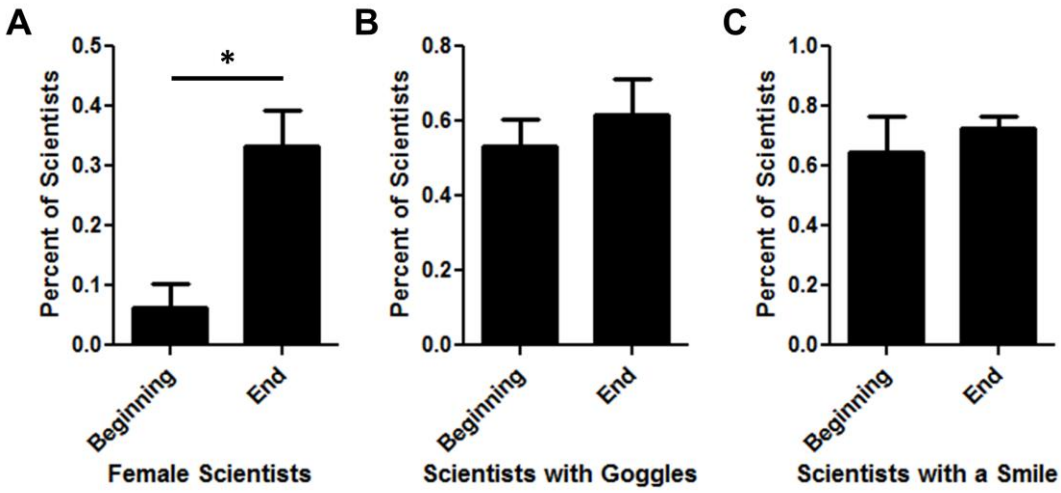

Figure 6.5. Quantification of the scientist drawings. (A) Students drew significantly more female scientists at the end of the school year. The same number of scientists were wearing (B) safety goggles or (C) a smile in drawings completed at the beginning and end of the school year.

6.7 Conclusions

Creating collaborations between researchers and high school classrooms can prove to be beneficial for everyone involved. Being the resident scientist in a high school classroom allows graduate students to work with educators to create useful and meaningful science curriculum materials related to BME research and has directly impacted the students, some of whom have now decided to pursue a career in a science-related field. It also allows high school students to interact with and "real-life scientists" and helps them to understand that we are not so different from them. Prior to my first day in the classroom and again at the end of the school year, Laura had her students draw a scientist. Importantly, at the end of the school year, students drew scientists that were qualitatively more like themselves. In fact, significantly more of the scientists that were drawn were female and there were also slight increases in the

number of scientists wearing goggles or with smiles (Figure 6.5). Being a GK-12 fellow was highly rewarding experience that taught me how to communicate complex concepts in an interesting and engaging way to non-scientists. These skills will continue to be important during the rest of my career.

CHAPTER 7

CONCLUSIONS AND FUTURE DIRECTIONS

7.1 Conclusions

As our knowledge of the mechanical and chemical regulation of angiogenesis continues to expand, so will our ability to develop therapeutics to influence the process of angiogenesis. This thesis contributes to the knowledge of angiogenesis by identifying three-dimensional matrix stiffness as a regulator of the formation and function of the angiogenic vasculature. It also describes a tractable method to modulate the stiffness of the matrix without changing collagen density. We utilized non-enzymatic collagen glycation to cross-link and stiffen three-dimensional collagen gels with only minimal changes to the collagen fiber arrangements. Using these matrices, we demonstrate that angiogenic outgrowth, branching, and cell-cell junctional integrity are altered by increases in matrix stiffness. Together, these data suggest that therapeutically targeting stiffness or endothelial cell response to stiffening may help maintain and restore vessel structure and function in cases where it is disrupted, such as in the tumor vasculature.

In Chapter 2, we characterized the physical properties of collagen matrices that had been stiffened by non-enzymatic glycation cross-linking. We were motivated by work done by Roy et al. that demonstrated the mechanical properties of collagen gels can be modulated by pre-glycating collagen solutions prior to collagen polymerization;

allowing for cells to be completely embedded within the cross-linked gel upon polymerization[1,2]. By using confocal reflectance microscopy and TRITC-labeled collagen, we showed that while increasing the concentration of ribose from 0-250 mM increases collagen gel stiffness, the collagen fiber architecture is modified in gels glycated with 150 mM ribose or greater. We demonstrated that glycating collagen gels with 0-100 mM ribose only minimally altered collagen fiber distributions while increasing the equilibrium compressive moduli three-fold.

A number of methods have been utilized to modulate the mechanical stiffness of three-dimensional matrices. Among the methods used to create naturally derived hydrogels, altering the density of extracellular matrix components such as collagen, fibrin, or hyaluronic acid is the most basic and commonly utilized[3–5]. However, in addition to changing the stiffness of the matrix, altering the density can also modulate the porosity, fiber structure and binding site frequency[3,4,6]. Importantly, when we cross-linked collagen gels by glycating with 0-100 mM ribose, there were significant increases in gel stiffness but there was not a significant difference in the collagen fiber structure within gels.

Previous work in our lab has shown that the stiffness of two-dimensional matrices regulates the formation of vascular networks[7]. Additionally, tissue stiffness is known to be altered in a number of disease states that are also known to have aberrant vasculature such as diabetes and cancer. Thus, we hypothesized that three-dimensional matrix stiffness would modulate the angiogenic response of endothelial

cells. We found that increased gel stiffness significantly altered the morphology of spreading or angiogenic outgrowth in single cells or spheroids, respectively. The work presented in Chapter 2 was the first to show that increasing three-dimensional stiffness independently of matrix density increases angiogenic outgrowth. Recently, others have confirmed our findings by utilizing collagen matrices that are cross-linked with microbial transglutaminase or by varying the ratio of collagen monomers to oligomers[8,9].

We further investigated the role of extracellular matrix stiffness on angiogenic function in Chapter 3 where we modulated matrix stiffness by glycating collagen gels of different densities. As expected, increasing the density or the extent of glycation cross-links increased the equilibrium compressive moduli of the collagen gels. Methods to study the role of stiffness on angiogenesis in naturally-derived hydrogels have primarily focused on altering matrix density and have typically found that increased density decreases angiogenesis[3,4,10,11]. We also observed that increasing collagen density decreases angiogenic outgrowth from endothelial cell spheroids. Importantly, we found that increasing matrix cross-linking increased angiogenic outgrowth both in vitro and in the ex ovo embryonic chick model. Additionally, we demonstrated that the increased outgrowth in the stiffer collagen matrices was prevented by inhibition of matrix metalloproteinase activity with GM6001. Together, these results demonstrate that matrix stiffness, and specifically matrix cross-linking, plays an important role in regulating angiogenesis in three-dimensional matrices.

Inspired by work in our lab that showed that endothelial cell-cell connectivity is altered by matrix stiffness on two-dimensional substrates[7,12], we chose to investigate the role of stiffness on cell-cell junctional properties in angiogenic outgrowths. Interestingly, we demonstrate that endothelial cell-cell junctional widths are modulated by the stiffness of the matrix. Angiogenic "stalk" cell junction widths increase with increasing three-dimensional matrix stiffness. Additionally, we found that "tip" junctions are significantly wider than "stalk" junctions in all conditions studied. Recently published work has also shown that VE-cadherin junctions are qualitatively different in tip and stalk cells[13]. However, our data is the first to demonstrate that three-dimensional matrix stiffness modulates VE-cadherin junction widths. We further show that the localization of VE-cadherin and the permeability of endothelial monolayers are significantly altered by matrix stiffness. These results show that the stiffness of the matrix modulates endothelial cell-cell junctions and alters vascular integrity.

In Chapter 4, we investigated how tumor stiffness regulates the vasculature by performing histological staining of murine and human mammary tumors. It is well known that the tumor vasculature is more dense, disordered, and permeable than the vasculature in normal tissue. Additionally, cells within the tumor deposit and cross-link matrix proteins during the process of tumorigenesis, thereby creating a stiffer extracellular environment with altered protein expression. We collaborated with Prof. Valerie Weaver's lab to study how tumor stiffness and integrin clustering influences vascular density and the presence of vessel-associated mural cells in murine mammary

tumors. When tumor stiffness was modulated by inhibiting collagen cross-linking, we found that the vascular density and mural cell localization were altered. Additionally, in both normal and mammary tumors tissues where the clustering of β_1 integrins had been increased with the V737N mutation, we observed increased vessel density. Interestingly, we found that a specific splice variant of fibronectin (EDB-FN) that is known to be associated with angiogenesis was expressed within the human tumor vasculature but not in patient-matched normal mammary tissue. Together, these data show that the tumor vasculature is inherently different in composition and density than that of normal tissue and suggests that matrix stiffness may play a role in these alterations.

Finally, in Chapter 5, we hypothesized that the stiffness of the matrix would modulate endothelial cell response to chemical cues such as VEGF. To test this hypothesis, we developed a novel microfluidic device to expose cells cultured on substrates of well-characterized, tunable stiffness to well-defined, stable chemical gradients. While the microfluidic device was not well-suited to experiments involving the chemotaxis of endothelial cells to VEGF, we did demonstrate that gradients of the phorbol ester PDBu stimulated podosomes in a directed manner in vascular smooth muscle cells.

The findings presented in this dissertation aid in our understanding of how the extracellular matrix mechanical environment regulates the formation and stabilization of angiogenic vessels. Importantly, we show that matrix stiffness influences the formation of angiogenic vasculature in vitro, ex ovo, and in histological sections from

murine and human models. We were the first to show that increasing three-dimensional stiffness independently of matrix density increases angiogenic outgrowth and modulates VE-cadherin junction widths. We also demonstrate that endothelial monolayer barrier function, mural cell localization, and vascular density are modulated by the stiffness of the matrix. Together, these results demonstrate that matrix stiffness, and specifically matrix cross-linking, plays an important role in regulating angiogenesis, endothelial cell-cell junctions, and vascular integrity in three-dimensional matrices.

Perhaps most importantly, this dissertation extends work done by Roy et al. to describe a tractable platform for tuning collagen gel stiffness independently of collagen fiber structure and matrix density[1,2]. By utilizing non-enzymatic glycation while collagen is in solution, cells can be embedded at the time of polymerization which allows for complete cell encapsulation and excellent cell viability. These gels could be used to study the effects of mechanical stiffness on a multitude of cellular behaviors including migration, cellular signaling, and tissue formation. Additionally, since collagen is the most abundant protein within the body and non-enzymatic glycation is a naturally occurring process in vivo, this method of matrix stiffening is physiologically relevant.

A number of studies have investigated the effects of stiffness on endothelial cell behavior and function (Table 7.1). Previous work from the Reinhart-King lab has demonstrated that two-dimensional matrix stiffness influences endothelial cell

network formation, force generation, and monolayer permeability[7,12,14]. Increasing the density of the matrix has traditionally been the most commonly used method to investigate the effects of three-dimensional matrix stiffness on cellular behavior and, generally, increased collagen or fibrin matrix density results in decreased vessel formation[3,4,9,10,15]. Here, we have also reported that increased collagen density resulted in decreased angiogenesis from multicellular endothelial cell spheroids (Figure 3.2). Interestingly, recent studies have confirmed our findings showing that increasing matrix stiffness via cross-linking and independently of matrix density increases angiogenesis[8,9].

These findings are important and relevant to aging, diabetes, and cancer because these conditions are correlated with increased matrix stiffness and angiogenesis and vascular integrity are known to be disrupted[16–18]. Increased matrix stiffness in tumors is correlated with increased vessel density, tortuosity, and permeability. Traditionally, the changes to the tumor vasculature have been thought to be associated with altered vascular endothelial growth factor signaling within the tumor microenvironment. Interestingly, increases in tissue stiffness in diabetic and elderly patients are also correlated with increased vessel permeability as well as delayed and disrupted angiogenesis resulting in a decreased wound healing ability. Importantly, our data suggest that the decreased vascular integrity observed in these conditions is caused by increased tissue stiffness. Further, if our findings are integrated with data previously collected in our lab, the results suggest that decreasing cellular contractility on

Table 7.1. Increased matrix stiffness influences endothelial cell behavior.

	Method	Stiffness, Density, or Concentration	Cell Type	Response
Findings from our lab and others:				
2D	Polyacrylamide Hydrogels	0.2-10 kPa	Bovine aortic endothelial cells	Decreased network formation[7]
		1-10 kPa	Bovine aortic endothelial cells	Increased traction force generation[14]
		2.5-10 kPa	Bovine aortic endothelial cells	Increased endothelial monolayer permeability[12]
	Polyacrylamide Hydrogels	1.2-11 kPa	Human umbilical vein endothelial cells	Increased cell-cell and cell-substrate forces[19]
3D	Collagen Density	3-20 mg/ml	Human umbilical vein endothelial cells	Decreased lumen density, lumen area, and cell invasion[3]
		0.5-3.5 mg/ml	Human umbilical cord blood endothelial colony forming cells	Decreased vessel formation and increased vessel cross-sectional area[15]
		0.3-2.7 mg/ml	Human dermal microvascular endothelial cells	Intermediate density promoted the most angiogenesis[20]
		2-4 mg/ml	Rat microvessel fragments	Decreased vessel formation[10]
		0.5-3 mg/ml	Endothelial colony forming cells	Decreased vessel formation[9]
3D	Collagen Cross-linking			
	Glucose-6-phosphate	0-375 mM	Human umbilical vein endothelial cells	Decreased vessel formation[21]
	Transglutaminase	0-500 μg/ml	Human umbilical vein endothelial cells	Increased angiogenic sprouting
	Oligomer: Monomer		Endothelial colony forming cells	Increased total vessel length and vessel volume[8]
3D	Fibrin Density	2.5-10 mg/ml	Human umbilical vein endothelial cells	Decreased vessel formation[22]
3D	Collagen: Fibrin	2.5 mg/ml	Human umbilical vein endothelial cells	Decreased vessel formation[23]
Findings reported in this dissertation:				
3D	Collagen Cross-linking (*Ribose*)	0-100 mM	Bovine aortic endothelial cells	Increased vessel formation[24]
3D	Collagen Density	1.5-10 mg/ml	Bovine aortic endothelial cells	Decreased vessel formation

matrices of increased stiffness could provide a mechanism to stabilize the vasculature[12].

The knowledge gained through these experiments could also be used to assist in the development of vascularized tissue-engineered organs. One of the greatest challenges in the field of tissue engineering is to create matrices that are capable of being vascularized so that nutrients can be delivered and waste products can be removed from the encapsulated cells. Without the formation of a functional vascular network, tissue-engineered therapies are limited to a thickness of less than 200 μm[25]. Importantly, the impact of creating vascularized tissue-engineered organs is enormous. According to Donate Life America, an average of 18 people die each day due to the lack of organs available for transplantation. Our results demonstrate that matrix cross-linking and density are critically important to the resultant angiogenic potential of the matrices used in tissue engineering therapies. Integrating our findings into current tissue engineering research could help fill the gap between the availability and need for organs.

7.2 Future Directions

Although the work described in this dissertation contributed significantly to our knowledge about the mechanical regulation of angiogenic vessel formation and vascular integrity, additional work is required to fully understand how mechanical stimuli regulate angiogenesis. Future directions of this work will provide additional

insights into how matrix stiffness mediates angiogenesis and facilitates vascular branching and integrity and may inform the development of therapeutics to regulate angiogenesis. There are several avenues of approach which should be completed.

1. **What are the molecular signaling pathways involved in the increased angiogenic outgrowth that is observed in stiffer matrices?**

While the work described in this dissertation focuses primarily on the biophysical mechanisms of angiogenesis, future work should further investigate the roles of cellular contractility and matrix degradation on angiogenic outgrowth in response to matrix stiffness in our system. Matrix degradation by matrix metalloproteinases (MMPs) has been shown to be crucial to the formation and stabilization of angiogenic structures[4,11,26–28]. In Chapter 3 we show that inhibiting MMP activity with GM6001 decreases angiogenic outgrowth from spheroids embedded within stiffer, cross-linked matrices. Additionally, previously published work from our lab has shown that endothelial cells sense and respond to increased matrix stiffness by increasing cell traction force generation and Rho GTPase activity[12,14]. Cellular contractility has also been implicated in mediating a number of angiogenic responses including endothelial cell survival, proliferation, migration, stress fiber formation, sprouting, cord formation, and permeability[11,29–32]. Based on these studies, we hypothesize increased matrix metalloproteinase activity, possibly coupled with increased cellular contractility, in the stiffer, glycated matrices is triggering the increased angiogenic response.

To test this hypothesis, the effects of cell contractility could be investigated by using the small molecule inhibitors Y27632 or ML7. Y27632 is an inhibitor of Rho-associated protein kinase (ROCK) which is known to be an important regulator of cellular contractility, motility, and polarity. Inhibiting ROCK with Y27632 has been shown to inhibit the formation of vascular networks[11,30]. ML7 is a selective inhibitor of myosin light chain kinase and has been shown to decrease angiogenic sprouting and vessel formation[11]. To investigate the role of Y27632 or ML7 on mediating angiogenic outgrowth in response to increased collagen stiffness in our system, the branching and extent of outgrowth of spheroids could be quantified. Spheroids embedded within 1.5 mg ml^{-1} collagen gels that had been glycated with 0 or 100 mM ribose could be treated with Y27632, ML7, or vehicle-controls. The qualitative and quantitative outgrowth of spheroids would be studied by imaging spheroids with phase microscopy and measuring the total projected area, respectively. After five days of outgrowth, the density of branching would be studied in response to the inhibitor molecule.

As a preliminary study, we inhibited cellular contractility with the small molecule Y27632. Bovine aortic endothelial cell (BAEC) spheroids were embedded within 1.5 mg ml^{-1} collagen gels that had been glycated with 0 or 100 mM ribose. Collagen gels were allowed to polymerize for 45 minutes and then overlaid with complete medium which was exchanged after 1 hour. After an additional 3 hours, medium was exchanged with complete medium with or without 10 μM Y27632. Spheroids were fed every other day with the respective medium. Spheroid outgrowth was monitored

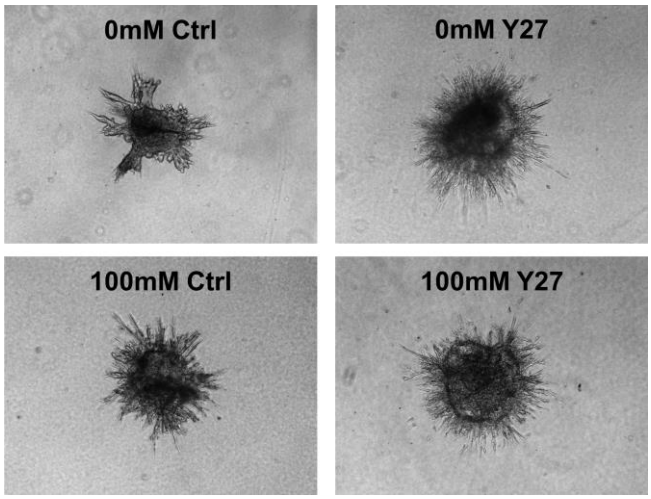

Figure 7.1. Endothelial cell spheroid outgrowth increases with Y27632 treatment. Endothelial cell spheroids were embedded within 1.5 mg/ml collagen that had been glycated with 0 or 100 mM ribose and were fed with complete media with or without 10 μM of Y27632. Y27632 treatment increases spheroid outgrowth in spheroids within 0 and 100 mM glycated collagen gels.

by imaging the spheroids using brightfield microscopy on a Zeiss Z1 microscope daily.

We found that spheroids treated with Y27632 exhibited increased outgrowth in collagen gels glycated with 0 or 100 mM ribose when compared to controls (Figure 7.1). While most studies have shown that decreasing ROCK activity decreases angiogenic potential, inhibition of ROCK with Y27632 has also been shown to enhance endothelial cell sprouting and angiogenesis both in vitro and in vivo[33,34]. Our preliminary data show that decreasing cellular contractility with Y27632 leads to increased angiogenic sprouting and outgrowth.

Based on the data discussed in Chapter 3 and the preliminary data discussed here, I expect that matrix degradation will play a larger role in mediating angiogenic

outgrowth than cellular contractility in response to matrix stiffness in our system. However, more work needs to be done to determine how MMP activity is altered by glycated collagen matrices and with GM6001 inhibition in our system.

2. How does matrix stiffness mediate tip cell formation and branching?

More work is needed to fully understand how matrix stiffness is mediating the formation of angiogenic outgrowths. Because we have shown an increase in sprouting and branching from endothelial cell spheroids in stiffer three-dimensional matrices, it would be interesting to study whether matrix stiffness is mediating the formation of tip cells. The Notch inhibitor, delta-like ligand 4 (Dll4) has been shown be expressed in the tip cells of angiogenic vasculature in response to VEGF stimulation[35]. The up-regulation of Dll4 causes adjacent cells to down-regulate VEGFR-2 and up-regulate VEGFR-1 and consequently specifies their fate as "stalk" cells[36]. Dll4 up-regulation is correlated with a decrease in sprouting and Dll4 expression has been, surprisingly, shown to be elevated in the vessels of a number of tumors[37–39]. Interestingly, inhibiting Dll4 leads to an increase in sprouting but has also been correlated with a decrease in tumor volume because the resultant vessels are non-functional[40–42]. Since tumors are known to have altered matrix mechanical properties and vascular densities, we hypothesize that Dll4 is mediated by matrix stiffness in addition to VEGF stimulation.

To investigate whether Dll4 expression is altered in response to matrix stiffness, endothelial spheroids could be embedded in 1.5 mg ml^{-1} collagen gels that had been

glycated with 0, 50, or 100 mM ribose. After 6, 24 or 48 hours of outgrowth, spheroids could be fixed and Dll4 localization would be studied with immunocytochemistry and confocal imaging. Since we observe an increase in angiogenic sprouting and branching in stiffer matrices, I would expect that increasing matrix stiffness will decrease Dll4 staining in spheroids (and thus decrease the proportion of cells that are specified as stalk cells). To further interrogate the system and ensure altered Notch activity is regulating angiogenic sprouting in response to matrix stiffness, inhibition of Notch signaling could be studied using *N*-[*N*-(3,5-difluorophenacetyl)-L-ananyl]-*S*-phenylglycine *t*-butyl ester (DAPT) in glycated and non-glycated collagen gels. If stiffness is indeed mediating Notch activity, I would expect that the inhibition of Notch with DAPT would increase the extent of angiogenic sprouting in softer matrices to a greater extent than it would in stiffer matrices.

As a preliminary experiment, we embedded BAEC endothelial cell spheroids within 1.5 mg ml^{-1} collagen gels and fixed the gels after 6, 24, or 48 hours. Spheroids were

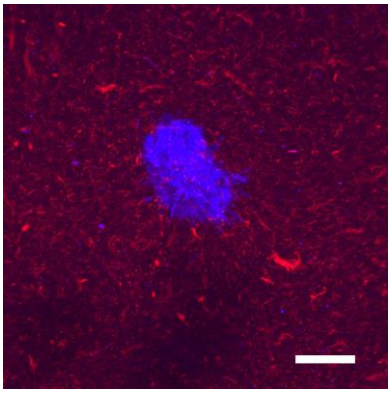

Figure 7.2. Spheroids stained for delta-like ligand 4 (DLL4). Endothelial cell spheroids were embedded within collagen gels and stained for DLL4 (red) and DAPI (blue). Extensive background staining was observed. Scale is 200 μm**.**

stained for Dll4 using a monoclonal rat IgG (R&D Systems, Clone#207822) and DAPI. Unfortunately, since the collagen we use is derived from rat tail tendons, there was significant background staining within the gel (Figure 7.2). This experiment should be repeated using a different antibody that is specific to bovine Dll4 but not of rat origin.

3. How does matrix stiffness influence the perfusion of tumors in vivo?

The work we have presented indicates that inhibiting collagen cross-linking in vivo modulates vascular density and mural cell localization in the tumor vasculature. We have also shown that the matrix stiffness mediates endothelial cell-cell junctional integrity in vitro. Future work should focus on understanding how matrix stiffness alters the perfusion of tumors and the permeability of the vasculature.

We have already received approval from the Cornell Institutional Animal Care and Use Committee to study the role of matrix stiffness on angiogenesis in a murine model. We hypothesize that matrix stiffness will influence angiogenesis and vascular integrity in vivo. To test this hypothesis, we have proposed two different approaches. We propose to study the angiogenic response to matrix stiffness by using multiphoton microscopy to monitor angiogenesis into glycated and non-glycated collagen gels that have been implanted intra-dermally. We also propose to modify the inherent cross-linking of mouse tissues in the MMTV-PyMT mouse model. PyMT mice spontaneously form palpable mammary tumors at as early as 5 weeks of age. In some animals, tissue cross-linking will be inhibited by beta-aminopropionitrile (BAPN).

Previous work has demonstrated that inhibiting lysyl oxidase-mediated collagen cross-linking with BAPN significantly alters the resultant mechanical properties of mammary tumors[43,44]. We have proposed to investigate a number of metrics including the extent of angiogenesis, extracellular matrix and vessel architecture, permeability and blood flow. Patent, angiogenic vessels will be visualized by injecting fluorescent contrast agents into the vasculature either retro-orbitally (for single injections) or using a tail-vein implanted catheter (for repeated injections). While we had initially envisioned determining the extent of angiogenic sprouting and tissue perfusion using multiphoton imaging, I anticipate that this type of study could be approached using a number of other methodologies currently available at Cornell including optical coherence tomography or ultrasound. End-point histological analysis of tissues should also be completed to determine the morphology, density, and organization of the vasculature.

4. How can endothelial cell response to stiffness be regulated in vivo?

Our in vitro, ex ovo, and histology results demonstrate that matrix stiffness is a key regulator of angiogenesis. In order for this observation to have impactful, clinical significance, matrix stiffness or cellular response to matrix stiffness needs to be specifically controlled in vivo. Since collagen cross-linking is needed to maintain tissue integrity, the systemic approaches to ubiquitously to regulate matrix stiffness by inhibiting collagen cross-linking in murine models are inappropriate for use in humans. We have also proposed the use of molecules such as Y27632 and GM6001 to interrogate endothelial cells response to matrix stiffness in controlled, in vitro

environments. However, since these molecules are not specific to endothelial cells and cellular contractility and matrix degradation mediate a multitude of normal and essential processes in vivo, broad-spectrum inhibitors are poor choices for clinical use. Additionally, prolonged exposure to small molecules inhibitors such as Y27632 has been shown to induce apoptosis in endothelial cells[30].

Ultimately, being able to specifically stimulate angiogenesis in wound healing and inhibit angiogenesis in cancer, would allow clinicians to better- manage patient care. Additionally, since many current tissue-engineered approaches are limited due to the inability to selectively and specifically control the angiogenesis, understating how to regulate angiogenesis as a function of matrix stiffness could allow for the development of tissue-engineered organs. Thus, future work should focus on elucidating therapeutics to control matrix stiffness or endothelial cell response in a localized manner.

REFERENCES

1 Roy R, Boskey A, Bonassar LJ. Processing of type I collagen gels using nonenzymatic glycation. J Biomed Mater Res A 2010; 93A:843–851.

2 Roy R, Boskey AL, Bonassar LJ. Non-enzymatic glycation of chondrocyte-seeded collagen gels for cartilage tissue engineering. J Orthop Res 2008; 26:1434–1439.

3 Cross VL, Zheng Y, Won Choi N, Verbridge SS, Sutermaster BA, Bonassar LJ, Fischbach C, et al. Dense type I collagen matrices that support cellular remodeling and microfabrication for studies of tumor angiogenesis and vasculogenesis in vitro. Biomaterials 2010; 31:8596–8607.

4 Ghajar CM, Blevins KS, Hughes CC, George SC, Putnam AJ. Mesenchymal Stem Cells Enhance Angiogenesis Early Matrix Metalloproteinase Upregulation. Tissue Eng 2006; 12:2875–88.

5 Seidlits SK, Drinnan CT, Petersen RR, Shear JB, Suggs LJ, Schmidt CE. Fibronectin-hyaluronic acid composite hydrogels for three-dimensional endothelial cell culture. Acta Biomater 2011; 7:2401–9.

6 Zaman MH, Kamm RD, Matsudaira P, Lauffenburger D a. Computational model for cell migration in three-dimensional matrices. Biophysical journal 2005; 89:1389–97.

7 Califano JP, Reinhart-King CA. A Balance of Substrate Mechanics and Matrix Chemistry Regulates Endothelial Cell Network Assembly. Cell Mol Bioeng 2008; 1:122–132.

8 Lee P-F, Bai Y, Smith RL, Bayless KJ, Yeh a T. Angiogenic responses are enhanced in mechanically and microscopically characterized, microbial transglutaminase crosslinked collagen matrices with increased stiffness. Acta biomaterialia 2013; 9:7178–90.

9 Whittington CF, Yoder MC, Voytik-Harbin SL. Collagen-polymer guidance of vessel network formation and stabilization by endothelial colony forming cells in vitro. Macromol Biosci 2013; 13:1135–49.

10 Edgar LT, Underwood CJ, Guilkey JE, Hoying JB, Weiss J a. Extracellular matrix density regulates the rate of neovessel growth and branching in sprouting angiogenesis. PloS One 2014; 9:e85178.

11 Kniazeva E, Putnam AJ. Endothelial cell traction and ECM density influence both capillary morphogenesis and maintenance in 3-D. Am J Physiol Cell Physiol 2009; 297:C179–87.

12 Huynh J, Nishimura N, Rana K, Peloquin JM, Califano JP, Montague CR, King MR, et al. Age-related intimal stiffening enhances endothelial permeability and leukocyte transmigration. Sci Transl Med 2011; 3:112ra122.

13 Bentley K, Franco CA, Philippides A, Blanco R, Dierkes M, Gebala V, Stanchi F, et al. The role of differential VE-cadherin dynamics in cell rearrangement during angiogenesis. Nat Cell Biol 2014; 16:309–21.

14 Califano JP, Reinhart-King CA. Substrate stiffness and cell area drive cellular traction stresses in single cells and cells in contact. Cell Mol Bioeng 2010; 3:68–75.

15 Crister PJ, Kreger ST, Voytik-Harbin SL, Yoder MC. Collagen matrix physical properties modulate endothelial colony forming cell-derived vessels in vivo. Microvasc Res 2010; 80:23–30.

16 Carmeliet P, Jain RK. Angiogenesis in cancer and other diseases. Nature 2000; 407:249–257.

17 Martin A, Komada MR, Sane DC. Abnormal angiogenesis in diabetes mellitus. Med Res Rev 2003; 23:117–145.

18 Sadoun E, Reed MJ. Impaired angiogenesis in aging is associated with alterations in vessel density, matrix composition, inflammatory response, and growth factor expression. J Histochem Cytochem 2003; 51:1119–1130.

19 Krishnan R, Klumpers DD, Park CY, Rajendran K, Trepat X, Van Bezu J, Van Hinsbergh VWM, et al. Substrate stiffening promotes endothelial monolayer disruption through enhanced physical forces. Am J Physiol Cell Physiol 2011; 300:C146–C154.

20 Shamloo A, Heilshorn SC. Matrix density mediates polarization and lumen formation of endothelial sprouts in VEGF gradients. Lab Chip 2010; 10:3061–3068.

21 Francis-Sedlak ME, Moya ML, Huang J-J, Lucas SA, Chandrasekharan N, Larson JC, Cheng M-H, et al. Collagen glycation alters neovascularization in vitro and in vivo. Microvasc Res 2010; 80:3–9.

22 Ghajar CM, Chen X, Harris JW, Suresh V, Hughes CCW, Jeon NL, Putnam AJ, et al. The effect of matrix density on the regulation of 3-D capillary morphogenesis. Biophys J 2008; 94:1930–1941.

23 Rao RR, Peterson AW, Ceccarelli J, Putnam AJ, Stegemann JP. Matrix composition regulates three-dimensional network formation by endothelial cells and mesenchymal stem cells in collagen/fibrin materials. Angiogenesis 2012; 15:253–264.

24 Mason BN, Mazzola MC, Somasegar S, Califano JP, Montague CR, Kang Y, LaValley D, et al. Collagen cross-linking increases angiogenesis and disrupts barrier integrity. In Preparation 2014;

25 Jain RK, Au P, Tam J, Duda DG, Fukumura D. Engineering vascularized tissue. Nat Biotechnol 2005; 23:821–3.

26 Stratman AN, Malotte KM, Mahan RD, Davis MJ, Davis GE. Pericyte recruitment during vasculogenic tube assembly stimulates endothelial basement membrane matrix formation. Blood 2009; 114:5091–5101.

27 Bayless KJ, Davis GE. Sphingosine-1-phosphate markedly induces matrix metalloproteinase and integrin-dependent human endothelial cell invasion and lumen formation in three-dimensional collagen and fibrin matrices. Biochem Biophys Res Commun 2003; 312:903–913.

28 Saunders WB, Bohnsack BL, Faske JB, Anthis NJ, Bayless KJ, Hirschi KK, Davis GE. Coregulation of vascular tube stabilization by endothelial cell TIMP-2 and pericyte TIMP-3. J Cell Biol 2006; 175:179–91.

29 Hoang M V, Whelan MC, Senger DR. Rho activity critically and selectively regulates endothelial cell organization during angiogenesis. Proc Natl Acad Sci U S A 2004; 101:1874–9.

30 Bryan BA, Dennstedt E, Mitchell DC, Walshe TE, Noma K, Loureiro R, Saint-Geniez M, et al. RhoA/ROCK signaling is essential for multiple aspects of VEGF-mediated angiogenesis. FASEB J 2010; 24:3186–95.

31 Liu Y, Senger DR. Matrix-specific activation of Src and Rho initiates capillary morphogenesis of endothelial cells. FASEB J 2004; 18:457–68.

32 Whelan MC, Senger DR. Collagen I initiates endothelial cell morphogenesis by inducing actin polymerization through suppression of cyclic AMP and protein kinase A. J Biol Chem 2003; 278:327–34.

33 Kroll J, Epting D, Kern K, Dietz CT, Feng Y, Hammes H-P, Wieland T, et al. Inhibition of Rho-dependent kinases ROCK I/II activates VEGF-driven retinal neovascularization and sprouting angiogenesis. Am J Physiol Heart Circ Physiol 2009; 296:H893–9.

34 Van Nieuw Amerongen GP, Koolwijk P, Versteilen A, Van Hinsbergh V. Involvement of RhoA/Rho Kinase Signaling in VEGF-Induced Endothelial Cell Migration and Angiogenesis In Vitro. Arterioscler Thromb Vasc Biol 2002; 23:211–217.

35 Hellström M, Phng L-K, Hofmann JJ, Wallgard E, Coultas L, Lindblom P, Alva J, et al. Dll4 signalling through Notch1 regulates formation of tip cells during angiogenesis. Nature 2007; 445:776–780.

36 Jakobsson L, Franco CA, Bentley K, Collins RT, Ponsioen B, Aspalter IM, Rosewell I, et al. Endothelial cells dynamically compete for the tip cell position during angiogenic sprouting. Nat Cell Biol 2010; 12:943–953.

37 Mailhos C, Modlich U, Lewis J, Harris A, Bicknell R, Ish-Horowicz D. Delta4, an endothelial specific notch ligand expressed at sites of physiological and tumor angiogenesis. Differentiation 2001; 69:135–144.

38 Patel NS, Dobbie MS, Rochester M, Steers G, Poulsom R, Le Monnier K, Cranston DW, et al. Up-regulation of endothelial delta-like 4 expression correlates with vessel maturation in bladder cancer. Clin Cancer Res 2006; 12:4836–4844.

39 Patel NS, Li J-L, Generali D, Poulsom R, Cranston DW, Harris AL. Up-regulation of delta-like 4 ligand in human tumor vasculature and the role of basal expression in endothelial cell function. Cancer Res 2005; 65:8690–8697.

40 Noguera-Troise I, Daly C, Papadopoulos NJ, Coetzee S, Boland P, Gale NW, Lin HC, et al. Blockade of Dll4 inhibits tumour growth by promoting non-productive angiogenesis. Nature 2006; 444:1032–7.

41 Ridgway J, Zhang G, Wu Y, Stawicki S, Liang W-C, Chanthery Y, Kowalski J, et al. Inhibition of Dll4 signalling inhibits tumour growth by deregulating angiogenesis. Nature 2006; 444:1083–1087.

42 Scehnet JS, Jiang W, Kumar SR, Krasnoperov V, Trindade A, Benedito R, Djokovic D, et al. Inhibition of Dll4-mediated signaling induces proliferation of immature vessels and results in poor tissue perfusion. Blood 2007; 109:4753–4760.

43 Lopez JI, Kang I, You W-K, McDonald DM, Weaver VM. In situ force mapping of mammary gland transformation. Integr Biol (Camb) 2011; 3:910–921.

44 Pickup MW, Laklai H, Acerbi I, Owens P, Gorska AE, Chytil A, Aakre M, et al. Stromally derived lysyl oxidase promotes metastasis of transforming growth factor-β-deficient mouse mammary carcinomas. Cancer Res 2013; 73:5336–46.

APPENDIX A

OTHER RESULTS

This appendix details other work that has been completed but is not included in the chapters of the dissertation.

A.1 Endothelial cell invasion is modulated by collagen glycation

These experiments were completed in collaboration with Sahana Somasegar and Michael Mazzola, undergraduate researchers in the Reinhart-King Lab.

In Chapters 2 and 3 we primarily use an in vitro multicellular endothelial cell spheroid model to determine the effects of three-dimensional matrix stiffening on angiogenic sprouting. Another commonly used technique to assess the angiogenic potential of

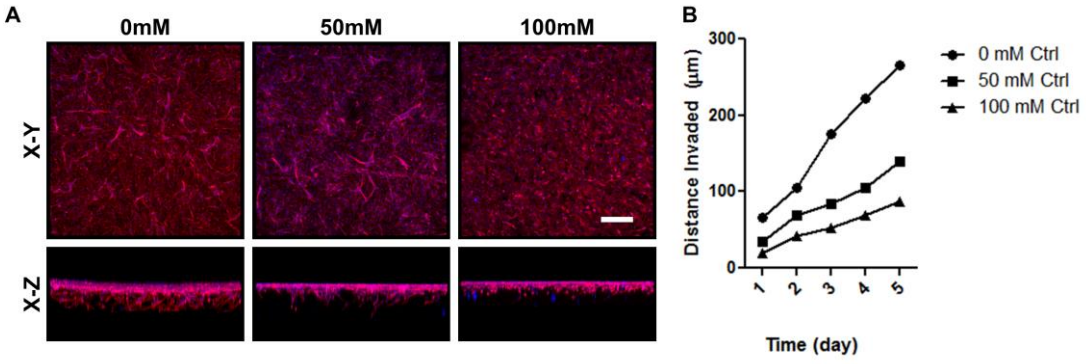

Figure A.1.1. Endothelial cell invasion is altered with matrix stiffness in glycated collagen gels. (A) Confocal imaging of the invasion of bovine aortic endothelial cells stained for actin (red) and DAPI (blue) into 1.5 mg/ml collagen gels glycated with 0, 50, or 100 mM ribose at day 5. (B) The distance of invasion was measured over 5 days. Data presented as mean ± SEM.

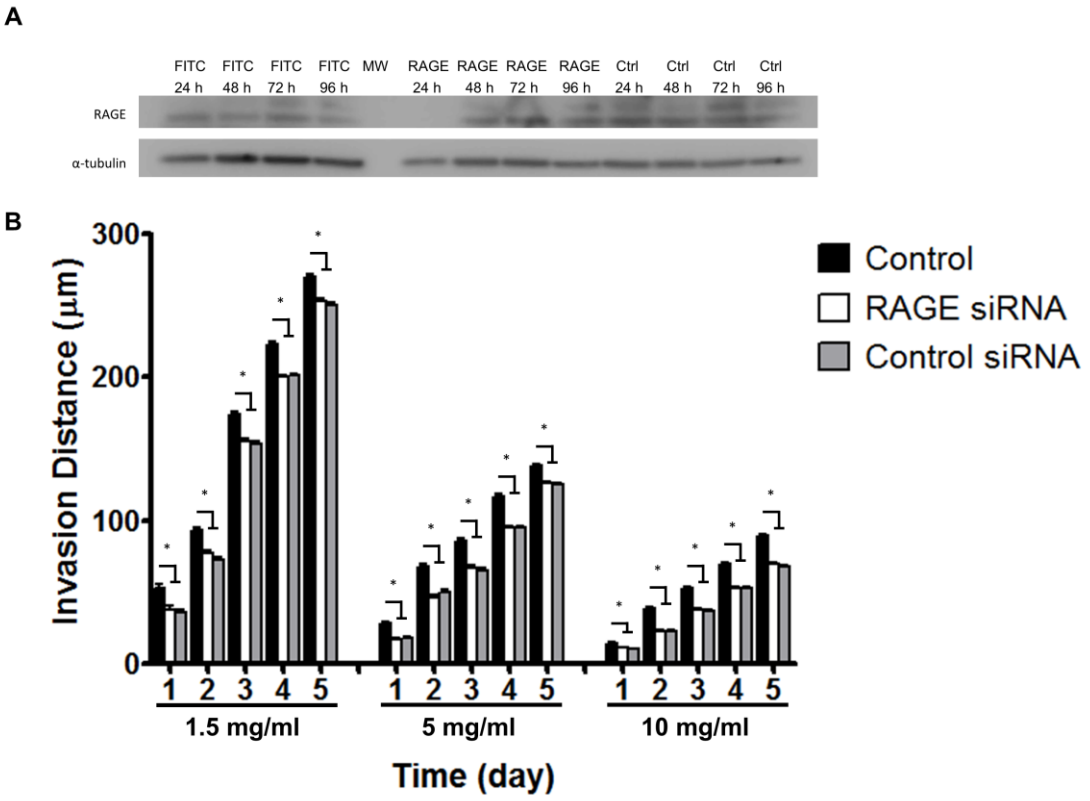

Figure A.1.2. Endothelial cell invasion is independent of RAGE activity. (A) Western blot demonstrating knockdown of RAGE at 24 and partial recovery beginning at 48 hours after transfection. 20 pmol control FITC siRNA (FITC); 20 pmol RAGE siRNA (RAGE); Opti-MEM control (Ctrl) (B) Quantification of endothelial cell migration fed with control media or media containing 20 pmol RAGE siRNA or FITC control siRNA. Data presented as mean + SEM.

endothelial cells is an invasion assay where cells are seeded atop of a biomaterial and their sprouting is monitored[9].

To better understand how matrix stiffness influences endothelial cell sprouting and angiogenesis, we performed invasion assays with BAECs seeded on 1.5, 5, or 10 mg ml^{-1} collagen gels that had been glycated with 0, 50, or 100 mM ribose. Endothelial cell invasion into the collagen gels was monitored using phase microscopy over 5 days. Surprisingly, BAECs seeded on the softer (0 mM ribose) gels invaded further

than those seeded on the stiffer (100 mM ribose) gels (Figure A.1.1). Interestingly, BAEC invasion was relatively individualized and the resultant sprouts did not resemble the long, continuous angiogenic cords we had previously seen with BAECS in the spheroid model. These observations suggest that there may be differences in endothelial cell migration and sprouting behaviors between the cells embedded as spheroids within the collagen gels or seeded as monolayers atop of a collagen gels.

Glycating the collagen gels creates cross-links termed advanced glycation endproducts (AGE) and endothelial cells are known to have receptors for advanced glycation endproducts (RAGE). Since it is possible that the increased concentration of AGE cross-links in the stiffer (100 mM ribose) gels was mediating the endothelial cell invasion, we blocked the AGE/RAGE interaction using siRNA against RAGE. BAECs were transfected with 20 pmol of RAGE siRNA (Santa Cruz, sc-270508) or a control FITC siRNA (Invitrogen, #2013) using lipofectamine. An Opti-MEM control was also used and the knockdown of RAGE was quantified with a Western Blot (Figure A.1.2A). We found that RAGE siRNA knocks down RAGE in BAECs for at least 24 hours and partial recovery begins at 48 hours. We quantified the invasion of BAECs that had been transfected with either the RAGE or control FITC siRNAs and found that while both the control and RAGE siRNA treatment decreased overall invasion in 1.5, 5, or 10 mg ml^{-1} gels when compared to Opti-MEM controls, there were no significant differences between the invasion in response to the control or RAGE siRNAs (Figure A.1.2B). These results suggest that the AGE/RAGE

interaction is not playing a significant role in the invasion of endothelial cells into the collagen matrices.

We repeated the invasion assay with human umbilical vein endothelial cells (HUVEC) seeded on 1.5 mg ml^{-1} collagen gels that had been glycated with 0, 50, or 100 mM ribose. Cells were fed with either complete M200 (CM200) or angiogenic medium (AM200; CM200 supplemented with 40 ng ml^{-1} vascular endotheial growth factor, 40 ng ml^{-1} basic fibroblast growth factor, 50 ng ml^{-1} phorbol-12-myristate-13-acetate, and 50 μg ml^{-1} ascorbic acid). Interestingly, HUVECs invade into the gels collectively and form open, lumen-like structures (Figure A.1.3). Quantification of the HUVEC invasion shows that HUVECs atop of the stiffer gels invade slightly more than those on the softer gels when cells are fed either with CM200 or AM200 (Figure A.1.4). These results show that HUVECs only slightly modulate the distance of invasion in response to matrix stiffness and suggest that other metrics that measure the number of lumens or lumen size may be potentially useful.

A.2 Endothelial cell migration is modulated by matrix stiffness

These experiments were completed in collaboration with Michael Mazzola and Lulu Bai, undergraduate students in the Reinhart-King Lab.

Since we have found differences in BAEC migration in glycated collagen gels of different stiffness (Chapter 3), we decided to investigate the migration response BAECs in response to 2D stiffness and ligand density using polyacrylamide hydrogels. Previous studies have shown that ligand density influences the migration of

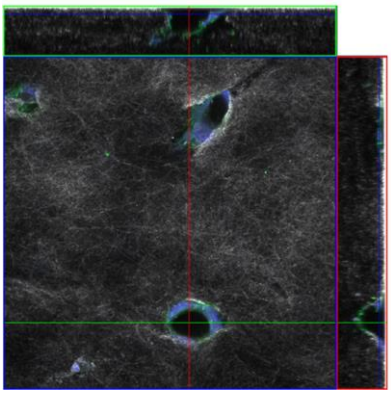

Figure A.1.3. Endothelial cell invasion of human umbilical vein endothelial cells into glycated collagen matrices. Orthogonal projection of confocal z-stack of human umbilical vein endothelial cell invasion into collagen gels demonstrates collective invasion and lumen formation. Cells were stained for actin (green) and DAPI (blue) and confocal reflectance of the collagen fibers is also shown.

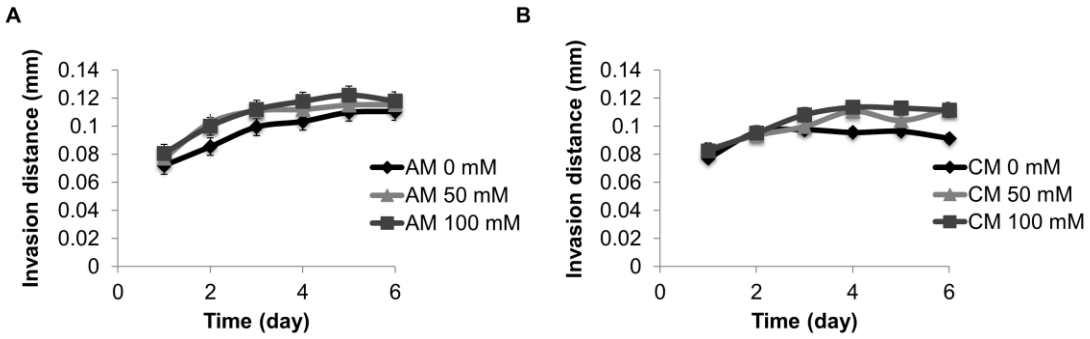

Figure A.1.4. Endothelial cell invasion is altered with matrix stiffness in glycated collagen gels. The distance of human umbilical vein endothelial cell invasion was measured over 5 days for cells seeded with (A) angiogenic medium (AM) or (B) complete medium (CM). Data presented as mean ± SEM.

cells in a biphasic manner[10]. Additionally, because we had seen differences in the invasion of BAECs and HUVECs, we quantified the migration speed of HUVECs in glycated collagen gels.

The stiffness of polyacrylamide hydrogels can be tuned by varying the ratio of acrylamide to bis-acrylamide. BAECs were seeded on 1, 5, 10, or 20 kPA

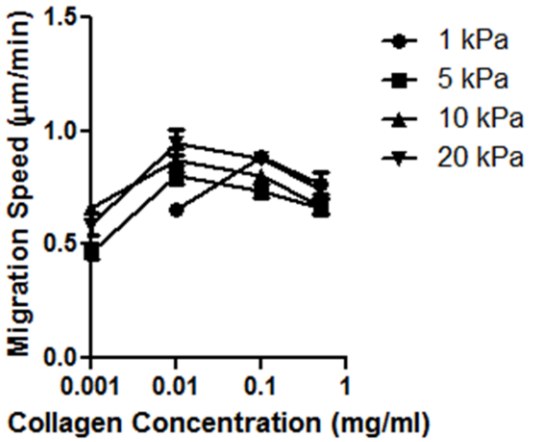

Figure A.2.1. Endothelial cell migration is altered by 2D matrix stiffness and collagen concentration. Endothelial cells were seeded on 1-20 kPa polyacrylamide hydrogels functionalized with 0.001-1 mg/ml collagen and the cell migration speeds were quantified. Data presented as mean ± SEM.

polyacrylamide gels that had been functionalized with 0.001, 0.01, 0.1, or 0.5 mg ml^{-1} collagen and their migration speed was quantified. We found that the BAECs altered their migration speed in a biphasic manner when seeded on gels functionalized with different amounts of collagen (Figure A.2.1). Interestingly, cells on stiff (5, 10, or 20 kPa) gels had a peak migration speed on gels functionalized with 0.01 mg ml^{-1} collagen while the migration speed of cells on the softest matrices (1 kPa) peaked at 0.1 mg ml^{-1} collagen. We hypothesize that this is due to a balance between substrate mechanics and cellular adhesion as demonstrated previously in our lab by Califano et al.[11].

Because the migration and invasion of BAECs is significantly altered in three-dimensional glycated collagen matrices (Chapter 3 and Figure A.1.1) and because we did not observe differences in HUVEC invasion (Figure A.1.4), we were interested in

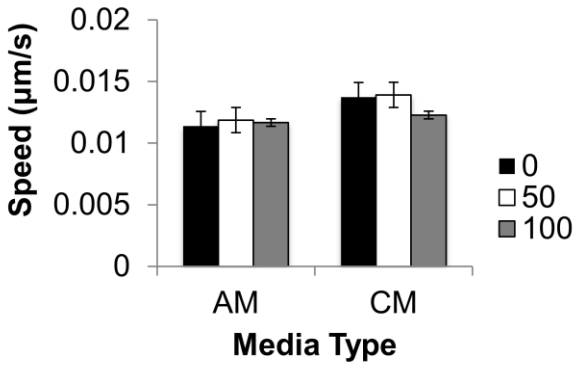

Figure A.2.2. Endothelial cell migration is not altered with matrix stiffness in glycated collagen gels. Human umbilical vein endothelial cells were seeded within 1.5 mg/ml collagen gels and their migration speed in response to angiogenic medium (AM) or complete medium (CM) was quantified. Data presented as mean ± SEM.

determining whether collagen stiffness mediates individual HUVEC migration. HUVECs were embedded within 1.5 mg ml^{-1} collagen gels that were glycated with 0, 50, or 100 mM ribose. Cells were fed with either CM200 or AM200 and their migration was monitored using timelapse microscopy. The cell centroid was tracked using Image J and the cell speed was calculated. HUVEC cell migration was only minimally modulated by three-dimensional matrix stiffness in both cells fed with AM200 or CM200 (Figure A.2.2).

A.3 Human umbilical vein endothelial cell spheroids in glycated collagen

Since we had seen differences in BAEC spheroid outgrowth with three-dimensional matrix stiffness and because BAEC spheroid extensions do not form lumens (Chapters 2,3), we decided to investigate HUVEC spheroid outgrowth. We had previously found that HUVECs form lumens in the glycated collagen gels during vasculogenesis (Chapter 3).

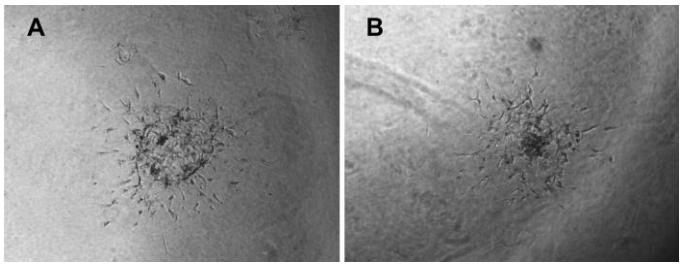

Figure A.3.1. Human umbilical vein endothelial cell spheroids. (A) HUVEC spheroids do not form continuous cord-like sprouts into collagen gels. (B) In some spheroids a dense region towards the center of the spheroid is observed.

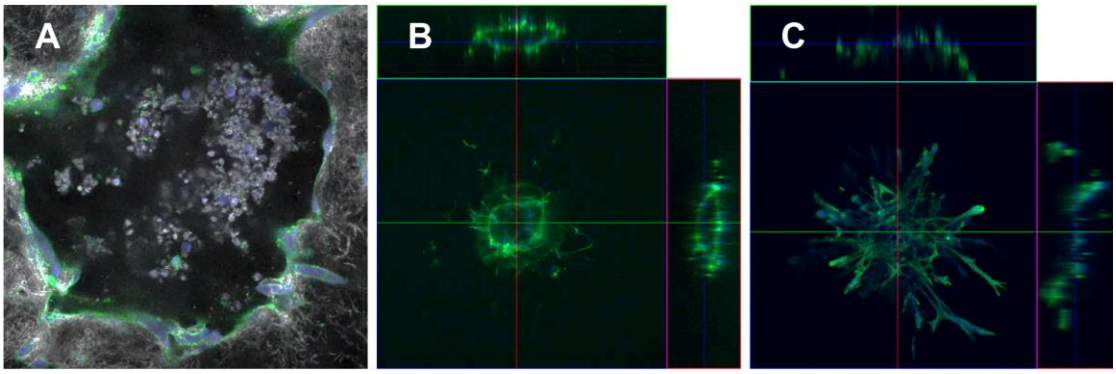

Figure A.3.2. Confocal imaging of human umbilical vein endothelial cell spheroids. (A) Confocal image showing what appears to be nuclear fragmentation at the center of a HUVEC spheroid. (B) Orthogonal projection of a confocal stack showing a fully-enclosed, lumen-like structure at the center of a HUVEC spheroids. (C) Orthogonal projection of bovine aortic endothelial cell spheroids shows sprouting at the spheroid center with no lumen-like structures.

HUVEC multicellular spheroids with 100, 500, 5000, 10000 cells were embedded within 1.5 mg ml^{-1} collagen gels that had been glycated with 0, 50, or 100 mM ribose. HUVECs embedded within the collagen gels did not have consistent outgrowth and spheroids tended to appear as though they fell apart and did not form continuous angiogenic extensions (Figure A.3.1). Additionally, in some spheroids, a dense region towards the center of the spheroids was observed that appeared to be a cluster of

apoptotic cells (Figure A.3.1B). HUVEC spheroids were fixed and stained for actin and DAPI and imaged using confocal microscopy. We found that the dense region in the center of the spheroids did indeed appear to be apoptotic cells with fragmented nuclei (Figure A.3.2A). Interestingly, when took a confocal z-stack of the HUVEC spheroids, we noticed that some of the spheroids had formed fully enclosed lumens (Figure A.3.2B) whereas individual sprouts were seen within the interior of BAEC spheroids (Figure A.3.2C). Our results indicate that HUVEC spheroids do not form the classical angiogenic sprouts when embedded within our glycated collagen gels.

A.4 Microcarrier bead culture of endothelial cells

Several labs have utilized microcarrier beads to culture endothelial cells and embedded them within fibrin gels as an in vitro model of angiogenesis[4,12,13]. Since we were unable to produce HUVEC spheroids that with consistent sprouting behaviors, we attempted to use microcarrier beads to model angiogenic sprouting within our system.

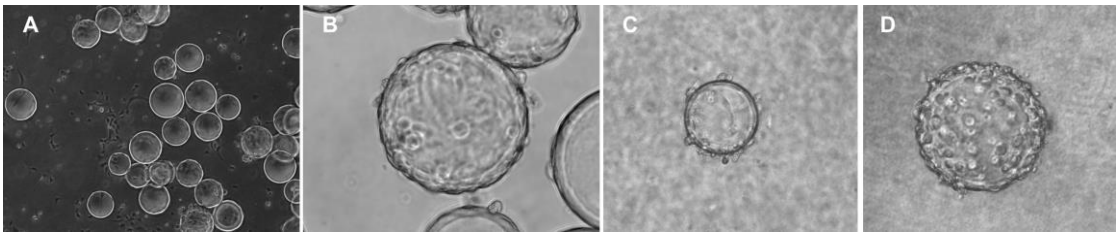

Figure A.4.1. Microcarrier beads seeded with endothelial cells. (A,B) Endothelial cells were allowed to attach to microcarrier beads in a 35 mm dish. Microcarrier beads coated with (C) human umbilical vein or (D) bovine aortic endothelial cells were embedded within collagen gels. Endothelial cells remained adherent to the microcarrier bead.

HUVECs and BAECs were successfully seeded onto Cytodex3 microcarrier beads (Sigma) using an orbital shaker (Figure A.4.1A,B). Cell-seeded microcarrier beads were embedded within collagen gels and monitored for outgrowth. Unfortunately, HUVEC and BAECs did not migrate off of the microcarrier bead and into the collagen (Figure A.4.1C,D). Even when we attempted to use AM200 with the HUVECs to stimulate angiogenesis, the endothelial cells did not consistently migrate into the collagen solutions (not shown). Our unsuccessful attempts taken together with successfully reported microcarrier experiments in collagen gels[14] suggest that we may need to dope the collagen gels with fibronectin to encourage endothelial cells invasion and sprouting.

A.5 Microchannel culture of endothelial cells

These experiments were completed in collaboration with Joseph Miller, a PhD student in the Reinhart-King Lab.

In Chapter 3, we utilize a method previously developed in our lab to investigate endothelial cell permeability in response to two-dimensional matrix stiffness using polyacrylamide hydrogels[2]. However, since this two-dimensional system more closely models large vessels and because it is difficult to form good monolayers on soft substrates (<1 kPa), we attempted to create a device that would allow us to quantify the permeability of microvessels within our glycated collagen gels. Our device was modeled from a number of other devices that have successfully created three-dimensional microvessels within collagen gels[15–18].

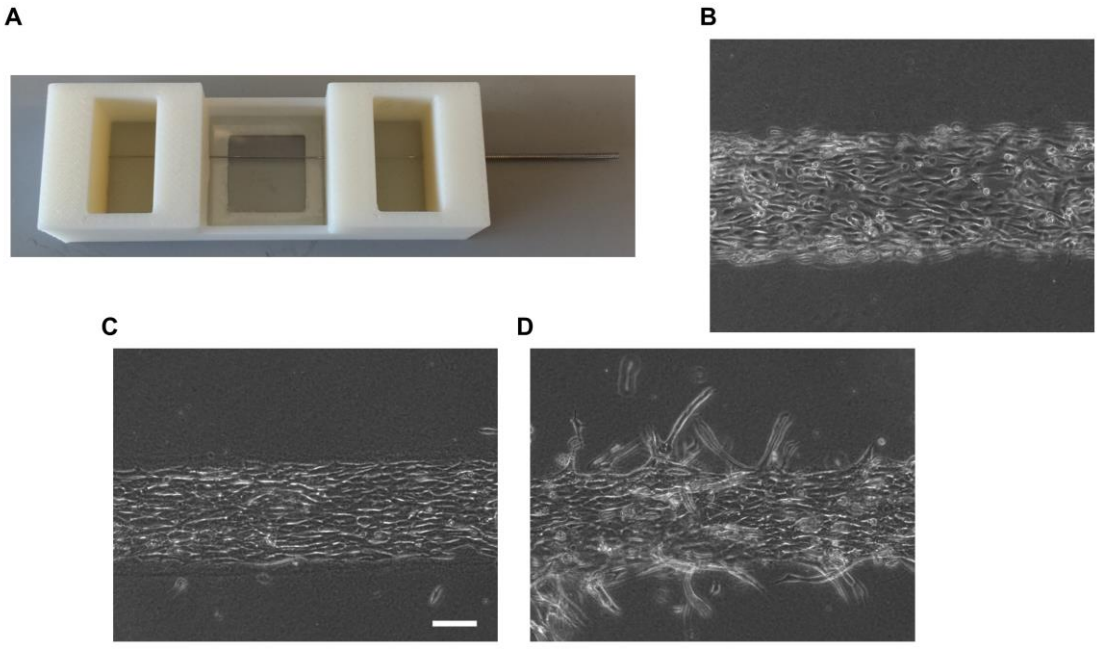

Figure A.5.1. Microchannels seeded with endothelial cells in collagen gels. (A) Microchannels were created by polymerizing collagen around an acupuncture needle. (B) Endothelial cells were injected into the channels and allowed to adhere to the collagen. Some endothelial cells form (C) tube-like structures in the microchannels while other areas (D) have a high degree of branching.

Joseph Miller and I created a manifold design that contained a central "culture" chamber with two external chambers to hold media (Figure A.5.1A). Manifolds were activated using polyethylenemine and glutaraldehyde as described in Appendix F and were dried using a lyophilizer (the 3D-printed ABS plastic is slightly porous). Vacuum grease was used to seal a 22x22 mm coverslip into the central culture channel and devices were UV sterilized in the biosafety cabinet. Microchannels within the collagen gels were created by threading acupuncture needles (0.3 x 75 mm) were threaded through holes in walls of the device and polymerizing 1.5 mg/ml collagen around them for 1 hour. The needles were carefully removed and a dense cell suspension (1,000,000 cells/ml) was injected into the channels. Manifolds were

placed upside-down in a 37^{O}C, 5% CO_2 incubator for 30 minutes to allow cells to attach to the top surface of the collagen microchannel (Figure A.5.1B). CM200 supplemented with 1% v/v penicillin-streptomycin was added to the collagen gels and outer wells. Endothelial cell outgrowth was monitored for up to a week. Unfortunately, HUVEC behavior within the microchannels was inconsistent with some areas forming tube-like structures while other areas were highly-branched (Figure A.5.1). Further optimization and experimentation may allow the experiments to be more consistent and feasible for 3D permeability measurements. If so, I would recommend using a fixable Texas Red dextran molecule to assess permeability as done previously by the Putnam lab[19].

A.6 Young investigator trans-network project with Moffitt Cancer Center: Investigating in vivo angiogenesis in response to matrix stiffness

These experiments were completed in collaboration with Mark Lloyd and Veronica Estrella at the Moffitt Cancer Center.

I was awarded a Young Investigator Trans-Network Project Grant from the National Cancer Institute, Physical Sciences Oncology Center for work entitled "The Role of the 3-D mechanical Environment in Regulating Angiogenesis" with Mark Lloyd at the Moffitt Cancer Center. In this PS-OC young investigator trans-network project, we explored the effects of 3D matrix stiffness on the organization and quantity of angiogenesis both in vitro and in vivo. We utilized collagen gels stiffened via non-enzymatic glycation implanted within a murine dorsal window chamber model.

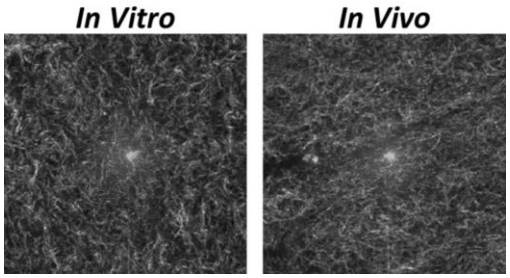

Figure A.6.1. Collagen fiber arrangements in vitro and in vivo. Collagen gels were polymerized and imaged with reflectance using multiphoton microscopy in vitro in Mattek dishes and in vivo in a dorsal window chamber. The arrangement of collagen fibrils was similar in both cases.

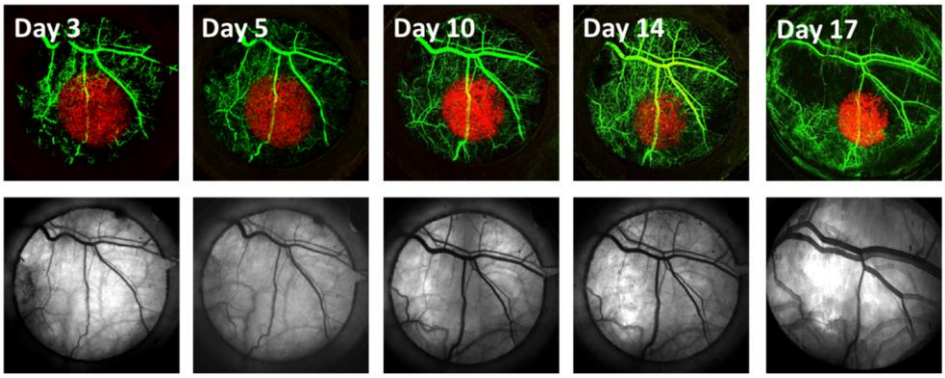

Figure A.6.2. Blood vessel growth visualized in murine dorsal window chambers. Murine dorsal window chambers were inoculated with collagen gels containing HCT116/RFP colon cancer cell tumors (red). After 3, 5, 10, 14, or 17 days of culture, the vasculature (green) and tumor tissues were imaged.

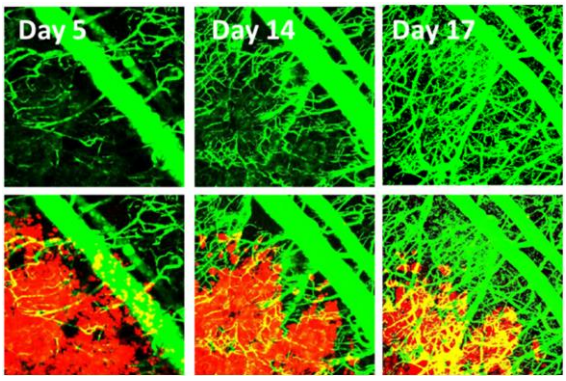

Figure A.6.3. A magnified view of the implants shows the vasculature (green) growing into the HCT116/RFP tumor tissue (red) at days 5, 14, and 17.

During solid tumor progression, tumor tissue tends to stiffen. Notably, angiogenesis in tumor tissue is perturbed. Compared to capillaries in healthy tissue, vessels in tumor tissue tend to be malformed, more permeable and more tortuous. In Chapters 2 and 3, we show that matrix stiffening via non-enzymatic collagen glycation alters the spreading, angiogenic sprouting, and spheroid outgrowth of bovine aortic endothelial cells in vitro[1]. Based on our in vitro results, we hypothesized that 3D mechanical stiffness will also regulate the dynamics of angiogenesis in vivo.

In this project, we utilized the glycated collagen matrices coupled with a murine dorsal window chamber model to monitor angiogenesis in vivo as a function of matrix stiffness. Since we have previously shown that different collagen fiber arrangements can influence cellular behavior[24], we confirmed that the glycated collagen matrices have similar fiber arrangements in vitro and in vivo (Figure A.6.1).

Initial in vitro experiments were performed to determine the optimal cell and glycated collagen mixtures to use within the dorsal window chambers. Murine dorsal window chambers were inoculated with collagen constructs and allowed to heal for 2 days. Subsequently, the vasculature was visualized by perfusing the mouse with 2000 kDA FITC-dextran and imaged using multiphoton microscopy. Constructs were imaged over the course at least 2 weeks and the development of the vasculature network was monitored. During this time, angiogenic blood vessels invade the glycated collagen gels in vivo and perfuse the tumor structure (Figures A.6.2, A.6.3). Our data have validated the feasibility of monitoring the response of vascular structures to matrix

stiffness with the glycated collagen gels. Future work should expand the number of experiments completed to determine the role of matrix stiffness on the formation of angiogenic vessels within the glycated collagen gels.

A.7 Collaboration with the Bonassar lab: Printed collagen interfaces and riboflavin cross-linking of collagen

These experiments were completed in collaboration with Stephanie Rhee, Nithin Reddy, and Timur Ozekcin from Lawerence J. Bonassar's laboratory at Cornell University.

To investigate whether collagen interfaces could be created to expose cells to a boundary between two distinct collagen domains, I worked with Stephanie Rhee in the Bonassar lab to utilize 3D printing technology. Neutralized 10 mg ml^{-1} collagen gel solutions that had been glycated with 0 or 100 mM ribose mixed with red and green beads, respectively and printed onto a heated plate. After printing, gels were

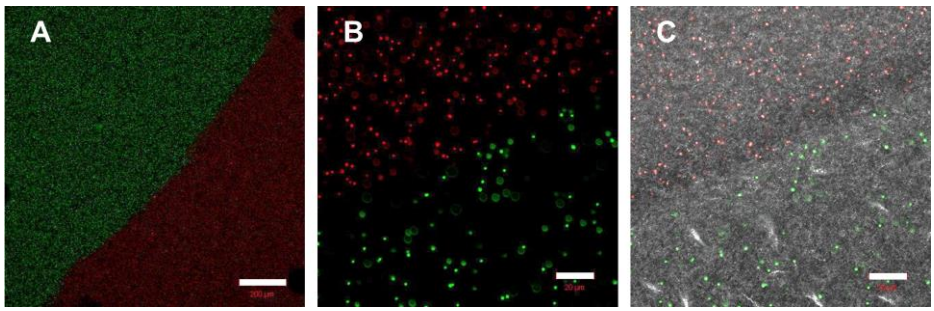

Figure A.7.1. Printed collagen interfaces. Collagen gels were printed using 10 mg/ml collagen solutions that had been glycated with 0 or 100 mM ribose and mixed with red or green beads, respectively. (A) The printed collagen interface between the collagen solutions is distinct. Scale is 200 μm. Zoomed in view of the printed interface (B) without and (C) with confocal reflectance microscopy imaging shows the separate collagen regions. Scale is 20 μm.

transferred to a 37^{O}C, 5% CO_2 incubator for 30 minutes to allow polymerization to be completed. Confocal microscopy was used to visualize the interface that was created between the gels. A distinct boundary between the gels was observed (Figure A.7.1). This technique may be useful to investigate how matrix stiffness heterogeneities within tissues influence angiogenesis.

Additionally, to investigate how riboflavin cross-linking concentration and matrix density would influence collagen gel structure and mechanics, I worked Nithin Reddy and Timur Ozekcin in the Bonassar lab. Riboflavin has been used in vivo to cross-link and strengthen corneal tissue[25,26]. Additionally, riboflavin has been shown to modulate collagen gel mechanical properties in vitro[27,28]. Collagen solutions were mixed with 0-0.5 mM riboflavin and neutralized to form 1.5 or 5 mg ml^{-1}gels. Gels were exposed to a UV lamp to cross-link the collagen and gels were polymerized for

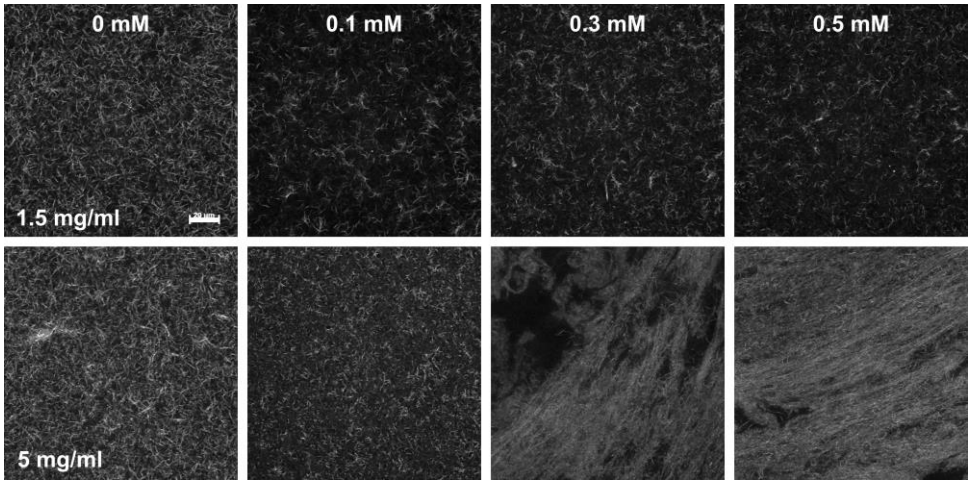

Figure A.7.2. Riboflavin cross-linking of affects collagen fiber structure and arrangement. Collagen gels were mixed with 0 – 0.5 mM riboflavin, polymerized, then cross-linked with UV light. Scale is 20 μm.

45 minutes at 37^{O}C 5% CO_2. Confocal reflectance microscopy was used to assess the internal fiber structure of the collagen gels. We found that riboflavin visibly altered the collagen fiber structure in both the 1.5 and 5 mg ml^{-1} collagen gels. Future experiments should be completed to determine the effects of adding riboflavin to collagen gels post-polymerization.

REFERENCES

1 Mason BN, Starchenko A, Williams RM, Bonassar LJ, Reinhart-King CA. Tuning three-dimensional collagen matrix stiffness independently of collagen concentration modulates endothelial cell behavior. Acta Biomater 2013; 9:4635–44.

2 Huynh J, Nishimura N, Rana K, Peloquin JM, Califano JP, Montague CR, King MR, et al. Age-related intimal stiffening enhances endothelial permeability and leukocyte transmigration. Sci Transl Med 2011; 3:112ra122.

3 Califano JP, Reinhart-King CA. Substrate stiffness and cell area drive cellular traction stresses in single cells and cells in contact. Cell Mol Bioeng 2010; 3:68–75.

4 Kniazeva E, Putnam AJ. Endothelial cell traction and ECM density influence both capillary morphogenesis and maintenance in 3-D. Am J Physiol Cell Physiol 2009; 297:C179–87.

5 Hoang M V, Whelan MC, Senger DR. Rho activity critically and selectively regulates endothelial cell organization during angiogenesis. Proc Natl Acad Sci U S A 2004; 101:1874–9.

6 Bryan BA, Dennstedt E, Mitchell DC, Walshe TE, Noma K, Loureiro R, Saint-Geniez M, et al. RhoA/ROCK signaling is essential for multiple aspects of VEGF-mediated angiogenesis. FASEB J 2010; 24:3186–95.

7 Kroll J, Epting D, Kern K, Dietz CT, Feng Y, Hammes H-P, Wieland T, et al. Inhibition of Rho-dependent kinases ROCK I/II activates VEGF-driven retinal neovascularization and sprouting angiogenesis. Am J Physiol Heart Circ Physiol 2009; 296:H893–9.

8 Van Nieuw Amerongen GP, Koolwijk P, Versteilen A, Van Hinsbergh V. Involvement of RhoA/Rho Kinase Signaling in VEGF-Induced Endothelial Cell Migration and Angiogenesis In Vitro. Arterioscler Thromb Vasc Biol 2002; 23:211–217.

9 Davis GE, Stratman AN, Sacharidou A, Koh W. Molecular basis for endothelial lumen formation and tubulogenesis during vasculogenesis and angiogenic sprouting. Int Rev Cell Mol Biol 2011; 288:101–65.

10 Gaudet C, Marganski WA, Kim S, Brown CT, Gunderia V, Dembo M, Wong JY. Influence of type I collagen surface density on fibroblast spreading, motility, and contractility. Biophys J 2003; 85:3329–3335.

11 Califano JP, Reinhart-King CA. A Balance of Substrate Mechanics and Matrix Chemistry Regulates Endothelial Cell Network Assembly. Cell Mol Bioeng 2008; 1:122–132.

12 Bing RJ, Binder T, Pataricza J, Kibira S, Narayan KS. The use of microcarrier beads in the production of endothelium-derived relaxing factor by freshly harvested endothelial cells. Tissue & Cell 1991; 23:151–159.

13 Ghajar CM, Blevins KS, Hughes CC, George SC, Putnam AJ. Mesenchymal Stem Cells Enhance Angiogenesis Early Matrix Metalloproteinase Upregulation. Tissue Eng 2006; 12:2875–88.

14 Shamloo A, Heilshorn SC. Matrix density mediates polarization and lumen formation of endothelial sprouts in VEGF gradients. Lab Chip 2010; 10:3061–3068.

15 Sakaguchi K, Shimizu T, Horaguchi S, Sekine H, Yamato M, Umezu M, Okano T. In vitro engineering of vascularized tissue surrogates. Sci Rep 2013; 3:1316.

16 Chrobak KM, Potter DR, Tien J. Formation of perfused, functional microvascular tubes in vitro. Microvasc Res 2006; 71:185–196.

17 Zervantonakis IK, Hughes-Alford SK, Charest JL, Condeelis JS, Gertler FB, Kamm RD. Three-dimensional microfluidic model for tumor cell intravasation and endothelial barrier function. Proc Natl Acad Sci U S A 2012; 109:13515–13520.

18 Bischel LL, Young EWK, Mader BR, Beebe DJ. Tubeless microfluidic angiogenesis assay with three-dimensional endothelial-lined microvessels. Biomaterials 2013; 34:1471–1477.

19 Grainger SJ, Putnam AJ. Assessing the permeability of engineered capillary networks in a 3D culture. PLoS ONE 2011; 6. doi:10.1371/journal.pone.0022086.

20 Bentley K, Franco CA, Philippides A, Blanco R, Dierkes M, Gebala V, Stanchi F, et al. The role of differential VE-cadherin dynamics in cell rearrangement during angiogenesis. Nat Cell Biol 2014; 16:309–21.

21 Jakobsson L, Franco CA, Bentley K, Collins RT, Ponsioen B, Aspalter IM, Rosewell I, et al. Endothelial cells dynamically compete for the tip cell position during angiogenic sprouting. Nat Cell Biol 2010; 12:943–953.

22 Hellström M, Phng L-K, Hofmann JJ, Wallgard E, Coultas L, Lindblom P, Alva J, et al. Dll4 signalling through Notch1 regulates formation of tip cells during angiogenesis. Nature 2007; 445:776–780.

23 Tung JJ, Tattersall IW, Kitajewski J. Tips, stalks, tubes: notch-mediated cell fate determination and mechanisms of tubulogenesis during angiogenesis. Cold Spring Harb Perspect Med 2012; 2:a006601.

24 Carey SP, Kraning-Rush CM, Williams RM, Reinhart-King CA. Biophysical control of invasive tumor cell behavior by extracellular matrix microarchitecture. Biomaterials 2012; 33:4157–4165.

25 Wollensak G, Spoerl E, Seiler T. Riboflavin/ultraviolet-a–induced collagen crosslinking for the treatment of keratoconus. Am J Ophthalmol 2003; 135:620–627.

26 Raiskup-Wolf F, Hoyer A, Spoerl E, Pillunat LE. Collagen crosslinking with riboflavin and ultraviolet-A light in keratoconus: long-term results. J Cataract Refract Surg 2008; 34:796–801.

27 Mi S, Khutoryanskiy V V, Jones RR, Zhu X, Hamley IW, Connon CJ. Photochemical cross-linking of plastically compressed collagen gel produces an optimal scaffold for corneal tissue engineering. J Biomed Mater Res A 2011; 99:1–8.

28 Wong JPF, MacRobert AJ, Cheema U, Brown R a. Mechanical anisotropy in compressed collagen produced by localised photodynamic cross-linking. J Mech Behav Biomed Mater 2013; 18:132–9.

APPENDIX B

PREPARATION OF GLYCATED COLLAGEN GELS

Materials:

Stock Collagen (10 mg/ml)

0.1% Sterile Acetic Acid

Hepes Buffer Solution (250 mM Hepes, 440 mM Sodium Bicarbonate, 1.1 g/L phenol red, in 10X PBS)

Cell Suspension / Media

1 N Sodium Hydroxide

Excel file for the collagen density and glycation concentrations (see 1.5 mg/ml protocol table below for an example)

Protocol:

1. Mix collagen, acetic acid, and ribose solutions together in a 15 ml tube to achieve desired ribose and collagen concentrations.
    a. It is difficult to mix more than 3 ml of gel solution when using pipets (you can get around this limitation by using syringes)
    b. See table below for an example of 1.5 mg/ml collagen gel solutions.
2. Incubate collagen solutions at $4^{O}C$ for **5 days** to allow for glycation reaction to occur**.**

a. NOTE: This must be done 5 days before polymerization if you are glycating gels or comparing controls to glycated gels BUT if you are only using control (0 mM gels), you can proceed to step 3 immediately

3. Add the HEPES buffer solution and mix well
4. Add the appropriate amount of sodium hydroxide to the solution and mix well
    a. NOTE: the table below displays an approximate volume for 1 ml of collagen solution but this will need to be adjusted until the collagen solution is approximately the color of complete medium (phenol red is a pH indicator and is present in the HEPES buffer solution)
5. Add in the cell suspension (or complete medium) and mix well
6. Pipet solutions into appropriate dish and allow to polymerize 20-60 mins dependent upon the collagen concentration (10 mg/ml collagen will polymerize much more quickly than 1.5 mg/ml collagen)
    a. Commonly used collagen gel volumes:
        i. 11 mm Mattek dish = 150 μl
        ii. 14 mm Mattek dish = 250 μl
        iii. 24 well Mattek dish = 500 μl
    b. NOTE: volume is an important determining factor of collagen fiber formation (see Carey et al., Biomaterials 2012)
7. After the gel has polymerized, add complete medium to the collagen gel.
8. Incubate with the media 1 hour and then remove media and add in fresh complete medium

a. NOTE: This is especially important if using glycated collagen gels so that the excess ribose is rinsed out of the gel.

To make 1 mL of collagen solution with the following glycation concentrations:

	Initial Volume	0.846	ml			
	Final Volume	1	ml			
	Collagen	1.5	mg/ml			
	D-PBS	1	X	**HEPES**	25	mM
	Cells	50	k cells/ml	**NaHCO3**	44	mM
From the following stock solutions.						
	Cell Conc.	1000	k cells/ml			
	Collagen	10	mg/ml			
	D-PBS	10	X	**HEPES**	250	mM
	Ribose	500	mM	**NaHCO3**	440	mM
	Glycation (mix 5 days prior to polymerization and store at 4^{o}C)			**Polymerization**		**Neutralize**
C_{ribose} (mM)	**collagen (ml)**	**Ribose (ml)**	**0.1% Acetic Acid (ml)**	**HEPES Stock (ml)**	**Cell Suspension or buffer (ml)**	**1N NaOH (ml)**
0	0.150	0.000	0.696	0.100	0.050	0.004
25	0.150	0.042	0.654	0.100	0.050	0.004
50	0.150	0.085	0.611	0.100	0.050	0.004
100	0.150	0.169	0.527	0.100	0.050	0.004
150	0.150	0.254	0.442	0.100	0.050	0.004
200	0.150	0.338	0.358	0.100	0.050	0.004
250	0.150	0.423	0.273	0.100	0.050	0.004
Collagen Density during Glycation:			1.773	mg/ml		

APPENDIX C

PREPARATION OF TRITC-LABELED COLLAGEN

Materials:

Lyophilized collagen

0.1M Sodium bicarbonate at pH=9

TRITC (Invitrogen: T490)

Dimethylsulfoxide (DMSO)

20000MW Dialysis tubing (Spectrum Laboratories: 131348)

Sterile water

Dialysis tubing clamps

Large Beaker or Erlenmeyer flask (washed and autoclaved)

Stir Plate

**Note all materials and reagents should be sterile.

Protocol:

1. Determine the weight of the lyophilized collagen.
2. Add cold 0.1 M, pH 9 sodium bicarbonate to the collagen to achieve a final collagen concentration of 10 mg/ml (or 20-30 mg/ml depending on the stock concentration you desire). Shake the collagen solution to mix well.
3. Add a 1:30 (mol collagen/mol TRITC) dilution of TRITC (at 10 mg/ml in DMSO).

4. Cover the collagen/sodium barcarbonate/TRITC solution with aluminum foil and place on a rocker at 4degC. Incubate the solution and allow it to react for 24 hours at 4degC.
    a. NOTE: At this stage, the collagen will not look very homogeneously dispersed in the sodium bicarbonate, it will appear very clumped and aggregated due to the basic solution.
5. Prepare sterile acetic acid solution for dialysis (you will need many liters of the 0.1% sterile acetic acid for the dialysis). Put the acetic acid in the cold room or refrigerator to chill it to 4degC.
6. Prepare the dialysis tubing by soaking it in sterile water for about 30 minutes to remove the sodium azide preservative.
    a. NOTE: Calculate the length of tubing you will need based on the diameter of the tubing and the volume of your collagen solution. The manufacturer should have information regarding how to do this. You will want some excess tubing at one end so that it can be suspended in the following steps.
7. Load the collagen solution into dialysis tubing (you can use a serological pipette), secure both ends with dialysis tubing clamps and leave a small “head space” or air bubble at the top end of the tubing.
8. Suspend the tubing within a large beaker or Erlenmeyer flask (I used a 5L flask) containing cold 0.1% sterile acetic acid. Add a stir bar to the flask and place the entire setup onto a stir plate at 4degC.

a. NOTE: Ensure that photobleaching of your labeled collagen does not occur by covering the entire flask setup with aluminum foil.

9. Change the acetic acid after about 1 hour and then daily (or more if needed) until the acetic acid solution is clear (i.e. no more TRITC is leaving the collagen) and the collagen solutions look opaque and uniform (i.e. no clumps or aggregates are visible). When I did this, it took about 8 days to get to this point.
10. Once dialysis is complete, remove the collagen solution from the dialysis tubing and place in a 50 ml centrifuge tube. Ensure that the tube is covered with aluminum foil to avoid photobleaching and store the collagen at 4degC until use.

References:

1. Mason B.N., A. Starchenko, R.M. Williams, L.J. Bonassar, C.A. Reinhart-King. Tuning 3D Collagen Matrix Stiffness Independently of Collagen Concentration Modulates Endothelial Cell Behavior. Acta Biomaterialia, 2013. 9(1):4635-4644.
2. Hermanson GT. Bioconjugate techniques. New York: Academic Press; 1996

APPENDIX D

SPHEROID GENERATION AND EMBEDDING

Materials:

MethoCult (H4100, 40 ml from Stemcell Technologies)

Complete Medium

Non-adherent 96-well round bottom plates

Orbital shaker

Collagen solutions (see glycated collagen protocol)

24 –well, glass bottom plates that have been coated Rain-X

Wide bore pipet tips

Spheroid Timeline with Glycated Collagen Gels:

Day 1: Prepare glycated collagen solutions

Day 3: Make spheroids

Day 5: Embed spheroids

Days 6-10: Monitor spheroid invasion

Methocult preparation:

1. Allow MethoCult to thaw at $4^{O}C$ overnight
2. Add 98 ml complete media to the bottle. Shake well to mix.
3. Let the MethoCult stand to allow the bubbles to rise to the surface.

a. NOTE: This 0.75% solution of MethoCult can be stored at 4^{O}C for up to 1 month.

Spheroid Generation:

NOTE: the numbers in this protocol will generate 1 plate of spheroids at 10,000 cells/spheroid

1. Pass cells according to protocol.
2. Count the cells and determine the cell density.
    a. For 1 – 96 well plate with 10,000 cells/spheroid, ~1,000,000 cells are needed.
    b. Determine the volume of cell suspension needed
3. In a 50 ml tube, mix the cell suspension with compete media to get 14.6 ml total.
4. Add 7.3 ml of the 0.75% MethoCult and mix well.
5. Transfer the mixture to a multi-channel pipet well.
6. Pipet 200 µl of the mixture into each well using a multi-channel pipet.
7. Centrifuge the plate at 1000RPM for 5 minutes.
8. Place plate on orbital shaker for 2 hours at ~30-45 RPM.
9. Culture cells for 2 days prior to embedding.

Spheroid Embedding

1. Pipet up-and-down in a well with a spheroid using a wide bore pipet tip. Find the spheroid in the media within the tip and isolate it into a small (~30 µl) volume of media on the lid of the well plate.
2. Repeat for ~12-15 spheroids.
3. Neutralize collagen solution
4. Pipet up 30 µl of collagen solution and collect spheroid into pipet tip
    a. Find the spheroid in the bubble on the lid
    b. Gently depress a small amount of collagen from the tip and "draw up" the spheroid into the tip
5. Deposit the spheroid and collagen onto the bottom of the 24-well glass bottom plate
6. Repeat for the remaining spheroids in that plate.
7. Move plate to the incubator. Plates will need to be incubated right-side-up, inverted, and then returned to right-side-up. The timing depends on the polymerization dynamics. I have found the following times to work well for 1.5 mg/ml collagen gels glycated with 0, 50, or 100 mM ribose.

Timing (min)	**0 mM**	**50 mM**	**100 mM**
Right-side-up	2	4	4
Inverted	4	5	8
Right-side-up	2	2	5

8. Add 450 µl of neutralized collagen per well. Incubate for an additional 30 minutes (right-side-up).
9. Add 1 ml complete media per well. Incubate 1 hour.

10. Exchange media for 1 ml of fresh complete medium (this step is important to wash away any excess ribose that may not have cross-linked within the gels).
11. Image spheroids using phase contrast microscopy.
12. Repeat step 11 for the rest of the experimental timing.

APPENDIX E

CONFINED COMPRESSION TESTING OF COLLAGEN GELS

Construct Fabrication:

1. Assemble the following materials in the biosafety cabinet:
    - Collagen and neutralization solutions
    - 24 well plate
2. Neutralize collagen gel solutions according to protocol
3. Polymerize 0.9 ml collagen per well for 1 hour at 37^{O}C and 5% CO_2
4. Add 1 ml media/well and incubate overnight at 37^{O}C and 5% CO_2
5. Remove media
6. Freeze gels at -20^{O}C
7. Cut constructs using 6 mm biopsy punch and place into individual 1.7 ml Eppendorf tubes
8. Freeze constructs at -20^{O}C until use

Mechanical Testing on Enduratec:

Machine Setup

NOTE: Do all setup with machine OFF

1. Screw 250 g for 1.5-5 mg/ml samples (or 1kg for 10-20 mg/ml samples) load cell onto the bottom, finger tight

2. Ensure load cell is connected to the controller (it should be plugged into the back of the console)
3. Screw appropriate size confined compression disk (3, 4, 6, or 8 mm) into the tissue cup
4. Screw the tissue cup onto the load cell
5. Connect impactor to the top of the system with 4 screws
    a. Put screws in from the top-down
    b. Be careful not to move the top load cell much – very important and sensitive for measuring loads
    c. Tighten screws with hex key to make the impactor as flat as possible on the bottom
6. Move stage up to comfortable position using black hatched pieces on the bars
    a. Note you will still be able to adjust height of tissue cup moderately using the rod and screw under the load cell

Computer Setup

1. Turn on Enduratec power box and load cell controller
2. Open the following on the computer

    NOTE: these files are pre-set to control the Enduratec and apply a 5% step-wise strain for 1.5 mm thick samples and can be modified for each individual test setup

    a. Wintest
    b. C:ProgramFiles:Enduratec

c. Brooke_Confinedcompression

NOTE: Go to Meniscus1mm if something is deleted on your file and re-save under your own name

3. Turn on the top load cell by clicking the "Local" button (green button towards the top right)
    a. Select "High"
    b. Close
4. Define the steps for confined compression
    a. 5% steps of sample thickness (originally set up for 2 mm samples)
    b. May need to change step size
    c. Need enough steps to go at least ½ way through normal thickness
5. Click "Setup" → "Channels" → "Load 1" in dropdown
6. "Tare" the load cell by bringing the load down in value on the main screen
7. "Home" the system by pressing the Home button then clicking "OK"

Sample Prep and Measurement

NOTE: It is generally easier to work with frozen samples; use PBS to gently transfer samples from the Eppendorf tube to a glass plate then into the tissue cup.

1. Measure the height of the sample with a caliper and record
2. Use PBS to hydrate and transfer the collagen construct (if cells are present, use a protease inhibitor in PBS)
3. Find appropriate sized porous plug
    a. Want the plug to be VERY level

b. The plug will go on top of sample and is porous to allow liquid to move through
c. The plug should be tight in the hole yet move relatively easily so you can do the testing and are measuring the load needed to compress the collagen

4. Transfer the collagen construct into the tissue cup with some PBS
5. Carefully move the construct into the compression disk hole using some PBS and a plastic pipet
6. Gently place the porous plug on top of the collagen construct
7. Bring the load cell and tissue cup up so that the top of the porous plug is almost touching the top piece
8. Move micrometer and bring top piece down slightly until it is touching the porous plug and the green load line on the screen drops (and recovers) slightly
9. Fill tissue cup with PBS so liquid level is above the porous plug
10. "Tare" the system again so the load is near "0"
11. Add up the amount of time the test will take
    a. Frequency → Time/step x # steps
    b. Max Scan Time = 1000 seconds
    c. # Scans = Total Time / 1000
    d. Figure out how much Time/Scan and set (overestimate!)
12. Ensure that "Displacement" and "Load 1" are clicked
13. Choose location to save files to
14. Click "Start" (button will turn yellow when it starts recording data)

a. Allow the load cell to record for ~30 seconds to set the basal level

15. Click green "Run" button to begin the loading program
    a. Click "0 – Start"
    b. Click "Yes"
    c. Click "Yes"

Data Analysis – Matlab Code

NOTE: The analysis code was developed by the Bonassar lab and the commands that follow describe how process the data through the code to quantify the gel modulus.

Preparing Data Folders

1. For each data set, prepare a folder that contains the "analysis" and "steps" folders as well as the "info.txt" file.
2. Label the data set "data.txt" so Matlab will recognize the file

Command Codes

1. File → Set Path → set to the Confined Compression Code folder (wherever you have it saved)
    a. Save and Close
2. Set Directory to folder with data set you wish to analyze
3. Commands:
    a. Chunkdata
        i. "0" enter
    b. SRcurvefit

i. close image

c. dataanalysis

i. “[x,y,z]” where x, y, z are rows that you want dropped or removed

ii. when happy with the data, “0” enter

iii. enter the linear region of the curve by

APPENDIX F

ACTIVATION OF PLATES AND COVERSLIPS FOR COLLAGEN OR POLYACRYLAMIDE ATTACHMENT

Materials:

Glass-bottomed plate or glass to be activated

Solution of 1% polyethylenemine (PEI) in water

Solution of 0.1% glutaraldehyde in 1X PBS

Distilled, Deionized (MilliQ) water for washing

Pipets and Pipettors

Appropriate waste containers (see note 3 above)

Protocol:

1. Put plate into plasma cleaner. Close the door to the plasma cleaner, check to make sure that the valve is closed, and turn on the vacuum pump to evacuate the chamber.
    a. Glass coverslips can be plasma cleaned in a petri dish. 5-6 glass 22x22 mm coverslips will fit in a petri dish bottom and 2 dishes can fit in the chamber at a time.
2. Once the pump has pulled a vacuum, turn the plasma cleaner onto the "high" setting. When the plasma is on, a pink haze can be seen through window. Leave plate in plasma for 2 minutes.

3. Turn off plasma and vacuum pump. Open valve to allow air to enter chamber and remove plate.
4. Place plate into the chemical fume hood and add in the PEI solution
    a. For a 24 well plate, use 1 ml per well
    b. For a 96 well plate, use 0.2 ml per well (can use the multichannel pipet for this)
    c. For glass coverslips, ensure that glass is submerged in the PEI (~5ml / petri dish)
5. Incubate the plates with the 1% PEI solution for 10 minutes.
    a. At this point, plates can be transferred to the Reinhart-King lab using secondary containment
6. Remove the PEI solution and put it into the appropriate waste container in the chemical fume hood. Rinse plates with water (3 x 5 minute incubations should work well)
    a. Remove the majority of the water from the plates and coverslips
7. Add 0.1% glutaraldehyde solution to the plates and incubate for 30 minutes.
    a. The same volumes used in step 4 can be used here EXCEPT invert glass onto 200 ul drops of glutaraldehyde on parafilm.
8. Remove the glutaraldehyde solution and put it into the appropriate waste container in the chemical fume hood. Rinse plates with water (4 x 15 minute incubations should work well for plates, 3 x 5 minute incubations should work well for glass coverslips).
9. Dry completely

10. If using for cell culture, UV the plate in the biosafety cabinet for at least 20 minutes to sterilize.

NOTES:

1. If you are using a Mattek dish/well plate, clean used plates with Alcanox and ethanol and rinse thoroughly with water before use.
2. Polyethylenemine and glutaraldehyde solutions should be disposed of in their respective, labeled hazardous waste containers in the chemical fume hood.
3. All items that are transported MUST be in a secondary container.
4. Collagen will adhere to the wells/glass if it is polymerized directly on the activated surface (the surface will NOT bind to collagen that is placed on the surface after polymerization)
5. Polyethlyenemine is VERY difficult to pipet but it can be kept in its diluted state until use. I have found that it is easiest to make the 1% PEI solution in 500 ml bottles. In the chemical fume hood, use a 25 ml serological pipet to slowly draw up ~8 ml of PEI and put it into 500 ml of water. I have found this to provide a good working concentration since much of the PEI is lost in the pipet.

APPENDIX G

MEASUREMENT OF ENDOTHELIAL CELL PERMEABILITY USING THE ZEISS LSM700 CONFOCAL MICROSCOPE

This protocol was modified from John Huynh's protocol for the Leica upright confocal and expanded to include analysis instructions

Materials:

Timer

Forceps

50 mm Mattek glass bottom petri dishes (with a 30 mm diameter glass opening)

10 μM 40 kDa FITC-dextran in Complete M199

Protocol:

1. Culture endothelial cells to 100% confluency on 18 mm circular polyacrylamide gels made on 18x18 mm glass coverslips in 6-well plates.
    a. NOTE: it is important to use the 18x18 mm glass coverslips so that they fit inside of the 30 mm diameter opening in the Mattek dish
2. Make enough 10 μM solution of 40 kDa FITC-dextran for all of your samples. Each sample requires 4 ml of dextran solution. For example, for 25 samples, make 100 ml of dextran solution.

a. NOTE: Dissolve 0.02 g 40 kDa FITC-dextran into 50 ml of Complete M199 to make a 10 μM solution. Media can be mixed by vortexing.
b. The 40 kDa FITC-dextran solution is stored in desiccant at 4°C and should be allowed to warm to room temperature before opening because it is hydroscopic

3. For each sample, aliquot 4 ml of dextran solution into a 50 mm Mattek petri dish. Place these petri dishes in the incubator to warm to 37°C.

NOTE: The following instructions are specific to the use of a Zeiss LSM700 microscope equipped with an environmental chamber and Zen 2012 software.

4. Warm the environmental chamber on the Zeiss LSM700 microscope to 37°C. Once warm, turn on the CO_2 to 5%.
5. Turn on the Zeiss LSM700 microscope (there is no need to turn on the fluorescent lamp).
6. Start Zen software.
    a. Turn off the 405 nm and 555 nm lasers (we will only use the 488 nm laser).
    b. Move the objectives to the "Load position" and put the individual sample holder on the stage
    c. Select the 40X water immersion objective and place a small drop of MilliQ water on the objective.
    d. Prepare software

7. Using forceps or the back end of a cotton swab, move a gel from the 6-well plate into a dextran-filled 50 mm Mattek petri dish. Start a timer for 5 minutes. Place the plate into the incubator and bring the immersed sample to the microscope and place it on the stage.
8. Prepare the microscope to acquire images of the gel.
    a. Locate the gel surface by doing a "Live" scan while moving the stage up and down in the z-axis and observing when the fluorescent intensity of the solution changes from being homogeneously bright to slightly dimmer (on gels with cells, you should be able to make out the cell outlines)
    b. In the XYZ mode on the touchpad, set the surface of the gel to "0"
    c. Move 100 um above the surface of the gel and set the point to be the upmost point of the z-stack
    d. Move 200 um below the surface of the gel and set the point to be the lowest point of the z-stack
    e. Check to make sure that your scan will encompass the entire gel by clicking "Start Experiment"
    f. Once the timer has reached 5 minutes, acquire 4 images in quick succession near the center of the polyacrylamide gel.
9. Repeat steps 7-8 with all samples.
10. Pro-tip: while waiting for timer to count down before step 8, you can place another gel in dextran and start a second timer to stagger your samples every ~3 minutes.

For data analysis:

Note that these analysis instructions assume that the intensity image is inverted such that the fluorescent solution appears to be at the bottom of the image with the gel at the top.

Do the following in the program ImageJ

1. Click on “Analyze” and choose “Set Scale”
    a. Check “Global”
    b. Press “Click to Remove Scale”
    c. Click “Ok”
2. Click on “Analyze” and choose “Set Measurement”
    a. Select area, min & max, integrated density, mean gray value, and display label from the list
3. Choose the rectangular selection tool
    a. Draw a box above the gel that is 400 pixels wide x 50 pixels high and place it about 50 pixels below the top of the gel (in the fluorescent region)
    b. Press “M” to measure
    c. Move the box to the other side of the endothelial cell monolayer such that the bottom of the box is just above the EC monolayer. Drag the top of the box to encompass the entire gel.
    d. Press “M” to measure

4. Repeat step 3 for all data
5. Copy the measurements from the results box and paste into Excel

Do the following in Excel

1. Create a column next to the imported data and divide the "mean gray value" measurement from inside the gel with the value above the gel
    a. =(Mean Gray Value Inside)/(Mean Gray Value Above)=Normalized Gray Value
2. Create another column to average the images from each gel together
    a. =AVERAGE[$(\text{Normalized Gray Value})_1$, $(\text{Normalized Gray Value})_2$, $(\text{Normalized Gray Value})_3$, $(\text{Normalized Gray Value})_4$]=Gel Averaged Gray Value
3. Create another column to normalize the cell permeability values to their controls (i.e. divide the 10 kPa cells by the 10 kPa controls to normalize for any differences in the diffusion of the 40 kDa FITC-Dextran into the gel)
    a. =(Gel Averaged Gray Value Cells)/(Gel Averaged Gray Value Control)

APPENDIX H

EMBRYONIC CHICKEN CHORIOALLANTOIC MEMBRANE MODEL OF ANGIOGENESIS

This protocol was developed with Michael Mazzola. Incubation and cracking protocols were modified from:

Yalcin et al., J Vis Exp 2010; (44) e2154

Timing Outline:

Day 0: Put eggs in incubator

Day 3: Crack Eggs

Day 5: Glycate collagen

Day 10: Preparation and implantation of collagen meshes

Day 15: Mesh fixation

Imaging and quantification

Protocol:

Day 0: Incubating Eggs

1. Order fertilized chicken eggs. In the Reinhart-King lab, we utilize the Cornell Poultry facility.

2. Label all eggs with your initials and the date. Place eggs in a 37.5^{O}C, 60% humidity, rocking incubator. Eggs are considered to be at embryonic Day 0 at the time of incubation.
    a. NOTE: Eggs can be stored in a wine cooler at 13^{O}C to arrest embryonic growth for a few days prior to incubation. Viability may decrease with the length of time stored so eggs should be used as soon as possible after delivery.
3. At embryonic Day 2.5-3, eggs are ready to be cracked and embryonic development can continue *ex ovo*.

Day 3: Cracking Eggs

1. The following materials should be assembled into a laminar flow hood:
    - Absorbent pad (laid out to cover the surface)
    - Plastic cups, 9 oz
    - Warm water
    - Plastic wrap
    - Rubber bands
    - Petri dishes
    - Beaker or metal bucket (sharp edge for cracking eggs)
    - Paper towels
    - 70% Ethanol
    - Autoclaved eggshells (ground to a powder using mortar and pestle)
2. Fill cups approximately 2/3 full with warm water

3. Cut a piece of plastic wrap, lay it over top of the plastic cup, and push down the center slightly so that it touches the water. Place rubber band around the cup to hold the plastic wrap in place (see photos 1 & 2).
4. Repeat steps 2-3 to get enough cups for all eggs.
    a. Alternatively, make hammocks in sets (for example, ten hammocks) to avoid preparing more cups than successful cracks, as it is unlikely all cracks will produce viable cultures (see photo 3).
5. Spray 70% ethanol onto the plastic wrap and allow it to incubate for at least 30 seconds. Dry plastic wrap with kimwipes.
6. Retrieve eggs from incubator 4-6 at a time and spray with EtOH.
    a. NOTE: Lay eggs on their side in an egg carton to allow the embryo to rotate to the top (see photo 4)
7. Gently crack the eggs on the edge of the beaker (see photo 6) and carefully deposit the egg onto the plastic wrap in a plastic cup.
    a. Tips for successful cracks:
        i. Softly crack until the shell membrane is broken and a small amount of albumin dribbles out of the egg.
        ii. After the shell membrane is broken, use the tips of your thumbs to separate the shell a bit further without completely cracking the egg. This will allow the egg shell to crack up the egg without releasing its contents so that crack will be more easily maneuvered.

iii. Swiftly separate the eggshell by pulling the crack apart. The swifter this motion, the less likely something (i.e. finger, egg shell) will puncture the yolk. It helps to pull apart on a diagonal to avoid contact with the yolk.

iv. Discard embryos whose yolks leak heavily, as they are unlikely to survive.

8. Ensure that the embryo is on top of the yolk and that the heart is beating. If the embryo is not at the surface, use your finger to gently rub the top of the yolk swiftly and repeatedly until the embryo appears.
9. Deposit a small amount of autoclaved eggshells (roughly a few grams) on the side of the hammock over the albumin.
    a. A plastic pipette with half its bulb cut off is a good way to transfer the eggshells from a conical tube to the albumin (see photo 5).
10. Put the top or bottom of a plastic petri dish over the cup and label before putting the embryo in the incubator.
11. Put plastic cups with water in the incubator to maintain incubator humidity.

Day 5: Preparing Glycated Collagen Solutions

1. Mix glycated collagen solutions and store at $4^{O}C$ for 5 days (for mesh placement at day 10).
    a. Refer to the glycated collagen protocol for preparing these solutions.

Day 10: Preparation and Implantation of Polymerized Collagen Meshes

1. Cut nylon meshes into 5 mm x 5 mm squares. Autoclave forceps and meshes before implanting.
    a. Meshes have square openings that are approximately ~200 μm square and can be ordered from Small Parts (#7050-1220-000-29) http://www.smallparts.com/dp/B0015H6LAK/ref=sp_dp_g2c_box
2. The following materials should be assembled into a biosafety hood:
    - Petri dishes
    - Parafilm (to cover bottom of a petri dish)
    - Autoclaved forceps
    - Autoclaved 5 mm x 5 mm meshes
    - Glycated collagen solutions mixed on day 5
    - VEGF (100 μg/ml) stock
    - HEPES stock and 1 N NaOH for neutralization
3. In the biosafety cabinet, line the bottoms of petri dishes with parafilm (one petri dish per condition).
4. Using the autoclaved forceps, place sets of two meshes of equal sizes/shapes (stacked on top of one another) on the petridishes.
5. Neutralize collagen solutions with HEPES and NaOH and mix well.
6. Add VEGF to neutralized solutions for a final [VEGF] of 5 μg/ml.
    a. NOTE: Substitute the PBS/Cell Suspension in the gel neutralization recipe for the 100 μg/ml VEGF stock solution.
7. Add 30 μl of neutralized collagen per mesh.

8. Incubate meshes in 37^{O}C incubator for 30 minutes.
9. Bring incubator with chick embryos and polymerized collagen meshes to location with laminar flow hood.
10. Remove 1 chick embryo at a time. In the laminar flow hood, place 5 polymerized collagen meshes around the chicken embryo vitelline membrane using the autoclaved forceps. Record location and conditions of meshes for each embryo (see photo 7).
11. Return chicken embryo to incubator after implantation.
12. Allow angiogenesis to occur until Day 15.

Day 15: Mesh Fixation

1. In the laminar flow hood, inject approx. 200 microliters of 0.25% Texas-Red Dextran in PBS using a 30G x 1 needle into the vasculature under the chorioallantoic membrane (CAM).
    a. Target injections to forks in the vasculature.
2. Return the embryo to the incubator. Allow 45 minutes for the dye to circulate.
3. Add 10-15 mL of 3.7% formaldehyde in PBS on top of the embryo.
    a. Cover the cultures with paper towel or aluminum foil to limit their exposure to light, as exposure to light weakens the fluorescent signal over time.
4. Remove the formaldehyde and dispose of appropriately in the hazardous waste.
5. Using scissors, cut the mesh from the CAM and put into 24-well plate.
    a. Note: chick should be decapitated before disposal

6. Incubate meshes in 3.7% formaldehyde for 45 minutes on rocker.
7. Wash 3x with PBS for 20 minutes on rocker.
8. Store at 4^{O}C until imaging is completed.

Imaging

1. On a glass slide, position the mesh with the CAM up (opposite the glass).
2. Using the 10x objective on the LSM, set up a tile scan that covers the mesh.
3. Run a z-stack, spanning the top (CAM) of the mesh to the lowest plane of fluorescent signal.

Quantification

1. Choose a 6x6 mesh square area that covers the most angiogenic vessels (those that branch off the CAM into the collagen of the mesh).
2. Count and record the number of squares within the 6x6 that have angiogenesis vessels.
    a. A max intensity z-projection on ImageJ (Image -> Stacks -> Z project) may help discern angiogenic vessels from CAM vessels by compiling the fluorescence from multiple z-planes

Photos:

Photos 1&2: Images of the hammocks used for chick culture

Photo 3: Make enough hammocks for each set of cracks. In this case, 6 eggs were removed from the incubator.

Photo 4: Lay eggs on side of cartoon so that embryo will float to the top before cracking the bottom side of the egg.

Photo 5: Autoclaved and ground eggshells transferred via the bulb of a severed pipette bulb.

Photo 6: Metal beaker for egg cracking and disposal.

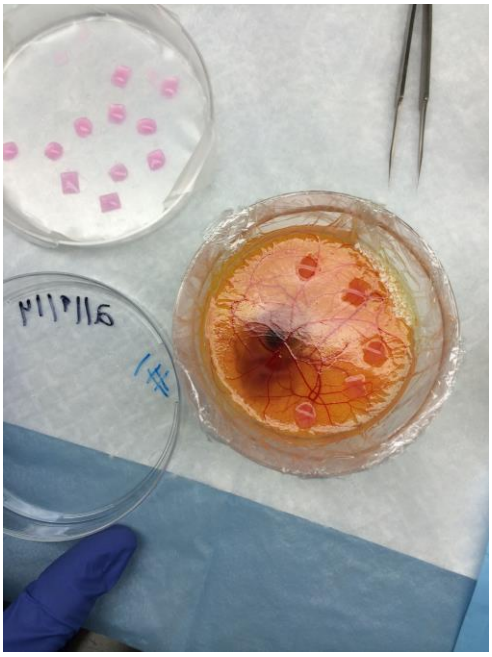

Photo 7: Collagen meshes (top left) implanted over vitelline (middle right)

APPENDIX I

HISTOLOGY PROTOCOL

Deparaffinization and Rehydration:

1. Label slides with conditions you will be using
    a. Pencil is best but lab markers can be used
    b. Include the markers you will be staining for and the date
2. Bake slides at 60^{O}C for 10 minutes
3. Cool slides at room temp for 5 minutes
4. Place samples into a slide holder/carriage (1 slide per spot)
5. Deparaffinize and rehydrate samples using the following washes
    a. 3X 5 min in 100% Xylene
    b. 1X 5 min in 100% Ethanol
    c. 1X 5 min in 95% Ethanol
    d. 1X 5 min in 70% Ethanol
    e. 1X 5 min in tap water

    NOTE: When moving to next wash, gently move carriage up and down in the container 5-10 times. Lift carriage and drain into container. Briefly tap the carriage onto paper towels and place into the next container
6. Move slide holder to a dish with water and exchange with water 5-6 times. Use tap water for the first 3-4 washes and DI water for the last 2 washes.

NOTE: Make sure to add water to the dish then add the carriage to avoid damaging the samples

7. Fill container with DI water, place carriage inside and place on the orbital shaker.

Antigen Retrieval:

8. Fill a plastic Coplin jar (with a lid) with 10 mM Citrate Buffer (pH 6)
9. Remove 1 slide at a time from the slide holder in the DI water. Use a Kimwipe (nicely folded) to wipe off the back of the slide and around the tissue sample on the front of the slide

NOTE: DO NOT touch the tissue section with the Kimwipe

10. Place the slide into the Coplin jar with the citrate buffer. Repeat for all slides

NOTE: Slides should have the tissue side faced inwards towards the buffer solution

11. Microwave for 1 min on "high" power

NOTE: The microwave powers and times are for the Shuler lab microwave. These may need to be adjusted if a different microwave is used.

12. Set the microwave to "warm" and microwave for 5 min.
13. Rest for 5 min
14. Microwave 5 min on "warm"
15. Rest for 2 min
16. Microwave 2 min on "warm"
17. Cool for 20 minutes to RT on counter.

18. Wash off citrate buffer with PBST (1X PBS + 0.05% Tween20)
19. Wash samples 2X 5 min with PBST on orbital shaker in the large Coplin jar.

Blocking and Staining:

1. Make blocking solution (usually 2-10% goat serum in 1X PBS) (will need approximately 100-200 ul/sample depending on area)
    a. For mouse-on-mouse staining, use the Vector Lab mouse-on-mouse kit blocking reagent
2. Dry slide (but do not touch tissue), circle each sample with hydrophobic pen and apply blocking reagent
3. Incubate in humidified chamber for 1 hour at room temperature or 37^{O}C
4. Dilute 1^{O} antibody in appropriate solution (usually 1:100 – 1:500 in 1% BSA in 1X PBS with 0.3% Triton-X)
    a. Note: can often mix multiple 1^{O} antibodies together for staining at the same time
    b. For mouse-on-mouse staining, use the Vector Lab mouse-on-mouse kit diluent solution
    c. Briefly vortex and store at 4^{O}C until use
5. Aspirate blocking solution
6. Wash slides 3X 5 min with PBST
7. Dry slide (but do not touch tissue) and apply 1^{O} antibody solution

8. Incubate overnight at 4^{O}C or 1-2 hours at room temperature (as optimized for protocol)
9. Aspirate antibody solution
10. Wash slides 3X 5 min with PBST
11. Dilute 2^{O} antibody in PBS (usually 1:100-1:200 works well)
12. Apply 2^{O} antibody to tissue and incubate for 30 minutes at room temperature (covered with foil)
13. Wash slides 3X 5 min with PBST
14. Repeat as necessary for all 2^{O} antibodies
15. Wash slides 3X 5 min with PBST
16. Mount slides using Vector Labs mounting medium and a coverslip (can use nail polish to seal)

APPENDIX J

MICROFLUIDIC DEVICE SETUP

Cell Seeding for 2D experiment: Should be completed ~6-24 hours before beginning device setup

1. Pass cells according to standard protocol
2. Seed a microscope slide (with or without polyacrylamide gel hydrogel) with cells by creating a cell suspension "bubble" of media on top of the slide
    a. ~15,000 BAECs/slide worked well for my single cell experiments
3. Incubate at 37^{O}C, 5% CO_2 for at least 6 hours to allow cells to attach
4. If not using cell slide immediately, fill petri dish with media and incubate until use

Creating Agarose Mold of Features:

1. Assemble the following at the lab bench:
    - Silicon master
    - 1 mm thick PDMS spacer
    - Agarose powder
    - 1X PBS
    - Glass slide
    - Small beaker

2. Clean the silicon master, spacer, slide, and beaker using 70% ethanol. If the spacer is dusty, clean by gently pressing scotch tape onto it
3. Place spacer around features in silicon master and press down to seal
4. Make a 3% agarose solution my mixing 0.3 g of agarose with 10 ml of PBS
5. Heat the solution in the microwave with occasional mixing (mix by swirling) until the agarose is completely dissolved and solution is boiling
    a. NOTE: Swirl the agarose in the small beaker to prevent bubble formation, sometimes boiling the solution can actually decrease the amount of bubbles in solution
6. Pour the hot solution into the spacer and move any bubbles out from between the channels using a spatula
7. Place the glass slide on top of solution in the spacer. Press down on slide evenly to create a flat agarose mold of the microfluidic device features
8. Transfer the silicon master and agarose mold into the biosafety cabinet

Microfluidic Device Assembly:

1. Assemble the following in the biosafety cabinet:
    - Silicon master and agarose mold
    - Plastic tubing punch
    - Plexiglass microfluidic top
    - Stainless steel microfluidic bottom
    - Screws and screw driver
    - Glass slide or polyacrylamide gel on a glass slide seeded with cells

- Glass slides for transferring agarose
- Sterile PBS
- Large petri dish
- Thin plastic lifter (can be cut from the bottom of a weigh boat)

2. Remove slide from the top of agarose mold by sliding it off
3. Punch holes corresponding to the microfluidic device ports using the plastic tubing punch
    a. NOTE: Make sure to remove the agarose plugs from the mold
4. Gently lift the agarose mold and spacer off of the silicon master, transfer feature-side-up onto a glass slide
    a. NOTE: I have found it easiest to use the thin plastic lifter with some PBS
5. Transfer mold to another slide so that the feature-side-down
6. Align the mold ports with the microfluidic top ports and replace the spacer around the agarose
7. Place the slide or polyacrylamide gel that has been seeded with cells in the microfluidic bottom
8. Coat the slide with complete media
9. Gently lower the agarose and microfluidic top onto the microfluidic bottom being careful to avoid bubble formation
10. Apply gentle and even pressure to the device with one hand and alternate putting screws in with the other hand

a. NOTE: do not over-tighten screws or you will collapse the microfluidic channels, this is especially important when assembling the device on top of a polyacrylamide gel

11. Check to ensure that the ports are open by using a micropipette to flow solution through each of the channels
12. Ensure that all channels are filled in media, put PDMS filled pipet tip plugs into each port, place device in sterile petri dish, and put into 37^{O}C, 5% CO_2 incubator until microscope is ready

**If you are creating a 3D collagen suspension of cells in the center channel, allow the device to warm up in the incubator. Prepare your cells suspension in the neutralized collagen solution on ice. Inject collagen solution into both sides of the center channel. Plug channel ports with PDMS filled pipet tips so all collagen flow is stopped. Place the microfluidic device in the incubator, turn device upside down partway through so that cells do not all sink to the bottom.

Time Lapse Experiments:

1. Make tubing for experiment
    a. Generally, 0.25 mm ID tubing should be used. Most inlet tubing sets will be comprised of 3 parts – the peristaltic tubing with another tubing section connected to either end to connect to the microfluidic device
        i. Attach the peristaltic pump section to tubing connector sections with gel loading pipette tips.

ii. Pipette tips should also be used in tubing ends that will connect to the microfluidic device

b. Make outlet tubing for microfluidic device (tubing should have pipette tip connector but not be connected to pump for passive outlet flow)

2. Turn on heat in environmental chamber on microscope
3. Label tubing with media condition using tape for markers, connect to peristaltic pump and place the pump near the back of the environmental chamber
4. Prime tubing with 70% ethanol for ~5 minutes to sterilize
5. Prime tubing with PBS for ~10 mins to get rid of bubbles and clear out the ethanol
6. Prime tubing with media
7. Once the environmental chamber is warm and tubing is primed with media (just use complete media here), turn the fan down to low and place the microfluidic device on the stage
8. Set up positions and program to run time lapse microscopy
9. Prime tubing with media of the appropriate condition
    a. Put the media tubes in the environmental chamber so that they will be temperature and CO_2 controlled throughout the experiment
    b. It is best to run tubing through the sliding doors in the back of the chamber
10. Connect inlet and outlet tubing to microfluidic device

a. Outlet tubing should run to a collection vessel outside of the environmental chamber

11. Begin fluid flow at 5 ul/min (~0.66 RPM with 0.25 mm ID tubing) and note what time it is.
12. Re-focus positions for time lapse, begin imaging as optimized for experiment; note what time it is relative to the start of the flow.

Time Lapse Notes and Hints:

- Since the channels are so small, it is extremely important to keep the light intensity low so as to not overheat/overexpose the cells. I used a light intensity of ~1.03V with an exposure >1s.
- Care should be taken to make sure that the device has stable fluid flow (with no fluid accumulation) at any of the ports before leaving it on the microscope
- Keep the culture channel ports plugged with PDMS-filled pipet tips during the experiment to avoid media dehydration

APPENDIX K

TRANSFECTION OF ENDOTHELIAL CELLS

This protocol has been modified from Joe Califano's protocol

This procedure can be used for siRNA transfection of endothelial cells (bovine aortic or human umbilical vein)

Timeline for siRNA knockdown verification

Day -1: Plate cells in a vessel

Day 0: Transfect cells

Day 1: Collect Cell Lysate

Day 2: Collect Cell Lysate

Day 3: Collect Cell Lysate

Day 4: Collect Cell Lysate

Run Western

Materials:

- Cells
    - For siRNA: cells in a 6-well dish 60-80% confluent
- Lipofectamine 2000
- Optimem

- siRNA
- Sterile 15 mL centrifuge tubes

Optimization Notes:

- siRNA is administered at 10, 20, 50 pmol per well to optimize concentration
- 3 wells/condition/day of a 6 well plate are lysed for Western blotting
- Control Fluorescein-conjugated siRNA is used to verify transfection efficiency and as knockdown control

Procedure:

1. The day before transfection, seed
    - For plasmids: 300k cells/well in a 6-well dish
    - For siRNA: 200k cells/well in a 6-well dish

The day of transfection (Day 0)

1. Add 250 μL Optimem per well to 2 centrifuge tubes – 1 tube each for siRNA and lipofectamine dilutions
2. Add to the siRNA tube
    - siRNA: 1, 2, or 5 μL stock siRNA solution per well —mix and sit 5 min RT
    - NOTE: 1 μL per well of a 10 μM stock will be 10 pmol of siRNA
3. Add to the lipofectamine
    - For siRNA: 6 μL Lipofectamine per well and sit 5-15 min RT
    - NOTE: Do not exceed 25 min

4. Mix the Optimem tubes together (lipofectamine and siRNA)
    - sit 20 min RT
5. Was cells gently 2x with Optimem
6. Add 1.5 mL Optimem to well
7. Add the ~500 μL siRNA/Lipofectamine/Optimem mix to each well (2 mL final volume per well)
    - add dropwise to the well
    - swirl/rock to mix, avoid bubbles
8. Put in incubator 4-6 h. Check cells every few hours for significant debris or vacuole formation
9. Remove mix, wash 2x with sterile PBS
10. Replenish fresh media

Days 1-4

1. Collect cell lysates for Western blot to verify knock down

APPENDIX L

CELL INVASION ASSAY

This protocol was developed with Sahana Somasegar

Materials:

Collagen solutions and neutralization materials (HEPES buffer solution, 1 N NaOH, etc.) *NOTE: see Appendix B*

Activated 96-well glass-bottomed plate (UV sterilize plate after activation for at least 20 min) *NOTE: see Appendix F*

Flask of cells that are ready to passage and appropriate passaging solutions (media, trypsin, etc.)

Protocol:

1. Neutralize collagen gels by adding HEPES and 1 N NaOH to each of the collagen gels and mix well (or other buffers according to your protocol)
2. Pipette 100 μl of collagen gel mixture per well into activated 96-well plate – generally seed 6 wells per condition (0mM, 50mM, and 100mM)
3. Place in 37°C incubator for 30 minutes to allow for collagen polymerization
4. After 30 minutes, remove plate from incubator, carefully add 100 μl media on top of each gel, and place in incubator for another 1 hour to allow gels to hydrate.

5. During the 1 hour incubation step, passage your cells according to the appropriate protocol.
6. Seed the hemocytometer by adding 10 µl of cell suspension to each side.
7. Centrifuge the cells for 5 minutes at 1000 rpm
8. While the centrifuge is running, count the cells using the tissue culture microscope and hemocytometer
9. Determine the amount of media that will need to be added to the cell pellet so the density of the cell suspension is 500,000 cells/ml
10. Remove sample from centrifuge and remove supernatant so that only the cell pellet is remaining
11. Add media so that the cell concentration is 500,000 cells/ml (based on hemocytometer count) and mix well
12. After 1 hour has passed since the 96-well plate was placed in the incubator, remove plate and remove media from each well
13. Pipette 100 µl of the cell suspension solution with into each well
14. Place in incubator for 24 hours.

Data Collection and Imaging

15. For the next 5 days, examine the 96-well plate under the microscope at 24 hour intervals
16. When viewing under the microscope, zoom out to the top most layer of the microscope and zero the Z value.

17. Slowly zoom in, going deeper into the gel, to the last possible point when cells are clearly seen in focus. Record Z values for 5 positions within each well – left, center, right, top, and bottom of the well.
18. Record this Z value.
19. Repeat steps 21-23 every 24 hours for 5 days

APPENDIX M

COLLAGEN CONTRACTION ASSAY

Construct Fabrication:

1. Assemble the following materials in the biosafety cabinet:
    - 16 mm inner diameter silicone O-rings
    - 22x22 mm coverslips
    - forceps
    - beaker
    - paper towels (spread across cabinet surface)
    - petri dishes
    - 1X sterile PBS
    - 2% sterile gelatin in a petri dish
    - 70% ethanol
2. Place O-rings in the beaker and cover with 70% ethanol, incubate at least 5 minutes to sterilize.
3. Aspirate ethanol and rinse the O-rings with the sterile PBS
4. Place O-rings into 2% sterile gelatin petri dish
5. Lay out 22x22 mm coverslips on the paper towels
6. Select an O-ring out of the gelatin with the forceps and place it onto a glass coverslip.

a. NOTE: If there is a bubble of gelatin in the middle of the O-ring, pop it with a vacuum aspirator.

7. Repeat step 6 for all O-rings and coverslips.
8. UV sterilize constructs for at least 30 min
9. Place 4-5 constructs into each petri dish and incubate them at 4^{O}C for at least 1 hr or until the gelatin had adhered the O-ring to the coverslip.
    a. NOTE: You can incubate them for up to a few days

Collagen Gel Polymerization:

1. Assemble the following materials into the biosafety cabinet.
    - O-ring/coverslip constructs
    - Collagen and neutralization solutions
    - Cell flask and passaging solutions
    - 6 well plates
    - forceps
2. Place 1 construct/well into a 6 well plate
3. Trypsinize and re-suspend cells to desired concentration in cold media
    a. NOTE: If using glycated collagen gel protocol, re-suspend cells at 5,000,000 cells/ml
4. Neutralize collagen gel solutions according to protocol
5. Mix cell suspension with collagen solution
6. Pipet 500 µl of collagen/cells into the middle of the O-ring for each construct
7. Polymerize collagen for 45 min at 37^{O}C and 5% CO_2

8. Add 3 ml of complete media/well
9. Carefully remove O-ring from collagen gel using forceps
10. Image the collagen gel in each well with a ruler next to the plate for scaling
11. Repeat step 10 each day throughout the course of the experiment
12. To analyze data, measure the area of the gel at each time point and normalize to the first time point.

APPENDIX N

ENDOTHELIAL CELL MICROCARRIER BEAD PROTOCOL

Materials:

Sigmacote

Glass Bottle

Cytodex 3 microcarrier beads

PBS

Complete Medium

Cells ready for passage

Collagen and neutralization solutions

Sterilizing Microcarriers:

1. Silanize a glass bottle by coating with Sigmacote
    a. Put a small amount (~1 ml) of Sigmacote into the bottle and turned bottle so liquid coated all sides of interior
    b. Put excess into other bottle and repeated
    c. Put the bottles into fume hood and allow to dry overnight
    d. Wash the bottles with detergent and water
2. Suspend beads in PBS to allow them to swell
    a. Want ~10,000 beads/ml
    b. There are ~3,000,000 beads/g

c. $\frac{10{,}000\frac{beads}{ml} x\ 500\ ml}{3{,}000{,}000\frac{beads}{g}} = 1.67\ g\ beads\ into\ 500\ ml\ PBS$

3. Autoclave the beads to sterilize and allow to cool before using.
    a. Note: I used a liquid cycle for 32 minutes because of the 500 ml PBS

Seeding Microcarriers:

1. Wash 1 ml of beads 2X with complete medium.
    a. Resuspend beads by swirling in the PBS prior to aliquoting
    b. Spin beads for 1 min @ 1000 RPM to pellet between washes
2. Add the 1 ml of beads to a 35 mm petri dish.
3. Pass cells and resuspend to 500,000 cells/ml.
4. Add 2 ml of cell suspension to the 35 mm petri dish. (1,000,000 cells/dish; 200 cells/bead)
5. Place dish on orbital shaker and gently rock for ~4 hours to allow cells to attach.
6. Remove cells from petri dish and place into centrifuge tube. Spin for 1 min @ 1000 RPM.
7. Resuspend in a fresh media and a new petri dish
8. Incubate overnight.

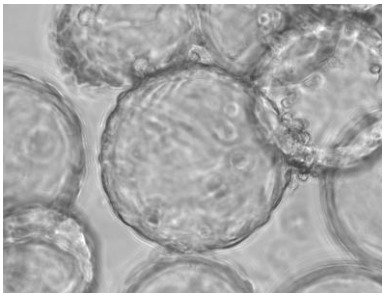

Microcarrier bead coated with human umbilical vein endothelial cells in a 35 mm petri dish.

Suspending Microcarriers in Collagen gels:

Note: the microcarrier beads are pretty "heavy" and sink through the collagen gels easily. I found this to be the easiest way to suspend the beads.

1. Spin the cells for 1 min @ 1000 RPM. Resuspend in 1.5 ml
    a. I have found that this density gives me some isolated microcarrier beads even though some may be aggregated
2. Neutralize a tube of collagen.
3. Pipet 100 µl of collagen per well into a 96-well plate.
4. Allow collagen to polymerize for ~5 min at 37^{O}C
5. Neutralize another tube of collagen solution but replace the "media" component with the microcarrier bead suspension.
6. Pipet an additional 50 µl of the microcarrier/collagen solution on top of the partially polymerized collagen.
7. Allow collagen to polymerize for 30 min at 37^{O}C.
8. Add 200 µl of complete medium to the polymerized gel.
9. Incubate 1 hour.
10. Exchange medium for fresh complete medium.

APPENDIX O

GK-12 TEACHING MATERIALS

O.1 Cornell BME CLIMB Module

Blood Vessel Transport and Tissue Perfusion	
Author:	Brooke N. Mason and Laura V. Austen
Date Created:	December 2012
Subject:	Intermediate Level Science
Level:	Middle/High School (Grade 8-11)
Standards:	NYS Standards: The Living Environment Core Curriculum http://www.p12.nysed.gov/ciai/mst/pub/livingen.pdf **Standard 1** Key Idea 1 – Scientific Inquiry: 1.1a, 1.3b Key Idea 2 – Scientific Testing: 2.1, 2.3, 2.4 Key Idea 3 – Analysis of Results: 3.1, 3.3 **Standard 4** Key Idea 1 – Living Things: 1.2a,b,e,f,g Key Idea 5 – Dynamic Equilibrium: 5.2a,h, 5.3a
Schedule:	**2 days, 1-hour periods**

Objectives:

Students will learn about blood vessels and the tissue properties that influence the exchange of nutrients and wastes.

Students will also learn about how the foods they eat contribute to changes in blood sugar. They will learn to use a glucose meter and discuss the changes to blood sugar regulation that occur in patients with diabetes.

Students will:

Vocabulary:

Circulation
Perfusion
Tissue Density
Hydrogel
Glucometer

Materials:

For Each Group:

Transport Lab

- Petri dishes
- Gelatin
- Straws
- Red food coloring
- Paper towels
- Pipettes or droppers

Transport Lab • Simulate blood vessel perfusion • Quantify the diffusion and describe how it will be influenced by tissue properties • Predict what would happen if disease altered the density of a tissue **Blood Sugar Lab** • Test for simple sugars using chemical indicators and a glucose meter • Explain diffusion through a membrane • Relate the process of digestion to the circulation of sugars in the blood • Predict how foods will influence blood sugar levels	• Rulers **Blood Sugar Lab** • Dialysis tubing • Water, milk, soda, juice, sports drink • Beakers • Glucose meter • Glucose meter test strips • Pipettes or droppers Safety: Goggles Wash hands after experiments

Science Content for the Teacher:

Note: This lab can be used to supplement the knowledge gained the NY State Laboratory "Diffusion through a Membrane" or can be used as a stand-alone module to discuss the concepts of diffusion and transport within our body.

Part 1 – The transport of molecules and perfusion of tissues via the circulatory system

The process of exchanging of oxygen, carbon dioxide, nutrients, and wastes is called tissue perfusion and occurs in small blood vessels called capillaries. The effective perfusion of tissues is dependent upon a variety of factors including the number of capillaries, the flow rate of blood through the capillaries, the permeability (or leakiness) of the capillaries, and the density of the tissue. For example, capillaries within many solid tumors tend to be leakier that blood vessels in healthy tissues. This leakiness allows excess nutrients to leave the blood vessels and diffuse into the tumor tissue and ultimately facilitates tumor growth. Interestingly, this process may also contribute to cancer cell metastasis (cancer cells leaving the tumor, entering the blood vessel, and making new tumors in different body sites) because the cells can enter the blood vessels easier.

Tissue density is influenced by the amount proteins and other molecules in the space surrounding the cells called the extracellular matrix. Tissue density is influenced by the function and type of tissue and can be altered during different diseases such as cancer. These changes in density can have large effects on tissue perfusion and

nutrient transfer because it takes longer for molecules to move through tissues of increased density. Since it more difficult to control the leakiness of a classroom-based vascular model, this lab focuses on the effects of tissue density on perfusion.

Part 1 – Laboratory Goals and Procedures
In this inquiry-based laboratory, students will design a set of experiments to test properties that influence tissue perfusion. They will discover and discuss how diseases that change the density of tissue influence the ability of blood to perfuse the tissue. Students will cut capillary structures into the tissue construct and then place red food coloring (simulating oxygenated blood) into each of the wells. Students will then monitor the experiment, record their results, and analyze the data.

Part 2 – The relationship of the food we eat and blood sugar levels
When we ingest foods and drinks, they enter into the digestive system and are eventually converted into the nutrients our cells need to survive. What we eat directly influences the nutrients our body receives, uses, and stores as fat. The process of digestion breaks down all of the usable nutrients from what we ingest so the nutritional content of the food we eat is very important. Generally, people should eat foods that are low in oils and fat and high in vegetable and fruit content with moderate protein and grain intake. Sugars can provide people with the energy they need to be active but, if people eat and drink too much sugar, the excess will be converted to glycogen or fatty acids and stored within the body.

People with diabetes must be especially careful about the amount of sugar they ingest because they do not produce enough insulin or are resistant to the insulin they do produce. In addition to controlling their dietary intake and exercising, diabetic patients also use insulin therapy to control their sugar levels. The most common way to measure the amount of sugar in the blood is to use a small device called a glucometer (or glucose meter) with a small drop of blood from a pricked finger.

Part 2 – Laboratory Goals and Procedures
In this laboratory, students will investigate how different drinks can influence blood sugar levels. Students will simulate the absorbance of nutrients into the blood stream from different liquids using dialysis tubing filled with fluid to model the blood vessel. They will test the amount of glucose that has entered the blood vessel using a glucose meter and compare between the conditions they chose.

Preparation:

Pre-lab lecture: A day before the lab, the teacher should introduce the students to the concepts of diffusion, circulation, digestion, and transport. Students should understand the basic principles of how the circulatory and digestive systems are related to each other.

Part 1: Transport

Materials

- 2 petri dishes per group (at least 1 for each student)
- 2%, 5%, and 15% (w/v) gelatin solutions
- Straws (McDonald's straws work well)
- Red food coloring
- Paper towels
- Pipettes or droppers
- Rulers

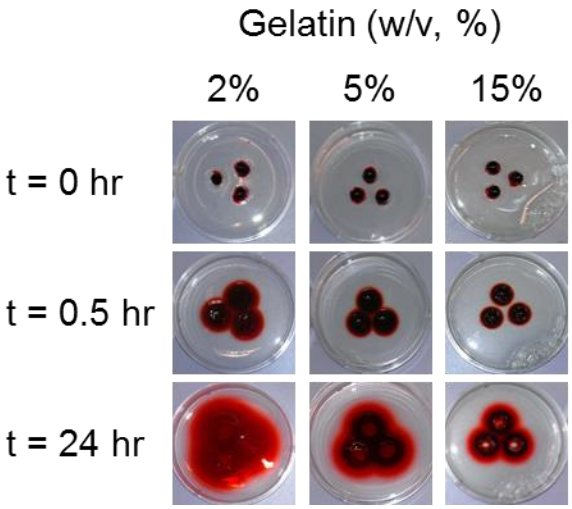

Figure 1. Example experimental setup and qualitative results of the transport laboratory. As the density of the gelatin increases, the amount of diffusion is decreased over the course of 24 hours.

Prepare Petri Dishes

At least 1 day prior to the laboratory, instructors should:

1. Dissolve gelatin in water to create 2%, 5%, and 15% solutions.

Note: The water may need to be heated to get the gelatin to dissolve completely

2. Pour gelatin into petri dishes and allow the gelatin to set in the refrigerator. Make sure to label the petri dishes with the % gelatin.

Transport Laboratory

Split the students into groups of 2-3

(Day 1)

1. **Decide on gelatin density and vessel layout:** Each group must decide which 2 gelatin conditions they will use and should determine the layout they plan to use for their vessel structures.

Note: If you are using having the students use the associated worksheet, they should complete Part 1, Questions #1-4.

2. **Cut the blood vessels:** Students should punch their capillary structures into the gelatin (tissue construct) using a straw or biopsy punch. Ensure that the gelatin is completely removed from the center of the well and then have the

students place 1 drop of red food coloring into each of the wells that are created.

3. **Measure the diffusion of the food coloring from the wells:** Students should measure the amount of diffusion that has occurred immediately after placing the food coloring in the wells and at the end of the first lab period.

Note: If you are using having the students use the associated worksheet, they should complete Part 1, Question #5.

4. **Label petri dishes and store overnight:** Students should label their petri dishes and they should be stored in the refrigerator overnight so that the students can make observations during the next lab period.

(Day 2)

5. **Measure the diffusion of the food coloring from the wells:** Students should measure the amount of diffusion that has occurred during the second lab period.

Note: If you are using having the students use the associated worksheet, they should complete Part 1, Question #6.

6. **Compiling results and conclusions:** Students should compile their results and graph the diffusion for the different density gels over time. They should draw conclusions from their data and discuss how changes in the density of tissues could influence overall perfusion.

Note: If you are using having the students use the associated worksheet, they should complete Part 1, Questions #7-11.

Part 2: Blood Sugar

Materials

- Dialysis tubing
- Water, milk, soda, juice, and sports drink
- Beakers
- Glucose meter
- Glucose meter test strips
- Red food coloring
- Pipettes or droppers
- Toothpicks

Prepare Dialysis Tubing and Drinks

Prior to the laboratory, instructors should:

1. Prepare dialysis tubing by cutting it into ~15-20 cm long segments. Place the dialysis tubing in a beaker of water to allow it to hydrate and facilitate handling.
2. Every brand of glucose meter is different. Instructors should determine the amount of dilution that is needed for the glucose meter to measure the amount

of sugar in the drink with the highest sugar content. All other drinks should be diluted by the same amount (i.e. 100 ml into 1 L of water) such that the glucose meter will read the amount of sugar in all drinks and the measurements scale to the original sugar content of the drinks.

3. Prepare a beaker of water with red food coloring to simulate the blood.

Blood Sugar Laboratory

Split the students into groups of 2-3 (can be same as the groups used above)

1. **Decide on drink selection:** Students should choose 2 drink conditions that they would like to test.

Note: If you are using having the students use the associated worksheet, they should complete Part 2, Questions #1-4.

2. **Create Blood Vessels:** Students should create their blood vessels from the dialysis tubing. Each student group should take 2 pieces of dialysis tubing and make a tight knot at one end of the tubing. They should next use the pipettors/droppers to fill the dialysis tubing with red colored water and tie off the other end of the dialysis tubing in a tight knot.

3. **Expose the vessels to the different liquids:** Students should place each of their dialysis tubing blood vessels into separate beakers and add their chosen liquid solution to the beaker until it just covers the blood vessel.

4. **Measure the "blood sugar":** Towards the end of the class period (or at least 30 minutes after the vessels have been placed in the different liquids), students should make qualitative observations about the blood vessels in the beakers (i.e. the blood has diffused out of the vessel because we can see the red color in the rest of the liquid). Students should then remove their vessels from the beakers and rinse them briefly in water. They should prepare the glucose meter with a test strip, puncture the dialysis tubing with a toothpick, and place a small amount of the liquid from inside the tubing onto the test strip.

Note: If you are using having the students use the associated worksheet, they should complete Part 2, Question #5.

5. **Recording results and conclusions:** Students should record the quantitative measurements from the glucose meter, compare between the conditions they chose, and draw conclusions. Instructors should facilitate a class discussion about all of the different conditions in class and ask the students to relate how the different drinks tested changed the blood sugar conditions. They should speculate as to how their results relate to overall health and nutrition.

Note: If you are using having the students use the associated worksheet, they should complete Part 2, Questions #5-8.

Classroom Procedure:

Engage (Time: 20 min over 2 days)

Introduce the lab by going over the information in the "Circulatory System Worksheet" and discussing the general procedure that they will be using. Explain to the students that they are using the same scientific process as real researchers and will be testing their own hypotheses, developing their own protocols, and collecting their own data.

Explore (Time: 70 min over 2 days)

Allow the students to work through the "Circulatory System Worksheet." Students should discuss their hypotheses with their lab group and develop methods to test their hypotheses. Instructors should move from group-to-group and check to make sure that the methods they have chosen are appropriate for the experiment but should not give them specific methods to perform. Once the instructor has checked to make sure that they are on the right track, students should start the experiments and complete their worksheet.

Explain (Time: 20 min over 2 days)

Work with the students to help them answer critical thinking questions and discuss data that their classmates have obtained. Ask the students to discover the overall trends and results of the experiment.

Expand (Time: 10 min over 2 days)

Discuss the implications of their findings to overall human health and disease and relate the information they gathered to other material covered in the class. Ask students how they would change their experimental methods if they were to run the experiment again.

Assessment:

The following rubric can be used to assess students during each part of the activity. The term "expectations" here refers to the content, process and attitudinal goals for this activity. Evidence for understanding may be in the form of oral as well as written communication, both with the teacher as well as observed communication with other students. Specifics are listed in the table below.

1= exceeds expectations
2= meets expectations consistently
3= meets expectations occasionally
4= not meeting expectations

	Engage	Explore	Explain	Expand/Synthesis
1	Shows high level of interest in the material, asks thoughtful questions relevant to the material	Prepares the lab well, is able to take accurate measurements and provide in-depth observations. Data is well organized and student constructs several plots clearly expressing data trends	Provides thoughtful, detailed answers to discussion and worksheet questions, and is able to clearly see correlations between data trends and overarching themes of diffusion and transport concepts.	Integrates knowledge gained from the experiment and asks questions that demonstrate deep understanding of the concepts as they relate to overall human health
2	Shows interest in the material, participates in the discussion while attempting to understand key concepts	Well organized and on-task and takes some measurements but needs some assistance to get started plotting data	Takes part in discussion and provides correct answers to worksheet questions	Understands the concepts being discussed and asks questions that demonstrate a basic understanding of how they relate to human health
3	Minimal discussion and participation but is on-task and is able to understand the concepts and material	Needs assistance on some parts of the lab but is making an effort to participate, attempts to take measurements and plots data but needs some help	Makes minimal effort to join discussion, provides answers to mostly correct answers to worksheet with a few minor misconceptions still evident	Minimal integration of knowledge from laboratory with concepts of human health
4	Does not take interest in the material and refuses to take part in the discussion	Does not participate in the experiments and does not attempt to understand concepts	No effort is made in the discussion, the worksheets are incomplete or incorrectly completed	No effort to understand how the concepts from the laboratory are related to course material

Extension Activities:

Part 1 – Transport

Additional demo materials can be made and used during the explore portion of this activity:

1. Extra petri dishes can be provided to the students and instructors can allow them to create artistic designs with the wells and different color food coloring. These can be observed over the course of the experiments to reinforce the concepts of diffusion and tissue perfusion.
2. Blood vessels made of dialysis tubing can be encapsulated within gelatin (clear plastic containers work well). The dialysis tubing can be filled with a concentrated solution of red food coloring and water (note, it should be filled during gelation so that it doesn't collapse and such that fluid can be pushed through). Students can observe how the food coloring diffuses out of the dialysis tubing in 3D, similarly to how it would occur in the body.

Part 2 – Blood Sugar

Additional demo materials can be made and used during the explore portion of this activity:

1. The nutritional information on the beverages can be used to determine the total amount of sugar per volume of the drinks. White sugar can be weighed out into bags and used visually illustrate the differences in sugar content between the drinks. (i.e. weigh out the amount of sugar per liter of each beverage into separate bags to show the students during the discussion section)

Supplemental Information:

Circulatory System Pre-Test

Circulatory System Pre-Test Answers

Circulatory System Worksheet

Safety:

- Safety goggles while in the laboratory.
- While all the laboratory chemicals used are non-toxic, all direct contact with them should be avoided.
- Students should be careful not to cut themselves when puncturing the dialysis tubing with the toothpick in the blood sugar laboratory. Instructors may want to assist their students with this procedure.
- Do not eat or drink in the laboratory.
- Everyone should wash their hands and work area when completed with the laboratory experiments or before leaving the classroom.

Acknowledgments:

Shivaun Archer, Chris Schaffer, and Cynthia Reinhart-King, Department of Biomedical Engineering, Cornell University

Nev Singhota, Cornell Center for Materials Research

National Science Foundation Cornell GK-12 Program: DGE 0841291

O.2 Circulatory System Pre-Test **Name:_____**

Fill in the blank

1. _____ is the process in which blood vessels exchange nutrients and oxygen in tissues.

2. _____ is one of the primary components of the extracellular matrix.

3. _____ is can be used to model tissue structures and is primarily composed of denatured collagen.

Multiple Choice: Choose the correct answer(s)

4. _____ are the primary blood vessel structures that exchange nutrients and wastes in tissues.

   a. arteries
   b. veins
   c. capillaries
   d. ventricles

5. Blood brings _____ to cells in the body and removes _____ _____ that have accumulated within the cells.

   a. oxygen
   b. carbon dioxide
   c. sugar
   d. toxins

Circle True/False for the following questions.

6. True or False: The number of blood vessels is the only important factor in getting nutrients to tissues.

7. True or False: What we eat and drink influences the amount of sugar in our blood.

Short Answer: be sure to write your response in complete sentences.

8. How does the density of the tissue influence perfusion?

9. What structures absorb nutrients from the digestive system and transport them to tissues?

10. The diffusion of nutrients through tissues can be simulated by watching the diffusion of food coloring through a hydrogel. The distance of diffusion has been measured using a ruler on the diagram below. Graph the amount of diffusion occurring over time.

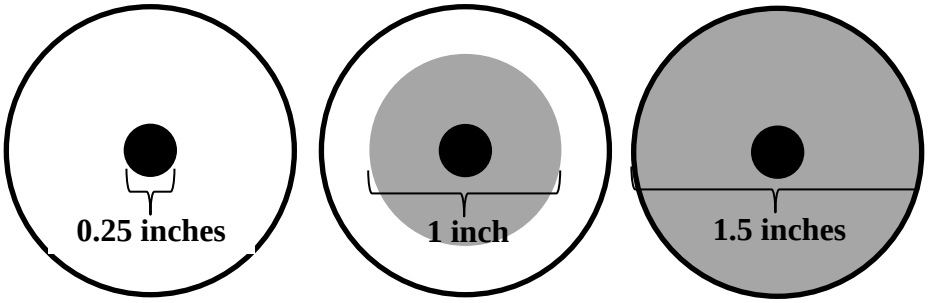

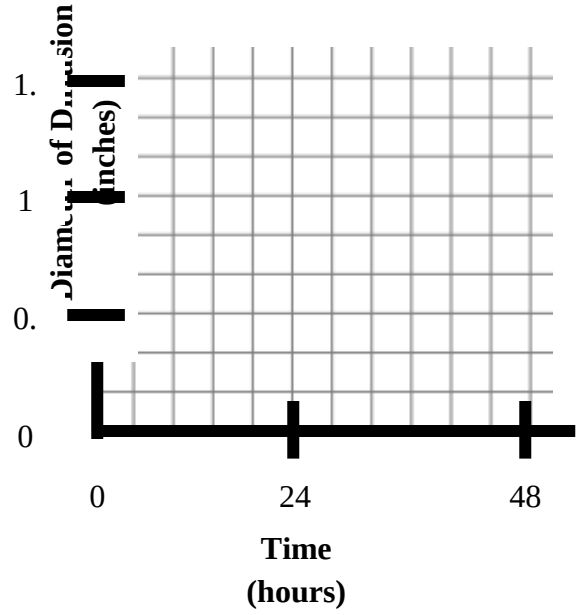

Time = 0 hours Time = 24 hours Time = 48 hours

O.3 Circulatory System Pre-Test Answer Sheet

Fill in the blank

1. _**Perfusion or Transport or Diffusion**_ is the process in which blood vessels exchange nutrients and oxygen in tissues.

2. __**Collagen**_____ is one of the primary components of the extracellular matrix.

3. __**Gelatin**_____ is can be used to model tissue structures and is primarily composed of denatured collagen.

Multiple Choice: Choose the correct answer(s)

4. __**C, Capillaries**_____ are the primary blood vessel structures that exchange nutrients and wastes in tissues.

e.	arteries	g.	capillaries
f.	veins	h.	ventricles

5. Blood brings _**A, Oxygen and C, Sugar**_____ to cells in the body and removes _**B, Carbon Dioxide and D, Toxins**_____ that have accumulated within the cells.

e.	oxygen	g.	sugar
f.	carbon dioxide	h.	toxins

Circle True/False for the following questions.

6. True or **False**: The number of blood vessels is the only important factor in getting nutrients to tissues.

There are many other factors that are important including the density of the tissue, the flow rate of blood through the capillaries, and the permeability/leakiness of the endothelial cell layer that makes up the capillaries.

7. **True** or False: What we eat and drink influences the amount of sugar in our blood.

Short Answer: be sure to write your response in complete sentences.

8. How does the density of the tissue influence perfusion?

Oxygen and nutrients will diffuse a shorter distance in a tissue that is more dense

9. What structures absorb nutrients from the digestive system and transport them to tissues?

Nutrients are absorbed by the capillaries in the digestive system and transported throughout the rest of the body.

10. The diffusion of nutrients through tissues can be simulated by watching the diffusion of food coloring through a hydrogel. The distance of diffusion has been measured using a ruler on the diagram below. Graph the amount of diffusion occurring over time.

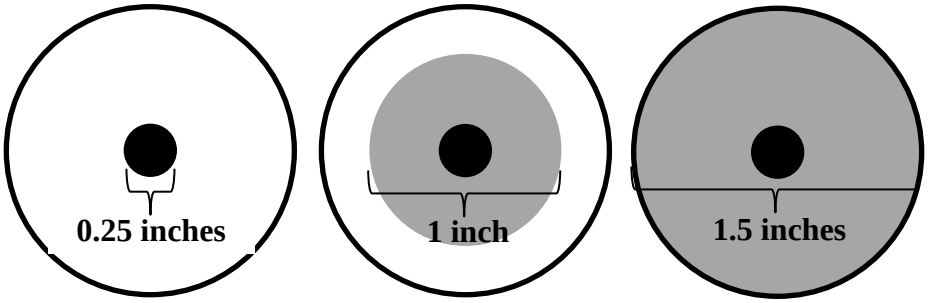

Time = Time = 24 hours Time = 48 hours

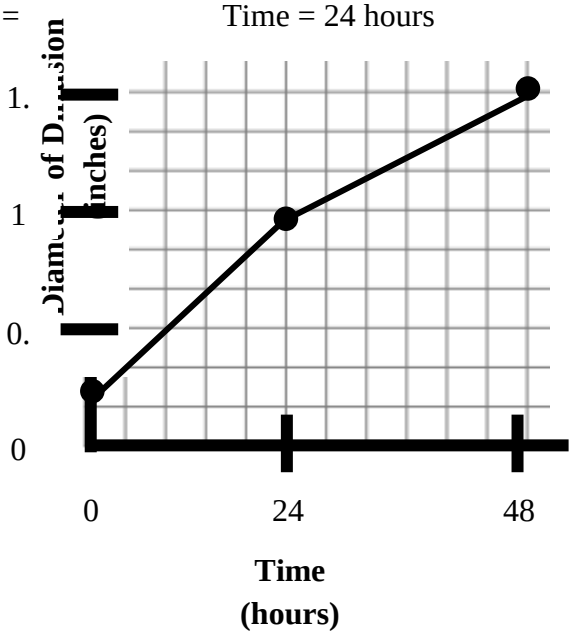

Alternate question that could be used.

1. Use numbers to order the following steps in the scientific method (1 is the first step, 8 is the last step).

___**1**_ Define Problem

___**8**_ Redesign experiment and repeat process

___**7**_ Develop conclusions

___**2**_ Learn about the topic

___**3**_ Develop a hypothesis

___**5**_ Gather Data and Results

___**4**_ Design Experiment

___**6**_ Interpret results

O.4 Circulatory System Worksheet **Name:_____**

Lab #_____

Part 1 – The transport of molecules and perfusion of tissues via the circulatory system

Circulation is the term used to describe the movement of blood through tube-like structures in the body called **blood vessels**. There are two primary categories of blood vessels: arteries and veins. **Arteries** transport blood away from the heart and carry oxygen and nutrients to the rest of the body and **veins** transport blood to the heart and help carry carbon dioxide and wastes away from the cells. The two exceptions to this are the pulmonary artery, which carries deoxygenated blood to the lungs, and the pulmonary vein, which carries oxygenated blood back to the heart. The process of exchanging of oxygen, carbon dioxide, nutrients, and wastes is called tissue **perfusion** and occurs in small blood vessels called **capillaries**.

The effective perfusion of tissues is dependent upon a variety of factors including the number of capillaries, the flow rate of blood through the capillaries, the permeability (or leakiness) of the capillaries, and the density of the tissue. **Tissue density** is influenced by the amount proteins and other molecules in the space surrounding the cells called the extracellular matrix. Tissue density is influenced by the function and type of tissue and can be altered during different diseases such as cancer. These changes in density can have large effects on tissue perfusion.

In animals, the most abundant protein component of tissues and the extracellular matrix is **collagen**. Collagen can be isolated from tissues and is commonly used to create **hydrogels** (a gel-like polymer that contains a high amount of water) for tissue engineering and research purposes. **Gelatin** is a made of denatured collagen can form a hydrogel when it is mixed with water and can be used to model tissue structures.

Laboratory Goals and Procedures

In this inquiry-based laboratory, you will design a set of experiments to test properties that influence tissue perfusion. Your goal is to perfuse the entire tissue construct (a gelatin coated petri dish) with the least number of capillaries (modeled by punching holes into the gelatin). You and your partner(s) will choose 2 tissue constructs that have been coated with a 2%, 5%, or 15% gelatin solution and determine the number of capillaries you think will be necessary to perfuse the entire tissue. You will cut your capillary structures into the tissue construct using a straw or biopsy punch and then place 1 drop of red food coloring (simulating oxygenated blood) into each of the wells

you create. You will monitor your experiment, record your results, and analyze your data.

Objectives

By the end of this laboratory, you should be able to:

- measure and graph the diffusion properties for tissues of different densities
- describe how the density and porosity of a tissue will influence diffusion
- predict what would happen if the density of a tissue were to be altered (as in some diseases)

Materials

- 35 mm petri dishes coated with 2%, 5%, or 15% gelatin
- 6 mm biopsy punch or straw
- red food coloring
- paper towels
- pipettes or droppers

Safety

- Wear safety goggles while in the laboratory.
- While all the laboratory chemicals used today are non-toxic, all direct contact with them should be avoided. The food coloring will stain.
- Do not eat or drink in the laboratory.
- Wash your hands and work area when completed with the laboratory experiments or before leaving the classroom.

1. **State the objective of this experiment. What problem are you trying to examine or solve?**

_____

_____

2. **Propose a hypothesis. What do you think is going to happen during your experiment?**

_____

_____

3. **How will you test your hypothesis? Write down your methods and fill in the diagrams with your proposed capillary layout (include the density of the gelatin you will test, how many capillaries you will make in each dish, where you will put the capillaries, etc.)**

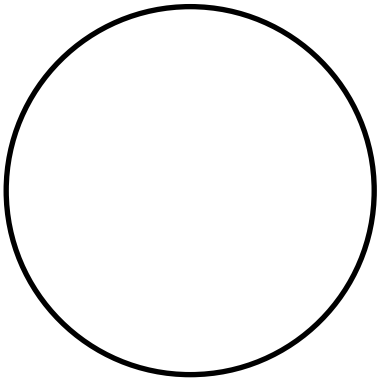

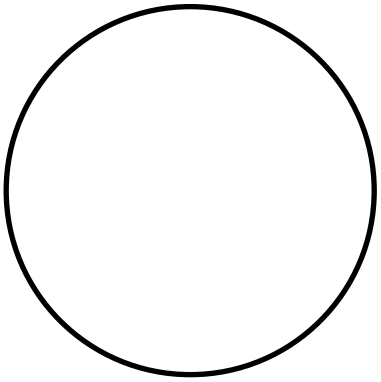

Write down the details of your methods here:

_____

_____

_____

4. **What method will you use to determine the extent of diffusion that occurs from the capillaries into your tissue constructs? How do you plan to measure the differences in diffusion between tissue constructs of different densities?**

_____

_____

5. **What are your initial (day 1) results and observations?**

Sample Density	Observations	Measurement of Perfusion	Other

Use the diagram below to draw your samples:

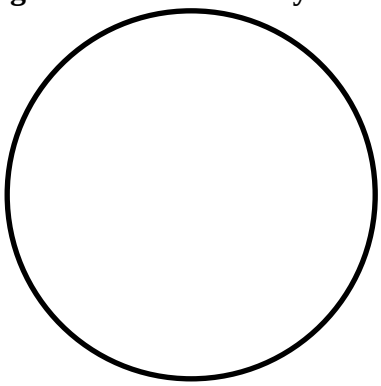

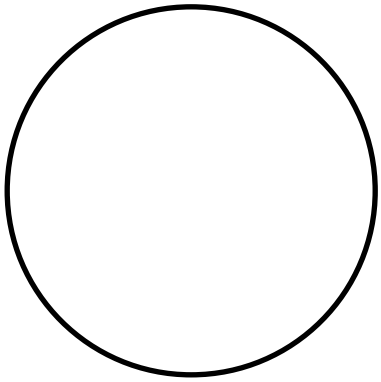

6. **What are your final (day 2) results and observations?**

Sample Density	Observations	Measurement of Perfusion	Other

Use the diagram below to draw your samples:

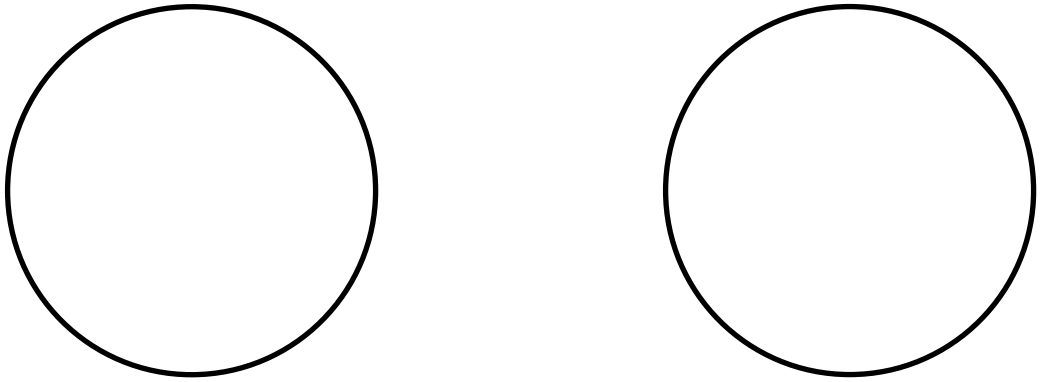

7. **Plot your results on the following graph. Be sure to put a title on the graph and label the axes. (Hint, use a line graph with a legend to plot the two different conditions over time)**

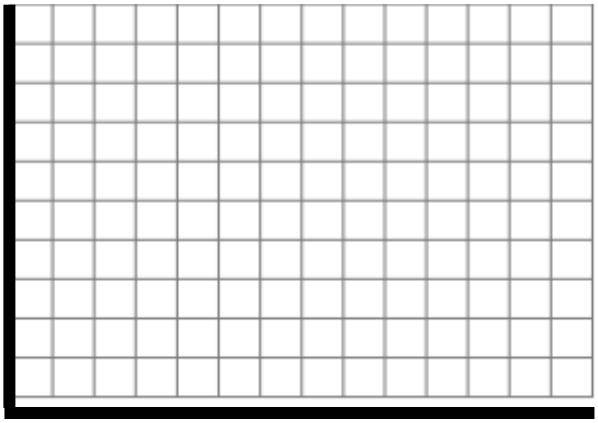

8. **What conclusions can you draw from your results?**

9. **In the body, how could changing the density of your tissues change the diffusion of nutrients into the tissue?**

10. **If the density of your tissues were to increase, what could you do to make sure that it remains well-perfused? (Hint: What could you change about your blood vessels so that they could perfuse the tissue more effectively?)**

11. **What other physical factors are present in the vasculature that could influence the perfusion of tissues?**

Part 2 – The relationship of the food we eat and blood sugar levels

When we ingest foods and drinks, they enter into the digestive system and are eventually converted into the nutrients our cells need to survive. The foods in our diet are mechanically degraded into smaller molecules in our mouth and stomach and chemical degradation is initiated. Once the food leaves the stomach (as a thick mixture called chyme) and enters the small intestine, the majority of chemical digestion occurs and the **nutrients begin to be absorbed directly into the blood stream**. Once in the blood, those nutrients travel throughout the whole body and are delivered to the cells via **perfusion** from capillaries.

What we eat directly influences the nutrients our body receives, uses, and stores as fat. The process of digestion breaks down all of the usable nutrients from what we ingest so the nutritional content of the food we eat is very important. Generally, people should eat foods that are low in oils and fat and high in vegetable and fruit content with moderate protein and grain intake. Sugars can provide people with the energy they need to be active but, if people eat and drink too much sugar, the excess will be converted to glycogen or fatty acids and stored within the body.

People with diabetes must be especially careful about the amount of sugar they ingest because they do not produce enough insulin or are resistant to the insulin they do produce. In addition to controlling their dietary intake and exercising, diabetic patients also use insulin therapy to control their sugar levels. The most common way to measure the amount of sugar in the blood is to use a small device called a **glucometer** (or glucose meter) with a small drop of blood from a pricked finger.

Laboratory Goals and Procedures

In this laboratory, you will investigate how different drinks can influence blood sugar levels. You and your partner(s) will simulate the absorbance of nutrients into the blood stream from different liquids using dialysis tubing filled with fluid to model the blood vessel. You will choose 2 different types of drinks (water, milk, soda, juice, or sport's drink) and put them into a beaker. To complete the setup, you will add a blood vessel made out of dialysis tubing and allow the nutrients to diffuse into the vessel. After about 1 hour, you will test the amount of glucose that has entered the blood vessel using a glucose meter and compare between the conditions you chose.

Objectives

By the end of this activity, you should be able to:

- demonstrate how to test for simple sugars using chemical indicators and a glucose meter

- explain diffusion through a membrane simulating the vascular wall
- relate the process of digestion to the circulation of simple sugars in the blood stream
- predict how foods will influence blood sugar levels

Materials

- dialysis tubing
- water, milk, soda, juice, sports drink
- beaker
- glucose meter
- glucose meter test strips
- pipettes

Safety

- Wear safety goggles while in the laboratory.
- While all the laboratory chemicals used today are non-toxic, all direct contact with them should be avoided.
- Do not eat or drink in the laboratory.
- Wash your hands and work area when completed with the laboratory experiments or before leaving the classroom.

1. **State the objective of this experiment. What problem are you trying to examine or solve?**

_____

_____

2. **Propose a hypothesis. What do you think is going to happen during your experiment?**

_____

_____

3. **How will you test your hypothesis? Write your methods here.**

_____

_____

4. **What method will you use to compare the amount of blood sugar that diffuses into you blood vessel from the test solution?**

_____

_____

5. **What are your results and observations?**

Test Solution	**Observations**	**Blood Sugar Measurement**	**Other**

_____

_____

6. **Plot your results on the following graph. Be sure to put a title on the graph and label the axes. (Hint, use a bar graph to plot the two different conditions)**

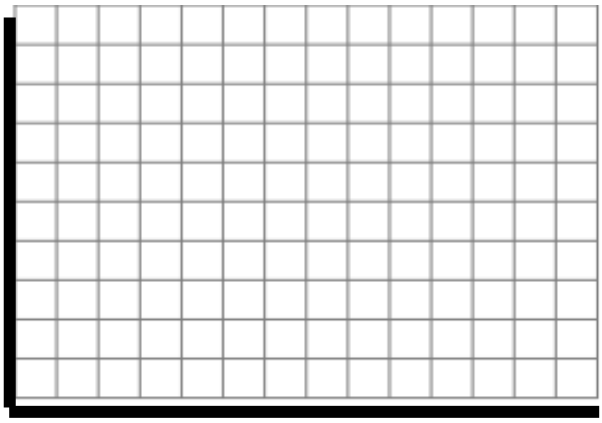

7. **What conclusions can you draw from your results?**

_____

_____

8. **People with diabetes must maintain their blood sugar at a relatively constant level and avoid large changes in blood sugar. Based on your data, what drinks should diabetics avoid?**
   a. **water**
   b. **milk**
   c. **juice**
   d. **sports drinks**
   e. **soda**

O.5 Turkey Time Lesson Plan

Background:

Food scientists and nutritionists investigate the properties of the food that we eat and design meals that contain the essential vitamins and nutrients that our bodies need to function properly. Generally, people should eat foods that are low in oils and fat and high in vegetable and fruit content with moderate protein and grain intake. ChooseMyPlate is a tool designed by nutritionists to help people determine the proportion of foods they should be eating to stay healthy. The diagram below shows the approximate breakdown and recommended intake of the primary food groups.

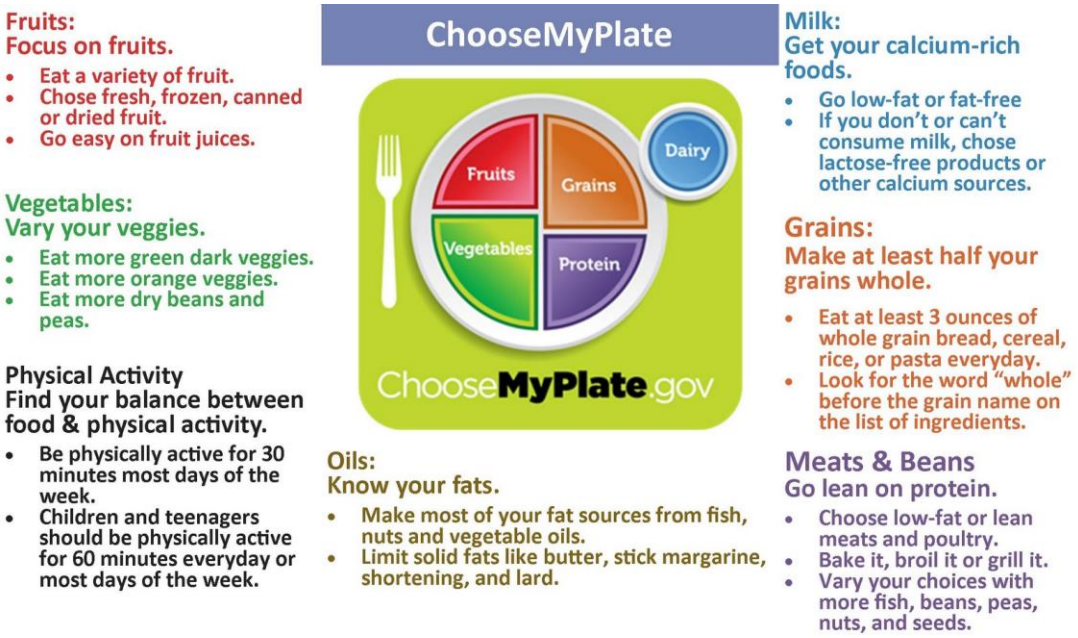

Project Motivation and Goals:

Thanksgiving dinner is delicious tradition but recent studies have found that the foods served during the holiday season can lead to weight gain, increased risks of cardiac events, and an overall decrease in health. You are a nutritional scientist at Good Food for You, a company that is responsible for creating and distributing healthy, well-balanced meals. Good Food for You is competing against other companies to win the rights to provide meals for next year's Thanksgiving meal and will be judged on the quality and composition of the food you produce. Before you send off samples of food to the national competition, you decided it would be a good idea to test the food you make to determine what it is comprised of. Your goal is to determine what is currently in the foods you produce and modify them to create a healthy, well-balanced meal so that you can win the competition.

Note: Much of the following information has been taken from or adapted from:
http://www.accessexcellence.org/pizza/pdf/fcbook.pdf
Food Chemistry Experiments; Institute of Food Technologists. The Society for Food Science and Technology.

Definitions and Vocabulary:
Polymers (the prefix "poly" means many) contain two or more monomers. Starch is a polymer of the monomer glucose. Protein is a polymer of amino acids.

Glucose is a simple sugar and the primary source of energy for all mammals and many plants. It is also known as dextrose, grape sugar, and corn sugar. The chemical structure is $C_6H_{12}O_6$ and a diagram of the molecule is shown below (Figure 1).

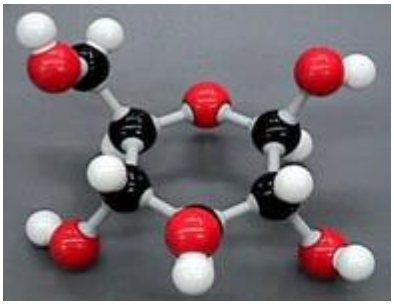

Figure 1: This ball and stick diagram depicts a molecule of glucose.

Carbohydrates/Starches:
Polysaccharides are formed when many single sugars are joined together chemically. Polysaccharides include starch, glycogen (storage starch in animals), cellulose (found in the cell walls of plants), and DNA.

Starch is the predominant storage molecule in plants and provides the majority of the food calories consumed by people worldwide. Starch is a polymer of simple sugar molecules such as glucose (see above). Animals store energy in the muscles and liver as glycogen (a storage starch in animals). For longer-term storage, animals convert the food calories from carbohydrates to fat.

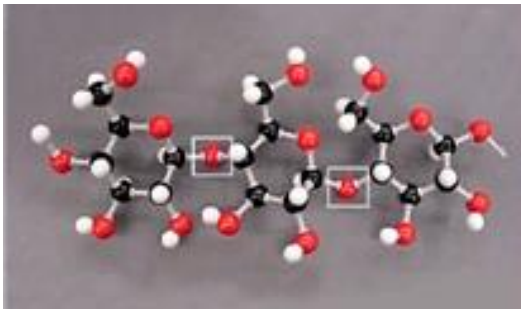

Figure 2: This ball and stick diagram depicts starch. Starch is a polysaccharide formed from multiple monosaccharides.

Lipids and Fatty Acids:

Lipids include fats, oils, waxes, cholesterol, other sterols, and most steroids. Lipids are biologically important for making barriers (membranes of animal cells), which control the flow of water and other materials into a cell.

Fats and oils make up 95% of food lipids and phospholipids, and sterols make up the other 5%. Animal fats are found in meats (beef, chicken, lamb, pork, and veal), milk products, eggs, and seafood (fish oil). Plant (vegetable) oils come from nuts (peanuts), olives, and seeds (soybean, canola, safflower, and corn). We use lipids for flavor (butter and olive oil), to cook foods (oils and shortening), to increase the palatability of foods by improving the texture or "mouthfeel" (cakes, creamy ice cream), and in food processing (emulsifiers).

Fatty acids are generally long, straight chains of carbon atoms with hydrogen atoms attached (hydrocarbons) with a carboxylic acid group (COOH) at one end and a methyl group (CH_3) at the other end (Figure 2). These long, straight chains combine with the glycerol molecule to form lipids.

In the body, fat serves as a source of energy, a thermal insulator and cushion around organs, and an important cellular component. Since fats have 2.25 times the energy content of carbohydrates and proteins, most people try to limit their intake of dietary fat to avoid becoming overweight. The food industry has a big market for low-fat and non-fat foods.

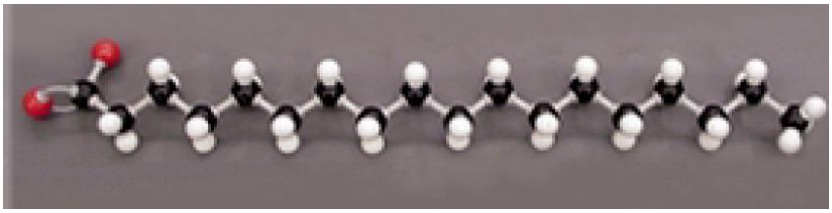

Figure 3: This ball and stick diagram depicts stearic acid. It is a saturated fatty acid found in foods from animal and plant sources.

Amino Acids and Proteins:

Amino acids contain carbon, hydrogen, nitrogen, and sometimes sulfur and serve as the monomers for making peptides and proteins. Amino acids have a basic structure that includes an amino group (NH_2) and a carboxyl group (COOH) attached to a carbon atom (see Figure 1A). This carbon atom also has a side chain (an "R" group). This side chain can be as simple as an -H or a -CH_3, or even a benzene group.

There are twenty amino acids found in the body. Eight of these amino acids are essential for adults and children, and nine are essential for infants. Essential means

that we cannot synthesize them in adequate quantities for growth and repair of our bodies, and therefore, must be included in the diet.
Amino acids are linked together by a peptide bond in which the carboxyl carbon of one amino acid forms a covalent bond with the amino nitrogen of the other amino acid (see Figure 1B). Short chains of amino acids are called peptides. Longer chains of amino acids are called polypeptides

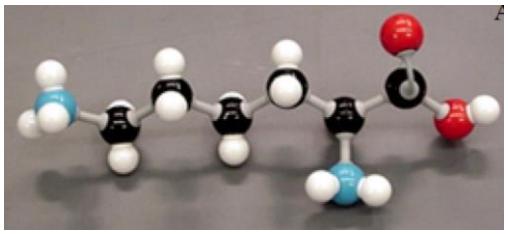

Figure 4: This ball and stick diagram depicts lysine, an essential amino acid we must get from our diet.

Proteins are complex polymers composed of amino acid monomers, and are considered to be the primary structure of all living organisms. Some examples of protein are muscle, hair, skin, hormones, and enzymes. Body builders and football players eat a lot of protein (eggs, cheese, and meat) to build muscle mass. You have probably seen protein-enriched drinks and protein-enriched foods (power bars) at the supermarket.

Proteins are the most complex and important group of molecules because they possess diverse functionality to support life. Every cell that makes up plants and animals requires proteins for structure and function.

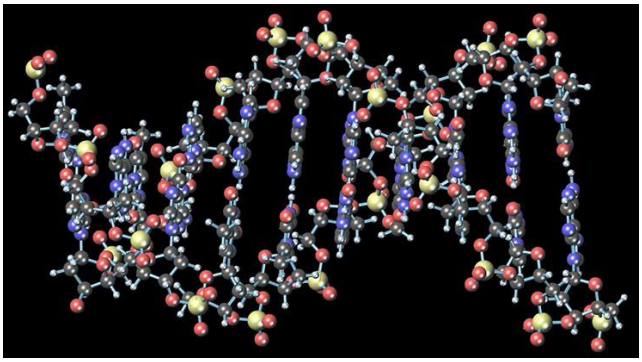

Figure 5: This complex ball and stick diagram depicts the structure of DNA. Notice that the structure is much more complex than a single amino acid.

Methods for Analyzing Food Components:

1. **Testing for Glucose – Benedict's Test**

How the Benedict's Test Works

Benedict Solution is light blue because it contains copper sulfate. When it is mixed and heated with a sugar, such as glucose, which has electrons available to donate, the copper will accept the electrons and become reduced, which turns it brownish-orange. During this process, the blue copper (II) ion is reduced to a red copper (I) ion. While the copper is being reduced, the glucose gives up an electron and is oxidized. Because glucose is able to reduce the copper in Benedict Solution, we call it a reducing sugar.

Reducing Sugars

Glucose is not the only reducing sugar. Any sugar that is structurally capable of donating electrons to Benedict Solution (or a similar reagent) falls into this category. Aldehyde-based sugars that are in their linear, acyclic form are able to donate electrons and reduce other molecules. Some sugars are "locked" into their cyclic form and structurally unable to open into their linear form. These are most commonly non-reducing sugars. Other examples of reducing sugars include ribose and sucrose.

Uses

The most common use for Benedict Solution is the detection of glucose in urine for the diagnosis of diabetes. Diabetics excrete glucose into their urine because they are unable to properly absorb it into their cells. After a positive diagnosis, additional tests are needed to quantify the amount of glucose excreted.

Method

1. Fill a test tube with a few ml of your test solution and add an equal amount of Benedict's Solution (20 drops of your test solution + 20 drops of Benedict's Solution).
2. After briefly mixing, heat the tube for a few minutes in the hot water bath.
3. Determine if your test is positive or negative. A positive result will produce a brownish-orange precipitate and a negative result will produce no change to the solution. If your tube turns a muddy green, your initial glucose concentration was likely so low that only some of the blue copper (II) ions reacted (this is still considered a positive test).

Read more: The Effect of Benedict Solution on Glucose
http://www.ehow.com/about_6584528_effect-benedict-solution-glucose.html

2. **Testing for Protein – Biuret Test**

How the Biuret Test Works

The Biuret solution is a mixture of 5% copper(+2) sulfate in 10% sodium hydroxide. Substances containing two or more peptide bonds (three or more amino acids) form a purple-violet complex with copper salts in alkali solution. The nature of the color is probably due to the formation of a tetra-coordinated cupric ion (Cu+2) with amino groups (the Cu+2 ion is surrounded by amino groups). A light blue color indicates a negative response, a purple/violet color a positive response.

Uses
The Biuret test can be used to detect the presence of proteins in a solution. The Biuret test can also be used to quantify the amount of proteins used in a solution when used with a spectrophotometer.

Method

1. Fill a test tube with a few ml of your test solution and add an equal amount of Biuret Solution (20 drops of your test solution + 20 drops of Biuret Solution).
2. Swirl mixture to mix and allow the mixture to stand for 5 minutes.
3. Determine if your test is positive or negative. A positive result will produce a pink or purple solution and a negative result will produce no change to the solution.

Read more about the Biuret Test
http://www.brilliantbiologystudent.com/biuret_test.html

3. Testing for Starch – Iodine Test

How the Iodine Test Works
A complex interconnected series of sugar molecules (saccharides) comprise starch molecules. To test for the presence of these polysaccharides (many sugar) structured starches you will need iodine. The iodine acts as an indicator, changing color when it combines with starches. A color change occurs from the complex network of starches trapping the iodine molecules, revealing a blue-black color. The iodine will not change color in reaction to simple sugars, such as sucrose or fructose, because these do not retain iodine between the sugar molecules the way starches do.

Uses
The Iodine test can be to test for the presence of starch within food samples.

Method

1. Fill a test tube with a few ml of your test solution and add an equal amount of Iodine (20 drops of your test solution + 20 drops of Iodine).
2. Swirl mixture to mix and allow the mixture to stand for 5 minutes.

3. Determine if your test is positive or negative. A positive result will produce a dark blue-black solution and a negative result will produce no change to the solution (it will remain an amber color).

Read more: How to Test Yogurt for Starch With Iodine
http://www.ehow.com/how_5682963_test-yogurt-starch-iodine.html#ixzz2BkLPp0sQ

4. Testing for Lipids – Paper towel or "floating" test

How the Paper Towel test Works

The Grease Spot test can also be used identify the presence of lipids in a sample. Lipids make unglazed paper, such as the outside of a paper bag, translucent.

How the Floating Test Works

Lipids do not dissolve in water since lipids are nonpolar molecules. When water and lipids are mixed together, the two solutions will separate and the lipids will form a layer or film on top of the water.

Method for the Paper Towel Test

1. Use a cotton swab to apply a few drops of the sample to the paper towel.
2. Allow the sample to dry on the bag for several minutes.
3. Hold the paper bag up to a light after the sample has dried completely. If a grease spot remains, the sample contains lipids (positive result).

Method for the Floating Test

1. Fill a test tube with a few ml of your test solution and an equal amount of water (20 drops of your test solution + 20 drops of water).
2. Swirl mixture to mix and allow the mixture to stand for 5 minutes.
3. Determine if your test is positive or negative. If the result is positive, the two solutions will form distinct layers and the lipids will float on top of the water solution. If the result is negative, no layer will form on top of the water solution. NOTE: The lipids can be easily viewed if the solution is cooled (the lipids will form a solid-like film on top of the water).

Read more about How to Test for Lipids
http://www.ehow.com/how_4829982_test-for-lipids.html#ixzz2BkLkIBsX

5. Testing for pH – pH strips

How the pH test works

The pH of a solution can be tested in a number of ways including the use of colorimetric indicators like pH test strips. When the pH strip is dipped into an acidic

solution, the acid donates a proton (H+) and a color change occurs on the strip. Likewise, when the pH strip is dipped into a basic solution, the base accepts a proton (H+) and a color change occurs on the strip. The pH of the solution can be determined by matching the color of the strip with the indicator legend.

Method for pH testing

1. Fill a test tube with a few ml of your test solution.
2. Briefly dip the pH strip into the solution and determine which indicator color the strip matches.

The following websites contain more information about the recommended allowances for a healthy diet:
http://www.choosemyplate.gov/
http://www.livestrong.com/article/555621-sugar-fat-protein-starches-used-in-the-human-body/
http://www.livestrong.com/article/288657-the-recommended-daily-intake-of-calories-carbs-fat-sodium-protein/

Turkey Time Worksheet **Name:**

Lab #_____

Use the packet to fill in the following table about testing methods:

Material Testing	Test Name	Positive Result	Negative Result
Starch			
	Biuret		
		Brown-orange precipitate	Light blue solution
pH			
	Paper towel or floating test		

What is the purpose/objective of this lab? What will you be testing for?

Choose 3 of the following foods and develop hypotheses for the different components that will be in each (write hypotheses below).

- Turkey
- Mashed Potatoes
- Gravy
- Bread
- Candied Yams
- Pumpkin Pie
- Apple Pie
- Lemon Meringue Pie

Hypotheses:

1.

2.

3.

Experimental Design and Methods:

Write out the procedure you will use to test the composition of these foods.

Results:

List your results (positive or negative) for each test in the table below:

Food Tested	Biuret Test	Benedict Test	Iodine Test	pH Test	Paper Towel or Floating Test

Write any additional results or observations here:

Conclusions: What can you conclude about the foods from your results?

Consider the proportions and dietary suggestions given by the food pyramid. What types of foods are healthiest for you to eat?

What could you do to make the “unhealthy” foods better for you to eat (what could you add to or remove from the foods)?